ROCK MECHANICS AN INTRODUCTION SECOND EDITION



NAGARATNAM SIVAKUGAN, SANJAY KUMAR SHUKLA, BRAJA M. DAS AND PETER TO

Rock Mechanics: An Introduction, Second Edition introduces rock mechanics fundamentals in a simple way with a strong practical bias, assuming no prior knowledge in the subject. It is an essential text for students at the graduate level who are facing careers as professional geotechnical engineers. The book is also suitable for undergraduates and engineering professionals in civil, mining, petroleum and geological engineering.

This new edition brings in a completely new chapter on tunnelling as well as more information on numerical analysis and software, and sections on slope failure mechanisms, rock-socketted piles and petroleum geology.

Nagaratnam Sivakugan is former Head of Civil and Environmental Engineering at James Cook University, Australia.

Sanjay Kumar Shukla is Civil Engineering Discipline Coordinator and Founding Geotechnical and Geoenvironmental Engineering Research Ground Leader at the School of Engineering, Edith Cowan University, Australia.

Braja M. Das (deceased) was Dean of the College of Engineering and Computer Science at California State University, Sacramento, USA.

Peter To is Discipline Coordinator in Civil Engineering at James Cook University, Australia.



Rock Mechanics An Introduction

Second Edition

Nagaratnam Sivakugan, Sanjay Kumar Shukla, Braja M. Das, and Peter To



Designed cover image: Dr. S. K. Navaratnarajah

Second edition published 2026

by CRC Press

4 Park Square, Milton Park, Abingdon, Oxon, OX14 4RN

and by CRC Press

2385 NW Executive Center Drive, Suite 320, Boca Raton FL 33431

© 2026 Nagaratnam Sivakugan, Sanjay Kumar Shukla, Braja M. Das, and Peter To

First edition published by CRC Press 2013

CRC Press is an imprint of Informa UK Limited

The right of Nagaratnam Sivakugan, Sanjay Kumar Shukla, Braja M. Das, and Peter To to be identified as authors of this work has been asserted in accordance with sections 77 and 78 of the Copyright, Designs and Patents Act 1988.

All rights reserved. No part of this book may be reprinted or reproduced or utilised in any form or by any electronic, mechanical, or other means, now known or hereafter invented, including photocopying and recording, or in any information storage or retrieval system, without permission in writing from the publishers.

For permission to photocopy or use material electronically from this work, access www.copyright.com or contact the Copyright Clearance Center, Inc. (CCC), 222 Rosewood Drive, Danvers, MA 01923, 978–750–8400. For works that are not available on CCC please contact mpkbookspermissions@tandf.co.uk

Trademark notice: Product or corporate names may be trademarks or registered trademarks, and are used only for identification and explanation without intent to infringe.

British Library Cataloguing-in-Publication Data

A catalogue record for this book is available from the British Library

Library of Congress Cataloging-in-Publication Data

Names: Sivakugan, N. (Nagaratnam), 1956– author | Shukla, Sanjay Kumar author | Das, Braja M., 1941– author | To. Peter author

Title: Rock mechanics: an introduction / Nagaratnam Sivakugan, Sanjay Kumar Shukla, Braja M. Das, and Peter To.

Description: Second edition. | Boca Raton, FL: CRC Press, 2026. | Includes bibliographical references and index.

Identifiers: LCCN 2025014822 (print) | LCCN 2025014823 (ebook) | ISBN 9781032714684 hardback | ISBN 9781032725147 paperback | ISBN 9781032725161 ebook

Subjects: LCSH: Rock mechanics

Classification: LCC TA760 .S49 2026 (print) | LCC TA760 (ebook) | DDC 624.1/5132—dcundefined LC record available at https://lccn.loc.gov/2025014822

LC ebook record available at https://lccn.loc.gov/2025014823

ISBN: 978-1-032-71468-4 (hbk) ISBN: 978-1-032-72514-7 (pbk) ISBN: 978-1-032-72516-1 (ebk)

DOI: 10.1201/9781032725161

Typeset in Times

by Apex CoVantage, LLC

Contents

Preface			ix	
About the A	uthors.		xi	
Chapter 1	Fundamentals of Engineering Geology		1	
	1.1 Introduction		1	
	1.2	Structure and Composition of the Earth		
	1.3	Minerals and Mineralogical Analysis		
	1.4	Rock Formations and Types		
	1.5	Geological Structures and Discontinuities		
	1.6 Weathering of Rocks and Soil Formation			
	1.8	Hydrogeology		
	1.9	Petroleum Geology		
	1.10	Site Investigation		
		1.10.1 Seismic Methods		
		1.10.2 Electrical Resistivity Methods		
	1.11	Geological Site Selection for Structures		
	1.12	Summary		
	Revie	ew Exercises		
	Refer	ences	55	
Chapter 2	Spher	rical Presentation of Geological Data	57	
-				
	2.1	Introduction		
	2.2	Orientations of Planes and Lines		
	2.3	Coordinate System with Longitudes and Latitudes		
	2.4	Intersection of a Plane and a Sphere		
	2.5	Spherical Projections		
		2.5.1 Equal Area Projection		
		2.5.2 Equal Angle Projection		
		2.5.3 Projections of Great Circles on Horizontal Planes		
		2.5.4 Polar Stereonet		
		2.5.5 Equatorial Stereonet		
		2.5.6 Intersection of Two Planes		
		2.5.7 Angle between Two Lines (or Planes)		
	2.6	2.5.8 Fault Estimation		
	2.6	Summary		
		ew Exercisesences		
	Neier	CHICAGO	0.1	

vi Contents

Chapter 3	Rock Properties and Laboratory Testing		
	3.1 Introduction		86
	3.2	Engineering Properties of Intact Rock	86
		3.2.1 Rotary versus Percussion Drilling	
		3.2.2 Rock Coring	
		3.2.3 Rock Quality Designation	
		3.2.4 Specimen Preparation	
		3.2.5 Standards	
	3.3	Uniaxial Compressive Strength Test	
		3.3.1 Soils versus Rocks	
		3.3.2 Test Procedure	92
	3.4	Indirect Tensile Strength Test	101
		3.4.1 Test Procedure	
	3.5	Point Load Strength Test	103
		3.5.1 Test Procedure	
	3.6	Slake Durability Test	106
· · · · · · · · · · · · · · · · · · ·		3.6.1 Test Procedure	108
	3.7	Schmidt Hammer Test	108
		3.7.1 Test Procedure	110
	3.8	Triaxial Test	111
		3.8.1 Test Procedure	111
	3.9	Empirical Correlations	112
	3.10	Summary	113
	Revie	w Exercises	114
	Refere	ences	116
Chapter 4	Rock	Mass Classification	119
	4.1	Introduction	119
	4.2	Intact Rock and Rock Mass	
	4.3	Factors Affecting Discontinuities	123
		4.3.1 Orientation	
		4.3.2 Spacing	124
		4.3.3 Persistence	
		4.3.4 Roughness	125
		4.3.5 Wall Strength	
		4.3.6 Aperture	
		4.3.7 Filling	
		4.3.8 Seepage	
		4.3.10 Block Size	
	4.4	Rock Mass Classification	
	4.5 Rock Mass Rating		
	4.6	Tunnelling Quality Index: Q-System	

Contents

	4.7	Geological Strength Index	146
	4.8	Summary	151
	Revie	ew Exercises	152
	References		
Chapter 5	Strength and Deformation Characteristics of Rocks		155
	5.1	Introduction	155
	5.2	In Situ Stresses and Strength	
	5.3	Stress–Strain Relations	
	0.0	5.3.1 Plane Strain Loading	
		5.3.2 Plane Stress Loading	
		5.3.3 Axisymmetric Loading	
		5.3.4 Strain–Displacement Relationships	
	5.4	Mohr–Coulomb Failure Criterion	
	5.5	Hoek–Brown Failure Criterion	
		5.5.1 Intact Rock	170
		5.5.2 Rock Mass	173
	5.6	Mohr–Coulomb c' and ϕ' for Rock Mass from the	
		Hoek-Brown Parameters	176
	5.7	Deformation Modulus	180
	5.8	Strength of Rock Mass with a Single Plane of Weakness.	181
	5.9	Summary	183
		ew Exercises	
	Refer	rences	186
Chapter 6	Rock	Slope Stability	188
	6.1	Introduction	188
	6.2	Modes of Rock Slope Failure	
	6.3	Slope Failure Mechanisms and Kinematic Analysis	
		6.3.1 Slope Failure Mechanisms	
		6.3.2 Kinematic Analysis	
	6.4	Slope Stability Analysis	201
		6.4.1 Factor of Safety	202
		6.4.2 Plane Failure	202
		6.4.3 Wedge Failure	208
		6.4.4 Circular Failure	212
		6.4.5 Toppling Failure	212
		6.4.6 Fall	
	6.5	Slope Stabilisation	
	6.6	Summary	
		ew Exercises	
	References		223

viii Contents

Chapter 7	Found	dations on Rock	225
	7.1	Introduction	225
	7.2	Shallow Foundations	225
		7.2.1 Meaning of Shallow Foundation	225
		7.2.2 Types of Shallow Foundations	
		7.2.3 Depth of Foundation	
		7.2.4 Load-Bearing Capacity Terms	
		7.2.5 Estimation of Load-Bearing Capacity	
	7.3	Deep Foundations	
		7.3.1 Meaning of Deep Foundation	
		7.3.2 Types of Deep Foundations	
		7.3.3 Estimation of Load-Carrying Capacity	
	7.4	Rock-Socketted Piles	
		7.4.1 Ultimate Load-Carrying Capacities $Q_{\text{side.ult}}$,	
		$Q_{ m base,ult}$, and $Q_{ m ult}$	236
		7.4.2 Ultimate Side Shear Resistance f_s	
		7.4.3 Ultimate End-Bearing Capacity q_b	240
	7.5	Foundation Construction and Treatment	248
	7.6	Summary	249
	Revie	ew Exercises	249
	Refer	rences	252
Chapter 8	Tunnelling within Rock Mass25		
	8.1	Introduction	255
	8.2	Key Aspects of Design of Tunnels	
		8.2.1 Stabilisation of Roof and Walls	
		8.2.2 Lining Support System	
		8.2.3 Drainage and Ventilation System	
	8.3	Construction of Tunnels	
		8.3.1 Construction Methods	
		8.3.2 Cares and Considerations	
	8.4	Numerical Analysis and Software	
	8.5	Summary	
	Revie	ew Exercises	
		rences	
Appendix			287
Index			289

Preface

Rock mechanics is not generally taught as a core subject in civil engineering undergraduate programmes. It is taught as an elective subject in the undergraduate programme or as a core or elective subject at the postgraduate level. Some geological engineering or mining engineering degree programmes may offer greater exposure to rock mechanics than their civil engineering counterparts.

A geotechnical engineering project may involve working with not just soils but also rocks. This can include rock slope stability, foundations on rocks, tunnelling, dams and more. A good understanding of rock mechanics and geology is very valuable for a practising geotechnical engineer.

While rocks are geomaterials like soils, their behaviour and failure mechanisms are different. Seeing the need for a simple English introductory textbook in rock mechanics, we came up with the first edition of *Rock Mechanics: An Introduction* in 2013. Now, 12 years later, we are bringing you the second edition with a new co-author, Dr Peter To. Sadly, one of our original co-authors and a very close collaborator, Professor Braja M. Das, passed away in April 2023.

Building on the foundation of the first edition, the second edition of this textbook includes numerous updates and enhancements across all chapters, including the following:

- Chapter 1 includes an introduction to the fundamental principles of petroleum geology and geological site selection for structures.
- The discussion of slope failure mechanisms and kinematic analysis, originally presented in Chapter 2, has been relocated to Chapter 6 for better coherence. Additionally, new sections on software applications and fault estimation have been integrated into this edition.
- In Chapter 6, the theoretical frameworks have been updated to incorporate recent advancements.
- Chapter 7 now includes a major section on rock-socketted piles, covering the design procedures in detail.
- Chapter 8, 'Tunnelling within Rock Mass', is a newly introduced chapter
 that addresses various aspects of tunnel engineering, supplemented with
 illustrative examples and practice exercises. Brief guidance on tunnel
 dimensioning has also been incorporated.
- The text has been refined throughout to enhance conceptual clarity and comprehension.
- Additional illustrative examples and practice problems have been included to reinforce learning and practical application.

These updates ensure that the textbook remains a comprehensive and up-to-date resource for students, researchers and practitioners in civil and geotechnical engineering.

x Preface

We gratefully acknowledge the cover photo of *Sigiriya*, Dambulla, Sri Lanka provided by Dr S. K. Navaratnarajah of the University of Peradeniya, Sri Lanka. The rock fortress Sigiriya is a popular tourist attraction, a UNESCO-listed World Heritage site and one of the world's wonders. It is a 180-metre-high granite column, with an ancient palace built on top of the rock in the fifth century. We would like to thank Mr Andrew Carmount, the editorial assistant, for liaising between us and the production team and for ensuring the timely publication of this second edition.

About the Authors



Dr Nagaratnam Sivakugan retired from James Cook University in 2025 where he was the head of the civil and environmental engineering department for more than 10 years. He graduated from the University of Peradeniya with first class honours and earned his MSCE and PhD from Purdue University, West Lafayette, USA. He is a registered professional engineer of Queensland and a chartered professional engineer with Engineers Australia. Dr Sivakugan does substantial consulting work for the geotechnical and mining industries in Australia and overseas, including the World Bank. He is a fellow of Engineers Australia and an honorary fellow of the American Society of Civil Engineers. He has co-authored 10 books including

some research monographs and best practice guidelines, some of which have been translated into other languages. Dr Sivakugan's writings include 175 peer-reviewed journal papers and 100 peer-reviewed conference papers, which have attracted more than 12,000 citations with an H-index of 47. He serves on the editorial boards of Canadian Geotechnical Journal, Indian Geotechnical Journal, International Journal of Geotechnical Engineering, and International Journal of Geosynthetics and Ground Engineering.



Dr Sanjay Kumar Shukla is the founding editor-in-chief of the *International Journal of Geosynthetics and Ground Engineering* and the founding leader of the Geotechnical and Geoenvironmental Engineering Research Group at Edith Cowan University, Perth, Australia. He holds distinguished professorships at several universities, including the esteemed Delhi Technological University, Delhi, India, and Southern Illinois University, Carbondale, USA. He is a registered Chartered Professional Engineer in Civil and Geotechnical Engineering with Engineers Australia, holds the designation of an Asia Pacific Economic Cooperation (APEC) Engineer in Civil Engineering, and is recognised

as an International Professional Engineer in Civil Engineering by the International Engineering Association. Dr Shukla is a distinguished fellow of the American Society of Civil Engineers and Engineers Australia, a life fellow of the Institution of Engineers (India) and the Indian Geotechnical Society, and a member of several other professional bodies. He has contributed significantly to academic literature, including 28 books and over 330 articles, placing him among the world's top 2% of scientists for several years by Elsevier, and among the top 0.5% globally by ScholarGPS. Recognised for his excellence, he has received prestigious honours including a 2024 Distinguished Honour by the Consulate General of India, Perth for

his academic contributions to geotechnical engineering, the 2021 ECU Aspire Award from Business Events Perth, Australia, and the highly esteemed 2018 IGS Award from the International Geosynthetics Society, USA in recognition of his outstanding contributions to the development and use of geosynthetics. His groundbreaking work, including his generalised expressions for seismic active thrust (2015) and passive resistance (2013), along with his innovative Shukla's wraparound reinforcement technique, has become an essential part of engineering education and is widely applied by engineers worldwide. His seven research mantras introduced in 2022 have been instrumental in promoting sustainable research practices globally. With an extensive academic and professional network spanning over 70 countries, Dr Shukla collaborates with top universities, institutions, industries and individuals on academic and field projects. As a consulting geotechnical engineer, he solves complex problems for engineering organisations. His expertise has greatly enriched the civil engineering field worldwide. A renowned speaker, Dr Shukla delivers keynote talks and short courses globally and is widely consulted on practical engineering solutions.



Dr Braja M. Das passed away in 2023. He earned BSc degrees with honours in physics and civil engineering from Utkal University, Orissa, India; an MS in civil engineering from the University of Iowa, USA; and a PhD in geotechnical engineering from the University of Wisconsin, USA. He was the author of several geotechnical engineering texts and reference books, some of which have been translated into several languages and are used worldwide, and he authored more than 250 technical papers in geotechnical

engineering. He was a fellow and life member of the American Society of Civil Engineers, as well as an emeritus member of the Committee on Chemical and Mechanical Stabilization of the Transportation Research Board of the National Research Council of the US. From 1994–2006, he served as the dean of the College of Engineering and Computer Science at California State University, Sacramento.



Dr Peter To was the coordinator for the civil engineering discipline at James Cook University. He earned his BSc and MSc degrees from St Petersburg State Polytechnic University, and his PhD from the University of Queensland, where he was recognised as a UQ Future Leader. Dr To is a member of Engineers Australia and the Australian Geomechanics Society. With 15 years of extensive expertise in various geotechnical software applications, Dr To is also an expert in parallel computation. He is proficient in nine programming languages. His professional portfolio includes numerous projects in hydraulic structures, including rockwork and traffic tunnel design.

1 Fundamentals of Engineering Geology

1.1 INTRODUCTION

The earth materials that make up the relatively thin outer shell, called the *crust*, of the Earth are categorised by civil engineers as soils and rocks. These materials are made up of small crystalline units known as *minerals*. A mineral is basically a naturally occurring inorganic substance composed of one or more elements, with a unique chemical composition, unique arrangement of elements (crystalline structure) and distinctive physical properties.

Soils and rocks have various meanings across different disciplines. In civil engineering, soil is considered a natural aggregate of mineral grains that can be separated by gentle mechanical means such as agitation in water. It comprises all the materials in the surface layer of the Earth's crust that are loose enough to be normally excavated by manual methods using a spade or shovel. Rock is a hard, compact and naturally occurring earth material composed of one or more minerals and is permanent and durable for engineering applications. Rocks generally require blasting and machinery for their excavation. Note that geologists consider engineering soils as unconsolidated rock materials composed of one or more minerals. One rock is distinguished from another primarily based on its mineralogical composition.

Geology is the science concerned with the study of the history of the Earth, the rocks of which it is composed, and the changes it has undergone or is undergoing. In short, geology is the science of rocks and earth processes. Engineering geology deals with the application of geologic fundamentals to engineering practice. Rock mechanics is the subject concerned with the study of the response of rock to an applied disturbance caused by natural or engineering processes. Rock engineering deals with the engineering applications of the basic principles and the information available in the subjects of engineering geology and rock mechanics in an economic way. All these subjects are closely related to several engineering disciplines such as civil, mining, petroleum and geological engineering.

Rock mechanics is a relatively young discipline that emerged in the 1950s, two decades after its sister discipline, soil mechanics. The failure of the Malpasset concrete arch dam in France (Figure 1.1a) on December 3, 1959, killing 450 people, and an upstream landslide that displaced a large volume of water, overtopping Vajont Dam in Italy (Figure 1.1b) on October 9, 1963, claiming more than 2,000 lives downstream, were two major disasters that triggered the need for better understanding of, and more research into, rock mechanics principles. The first proper rock mechanics textbook, La Mécanique des Roches, was written by J.A. Talobre in 1957. Rock mechanics is a multidisciplinary subject relating geology, geophysics and engineering, which is quite relevant to many areas of civil, mining, petroleum and geological

DOI: 10.1201/9781032725161-1

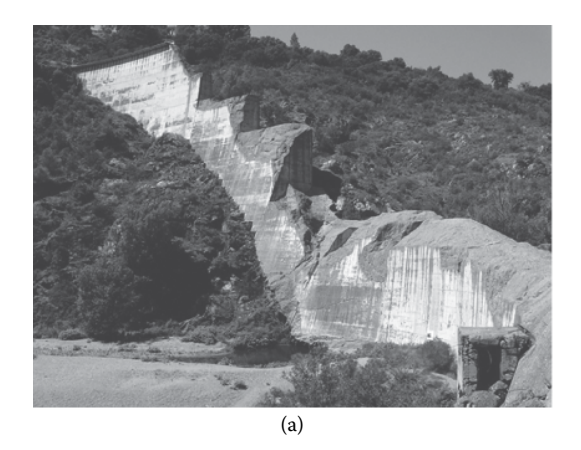




FIGURE 1.1 Dam failures: (a) Malpasset after failure and (b) Vajont dam currently.

engineering. A good grasp of rock mechanics would be invaluable to civil engineers, especially to those who specialise as geotechnical engineers. Here, we apply the principles we learnt in mechanics to study the engineering behaviour of the rock mass in the field. Applications of rock mechanics include the stability of rock slopes, rock bolting, foundations on rocks, tunnelling, blasting, open-pit and underground mining, mine subsidence, dams, bridges and highways.

This chapter presents the geological fundamentals and their relation to engineering. These concepts are essential for a better understanding of rock mechanics and its applications.

1.2 STRUCTURE AND COMPOSITION OF THE EARTH

The shape of the Earth is commonly described as a spheroid. It has an equatorial diameter of 12,756 km and a polar diameter of 12,714 km. The total mass of the Earth is estimated to be 5.975×10^{24} kg, and its mean density is 5,520 kg/m³.

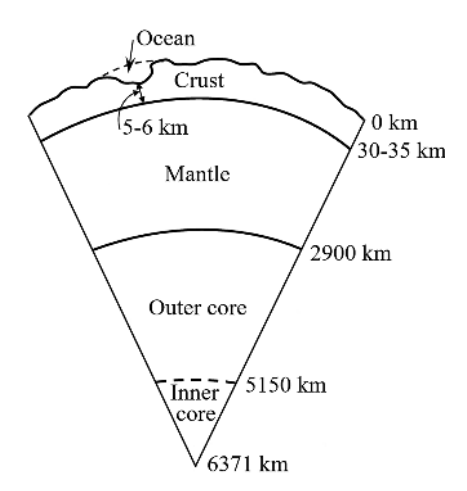


FIGURE 1.2 Structure of the Earth (*note*: not to scale).

Detailed scientific studies have indicated that the Earth is composed of three well-defined shells: crust, mantle and core (Figure 1.2). The topmost shell of the Earth is the *crust*, which has a thickness of 30–35 km in continents and 5–6 km in oceans. The oceanic crust is made up of heavier and darker rocks called basalts, while the continental crust consists of light-coloured and light-density granitic rocks. The Earth is basically an elastic solid, and when expressed in terms of oxides, it has silica (SiO₂) as the most dominant component, its value lying more than 50% by volume in oceanic crust and more than 62% in the continental crust. Alumina (Al_2O_3) is the next important oxide, varying between 13% and 16%. The zone of materials lying between the crust and a depth of 2,900 km is known as the mantle, which is made up of extremely basic materials – very rich in iron and magnesium but quite poor in silica. The mantle is believed to be a highly plastic or ductile solid in nature. The innermost structural shell of the Earth, known as the core, starts at a depth of 2,900 km below the surface and extends right up to the centre of the Earth at 6,370 km. The materials of the core are probably iron and nickel alloys. Seismic measurements reveal that the Earth's core consists of a solid inner core and a molten outer core. The outer core has almost no shear resistance, making it behave like a liquid. In contrast, the inner core is a ductile solid. The core has a very high density – more than 10,000 kg/m³ at the mantle– core boundary.

Lithosphere (Greek: *lithos* = stone) is a combination of the Earth's crust and the outer part of the upper mantle. It is an elastic solid. Its thickness is approximately 100 km. *Asthenosphere* is the upper mantle, which is ductile and 3% liquid (partially melting). Its thickness is approximately 600 km.

Below the Earth's surface, the temperature increases downwards at an average rate of 30°C/km. This rate is higher near a source of heat such as an active volcanic centre and is also affected by the thermal conductivity of the rocks in a particular locality.

EXAMPLE 1.1

Given that the Earth's crust temperature increases by about 30°C for every kilometre of depth, and assuming the surface temperature is 20°C, what would be the estimated temperature at a depth of 35 km? Do you believe the rock mass at this depth would melt? Please justify your answer with supporting reasoning.

Solution

Given: Temperature gradient = 30° C/km, Earth's surface temperature = 20° C, and depth below the Earth's surface = 35 km.

Temperature at a depth of 35 km

$$=20^{\circ}C + (30^{\circ}C / \text{km})(35 \text{ km}) = 1070^{\circ}C$$

With a temperature of 1,070°C, most rocks begin to melt, but it is unlikely that the rock mass at a depth of 35 km would melt. The reason is that the high pressure at this depth increases the melting point of the rock. Furthermore, the capacity of crustal rocks to conduct heat away from the Earth's interior may result in a temperature lower than the estimated temperature of 1,070°C. However, there will be a depth at which it becomes essentially a viscous fluid, and this defines the base of the lithosphere.

1.3 MINERALS AND MINERALOGICAL ANALYSIS

Minerals are the building blocks of soils and rocks present in the Earth, and they have distinctive physical properties, namely *colour, streak, hardness, cleavage, fracture, lustre, habit (or form), tenacity, specific gravity, magnetism, odour, taste and feel.* The streak of a mineral is the colour of its powder. The hardness of a mineral is its resistance to abrasion. The cleavage of a mineral is its tendency to break down along a particular direction; it is described as one set of cleavage, two sets of cleavage and so on. Fracture is the character of the broken surface of the mineral in a direction other than the cleavage direction. Lustre is the appearance of the mineral in reflected light. The habit (or form) of a mineral refers to the size and shape of its crystals. Tenacity describes the response of a mineral to hammer blows, cutting with a knife and bending.

Hardness and specific gravity are the most useful diagnostic physical properties of a mineral. Hardness is tested by scratching the minerals of known hardness with a specimen of the mineral of unknown hardness. In practice, a standard scale of 10 minerals, known as the Mohs scale of hardness (see Table 1.1), is used for this purpose. It was introduced by the German geologist and mineralogist Friedrich Mohs in 1812. The hardness of minerals listed in Table 1.1 increases from 1 for talc to 10 for diamond.

The specific gravity of a mineral is the ratio of its weight to the weight of an equal volume of water at a standard temperature, generally 4°C. The specific gravity of the common silicate minerals forming soils and rocks is about 2.65. For minerals forming ores, the specific gravity may be as high as 20; for example, native platinum has a specific gravity of 21.46. Most minerals have a specific gravity in the range of 2–6. Table 1.2 provides the specific gravity values of some common minerals.

TABLE 1.1

Mohs Scale of Hardness

Hardness	Mineral
1.	Talc (softest)
2.	Gypsum
3.	Calcite
4.	Fluorite
5.	Apatite
6.	Orthoclase
7.	Quartz
8.	Topaz
9.	Corundum
10.	Diamond (hardest)

TABLE 1.2

Specific Gravity of Some Common Minerals

Mineral	Specific gravity
Apatite	3.2
Calcite	2.71
Chlorite	2.6-3.3
Clay minerals	2.5-2.8
Dolomite	2.85
Feldspar	2.56-2.7
Garnet	3.7-4.3
Gypsum	2.32
Hornblende	3.2
Halite	2.16
Hematite	4.72
Magnetite	5.2
Pyrite	5.01
Muscovite	2.8-3.0
Quartz	2.65
Rutile	4.2
Topaz	3.6
Tourmaline	3.0-3.2
Zircon	4.7

Minerals are naturally occurring inorganic substances; however, coal and petroleum, despite being of organic origin, are also classified as minerals. Almost all minerals are solids, with the exception of mercury, water and mineral oil (crude petroleum).

In civil engineering practice, it is important to understand the minerals that form rocks, known as rock-forming minerals. Silicates and carbonates, as listed in Table 1.3, are the essential rock-forming minerals. Silicate minerals form the bulk (about 95%) of the Earth's crust. Silica and feldspars are the most common silicate minerals in the crust. Silica is found in several crystalline forms such as quartz, chalcedony, flint, opal and chert; quartz is one of the most common forms of silica. A high quartz content in a rock indicates that it will have high strength and hardness. Feldspars form a large group of minerals; orthoclase or K-feldspar (KAlSi₃O₈), albite (NaAlSi,O_o) and *anorthite* (CaAlSi,O_o) are the main members. The mixtures (solid solutions) of albite and anorthite in different proportions form a series of feldspars called *plagioclases*. A plagioclase containing 40% albite and 60% anorthite is called labradorite and denoted as Ab₄₀An₄₀. K-feldspars alter readily into kaolinite, which is one of the clay minerals. Hornblende is a major mineral of the amphibole group of minerals. Enstatite (MgSiO₃), hypersthene [(MgFe)SiO₃] and augite [(CaMgFe-Al)₂(SiAl)₂O₆] are the major minerals of the pyroxene group of minerals. There are two common types of micas: muscovite (white mica) [KAl₂(Si₂Al)O₁₀(OH)₂], which is rich in aluminium and generally colourless, and biotite (black mica) [K(MgFe)₃(-Si₃Al)O₁₀(OH)₂], which is rich in iron and magnesium and generally dark brown to nearly black. Both types occur in foliated form, and they can be split easily into thin sheets. The composition of common olivine is [(MgFe),SiO₄]. Since olivine crystallises at a high temperature (higher than 1,000°C), it is one of the first minerals to form from the molten rock material called magma. Garnets occur both as essential and as accessory minerals in rocks. Clay minerals are hydrous aluminium silicates. Kaolinite $[Al_4Si_4O_{10}(OH)_8]$, illite $[K_xAl_4(Si_{8x}Al_x)O_{20}(OH)_4$, with x varying between 1 and 1.5] and montmorillonite $[Al_aSi_8O_{20}(OH)_a]$ are the principal clay minerals, which are described in greater detail in Section 1.6. Calcite (CaCO₃) and dolomite [CaMg(CO₂)₂] are carbonate minerals present in some rocks.

In addition to essential minerals, there are *accessory minerals* such as *zircon*, *andalusite*, *sphene* and *tourmaline*, which are present in relatively small proportions in rocks. Some minerals, such as *chlorite*, *serpentine*, *talc*, *kaolinite* and *zeolite*, result from the alteration of pre-existent minerals, and they are called *secondary minerals*. Since these minerals have little mechanical strength, their presence on joint planes within the jointed rock mass can significantly reduce its stability.

The common rock-forming minerals can be identified in the hand specimen with a magnifying glass, especially when at least one dimension of the mineral grain is greater than about 1 mm. With practice, much smaller grains can also be identified. This task is easily done by experienced geologists. If it is difficult to identify minerals by physical observations and investigations, X-ray diffraction and electron microscopic analyses make the identification task easy. Figure 1.3 shows a typical X-ray diffractogram of an air-dried clay fraction ($<2~\mu m$) collected from a shear surface of a recent landslip in the South Cotswolds, the United Kingdom, where clay

TABLE 1.3

Essential Rock-Forming Minerals

Silicates

Silica (SiO₂)

Feldspars (Na, K, Ca and Al silicates)

Amphiboles (Na, Ca, Mg, Fe and Al silicates)

Pyroxenes (Mg, Fe, Ca and Al silicates)

Micas (K, Mg, Fe and Al silicates)

Garnets (Fe, Mg, Mn, Ca and Al silicates)

Olivines (Mg and Fe silicates)

Clay minerals (K, Fe, Mg and Al silicates)

Carbonates

Calcite (Ca carbonates)

Dolomite (Ca–Mg carbonates)

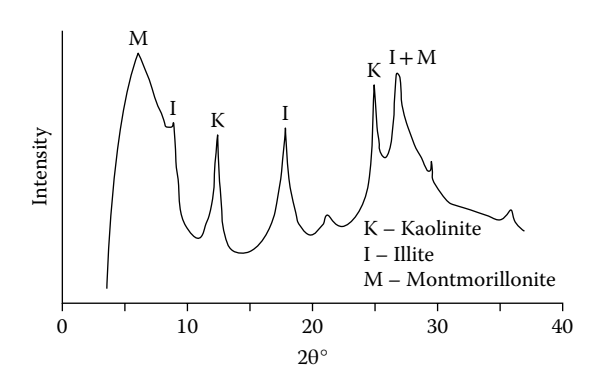


FIGURE 1.3 X-ray diffractogram of air-dried clay fraction (<2 μm). (Adapted from Anson, R.W.W. and A.B. Hawkins, *Geotechnique*, 49, 33–41, 1999.)

minerals (kaolinite, K; illite, I; and montmorillonite, M) are easily identified on the basis of a series of peaks of different intensities of X-rays reflected from the minerals, corresponding to different angular rotations (2 θ) of the detector of the X-ray diffractometer.

Figure 1.4 shows the photographs of some typical rock-forming minerals.

1.4 ROCK FORMATIONS AND TYPES

Rocks form a major part of the Earth's crust. They are formed by the following processes:

- 1 Cooling of molten material (magma)
- 2 Settling, depositional or precipitation processes
- 3 Heating or squeezing processes

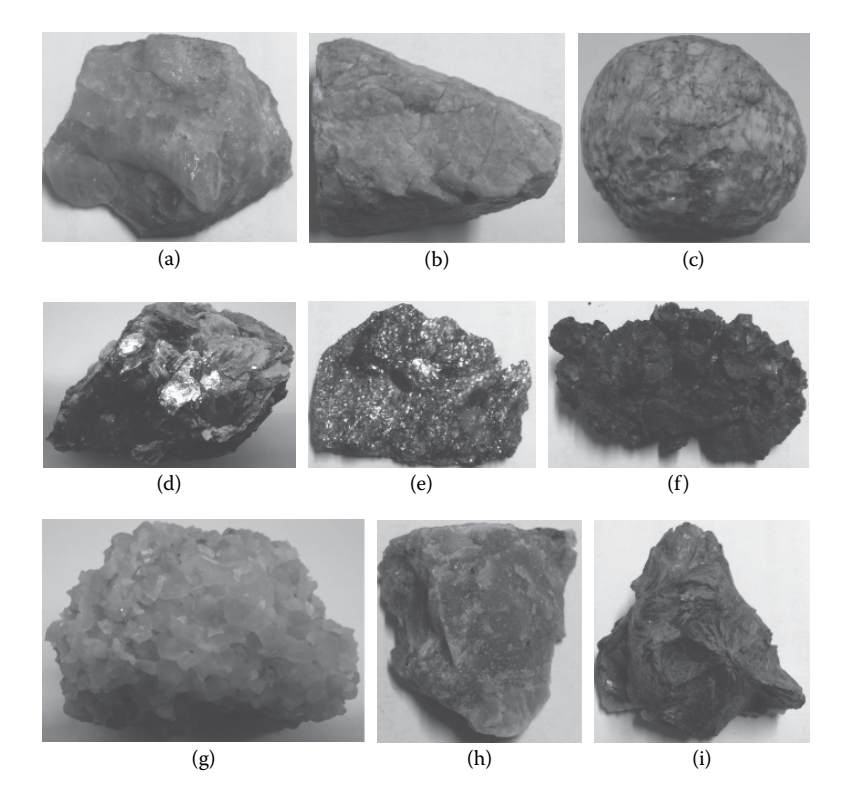


FIGURE 1.4 Photographs of some typical rock-forming minerals: (a) quartz, (b) orthoclase, (c) plagioclase, (d) muscovite, (e) biotite, (f) andradite garnet, (g) calcite, (h) dolomite and (i) chlorite. (Courtesy of Sanjay Kumar Shukla.)

These three processes form the basis for rock classification and are also significant factors in establishing the mechanical properties of rocks. Based on their formation, rocks are classified as follows:

- 1. Igneous rocks
- 2. Sedimentary rocks
- 3. Metamorphic rocks

Rocks derived from magma are called *igneous rocks*, which are usually hard and crystalline in character. Igneous rocks make up about 95% of the volume of the Earth's crust. Some examples are *granite*, *basalt*, *dolerite*, *gabbro*, *syenite*, *rhyolite* and *andesite*. The silicates are the common igneous rock-forming minerals. There are six of them: silica, feldspars, amphiboles, pyroxenes, micas and olivine. Granite is usually light coloured (white, reddish, greyish and so on) and has a medium specific gravity; feldspar and quartz are the essential minerals, and its grains are medium or coarse. Rhyolite is mostly light coloured (light grey, yellow, pale red and so on) and has low specific gravity; its grains are extremely fine, and therefore

constituent minerals cannot be easily identified. Basalt, composed of magnesium and iron silicates, is dark grey or black in colour and has high specific gravity; its mineral grains are too fine to be identified.

Igneous rocks are also known as *primary rocks* since they were the first rocks to form on the surface of the Earth. The characteristics of igneous rocks are controlled by two basic factors: the rate of cooling when they were formed and the chemical composition of the magma. Rapid cooling prevents the growth of crystals, while slow cooling allows their growth. The igneous rocks produced due to the rapid cooling of magma on the surface of the Earth are known as *extrusive igneous rocks*, whereas those formed beneath the surface of the Earth due to slow cooling are known as *intrusive igneous rocks*. For example, basalt, rhyolite and andesite are extrusive igneous rocks, whereas granite, dolerite, gabbro and syenite are intrusive igneous rocks.

Based on silica content, igneous rocks are broadly classified as (1) acidic (>66% of silica), (2) intermediate (between 55% and 66% of silica), (3) basic (between 44% and 55% of silica) and (4) ultrabasic (<44% of silica) (Mukerjee, 1984). Granite, rhyolite and pegmatite are acidic igneous rocks, whereas basalt, dolerite and gabbro are basic igneous rocks.

Field observations of igneous rocks are very important for determining the structure and extent of the exposed rock mass. Geological maps and satellite imagery are useful for identifying the mode of occurrence of rocks in the field. In civil engineering constructions, particularly for large structures, the extent and occurrence of igneous rocks must be known.

The products of weathering (disintegration of rocks, see Section 1.6) are subjected, under favourable conditions, to transportation – mostly by natural agencies such as running water, wind, glaciers and gravity – deposition, and subsequent compaction or consolidation, resulting in *sedimentary rocks*. Some examples are *sandstone, shale, conglomerate, breccias, limestone, coal* and *evaporites*. Minerals forming sedimentary rocks include kaolinite, illite, smectite, hematite, rutile, corundum, calcite, dolomite, gypsum, halite and so on. Sandstone is available in variable colours, and shades of grey, yellow, brown and red are frequent; it has low to medium specific gravity, and its grains are rounded or angular and are cemented together by siliceous, calcareous or ferruginous material. Sandstone is usually massive, but bedded structures may sometimes be visible. Limestone is generally fine-grained and found in lighter shades; calcite is the main constituent, although clay minerals, quartz, dolomite and others may also be present. Conglomerate has different shades of colour, and the fragments are generally rounded.

Rocks that have undergone some chemical or physical changes after their original form are called *metamorphic rocks*. The process by which the original character or form of rocks is more or less completely altered is called *metamorphism*. This is mainly due to four factors: temperature, uniform pressure, directed pressure and access to chemically reactive fluids. Metamorphism brings about changes in mineral composition and changes in the texture of rock. Examples include *quartzite*, *slate*, *mica schist*, *marble*, *graphite*, *gneiss* and *anthracite*. Common metamorphic minerals are serpentine, talc, chlorite, kyanite, biotite, hornblende, garnet and so on. Quartzite, formed from sandstone with high silica content, is light coloured with shades of grey, yellow, pink and so on, and has medium specific gravity. Slate,

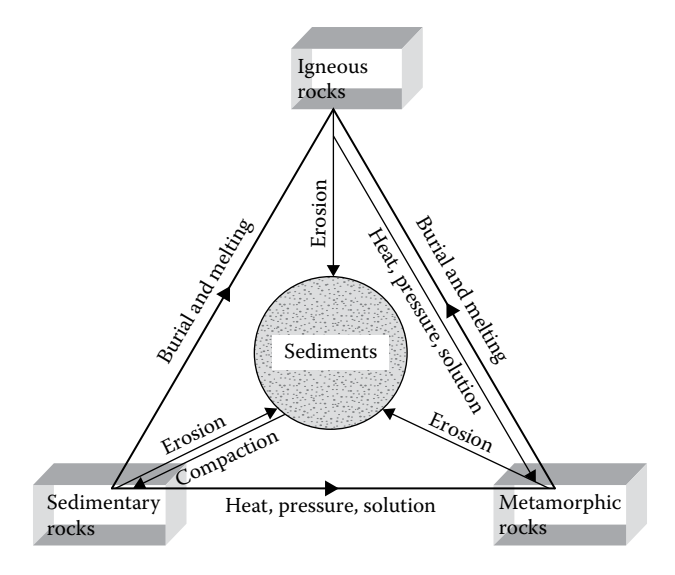


FIGURE 1.5 Rock cycle. (Adapted from Raymahashay, B.C., *Geochemistry for Hydrologists*, Allied Publishers Ltd., New Delhi, 1996.)

formed from shale, is a black or brown rock with low or medium specific gravity. Marble, formed from limestone, is commonly light coloured (white, grey, yellow, green, red and so on) and has a medium specific gravity; calcite is the main constituent of marble, and dolomite is frequently associated with it.

In nature, one type of rock changes slowly into another type, forming a rock cycle (Figure 1.5). At the surface of the Earth, igneous rocks are exposed to weathering, resulting in sediments, which may become sedimentary rocks due to hardening or cementation. If sedimentary and metamorphic rocks are deeply buried, the temperature and pressure may turn them into metamorphic rocks. Intense heat at great depths melts metamorphic and sedimentary rocks and produces magma, which may rise up and reach the Earth's surface where it cools to form igneous rocks.

Figure 1.6 shows photographs of some common types of rocks.

All kinds of rocks in the form of dressed blocks or slabs called *building stones*, or in any other form referred to as *building materials*, are frequently used in civil engineering projects. Building stones are used in the construction of buildings, bridges, pavements, retaining walls, dams, docks and harbours, and other masonry structures. Building materials are used as fine and coarse aggregates in cement and bituminous concrete, raw materials in the manufacture of lime and cement, soils for embankments and dams, ballasts for railway tracks and aggregates in sub-base and base courses of highway and runway pavements, and so on. As building stones and materials, rocks should have high strength and durability, which depend on their mineralogical composition, texture and structure. If the minerals in rocks are hard, free from cleavage and resistant to weathering, these rocks, when used as building stones and materials, are likely to be strong and durable. The rock granite, composed

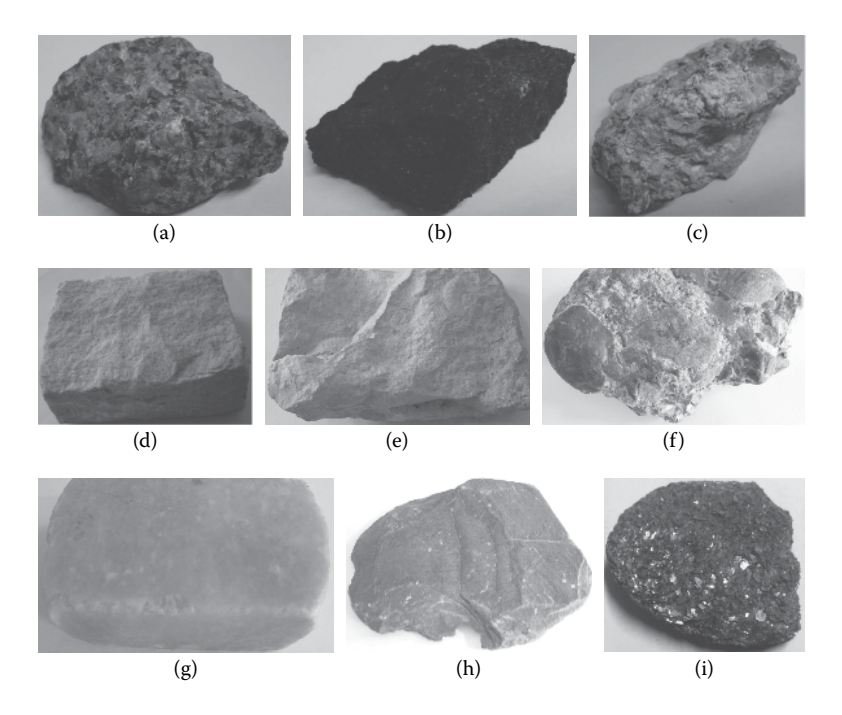


FIGURE 1.6 Photographs of some typical rocks: (a) granite, (b) basalt, (c) rhyolite, (d) sand-stone, (e) limestone, (f) conglomerate, (g) marble, (h) slate and (i) mica schist. (Courtesy of Sanjay Kumar Shukla.)

mainly of quartz and feldspar, is very strong and durable, while carbonate rocks such as marble and limestone are relatively weak and wear out more rapidly. The rock quartzite, composed mainly of quartz alone, is obviously strong and durable, while mica schist is rather weak as it contains a lot of mica, which is an easily cleavable material. In crystalline rocks of igneous and metamorphic origin, the mineral grains are mutually interlocked and no open space is usually left in between the constituent grains. The interlocking texture of the mineral grains contributes substantially to the strength of the crystalline rocks and the impervious nature of these rocks enables them to resist weathering.

In most sedimentary rocks, the mineral grains are held together by cementing materials of variable strength, and such rocks are generally porous due to the presence of voids or open spaces within them. The nature of the cementing materials determines the strength and durability of these rocks. Compared to igneous and metamorphic rocks, sedimentary rocks are weaker and less durable. Granite, marble and gneiss are, thus, stronger and more durable than sandstone, limestone and conglomerate. Experience has shown that granite, gneiss and fine-grained and well-cemented sandstone last for centuries while limestone and coarse-grained and poorly cemented sandstone generally have a much shorter lifespan.

For the selection of rocks as building stones and materials, their mineralogical composition and texture should be studied carefully, and at the same time, their

structural features should be closely observed in the field. It is also necessary to determine their porosity and absorption, crushing and flexural strength, resistance to frost, fire and abrasion, modulus of elasticity and other properties relevant to specific field applications.

1.5 GEOLOGICAL STRUCTURES AND DISCONTINUITIES

Geological structures such as *folds*, *faults*, *joints* and *unconformities*, encountered in geology, are regularly encountered in civil engineering work. For describing these structures, it is essential to understand the geometrical concept of the orientation of a plane and a line in space, as described in detail in Section 2.2.

Orientation (or attitude) of a plane (rock bed, discontinuity plane or sloping ground) in space is described in terms of strike (S-S) and dip (ψ), or dip (ψ) and dip direction (D) (Figure 1.7). The strike of a plane is the direction of a line considered to be drawn along the plane so that it is horizontal. It is basically a trace of the intersection of the inclined plane with the horizontal reference plane. It is obvious that there will be only one such direction for any rock bed or discontinuity plane or sloping ground. The line of maximum inclination on the inclined plane is called the line of dip. The dip (ψ) of a plane is its maximum inclination to the horizontal plane, measured at right angles to the strike. For a horizontal plane, the dip is 0°, and for a vertical plane, the same is 90°. Dip always refers to the true dip. Apparent dip is the inclination of any arbitrary line on the plane to the horizontal, and it is always smaller than the true dip. Dip direction (or dip azimuth) is the direction of the horizontal trace of the line of dip, expressed as an angle (α) measured clockwise from the north. It varies from 0° to 360°. In Figure 1.7, the rock bed strikes north—south, and therefore α is 90°.

Folds are defined as wavy undulations developed in the rocks of the Earth's crust due to horizontal compression resulting from gradual cooling of the Earth's crust, lateral deflection and intrusion of magma into the upper strata. Figure 1.8 shows a typical fold at an excavated site. Different elements of a fold are shown in Figure 1.9.

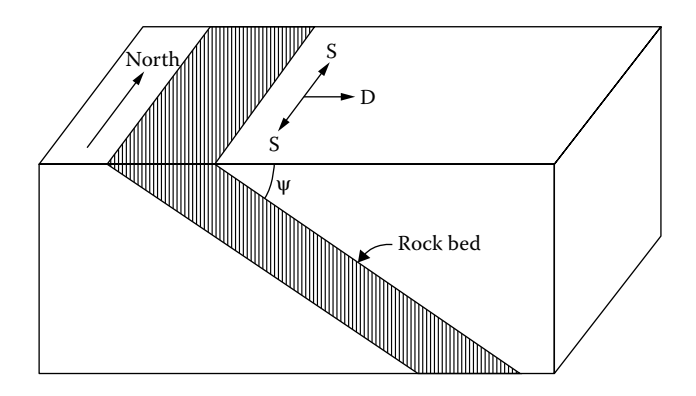


FIGURE 1.7 Dip and strike.

An *anticline* is an upfold where the limbs dip away from the axis of the fold on either side. A *syncline* is a downfold where the limbs dip towards the axis of the fold on either side. Anticline and syncline can be noticed easily in Figure 1.8. The highest point on the arch of an anticline is called the *crest* of the fold, and the lowest point on the syncline is called the *trough*. The sloping sides of a fold are called *limbs*. A reference plane that divides a fold into two equal halves is called an *axial plane*. The line of intersection of the axial plane and the surface of any constituent rock bed is called the *axis of the fold*, the inclination of which with the horizontal is called the *plunge* of the fold. In anticlines, the older rock beds generally occupy a position in the interior (or core) of the curvature, whereas in synclines, the rock beds in the interior are generally the youngest beds (Figure 1.9).



FIGURE 1.8 Folded rock beds. (Courtesy of Dr Dajkumar S. Jeyaraj.)

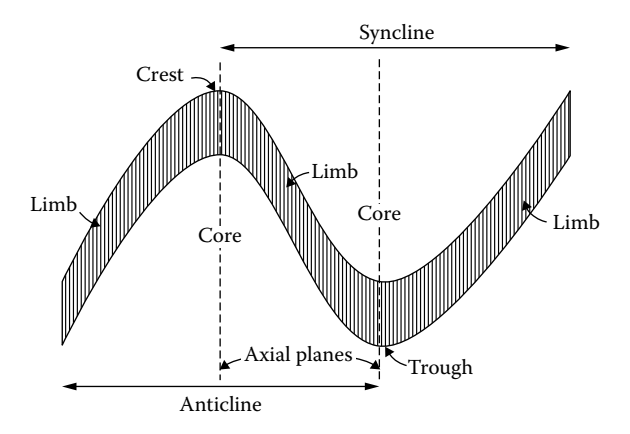


FIGURE 1.9 Elements of folds (anticline and syncline).

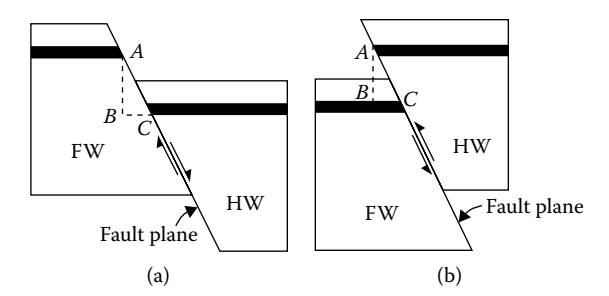


FIGURE 1.10 Inclined faults: (a) normal fault and (b) reverse fault.

Faults are fractures in crustal strata along which appreciable shear displacement of the adjacent rock blocks has occurred relative to each other, probably due to tectonic activities. The fracture along which the shear displacement has taken place is called a *fault plane*. In general, the term 'fault' includes both the fault plane and the displacement that has occurred along it.

Figure 1.10 shows inclined faults, namely normal fault (Figure 1.10a) and reverse fault (Figure 1.10b), where the fault plane is inclined to the vertical. The total displacement AC that occurs along the fault plane is called the net slip. The amount of net slip may vary from only a few tens of millimetres to several hundred kilometres. The vertical component AB of the net slip AC is called the throw or vertical slip, and the horizontal component BC of the net slip AC is called the heave or horizontal slip. The angle subtended between the fault plane and any vertical plane striking in the same direction is called the *hade* of the fault. In Figure 1.10, $\angle BAC$ is the hade of the fault. It is observed that the two blocks lying on either side of the inclined fault plane are dissimilar in their configuration and orientation in space. Of these two adjacent blocks, one appears to rest on the other. The former is known as the hanging wall (HW), while the latter, which supports the HW, is called the footwall (FW). In the normal fault, the HW appears to have moved relatively downwards in comparison with the adjoining FW, whereas in the reverse fault, the FW appears to have been shifted downwards in comparison with the adjoining HW. From a mechanical point of view, the presence of tensile stresses causes the development of normal faults, while compressive stresses lead to the formation of reverse faults. Fault plane, net slip, throw, heave and hade are called the *elements of the fault*.

Discontinuity is a collective term used for all structural breaks (bedding planes, fractures and joints) in solid geologic materials that usually have zero to low tensile strength. Bedding planes in sedimentary rocks form due to interruptions in the sedimentation process or repeated cycles of deposition. The material deposited often varies between cycles, typically occurring over geological time scales. A geological time scale is measured in millions of years, considering Earth's age of 4.54 billion years, as determined by radiometric dating of meteorites and ancient rocks. A fracture is where the continuity of the rock mass breaks. A joint is a fracture where little or no movement has taken place. This is the most common form of discontinuity encountered. These discontinuities can occur in several sets and are approximately parallel within a specific set (Figure 1.11). A discontinuity set is a series of discontinuities that have the same geologic origin, orientation, spacing and mechanical



FIGURE 1.11 Heavily jointed rock mass at 0.080 km of the Meja-Jirgo link canal, the site for the construction of a canal head regulator, Mirzapur, Uttar Pradesh, India. [After Sanjay Kumar Shukla, Allowable Bearing Pressure for the Foundation Rock/Soil at km 0.080 of the Meja-Jirgo Link Canal for the Proposed Construction of a Hydraulic Structure (Head Regulator), Mirzapur, UP, India. A technical report dated 11 June 2007, Department of Civil Engineering, Institute of Technology, Banaras Hindu University, Varanasi, India, 2007.]

characteristics. The discontinuities make the rock mass anisotropic. More details about the rock mass and discontinuities are given in Chapter 4.

EXAMPLE 1.2

In field situations, the fault plane can be vertical, and the fault is known as a *vertical fault*. Do you think the terms *hanging wall* and *footwall* are applicable here?

Solution

In the case of a vertical fault, the rock blocks on either side of the fault plane will have the same configuration and orientation in space; in other words, the structure remains the same irrespective of whether one block or the other has moved relatively downwards. Therefore, of the two adjacent blocks, one does not appear to rest on the other, and, therefore, the terms *hanging wall* and *footwall* are not applicable to vertical faults.

EXAMPLE 1.3

Can you write a relationship between the hade and the dip of a fault plane?

Solution

In Figure 1.10, $\angle BAC$ is the hade of the fault plane, and $\angle ACB$ is the dip of the fault plane. Since $\angle ABC$ is a right-angled triangle, $\angle BAC + \angle ACB = 90^{\circ}$.

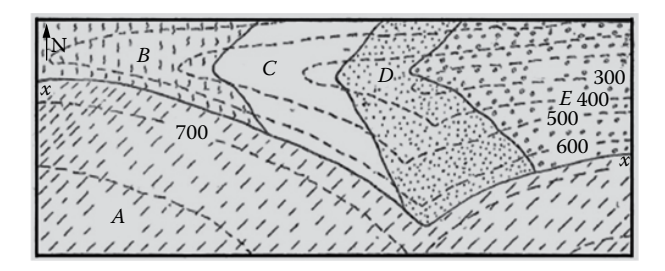


FIGURE 1.12 A typical geological map showing the presence of an unconformity (*Note*: Elevations are in metre).

The *plane of unconformity* or simply *unconformity* is the surface or plane of separation between two series of rock beds or geological formations that belong to two different geologic ages, and they are, in most cases, different in their geologic structure. The intersection of the plane of unconformity with the ground surface or topography constitutes the *line of unconformity* on the geological map. A geological map of an area exhibits the outcrops (portions of rocks exposed on the surface of the Earth) of the different rock types and geological formations and structures of that area, superimposed upon its topographical map. On a geological map, dashed lines represent the contour lines (imaginary lines that connect points of equal elevations) with the help of which the topographic features of the area are shown, and continuous lines represent the boundaries between the outcrops of rock beds (Figure 1.12).

When two series of beds are unconformably related, the following general relationships are typically observed: (1) some beds appear to overlie others; (2) the boundaries of the underlying beds often terminate abruptly against those of the overlying beds; (3) the dip angles of the beds differ between the two formations; and (4) a conglomerate bed is often present above the unconformity. The unconformity signifies a time gap between the deposition or formation of one series of beds and the other. It is either a surface of erosion or of non-deposition. In the field, an unconformity is commonly evidenced by the presence of a conglomerate bed. In Figure 1.12, bed *A* is horizontal. Beds *B*, *C*, *D* and *E* slope towards the west. The boundary of bed *A*, marked by the line *x-x*, is the line of unconformity in the map. Bed A is younger than the group of beds *B*, *C*, *D* and *E*, and appears to overlie them.

1.6 WEATHERING OF ROCKS AND SOIL FORMATION

The exposed rocks at the surface of the Earth are subject to continuous decay, disintegration and decomposition under the influence of certain physical, chemical and biological agencies; this phenomenon is called *weathering of rocks*. Temperature variations through a cycle of freezing and thawing of water in the openings inside the rock mass in the cold humid climates and thermal effects in hot dry (arid) regions are responsible for physical or mechanical weathering of rocks. Rainwater causes chemical weathering of rocks because of the chemical action of dissolved atmospheric gases (carbon dioxide, hydrogen, nitrogen and so on). Organisms (burrowing

animals such as earthworms, ants and rodents) and plants also cause degradation of rocks through their physical actions. Human beings also degrade rocks through various activities.

Weathering causes rocks to become more porous, individual grains to be weakened and bonding between mineral grains to be lost. Therefore, rocks lose strength and become more deformable, and their permeability may change depending on the nature of the rocks, the presence and type of weathering and the stage of weathering. The degree of weathering may be reflected by changes in index properties such as dry density, void ratio, clay content and seismic velocity. The engineering suitability of rocks greatly depends on two principal modes of weathering: physical or mechanical weathering (disintegration) and chemical weathering (decomposition). Disintegration of rocks gives rise to satisfactory engineering materials that can be used as pavement materials and concrete aggregates because physical breakdown of the rocks occurs without drastic changes in the minerals of the rock and hence without significant reduction in their durability. Decomposition, on the contrary, involves the chemical alteration of rocks and results in the transformation of most of the important minerals into some form of clay (Weinert, 1974). The assessment of rock weathering has been a challenging problem for engineering geologists and geotechnical engineers. For convenience, rock weathering has been classified into different types/grades by the researchers. Table 1.4 presents the classification suggested by Little (1969).

The processes of soil formation are complex, and they directly affect the engineering properties of the resulting soil mass. Soils are the result of interactions between five soil-forming factors: parent materials, topography, climate, organisms and time. Weathering of rocks as the parent materials plays a major role in the formation of soils and sediments. Minerals present in rocks have different degrees of resistance to weathering. Bowen's (1922) reaction series, which lists some minerals in the order of decreasing crystallisation temperature during their formation as a result of cooling of magma, is given in Figure 1.13. This list also follows the order of increasing resistance to weathering after their formation. Olivine, which crystallises earlier, that is, at higher temperature during the formation of rocks from magma, is the most weatherable mineral in rocks. Quartz, which crystallises later, that is, at lower temperature during the formation of rocks from magma, is the least weatherable mineral. Ouartz is the most common mineral in soils and sediments as a residue of weathering processes. Weathering of feldspar results in clay minerals (kaolinite or illite). In the tropical weathering environments, the clay minerals break down further, resulting in bauxite and laterite profiles.

Note that most rocks and soils found at or near the Earth's surface formed during the last one-eighth of geological time, spanning the 4.54 billion years of the Earth's and the Moon's existence. Approximately seven-eighths of geological history, described as the *Precambrian*, is poorly known. Based on their method of formation, soils are primarily classified as follows:

- 1. Sedimentary soils
- 2. Residual soils
- 3. Fills
- 4. Organic soils

TABLE 1.4 Engineering Rock Weathering Classification

Grade	Degree of weathering	Field recognition	Engineering properties
VI	Soil	Surface layer contains humus and plant roots; no recognisable rock structure; unstable on slopes when vegetative cover is destroyed.	Unsuitable for important foundations; unsuitable on slopes when cover is destroyed.
V	Completely weathered	Rock completely decomposed by weathering in place but texture still recognisable; in rock types of granite origin, feldspars com- pletely decomposed to clay minerals; cores cannot be recovered by ordinary rotary drilling methods; can be excavated by hand.	Can be excavated by hand or ripping without use of explosives; unsuitable for foundations of concrete dams or large structures; may be suitable for foundations of earth dams and for fill; unsuitable in high cuttings at steep slope angles; requires erosion protection.
IV	Highly weathered	Rock so weakened by weathering that fairly large pieces can be broken and crumbled in the hands; sometimes recovered as core by careful rotary drilling; stained by limonite.	Similar to grade V; unlikely to be suitable for foundations of concrete dams; erratic presence of boulders makes it an unreliable foundation stratum for large structures.
III	Moderately weathered	Considerably weathered; possessing some strength in large pieces (e.g. NX drill cores); often stained with limonite; difficult to excavate without use of explosives.	Excavated with difficulty without use of explosives; mostly crushes under bulldozer tracks; suitable for foundations of small concrete structures and rockfill dams; may be suitable for semi-pervious fill; stability in cuttings depends on structural features, especially joint attitudes.
II	Slightly weathered	Distinctly weathered with slight limonite staining; some decomposed feldspars in granites; strength approaching that of fresh rock; explosives required for excavation.	Requires explosives for excavation; suitable for concrete dam foundations; high permeability through open joints; often more permeable than zones above or below; questionable as concrete aggregate.
I	Fresh rock	Fresh rock may have some limonite-stained joints immediately beneath weathered rock.	Staining indicates water percolation along joints; individual pieces may be loosened by blasting or stress relief, and support may be required in tunnels and shafts.

Source: Little, A.L., Proceeding of the 7th International Conference on Soil Mechanics and Foundation Engineering, Vol. 1, pp. 1–10, 1969.

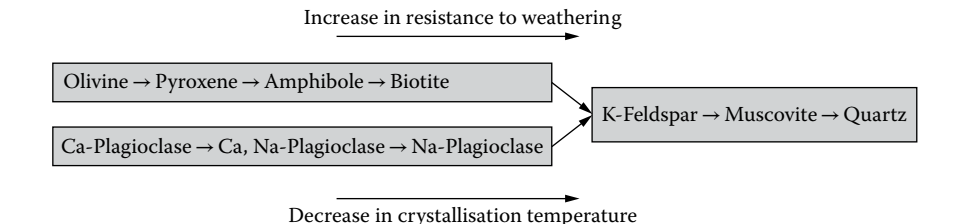


FIGURE 1.13 Bowen's reaction series.

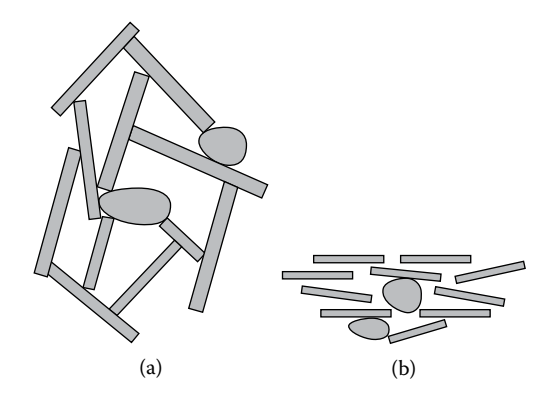


FIGURE 1.14 Soil structure: (a) flocculated and (b) dispersed.

The formation of *sedimentary soils* consists of three steps: *sediment formation* as a result of weathering of rocks; *sediment transport* by water, wind, ice, gravity and organisms, called the transporting agents; and *sediment deposition* in different environments. The orientation and distribution of particles in a soil mass, commonly termed *soil structure*, are governed by the environment of deposition. There are two types of soil structure, namely the *flocculated structure* and the *dispersed structure* (Figure 1.14). In the former structure, the particles have edge-to-face or edge-to-edge contacts, and there is a net attraction, whereas in the latter one, the particles tend to assume a face-to-face orientation, and there is a net repulsion. The engineering behaviour of soil is greatly controlled by the type of structure. Generally, an element of flocculated soil has higher strength, lower compressibility and higher permeability than an element of soil at the same void ratio but in a dispersed state. If the flocculated soil is subjected to a horizontal shear displacement, the particles will tend to line up in the dispersed structure.

Residual soils are products of the in situ weathering of bedrock. These soils are commonly situated above the groundwater table; therefore, they are often unsaturated. Fill is a man-made soil; the process of its formation is called filling. A fill is essentially a sedimentary soil where all the formation processes are carried out by humans. Organic soils, such as peats, are formed from the decomposition of organic materials, including decayed vegetation such as leaves and tree roots.

Clay minerals are a group of complex aluminosilicates, mainly formed during the chemical weathering of primary minerals. For example, the clay mineral *kaolinite* is formed by the breakdown of feldspar through the action of water and carbon dioxide. Most clay mineral particles are 'plate-like' in form, with a high specific area (surface area per unit mass), resulting in their properties being influenced significantly more by surface forces than by gravitational body forces. Long 'needle-shaped' particles can also occur (e.g. halloysite) but these are rare.

The basic structural units of most clay minerals consist of a *silica tetrahedron* and an *alumina octahedron* (Figure 1.15). These basic units combine to form sheet structures. Silicon and aluminium may be partially replaced by other elements in these units, a process known as *isomorphous substitution*. This can have the following two effects: a net unit charge deficiency results from each substitution, leading to a net negative charge, and a slight distortion of the crystal lattice occurs since the ions are not of identical size.

Several clay minerals are formed by the stacking of basic sheet structures, with different types of bonding between the layers. The three principal clay minerals are *kaolinite*, *illite* and *montmorillonite* (Grim, 1968).

The basic structure of kaolinite consists of a layer of alumina octahedron on the top of a layer of silica tetrahedron; this mineral is known as a 'two-layer' mineral. The thickness of the basic unit is about 7.2 Å. There is a very limited isomorphous substitution in kaolinite. The combined silica—alumina sheets are held together fairly tightly by hydrogen bonding. A kaolinite particle may consist of over 100 stacks.

The basic structure of illite consists of a sheet of alumina octahedron sandwiched between two sheets of silica tetrahedrons. The thickness of the basic unit is about 10 Å. In the octahedral sheet, there is a partial substitution of aluminium by magnesium and iron, and in the tetrahedral sheet, there is partial substitution of silicon by aluminium. The combined sheets are linked together by fairly weak bonding due to non-exchangeable potassium ions held between them.

Montmorillonite has the same basic structure as illite. In the octahedral sheet, there is partial substitution of aluminium by magnesium. The thickness of the basic unit is about 9 Å. The space between the combined sheets is occupied by water molecules and exchangeable cations other than potassium. There is a very weak bond

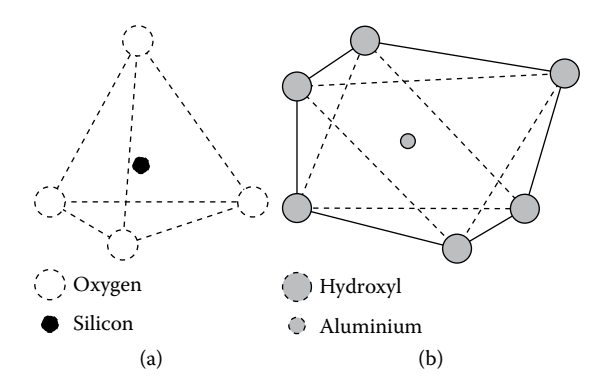


FIGURE 1.15 Basic structural units: (a) silica tetrahedron and (b) alumina octahedron.

between the combined sheets due to these ions. Considerable swelling of montmorillonite can occur due to the addition of water being adsorbed between the combined sheets.

The surfaces of clay mineral particles carry net negative charges, which may arise from any one or a combination of the following five factors: isomorphous substitution, surface disassociation of hydroxyl ions, absence of cations in the crystal lattice, adsorption of anions and presence of organic matter. Of these five factors, isomorphous substitution of aluminium or silicon atoms by atoms of lower valency is the most important.

A soil particle in nature attracts ions to neutralise its net negative charge. Since these attracted ions are usually weakly held on the particle surface and can be readily replaced by other ions, they are termed exchangeable ions, and the phenomenon is referred to as *cation exchange*. Calcium is a very common exchangeable ion in soils. The cations are attracted to a clay mineral particle because of the negative surface charges but at the same time tend to move away from each other because of their thermal energy. The net effect is that cations form a dispersed layer adjacent to the particle. The cation concentration decreases with increasing distance from the surface until the concentration becomes equal to that in the normal water in void space. The negatively charged particle surface and the dispersed layer of cations are commonly described as a *double layer*. Further details on the double layer can be found in some geotechnical textbooks (e.g. Shukla, 2014; Das, 2022).

1.7 EARTHQUAKES

Earthquakes are vibrations induced in the Earth's crust that virtually shake up a part of the Earth's surface and all the structures and objects lying within that area. Earthquakes may or may not result in the actual displacement of a land-mass on the Earth's surface. Strong earthquakes are among the most devastating natural disasters experienced on the Earth (Figure 1.16).



FIGURE 1.16 The damage done to a road and a house in Sukagawa city, Fukushima prefecture, in northern Japan, 11 March 2011. (Fukushima Minpo/AFP/Getty Images.)

Earthquakes Originate due to various causes, which can be classified as *tectonic* and *non-tectonic*. Tectonic causes include rupture and displacement in the Earth's crustal layers, and they relate to movement inside the Earth's structure. Earthquakes caused by tectonic activity are called tectonic earthquakes, and they are the most common and destructive type (Figure 1.16). Non-tectonic causes include natural activities (large-scale rockfalls or landslides, the dashing of sea waves along the coast, waterfalls, natural subsidence such as roof collapse into cavities and so on), human activity-based causes (underground nuclear, use of explosives for mineral exploration or excavation works, mining works, movement of heavy trucks and trains, dam construction, deep pumping, and so on) and *volcanic causes*. Many of the human activity-based causes result in less energetic earthquakes, but they are important to the engineers because they can cause damage to nearby standing structures and objects. Violent eruptions of volcanic lava often causes localised earthquakes. Earthquakes of volcanic origin are less severe and more limited in extent compared to earthquakes caused by tectonic causes.

Unlike most other disasters, earthquakes are nearly impossible to predict and occur without warning. However, while predicting them is difficult, people can still prepare to reduce the risks to lives and property through safety measures and disaster preparedness. The science that studies the causes of earthquakes and the propagation of waves within the Earth and on its surface is called *seismology*.

The causes of tectonic earthquakes are explained by the concept of *plate tectonics*. The basic hypothesis of plate tectonics is that the lithosphere consists of a number of large, intact, rigid blocks called *plates*, which float like large mats on the asthenosphere due to its viscosity and move as a result of convection currents, the force behind plate tectonics. Thus, the land-masses of the Earth have been moving for millions of years. For the study of the causes of the earthquakes, the Earth's crust is divided into six continental-sized plates (African, American, Antarctic, Indo-Australian, Eurasian and Pacific) and about 14 of subcontinental size (e.g. Caribbean, Cocos, Nazca and Philippine).

The point below the Earth's surface where a fault rupture first occurs is called the focus (or hypocentre) of the earthquake, which is its point of origin (point F in Figure 1.17a). The point vertically above the focus, located on the ground surface, is called the *epicentre* (point E in Figure 1.17). The vertical distance from the ground surface to the focus is called the focal depth (EF in Figure 1.17a). The horizontal distance between the epicentre and a given site is called the epicentric distance (EA in Figure 1.17), and the distance between a given site and the focus is called the hypocentric distance (FA in Figure 1.17a). The intensity of an earthquake decreases with the distance. If a line passing through the values of 'same intensity' in a particular earthquake record is imagined on the ground, it is called an isoseismal line; several such lines can be imagined.

Based on the focal depth, earthquakes are classified into the following three types:

- 1. *Deep-focus earthquakes*: These have focal depths of 300–700 km and constitute about 3% of all the earthquakes recorded around the world.
- 2. Intermediate-focus earthquakes: These have focal depths of 70–300 km.
- 3. *Shallow-focus earthquakes*: The focal depths of these earthquakes are less than 70 km. About 75% of all the earthquakes around the world belong to this category.

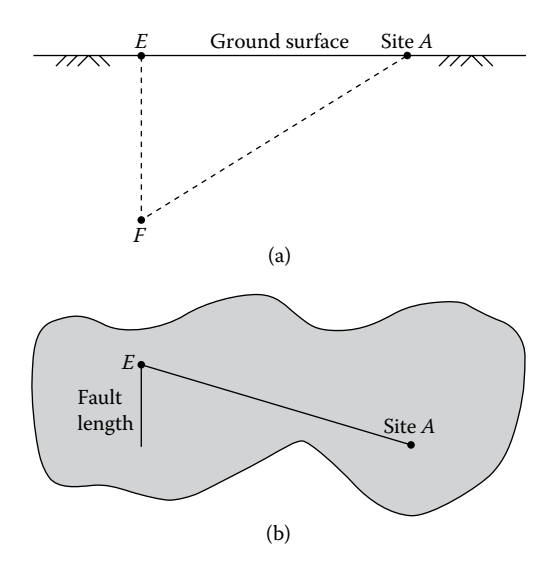


FIGURE 1.17 Definition of earthquake-related terms: (a) section and (b) plan. (Adapted from Das, B.M. and G.V. Ramana, *Principles of Soil Dynamics*, Cengage Learning, Stamford, CT, 2011.)

During the earthquake, seismic energy generated at the focus propagates in different directions in the form of waves, called the *shock* or *seismic waves*. Seismic waves are basically parcels of elastic strain energy that propagate outwards from a seismic source such as an earthquake, explosion or mechanical impact. Sources suitable for seismic investigation (see Section 1.9) usually generate short-lived wave trains, known as *pulses*, which typically contain a wide range of frequencies. Except in the immediate vicinity of the source, the strains associated with the passage of a seismic pulse are small and may be assumed to be elastic. On this assumption, the propagation velocities of seismic pulses are determined by the elastic modulus and density of the materials through which they pass.

There are two groups of seismic waves: *surface waves* and *body waves*. Surface waves, in the form of *Rayleigh waves* and *Love waves*, can propagate along the boundary of the solid. Surface waves are felt only near the surface of the Earth when earthquakes occur. They can also travel along the boundary between two media. They play a significant role in the destruction of buildings and other structures during earthquakes. These waves can be observed in a beam by blowing near its side. Rayleigh waves generate a form of swell on the solid surface, whereas Love waves are transverse shear waves on a horizontal surface.

Body waves can propagate through the internal volume of an elastic solid and are of two types: *Compressional waves* (*longitudinal*, *primary* or *P-waves*), which propagate by compressional and dilational uniaxial strains in the direction of wave travel, with particles oscillating about fixed points in the direction of wave propagation, and *shear waves* (*transverse*, *secondary* or *S-waves*), which propagate by a pure shear strain in a direction perpendicular to the direction of wave travel, with individual particles oscillating about fixed points in a plane at right angles to the direction of wave propagation.

P-waves can be observed in a beam by applying a compressional stress through striking its end. Each point on the beam vibrates in a sinusoidal movement in the direction of wave propagation, thus a P-wave is a longitudinal wave. When these waves move through the subsurface, they are the first waves perceived after an earthquake. S-waves can be observed in a beam by applying a shear stress to its upper surface. The points oscillate perpendicular to the direction of wave propagation; thus, an S-wave is a transverse wave. S-waves travel slower than P-waves and get absorbed in a liquid.

The velocity of a P-wave (V_p) relates to the elastic constants of the medium (bulk modulus of elasticity, K, and shear modulus or modulus of rigidity, G) and its density (ρ) as

$$V_{\rm p} = \sqrt{\frac{K + \frac{4}{3}G}{\rho}} \tag{1.1}$$

Since *K* is non-zero for all media (solids, liquids and gases), the P-wave velocity cannot be zero. Therefore, P-waves generated by earthquakes travel in all media and pass through all the layers (crust, mantle and core) of the Earth.

The velocity of an S-wave (V_s) relates only to the shear modulus or modulus of rigidity (G) of the medium and its density (ρ) as

$$V_{\rm s} = \sqrt{\frac{G}{\rho}} \tag{1.2}$$

Since the shear modulus (G) is negligible or zero for liquids and gases, the S-wave velocity can be zero. Therefore, S-waves generated by earthquakes travel mainly through solids. Past studies have shown that S-waves do not pass through the outer core of the Earth that extends approximately from 2,900 km to 5,150 km below the Earth's surface; this observation has indicated that the outer core of the Earth is in a liquid state although the inner core is a solid.

EXAMPLE 1.4

Derive an expression for the ratio of P-wave velocity (V_p) to S-wave velocity (V_s) . What do you notice based on this expression?

Solution

From Equations 1.1 and 1.2,

$$\frac{V_{\rm p}}{V_{\rm s}} = \sqrt{\frac{3K + 4G}{3G}} = \sqrt{\frac{4}{3} + \frac{K}{G}}$$
 (1.3)

To calculate V_p/V_s , both K and G of the medium should be known, but this is not essential if the following relationships are used to simplify Equation 1.3:

$$E = 2G(1+\nu) \tag{1.4}$$

$$E = 3K(1 - 2\nu) \tag{1.5}$$

where E is Young's modulus of elasticity and v is Poisson's ratio.

Eliminating E from Equations 1.4 and 1.5,

$$\frac{K}{G} = \frac{2(1+\nu)}{3(1-2\nu)} \tag{1.6}$$

Using Equation 1.6, Equation 1.3 becomes

$$\frac{V_{\rm p}}{V_{\rm s}} = \sqrt{\frac{1 - \nu}{0.5 - \nu}} \tag{1.7}$$

From Equation 1.7, note that the ratio of P-wave velocity to S-wave velocity depends only on Poisson's ratio of the medium. Thus, by measuring P- and S-wave velocities in the field, one can determine Poisson's ratio of the rocks and soils at a construction site. Poisson's ratio is an important material parameter in the numerical analysis of earth slopes and foundations for assessing their stability.

With Poisson's ratio for rocks typically around 0.25, the relationship $v_p \approx 1.7v_s$ holds, meaning that P-waves always travel faster than S-waves in the same medium.

EXAMPLE 1.5

The P-wave wave propagates vertically downwards through the continental crust of the Earth to a depth of 5 km from its surface and is reflected back to the surface. If the speed of the P-wave is 6.5 km/s, how long does it take for the P-wave to make the round trip?

Solution

Given: Travel distance = 5 km, and P-wave velocity = 6.5 km/s.

Travel time downwards to a depth of 5 km =
$$\frac{5}{6.5}$$
 = 0.77s

Travel time for the round trip = $2 \times 0.77 = 1.54s$

A *seismograph* is an instrument that detects and records seismic waves by capturing ground motion and converting it into data for analysis. The geophone serves as the sensor within the seismograph. The basic form of a seismograph contains a heavy weight suspended from a support that is attached to the ground. When waves from an earthquake reach the instrument, the inertia of the weight keeps it stationary while the support attached to the ground vibrates. The movement of the ground in relation to the stationary weight is recorded on a paper wrapped around a rotating drum.

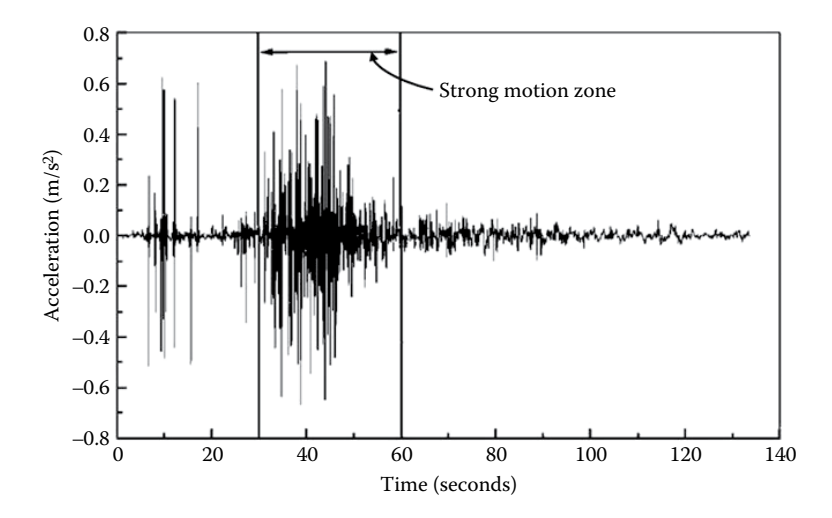


FIGURE 1.18 Time history of vertical ground acceleration during the Bhuj earthquake, 26 January 2001, India. (Adapted from Sitharam, T.G. and L. Govidaraju, *Geotechnical and Geological Engineering*, 22, 439–455, 2004.)

Modern seismographs are designed with electromagnetic sensors/geophones, along with electronic amplifiers, precision timing systems and recorders. Figure 1.18 shows a typical earthquake record given by a seismograph, called a *seismogram*. The measurements of seismic waves caused by a particular earthquake at three widely spaced stations can be analysed to work out how far these stations are from the epicentre.

The *intensity of an earthquake* is a measure of the local level of ground shaking as estimated based on human perceptibility and its destructiveness. Earthquakes are categorised into 12 grades according to the *Mercalli scale of intensity*, in which grade I refers to the earthquakes that are not felt but can be detected only by instruments, and grade XII refers to scenarios that result in situations such as total damage, ground warping, visible ground waves and objects being thrown upwards. Table 1.5 describes all the 12 grades of the earthquake intensity, with peak acceleration values provided for some grades.

The *magnitude of an earthquake* is a quantitative measure of its size, based on the amplitude of the elastic waves (P-waves) it generates at known distances from the epicentre. The earthquake magnitude scale presently in use was first developed by C.F. Richter (1958), who summarised its historical developments himself. Richter's earthquake magnitude is defined as

$$\log_{10} E = 11.4 + 1.5M \tag{1.8}$$

where E is the energy released (in ergs) and M is magnitude. Bath (1966) slightly modified the constant given in Equation 1.8 and presented it as

$$\log_{10} E = 12.24 + 1.44M \tag{1.9}$$

TABLE 1.5			
Mercalli Maximum	Earthquake	Intensity	/ Scale

Grades of earthquake intensity	Damage at epicentre (and peak acceleration, g being the acceleration due to gravity)
I	Not felt, detected only by instruments
II	Felt by some persons at rest; suspended objects may swing
III	Felt noticeably indoors; vibration like the passing of a truck
IV	Felt indoors by many persons, outdoors by some persons; windows and doors rattle $(<0.02g)$
V	Felt by nearly everyone; some windows broken
VI	Felt by all, many frightened; some heavy furniture moved; some fallen plaster; general damage slight
VII	Damage to poorly constructed buildings; weak chimneys fall (approx. 0.1 g)
VIII	Much damage to buildings, except those specially designed; tall chimneys and columns fall; sand and mud flow from cracks in the ground
IX	Foundations damaged; ground cracked; considerable damage in most buildings; buried pipes broken
X	Disastrous; buildings destroyed; rails bent; small landslides (> $0.6 g$)
XI	Few structures left standing; wide fissures opened in the ground with slumps and landslides
XII	Total destruction: ground wrapped; waves seen moving through ground; objects thrown upwards

Equation 1.9 shows that a one-unit increase in the magnitude (M) typically results in approximately a 30-fold increase in the energy (E) released during an earthquake. Earthquakes with a magnitude (M) of 2 to 2.5 are typically the smallest that can be felt, while those with $M \ge 5$ are considered damaging. Any earthquake exceeding M = 7 is regarded as a major disaster.

The length of fault rupture (or fault length) has been found to depend on the magnitude of the earthquake. Tocher (1958), based on observations of several earthquakes in California and Nevada, suggested the following relationship:

$$\log_{10} L = 1.02M - 5.77 \tag{1.10}$$

where L is the fault length in kilometres.

The Mercalli scale of earthquake intensity and the Richter scale of earthquake magnitude are not strictly comparable, but M = 5 corresponds roughly with grade VI. Table 1.6 presents an approximate comparison for other values of magnitude and intensity.

1.8 HYDROGEOLOGY

Hydrogeology deals with the occurrence, distribution, storage and movement of groundwater in the subsurface. All water located below the Earth's surface is referred

TABLE 1.6

Comparison of Richter Magnitude and Mercalli Maximum Intensity Scales

Richter earthquake magnitude scale, M	Mercalli maximum intensity scale
1–3	I
3–4	II–III
4–5	IV-V
5–6	VI–VII
6–7	VIII–IX
7–8+	X–XII



FIGURE 1.19 Air bubbles from the immersed dry weak sandstone sample collected from the proposed site for the construction of a coal handling plant (CHP), Northern Coalfields Limited, Gorbi, Madhya Pradesh, India. [After Sanjay Kumar Shukla, Subsoil Investigation for the Estimation of Load-Bearing Capacity of Foundation Soil at the Proposed Site for the Construction of a Coal Handling Plant (CHP), Northern Coalfields Limited, Gorbi, MP, India. A technical report dated 16 October 2006, Department of Civil Engineering, Institute of Technology, Banaras Hindu University, Varanasi, India, 2006.]

to as *groundwater* or *subsurface water*. Unlike surface water, groundwater needs very little treatment for use. Groundwater is one of the components of the hydrologic cycle in nature. It moves slowly through intergranular pores and natural cavities, called *primary openings*, and through discontinuities (joints, fractures and solution cavities), called *secondary openings* in rocks. Primary openings are generally found in sedimentary rocks, while secondary openings are found in most igneous and metamorphic rocks and in some sedimentary rocks. Figure 1.19 illustrates the physical evidence of pore spaces in a dry, weak sandstone sample when immersed in water.

The amount of groundwater or any other fluid (e.g. hydrocarbon fluids such as oil or gas) that can be stored in a rock mass depends on its *porosity*, which is estimated

as a ratio but expressed as the percentage of pore spaces, voids or openings relative to the total volume of the rock mass. Therefore, if *n* represents the porosity, then

$$n = \frac{V_{\nu}}{V} \tag{1.11}$$

where V_{y} is the void volume and V is the total volume of the rock mass element.

The property of rock that relates to its ability to transmit water or hydrocarbon fluids is called *permeability*, which is defined numerically as the flow through a unit area of the material per unit time under a unit hydraulic head. If *k* represents the permeability, then

$$k = \frac{q}{iA} \tag{1.12}$$

where q is the rate of flow in m³/s, A is the area through which flow takes places in m, $i = \Delta h/L$ is the hydraulic gradient, Δh is the hydraulic head causing the flow in m, and L is the flow path length in m. Note that the SI unit of permeability, called hydraulic conductivity or the coefficient of permeability, is metres per second; for convenience, it is expressed in metres per day for rocks.

Equation 1.2 may be expressed as

$$q = kiA \tag{1.13a}$$

or

$$v = ki \tag{1.13b}$$

where v is the discharge velocity in m/s. Equation 1.13a or Equation 1.13b is called Darcy's law, which holds good for all types of geomaterials as long as the fluid flows under laminar flow conditions, where a fluid particle follows a definite path and does not cross the paths of other fluid particles.

Table 1.7 gives values of porosity and permeability for some common rocks, soils and rock fracture zones.

EXAMPLE 1.6

A sandstone sample immersed in water absorbs 78 cc of water to become fully saturated. If its total volume is 458 cc, what is its porosity?

Solution

As the sample absorbs 78 cc of water, void volume, $V_{\nu}=78\,\mathrm{cc}$. Total volume, $V=458\,\mathrm{cc}$. From Equation 1.11, porosity of the sandstone is

$$n = \frac{78}{458} = 0.1703 \,\text{or} \, 17.03\%$$

TABLE 1.7

Typical Values of Porosity and Permeability for Some Common Rocks, Soils and Rock Fracture Zones

Rocks, soils and rock fracture zones	Porosity (%)	Permeability (m/day)
Fractured sandstone	15	5
Cavernous limestone	5	Erratic
Shale	3	0.0001
Granite	1	0.0001
Sand	30	20
Gravel	25	300
Clay	50	0.0002
Rock fracture zones	10	50

Source: Waltham, T., Foundations of Engineering Geology, Spon Press, London, 2002.

All porous rocks are not equally permeable. The permeability of a rock depends on the size of the pore spaces or openings present in the rock and the degree to which they are interconnected. Most soils transmit water through their pores, whereas transmission through most rocks occurs via pores and discontinuities such as joints and fractures. Fractures and joints normally transmit more water than pores. The loads from structures constructed on the ground can reduce the size of pores and fractures, resulting in reduced permeability. On the contrary, shrinkage due to desiccation can open cracks in clays, and dissolution can widen voids in soluble rocks, thus resulting in an increased permeability. Based on the water-bearing and water-yielding properties, geological formations are classified as follows:

Aquifers: Rocks and soils that are both porous and permeable.

Aquicludes: Rocks and soils that are porous but not permeable.

Aquitards: Rocks and soils that are porous but have limited permeability.

Aquifuges: Rocks and soils that are neither porous nor permeable.

Aquifers store groundwater in large quantities, and their permeability is sufficient to maintain a steady supply of water to ordinary or pumping wells or springs. The aquifers in which groundwater occurs under atmospheric pressure are called unconfined *aquifers*. If a well is drilled into an unconfined aquifer, the water level in that well represents the *water table*. An aquifer sandwiched between two relatively impermeable strata (aquicludes or aquifuges) is called a *confined aquifer*, also known as an *artesian* or *pressure aquifer*. Since impermeable strata do not allow the movement of groundwater across them, the groundwater within the aquifer remains under pressure greater than atmospheric pressure. The area through which rainwater infiltrates into the confined aquifer is called the *recharge area*. An imaginary surface coinciding

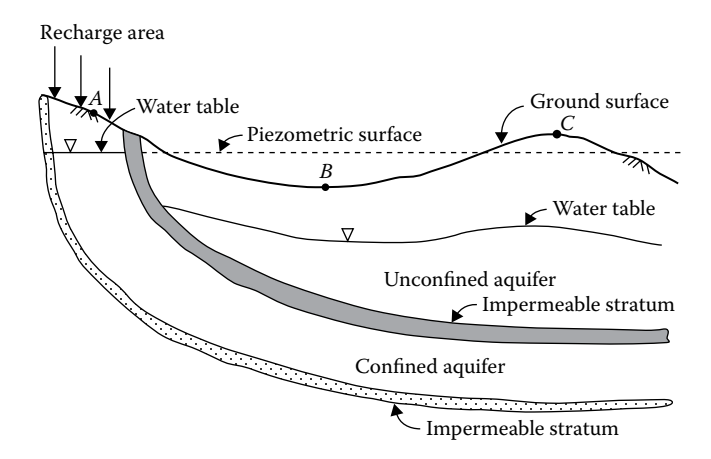


FIGURE 1.20 Unconfined and confined aguifers.

with the hydrostatic pressure level of water in the confined aquifer is called the *piezometric surface*. Figure 1.20 shows a typical schematic cross section of the confined and unconfined aquifers. A well drilled into the ground can be a *water table well* (site A and site B with the well bottom lying in the unconfined aquifer zone), a *flowing well* (site B with the well bottom lying in the confined aquifer zone) or *artesian well* (site C with the well bottom lying in the confined aquifer zone), depending on its depth and location on the ground. Thus, in any region, the possibility of obtaining an adequate supply of groundwater is dependent entirely on the location, extent and nature of the aquifers in that region. In river valleys, aquifers occur in abundance, and the water table generally lies near the ground. In such regions, the groundwater is usually drawn conveniently through both ordinary and pumping wells.

Typical aquifers are sand, gravel, sandstone, limestone, grit, conglomerate and so on. The fault zones, shear zones, joints and so on in igneous and metamorphic rocks may also act as aquifers. For a rock or soil to be an aquifer, its permeability should be greater than 1 m/day (Waltham, 2002). Clays, shales, mudstones and silt-stones are some examples of aquicludes. Clays with restricted amount of silt are aquitards, which are also called *leaky aquifers*. Massive compact granite, syenite, gabbro, gneiss and quartzite without discontinuities are typical examples of aquifuges. These rocks do not allow groundwater to percolate into them at all. For aquicludes and aquifuges – that is, for impermeable rocks or soils – their permeability is generally less than 0.01 m/day (Waltham, 2002).

1.9 PETROLEUM GEOLOGY

Petroleum is a mixture of hydrocarbon molecules and inorganic impurities that can exist in the solid, liquid (oil) or gas phase (Fanchi and Christiansen, 2017). Petroleum geology as a subject plays a significant role in the upstream oil and gas industry, serving as the foundation for the exploration, drilling and production of hydrocarbons

(crude oil and natural gas). This sector represents the first stage in the overall oil and gas supply chain, preceding the 'midstream' (transportation and storage) and 'downstream' (refining, distribution and marketing) sectors.

Understanding the Earth's subsurface is critical for locating and extracting oil and gas resources efficiently and sustainably. Geoscientists, including geologists, geophysicists and petroleum engineers, collaborate to analyse and interpret data from various sources to identify potential hydrocarbon reservoirs. Their work involves the integration of geological, geophysical and geomechanical data to assess the viability of drilling sites, estimate recoverable reserves and design extraction strategies that minimise environmental impact while maximising economic returns.

Underground hydrocarbon structures, comprising sedimentary rocks such as sandstone, limestone and shale, exhibit complex geological features and geomechanical properties. These factors, including porosity and permeability, are critical in determining the storage and flow of fluids within petroleum reservoirs, significantly influencing their performance during extraction.

Geomechanical properties, such as rock strength, stress distribution and fracture networks, also play a significant role in the stability of hydrocarbon reservoirs. Understanding these properties is essential for predicting how the reservoir will respond to drilling and production activities. The advanced techniques, including seismic imaging, well logging and core sampling, are used to characterise these features and assess the potential for successful hydrocarbon extraction.

The areas of the Earth's crust that are underlain by a thick sequence of sedimentary rocks are called sedimentary basins, which have been formed through a complex process that involves the deposition of sediments in subsiding areas of the Earth's crust. Rock in sedimentary basins can vary significantly due to different depositional environments and changes in pressure, density and composition. Tectonic forces such as folding, faulting and fracturing alter the orientation and continuity of rock strata, creating complex geological structures.

Petroleum-bearing sedimentary basins are regions where large quantities of organic material have accumulated and undergone transformation into hydrocarbons over geological time scales. These sediments, typically rich in organic matter, are buried under layers of overlying sediments, where they are subjected to increased temperature and pressure over millions of years. The process of diagenesis, involving the physical and chemical alteration of sediments through mainly compaction and/or cementation at relatively low pressure and temperature, leads to the formation of sedimentary rocks such as shale, sandstone, limestone and conglomerate. As these rocks are buried deeper, organic matter within them undergoes thermal maturation, transforming into hydrocarbons such as oil and natural gas. The size, shape and subsidence rate of the sedimentary basin influence the quantity and quality of hydrocarbons generated and stored.

The effectiveness of a *hydrocarbon source rock*, typically organic-rich, in generating hydrocarbons depends on several factors, including its organic content, thermal maturity and the presence of favourable conditions for hydrocarbon expulsion. These factors are assessed by analysing rock samples and using geochemical techniques, such as pyrolysis, to determine the hydrocarbon generation potential of the source rock. Understanding the characteristics of the source rock is important for predicting

the location and volume of hydrocarbons that may be present in a sedimentary basin. It should be noted that the volume of petroleum generated in a sedimentary basin depends on the area of the basin, the average total thickness of source rock and the efficiency of transforming organic matter to petroleum (Fanchi and Christiansen, 2017).

Hydrocarbon fluid migration refers to the movement of hydrocarbons from the source rock where they are generated to the reservoir rock where they accumulate. This process occurs in two stages:

- Primary migration: It involves the movement of hydrocarbons out of the source rock and into adjacent permeable formations.
- Secondary migration: It involves the movement of hydrocarbons through preamble formations, driven by buoyancy forces, until they are trapped in a suitable reservoir.

The density of hydrocarbon fluids generated in source rocks is usually lower than that of water. Hence, they tend to migrate upwards and follow permeable pathways until they encounter an impermeable boundary. The effectiveness of hydrocarbon fluid migration is influenced by several factors, including the permeability of the rocks, the presence of faults and fractures and the pressure gradient within the basin. Migration pathways are often complex, and hydrocarbons can be lost or altered during the migration process. A combination of geological modelling, seismic data and fluid flow simulations is used to map migration pathways and identify potential traps where hydrocarbons may have accumulated.

A *hydrocarbon trap*, often referred to as a *reservoir*, is a geological structure that allows the accumulation of hydrocarbon fluids and prevents their further movement. The base of each trap is typically the interface between water-saturated rock and hydrocarbon-saturated rock. Traps are classified into the following main types:

- Structural traps: They are formed by the deformation of the Earth's crust, such as folding, faulting or salt dome formation. Anticlines are a common type of structural trap (Figure 1.21). An anticline trap forms when hydrocarbons migrate upwards through porous reservoir rock and accumulate beneath an impermeable cap rock, preventing their escape and creating a reservoir.
- Stratigraphic traps: They are formed by changes in rock type or depositional environment, such as pinch-outs, unconformities or reef structures.
- Combination traps: They are formed as a combination of structural and stratigraphic features.

The effectiveness of a trap depends on the presence of a cap or seal, typically an impermeable rock layer such as shale or salt, that prevents hydrocarbons from escaping. The reservoir rock within the trap must have sufficient porosity and permeability to store and transmit hydrocarbon fluids. The characteristics of traps and reservoirs are often assessed using seismic surveys, well logs and core samples to estimate the size, shape and quality of the hydrocarbon accumulation.

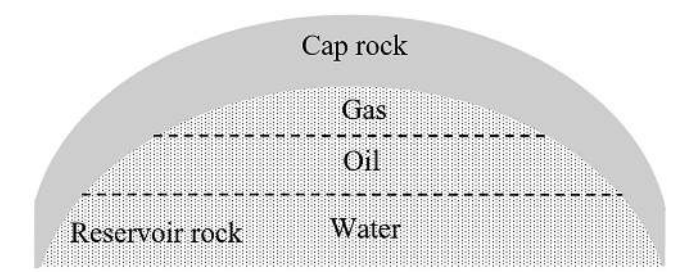


FIGURE 1.21 An anticline trap – an example of a structural trap.

Reservoir lithology refers to the type of rock that makes up the reservoir, which can significantly influence its ability to store and produce hydrocarbons. Common reservoir rocks include sandstone, limestone and dolomite. The physical properties of reservoir rocks are:

- 1. *Porosity* (n): The measure of void volume (V_{ν}) within the rock that can store fluid (oil, water and/or gas). It is expressed as a percentage of the total rock volume, as explained earlier (see Equation 1.11).
- 2. Degree of saturation or simply saturation (S): The fraction of pore volume occupied by each fluid (e.g. oil, gas, water) within the rock. For each fluid, it is expressed as a ratio but presented as a percentage of total void volume (V_p) .

Oil saturation,

$$S_0 = \frac{V_0}{V_{\nu}} \tag{1.14a}$$

Water saturation,

$$S_{w} = \frac{V_{w}}{V_{v}} \tag{1.14b}$$

and gas saturation,

$$S_g = \frac{V_g}{V_g} \tag{1.14c}$$

where V_o , V_w and V_g are volume of oil, water and gas, respectively.

The sum of saturations of oil, water and gas phases must equal unity. Mathematically,

$$V_{o} + V_{w} + V_{o} = 1 {(1.15)}$$

1. *Permeability* (K): In civil and ground infrastructure projects, permeability (k) is characteristic of both geomaterial and the fluid, and is often used and expressed in m/s, as explained in Section 1.8. In petroleum or reservoir engineering, permeability is also measured based on Darcy's law, but as the specific or absolute permeability ($K = (k\eta)/\gamma_f$), which depends

only on the properties of geomaterials, typically in square metres (m²) in the SI system or in darcy (D) (1 D = 0.987×10^{-12} m²). Note that η is the viscosity of fluid, and γ_f is the unit weight of fluid. Further details on Darcy's law, including the definition and units of permeability, can be found in Shukla (2014).

Reservoir rocks may have different porosity, saturation, permeability and mechanical properties. The texture, grain size and cementation of these rocks affect their pore space and the ease with which fluids can flow through them. The porosity of commercially viable reservoir systems ranges from a few percent for shale and coal to about 50% for diatomaceous formations. The porosity of most conventional oil and gas formations ranges from 15% to 25% (Fanchi and Christiansen, 2017).

The rock-fluid characteristics of a reservoir are crucial in determining its performance and guiding the design of efficient recovery methods. Key factors include wettability, which influences the distribution of hydrocarbons and water within the pores, as well as the viscosity, density and composition of the reservoir fluids. Wettability is a multiphase property that describes the tendency of a solid rock matrix to preferentially maintain contact with one fluid over another, influencing fluid distribution and flow within the porous medium. Interactions between the reservoir rock and fluids, such as capillary pressure and wettability, significantly affect fluid distribution, flow and overall recovery efficiency. Understanding these properties is essential for optimising techniques like water flooding, gas injection or enhanced oil recovery to maximise hydrocarbon extraction from the reservoir.

1.10 SITE INVESTIGATION

Site investigation involves assessing the surface and subsurface conditions at proposed engineering project sites. Engineering geological and geotechnical data and information are required since the planning stage of the project. A typical site investigation includes preliminary studies such as desk study and site reconnaissance, geophysical surveys, drilling boreholes, in situ testing, sampling and laboratory testing of samples, and groundwater observations and measurements. A desk study involves gathering as much existing information as possible about the site through geological maps, aerial and satellite photographs, soil survey reports, and site investigation reports from nearby locations, and so on. Site reconnaissance consists of a walkover survey, visually assessing the local conditions such as site access, adjacent properties and structures, topography and drainage.

All the findings of the site investigation are presented to the client in the form of a *site investigation report*, which consists of a site plan, several boring logs that summarise the soil and rock properties at each test pit and borehole, and the associated laboratory and in situ test data. The extent of a site investigation programme for a given project depends on type of project, importance of the project and nature of the subsurface materials involved. The level of investigation should be appropriate to the proposed site use and to the consequences of failure to meet the performance requirements. For example, a large dam project would usually require a more thorough site investigation than the investigation required for a highway project. A further example is loose sands or soft clays, which usually require more investigation

than the investigation required for dense sands or hard clays. Site investigation typically accounts for 0.1–1.0% of the total project construction cost, depending on the complexity and scale of the project. The lower percentage applies to smaller projects or those with less complex subsurface conditions, while the higher percentage is typically for larger projects or those with more critical subsurface conditions.

The purpose of the site investigation is to conduct a scientific examination of the site for collecting as much information as possible at minimal cost about the existing topographical and geological features of the site, for example, the exposed overburden, the course of nearby streams or rivers, rock outcrops, hillocks or valleys, vegetation and mainly the subsurface conditions underlying the site. Investigation of subsurface conditions at the site for the proposed construction of an engineered system is essential before the design is finalised. Subsurface investigation is needed basically to provide the following:

- 1. Sequence and extent of each soil and rock stratum underlying the site and likely to be affected by the proposed construction.
- 2. Engineering geological characteristics of each stratum and geotechnical properties mainly strength, compressibility and permeability of soil and rock, which may affect the design and construction procedures of the proposed engineered systems and their foundations.
- 3. Location of groundwater table (or water table) and possible harmful effects of soil, rock and water on materials to be used for construction of structural elements of foundation.

The preceding information is used for determining the type of foundation and its dimensions, estimating the load-carrying capacity of the proposed foundation, and identifying and solving the construction, environmental and other potential problems, enabling the civil engineer to arrive at an optimum design with due consideration to the subsurface material characterisation.

Shukla and Sivakugan (2011) have described several methods of subsurface exploration in detail. Experience has shown that making boreholes is the only direct practical method of subsurface exploration to greater depths. Rotary drilling is the most rapid method of advancing boreholes in rock masses unless it is highly fissured; however, it can also be used for all other soils. In this method, cores from rock as well as from concrete and asphalt pavements may be obtained using coring tools (coring bit and core catcher). Coring tools should be designed so that, in sound rock, continuous recovery of core is achieved. To obtain cores of rock, various types of core barrels are available; however, the NX type is commonly used in routine site investigation work, giving core samples with a diameter of 2 1/8 inches (53.98 mm) (Figure 1.22). It is important to ensure that boulders or layers of cemented soils are not mistaken for bedrock. This necessitates core drilling to a depth of at least 3 m into bedrock in areas where boulders are known to occur. Core photography in colour is performed on all cores to record permanently the unaltered appearance of the rock. Based on the length of rock core recovered from each run, the following quantities may be calculated for a general evaluation of the rock quality encountered:



FIGURE 1.22 Rock cores in a core box.

Core recovery =
$$\left(\frac{\text{Length of the core recovered}}{\text{Total length of the core run}} \times 100\right)\%$$
 (1.16)

and

Rock quality designation (RQD)
$$= \left(\frac{\Sigma \text{ lengths of intact pieces of recovered core} \ge 100 \,\text{mm}}{\text{Total length of the core run}} \times 100\right)\% \qquad (1.17)$$

A core recovery of 100% indicates the presence of intact rock; for fractured rocks, the core recovery will be less than 100%. More details on rock coring and assessment of rock quality are described in Chapter 3.

Geophysical methods can be used to determine the distributions of physical properties, for example, elastic moduli, electrical resistivity, density and magnetic susceptibility, at depths below the ground surface that reflect the local subsurface characteristics of the materials (soil, rock, water, oil or gas). These methods may be used for the investigation during the reconnaissance phase of the site investigation programme, as they provide a relatively rapid and cost-effective means of deriving aerially distributed information about subsurface stratification. Geophysical investigation can optimise detailed investigation programmes by maximising the rate of ground coverage and minimising the drilling and field-testing requirements. Since geophysical investigations may sometimes be prone to major ambiguities or uncertainties of interpretation, they are often verified by drilling or excavating test pits. In fact, geophysical investigation methods may be used to supplement borehole and outcrop data and to interpolate between boreholes.

A wide range of geophysical methods are available for subsurface investigation, each of which is sensitive to a specific physical property (Dobrin, 1976;

Kearey et al., 2002). The physical property to which a method responds clearly determines its range of applications. Seismic refraction or reflection and ground-penetrating radar methods can be used to map soil horizons and depth profiles, water tables and depth to bedrock in many situations. Electromagnetic induction, electrical resistivity and induced polarisation (or complex resistivity) methods may be used to map variations in water content, clay horizons, stratification and depth to aquifer or bedrock. The magnetic method is particularly suitable for locating magnetite and intrusive bodies such as dykes in subsurface rocks. Other geophysical methods such as gravity and shallow ground temperature methods may be useful under certain specific conditions. Crosshole shear wave velocity measurements offer critical soil and rock parameters for dynamic analysis.

In petroleum and reservoir engineering, hydrocarbon exploration involves the use of various techniques to identify and evaluate potential subsurface geological structures that may contain hydrocarbons. Seismic surveying is one of the most widely used methods, involving the generation of seismic waves that travel through the Earth's subsurface and are reflected to the surface by different rock layers. By analysing the travel time and amplitude of these reflections, the detailed images of the subsurface are created to identify potential traps and reservoirs. Other exploration techniques include gravity and magnetic surveys, which measure variations in the Earth's gravitational and magnetic fields caused by subsurface geological features. Well logging, which involves the measurement of physical properties of rocks and fluids in boreholes, provides direct information about the characteristics of the reservoir. Drilling exploratory wells, or wildcat wells, is often the final step in confirming the presence of hydrocarbons and assessing their commercial viability.

Seismic and electrical resistivity methods are commonly used alongside boring logs for subsurface investigations. These methods are discussed in detail in Sections 1.10.1 and 1.10.2.

1.10.1 Seismic Methods

Seismic methods require generation of shock or seismic waves. They generally use only P-waves, since this simplifies the investigation in two ways. First, seismic or shock detectors that are insensitive to the horizontal motion of S-waves, recording only vertical ground motion, can be used. Second, the higher velocity of P-waves ensures they always reach the detector before the corresponding S-waves, making them easier to identify (Kearey et al., 2002).

Seismic methods make use of the variation in elastic properties of the strata, which influence the velocity of seismic waves travelling through them. This allows for the determination of dynamic elastic moduli as well as the mapping of the subsurface horizons. The required shock waves are generated within the subsurface materials, at the ground surface or at a certain depth below it, by striking a plate on the soil or rock with a hammer or by detonating a small charge of explosives in the soil or rock. The radiating shock waves are picked up by the vibration detector, also called a seismometer (e.g. a geophone on land or a hydrophone offshore), where the travel times are recorded. Geophones and hydrophones are sensors: geophones convert ground motion into voltage to detect seismic vibrations, while hydrophones detect

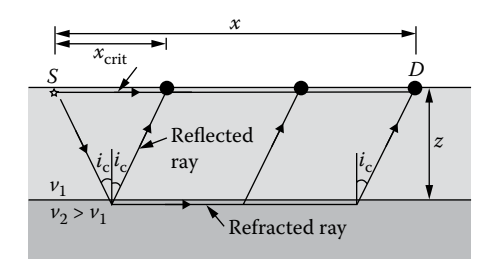


FIGURE 1.23 Seismic/shock ray paths from a near-surface source to a surface detector in the case of a two-layer system.

underwater sound by converting acoustic pressure into electrical signals, functioning like underwater microphones. On land, either a number of geophones are arranged in a line, or the shock-producing device is moved away from the geophone to produce shock waves at intervals. Figure 1.23 shows the travel paths of primary waves in a simple geological section involving two media (e.g. soil underlain by bedrock) with respective primary wave velocities of v_1 and v_2 (where $v_2 > v_1$), separated at a depth z. From the seismic source S, the energy reaches the detector D at the ground surface by three types of ray path. The *direct ray* travels along a straight line through the top layer from the source to the detector at velocity v_1 . The *reflected ray* is obliquely incident on the interface and is reflected back through the top layer to the detector, having its entire path within the top layer at velocity v_1 . The *refracted ray* travels obliquely down to the interface at velocity v_1 , propagates along the interface at the higher velocity v_2 , and then returns through the upper layer at velocity v_1 .

The travel time t_{dir} of a direct ray is given simply by

$$t_{\rm dir} = \frac{x}{\nu_1} \tag{1.18}$$

where x is the distance between the source S and the detector D.

The travel time of a reflected ray is given by

$$t_{\text{refl}} = \frac{\sqrt{x^2 + 4z^2}}{\nu_1} \tag{1.19}$$

The travel time of a refracted ray is given by

$$t_{\text{refr}} = \frac{z}{\nu_1 \cos i_c} + \frac{x - 2z \tan i_c}{\nu_1} + \frac{z}{\nu_1 \cos i_c}$$
 (1.20)

where i_c is the critical angle of incidence, expressed as

$$i_{\rm c} = \sin^{-1} \left(\frac{\nu_1}{\nu_2} \right) \tag{1.21}$$

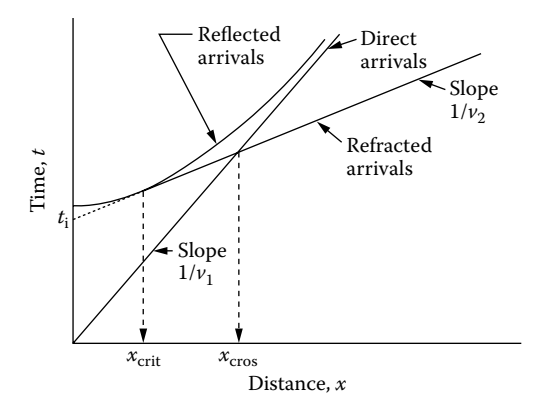


FIGURE 1.24 Time–distance curves for seismic/shock waves from a single horizontal discontinuity.

Substitution of Equation 1.21 into Equation 1.20 yields

$$t_{\text{refr}} = \frac{x}{\nu_2} + \frac{2z\sqrt{\nu_2^2 - \nu_1^2}}{\nu_1 \nu_2}$$
 (1.22)

Time-distance curves for direct, refracted and reflected rays are illustrated in Figure 1.24. By suitable analysis of the time-distance curve for reflected or refracted rays, it is possible to compute the depth to the underlying layer such as the bedrock. This provides two independent seismic methods, namely the seismic reflection method and the seismic refraction method, for locating the subsurface interfaces. The seismic refraction method is especially useful in determining the depth to rock in locations where successively denser strata are encountered, that is, when the velocity of shock or seismic waves increases successively with depth. This method is therefore commonly used in site investigation work. From Figure 1.24, it is evident that the first arrival of seismic energy at a surface detector offset from a surface is always a direct ray or a refracted ray. The direct ray is overtaken by a refracted ray at the crossover distance, x_{cross} . Beyond this crossover distance, the first arrival is always a refracted ray. Since critically refracted rays travel down to the interface at the critical angle, there is a certain distance, known as the *critical distance*, x_{crit} , within which refracted energy will not be returned to the surface. At the critical distance, the travel times of reflected rays and refracted rays coincide because they follow effectively the same path. In the refraction method of site investigation, the detector should be placed at a sufficiently large distance to ensure that the crossover distance is well exceeded, so that refracted rays are detected as first arrivals of seismic energy. In general, this approach means that the deeper a refractor, the greater the range over which recordings of refracted arrivals need to be taken.

In Figure 1.24, the intercept on the time axis of the time–distance plot for a refracted ray, known as the *intercept time*, t_i , is given by

$$t_{\rm i} = 2z \frac{\sqrt{\nu_2^2 - \nu_1^2}}{\nu_1 \nu_2} \tag{1.23}$$

Since t_i can be determined graphically as shown in Figure 1.24 or numerically from the relation $t_i = t_{refr} - x/v_2$, Equation 1.23 can be used to determine the depth to bedrock as

$$z = \frac{t_{\rm i}}{2} \frac{\nu_1 \nu_2}{\sqrt{\nu_2^2 - \nu_1^2}} \tag{1.24}$$

The seismic reflection method may be useful in delineating geological units at depths. Recordings are normally restricted to small offset distances, well within the critical distance for reflecting the interfaces of main interest. This method is not constrained by layers of low seismic velocity and is especially useful in areas of rapid stratigraphic changes.

1.10.2 ELECTRICAL RESISTIVITY METHODS

The electrical resistivity method may be useful in determining the depth to bedrock and anomalies in the stratigraphic profile, in evaluating stratified formations where a denser stratum overlies a less dense medium and in the location of prospective sand–gravel or other sources of borrow material. This method is based on the determination of the subsurface distribution of electrical resistivity of earth materials from measurements taken on the ground surface. Resistivity parameters are also required for the design of grounding systems and cathodic protection for buried structures. The resistivity of a material is defined as the resistance in ohms between the opposite faces of a unit cube of the material. If the resistance of a conducting cylinder having length L and cross-sectional area A is R, the resistivity ρ is expressed in ohm-metre $(\Omega-m)$ as

$$\rho = R \frac{A}{L} \tag{1.25}$$

The current I is related to the applied voltage V and the resistance R of the material by Ohm's law as

$$I = \frac{V}{R} \tag{1.26}$$

Each soil or rock has its own resistivity depending on water content, compaction and composition. Certain minerals such as native metals and graphite conduct electricity via the passage of electrons. Most of the rock-forming minerals are, however, insulators, and electric current is carried through a rock mainly by the passage of ions in the pore water. Thus, most rocks conduct electricity by electrolyte rather than electronic processes. It follows that porosity is the major control on the resistivity of rocks, and the resistivity generally increases as porosity decreases. However, even

TABLE 1.8
Resistivity of Subsurface Earth Materials

Subsurface earth materials	Mean resistivity (ohm-m
Marble	10^{12}
Quartz	10^{10}
Rock salt	$10^6 - 10^7$
Granite	5000-106
Sandstone	35-4000
Moraines	8-4000
Limestone	120-400
Clays	1–120

Source: Shukla, S.K. and N. Sivakugan, Geotechnical Engineering Handbook, J. Ross Publishing, Inc., Fort Lauderdale, FL, 2011.

crystalline rocks with negligible intergranular porosity are conductive along cracks and fissures. The range of resistivity among earth materials is enormous, extending from 10^{-5} to $10^{15} \Omega$ -m. For example, the resistivity is low for saturated clays and high for loose dry gravel or solid rock, as seen in Table 1.8. Since there is considerable overlap in resistivity values between different earth materials, identification of a rock is not possible solely based on resistivity data. Strictly speaking, Equation 1.25 refers to electronic conduction, but it may still be used to describe the *effective resistivity* of a rock or soil, that is, the resistivity of the rock or soil and its pore water. Archie (1942) proposed an empirical expression for effective resistivity as

$$\rho = an^{-b}S^{-c}\rho_{w} \tag{1.27}$$

where n is the porosity, S is the degree of saturation, ρ_w is the resistivity of water or the ionic solution in the pores, and a, b and c are empirical constants, known as the tortuosity factor, cementation exponent and saturation exponent, respectively. The tortuosity factor a depends on pore geometry, while the cementation exponent b depends on the degree of consolidation of the rock. In the case of sands, the empirical parameters a and b range from 0.35 to 4.78 and from 1.14 to 2.52, respectively (Bassiouni, 1994). The value ρ_w can vary considerably according to the quantity and conductivity of dissolved materials.

Equation (1.27), commonly known as Archie's equation, can be presented as

$$\rho_0 = an^{-b}\rho_w = F\rho_w \tag{1.28}$$

where ρ_0 is resistivity of saturated porous material, and

$$F = a\eta^{-b} \tag{1.29}$$

is the formation resistivity factor, or simply formation factor, of the porous material.

Normally, one would expect a fairly uniform increase in resistivity with geologic age because of the greater compaction associated with the increasing thickness of overburden. There is no consistent difference between the range of resistivity of igneous and sedimentary rocks, although metamorphic rocks appear to have a higher resistivity, statistically, than either of the other types of rock (Dobrin, 1976).

EXAMPLE 1.7

Given the following parameters for a rock formation:

- Tortuosity factor, a = 0.75
- Cementation parameter, b = 1.8
- Formation factor, F = 80

What is the porosity of the rock?

Solution

From Equation (1.29), the porosity of the rock,

$$n = \left(\frac{a}{F}\right)^{1/b} = \left(\frac{0.75}{80}\right)^{1/1.8} = 0.075 \text{ or } 7.5\%$$

The test involves sending direct currents or low-frequency alternating currents into the ground and measuring the resulting potential differences at the surface. For this purpose, four metal spikes are driven into the ground at the surface along a straight line, generally at equal distances; one pair serves as current electrodes, and the other pair as potential electrodes (Figure 1.25). The resistivity can be estimated using the following equation (Kearey et al., 2002):

$$\rho = \frac{2\pi V}{I\left[\left(\frac{1}{r_1} - \frac{1}{r_2}\right) - \left(\frac{1}{R_1} - \frac{1}{R_2}\right)\right]}$$
(1.30)

where V is the potential difference between electrodes P_1 and P_2 , r_1 and r_2 are the distances from potential electrode P_1 to current electrodes C_1 and C_2 , respectively, and R_1 and R_2 are the distances from potential electrode P_2 to current electrodes C_1 and C_2 , respectively.

When the ground is uniform, the resistivity calculated from Equation 1.30 should be constant and independent of both electrode spacing and surface location. When subsurface inhomogeneity exists, however, the resistivity will vary with the relative positions of the electrodes. Any computed value is then known as the *apparent resistivity* ρ_a and will be a function of the form of the inhomogeneity. Equation 1.30 is thus the basic equation for calculating the apparent resistivity for any electrode

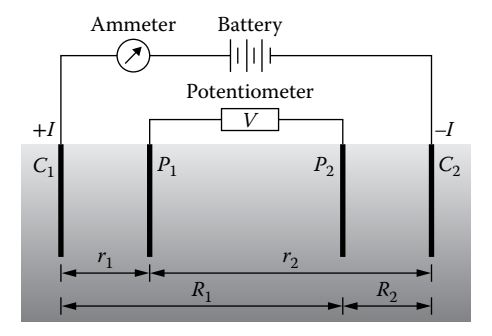


FIGURE 1.25 The generalised form of the electrode configuration used in the electrical resistivity method. (*Note:* C_1 and C_2 are current electrodes, and P_1 and P_2 are potential electrodes.)

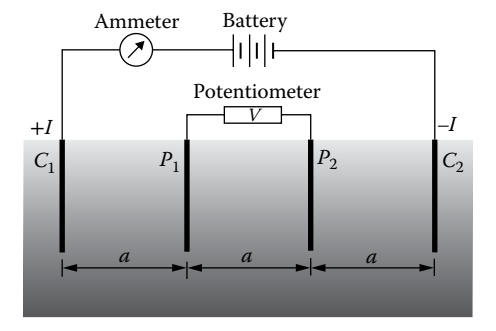


FIGURE 1.26 The Wenner electrode configuration used in the electrical resistivity method. (*Note*: C_1 and C_2 are current electrodes, and P_1 and P_2 are potential electrodes.)

configuration. The current electrode separation must be chosen so that the ground is energised to the required depth and should be at least equal to this depth. This places practical limits on the depths of penetration attainable by normal resistivity methods due to the difficulty in laying long lengths of cable and generating sufficient power. Depths of penetration of about 1 km are the limit for normal equipment.

There can be several configurations of electrodes, but the *Wenner configuration* is the simplest in that current and potential electrodes are maintained at an equal spacing, a (see Figure 1.26). Substitution of this condition, that is, $r_1 = a$, $r_2 = 2a$, $R_1 = 2a$ and $R_2 = a$, in Equation 1.30 yields

$$\rho_a = 2\pi a \frac{V}{I} \tag{1.31}$$

In the study of horizontal or near-horizontal overburden soil-bedrock interfaces, the spacing *a* is gradually increased about a fixed central point. Consequently, readings are taken as the current reaches progressively greater depths. This technique,

known as *vertical electrical sounding* (VES), also called the *electrical drilling* or *expanding probe*, is extensively used to determine overburden thickness and to define horizontal zones of porous media. To study the lateral variation of resistivity, the current and potential electrodes are maintained at a fixed separation and progressively moved along a profile. This technique, known as the *constant separation traversing* (CST), also called the *electrical profiling*, is used to determine variations in bedrock depth and the presence of steep discontinuities.

1.11 GEOLOGICAL SITE SELECTION FOR STRUCTURES

Geological site selection is a critical step in the design and construction of civil and infrastructure engineering projects. It ensures that the selected location can support the intended structural load while minimising risks from natural hazards such as landslides, earthquakes or subsidence. The geological conditions of a site directly impact design parameters, construction methods and the long-term performance of the structure. Poor site selection can lead to significant structural issues, higher construction costs and even catastrophic failures. Therefore, careful site selection is essential for ensuring the safety, durability and economic viability of a project, requiring a comprehensive understanding of the geological, geotechnical and environmental conditions of the area

The geological site selection involves evaluating the suitability of a location based on various geological factors, including the following:

- · Rock and soil types
- Topography
- · Groundwater conditions
- Seismic activity
- Presence of any potential geohazards

The type of rock and soil at a site plays a crucial role in determining its suitability for construction. Different types of rocks and soils have varying load-bearing capacity, compressibility and stability, which affect the foundation design. For instance, hard rocks such as granite and basalt offer excellent support for heavy structures, while loose soils such as sand or clay may require extensive ground improvement techniques. Soil and rock characterisation is typically performed through field investigations and laboratory testing, including soil borings, rock core sampling and geotechnical tests, as applicable. These tests help determine the mechanical properties of the subsurface materials, such as shear strength, permeability and consolidation characteristics.

Groundwater conditions significantly impact the stability and design of foundations. High groundwater levels can lead to problems in both rock and soil formations, such as water ingress during construction, reduced rock joint strength, reduced soil strength and increased risk of liquefaction during earthquakes. Additionally, fluctuations in groundwater levels can cause differential settlement, adversely affecting the integrity of the structure. Hydrogeological studies, including well tests, permeability assessments and piezometer installations, are essential to understand the

groundwater regime at a site. These studies help in designing appropriate dewatering systems, drainage solutions and foundation types that can withstand the groundwater conditions at the project site.

The topography of the site influences both the design and construction process. Sites with steep slopes may be prone to landslides or erosion, requiring additional stabilisation measures such as retaining walls, slope or rock reinforcement, or terracing. Conversely, flat sites may offer easier construction conditions but could be more susceptible to flooding. A topographical survey is typically conducted to map the elevation, slope and surface features of the site. This information is crucial for planning the site layout, drainage systems and access roads, as well as for identifying any potential geohazards.

Seismic activity is a critical factor in geological site selection, particularly in regions prone to earthquakes. The presence of active faults, seismic zones and the historical frequency and magnitude of earthquakes must be considered when selecting a site. Structures built on or near active faults may be at risk of ground shaking, surface rupture and soil liquefaction, all of which can lead to severe damage or collapse. Seismic hazard assessments, including the analysis of local fault lines, historical seismic data and ground motion studies, are essential for determining the seismic risk at a site. These assessments inform the design of earthquake-resistant structures, including the selection of foundation types, building materials and reinforcement techniques.

Geohazards, such as landslides, sinkholes and subsidence, pose significant risks to structures and must be carefully evaluated during site selection. Landslides can occur on slopes with weak or unstable materials, especially in areas of high rainfall or seismic activity. Sinkholes, often caused by the dissolution of soluble rocks such as limestone, can result in sudden ground collapse, while subsidence due to the extraction of groundwater or underground mining can lead to differential settlement and structural damage. Geohazard assessments involve geological mapping, remote sensing and geotechnical investigations to identify and quantify the risks associated with these natural phenomena. Mitigation measures, such as slope stabilisation, grouting or the avoidance of high-risk areas, may be necessary to reduce the potential impact of geohazards on the structure.

Note that in addition to geological factors, environmental considerations are increasingly important in geological site selection, particularly for projects located in sensitive areas or those with significant environmental impacts. Key environmental factors include ecological impact, water resources and ground contamination. The potential impact of construction activities on local ecosystems, including flora and fauna, must be assessed. This may involve environmental impact assessments (EIAs), habitat surveys and consultations with environmental agencies to ensure compliance with regulations and minimise ecological disruption. The availability and quality of water resources, including surface water and groundwater, are critical considerations. Construction activities can alter natural drainage patterns, affect water quality and reduce water availability for local communities. Mitigation measures, such as water management plans and pollution control strategies, are necessary to protect water resources. Sites with a history of industrial activity or waste disposal may have contaminated soils and rocks, posing a risk to human health and the environment.

Ground contamination assessments, including soil and rock sampling and chemical analysis, are essential for identifying and remediating contaminated areas before construction begins.

The ideal site for a dam should satisfy the following requirements:

- Presence of a narrow river valley with steeper, stable side slopes and a stable and impervious foundation and reservoir base area
- · Occurrence of bedrock at a shallow depth
- Absence of clay, thick overburden, fault and shear zones, extensive jointing with several sets, fractured and weathered formations, and anticlinal and synclinal structures
- Bedding planes and joints in formations, if present, should be dipping towards upstream or be horizontal to avoid loss of reservoir water through seepage, and to allow the resultant weight of the dam and reservoir water thrust to act almost normal to the bedding planes and joints
- Easy access to the site for the supply of materials during construction and for future maintenance

The ideal alignment for a tunnel should satisfy the following requirements:

- Straight alignment for ease of construction and cost efficiency
- Avoidance of fault zones, unstable or highly weathered rock, water-filled areas, high water table and landslide-prone regions
- Flexibility to introduce slight curves to bypass hazardous zones when necessary
- Minimal land acquisition issues and low environmental impact, and
- · Stability and safety maintained throughout the entire alignment

Note that the ideal requirements never exist at any project site, and hence proper ground/foundation treatments and other arrangements are often required for making the project successful.

A careful study of geological structures and orientation of rock beds is essential for selecting the most suitable sites for civil engineering structures, and it also helps in planning safe excavations of open pits, shafts, stopes and tunnels in civil and mining projects. For example, a site with horizontal rock beds is the most capable of supporting the weight of building structures, but such sites may not be an ideal for dams where water in the reservoir applies a horizontal force (thrust) on the dam embankment and sufficient seepage of water is expected, resulting in loss of reservoir water. Rock beds dipping upstream in the foundation may be the most competent to support the combined load R due to the weight (W) of the dam and thrust (T) from water in the reservoir, as illustrated in Figure 1.27. Additionally, such dipping rock beds do not generally allow the water in the reservoir to percolate below the dam. In fact, the percolating water flows upstream and returns to the reservoir area; thus, the reservoir does not lose much water due to seepage through the dam foundation. At the same time, the foundation remains watertight, and the dam is not subjected to any appreciable amount of uplift pressure.

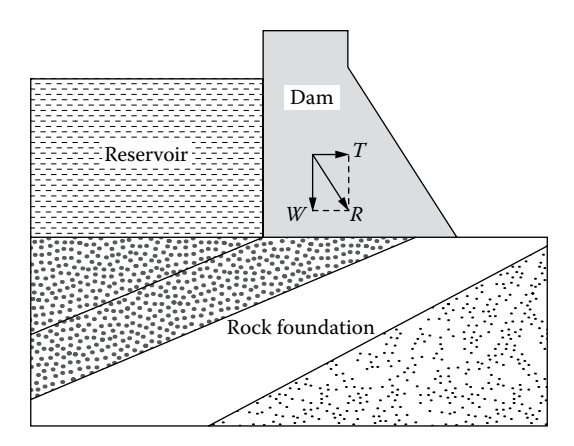


FIGURE 1.27 A dam resting on rock beds (rock foundation) dipping upstream.

In tunnels aligned along the strike of the strata, pressure tends to concentrate on one side, increasing the likelihood of rockfalls from the side where the beds dip into the tunnel. However, in tunnels crossing the strike and traversing beds of different rock types, the pressure is directed downwards from the roof. Water-related issues are more likely to occur in areas with porous rock layers.

In tunnels driven through synclinal folds, whether along or across the axis, joint blocks form inverted keystones in the arch, resulting in rockfalls and increased pressure on the roof and walls. If the rocks are water-bearing, water ingress can create significant challenges. Conversely, in tunnels aligned along or across the axis of an anticline, the risk of sudden rockfalls and water ingress is reduced, and the pressure on the roof and walls is generally lower.

Landslides in rock slopes are heavily influenced by the orientation of joints, bedding planes and other discontinuities. When these geological features are unfavourably oriented, they create planes of weakness, increasing the risk of slope failure. If bedding planes or joints dip in the same direction as the slope, known as 'daylighting', the likelihood of landslides rises, as rock blocks can slide along these planes under gravity. Additionally, steeply inclined joints or beds towards the slope face may lead to wedge failures where intersecting planes meet. Water infiltration further destabilises the slope by reducing friction along these planes, increasing pore pressure and triggering movement. Landslides are thus strongly governed by the structural geology and orientation of rock discontinuities.

By prioritising geological site selection with environmental considerations, project stakeholders can mitigate risks, reduce costs and ensure the long-term success of civil engineering and other infrastructure projects. In the past, several case studies have been reported to illustrate the importance of geological site selection.

The Tehri Dam is a multi-purpose rock and earth-fill embankment dam on the Bhagirathi River, a tributary of the Ganga, located in New Tehri, Tehri Garhwal district, Uttarakhand, India. Construction began in 1978 and was completed in 2006. The dam impounds a reservoir used for irrigation, municipal water supply and

hydroelectric power generation. With a height of 260.5 m, a crest length of 575 m, a base width of 1125 m at the riverbed and 20 m at the crest, it is one of the tallest dams in the world. The upstream and downstream slopes are designed at 1V:2.5H and 1V:2H, respectively (Singh, 2002; Adhikari, 2009). The dam is situated in the seismically active Himalayan region near the Main Central Thrust (MCT) fault. It is founded on Precambrian metamorphic rocks, including phyllites, quartzites and schists, which have moderate to good strength but are susceptible to weathering. The rock formations, which dip downstream, are intercalated with argillaceous and arenaceous bands (Gokhale, 2005). The area is prone to landslides due to steep slopes and fractured rocks. Extensive slope and foundation stabilisation, along with hydrogeological studies, were conducted to mitigate these risks. Reservoir-induced seismicity is a concern, and sediment deposition in the Bhagirathi River poses long-term challenges. The design of dam incorporates earthquake-resistant features to address seismic risks in this tectonically complex zone.

The world's tallest building, the Burj Khalifa, was constructed on a site with challenging geological conditions, including weak, compressible soils and high groundwater levels. The ground conditions consist of a horizontally stratified subsurface profile that is complex and highly variable due to the nature of deposition and the prevalent hot arid climatic conditions. Medium dense to very loose granular silty sands (marine deposits) are underlain by a succession of very weak to weak sandstone interbedded with weakly cemented sand, gypsiferous fine-grained sandstone/siltstone and weak to moderately weak conglomerate/calcisiltite (Poulos and Bunce, 2008). Extensive geotechnical investigations were conducted, and innovative foundation solutions, such as a deep piled raft foundation system and a cathodic protection system to prevent corrosion, were implemented to ensure the stability and longevity of the structure.

The Millennium Tower is a 58-story reinforced concrete building with one basement level (approximately 184 m tall) that was constructed in San Francisco, California, between 2005 and 2009. The Tower is founded on an embedded pile-supported mat, with pile tips bearing in dense marine deposits that overlie an over-consolidated marine clay layer known locally as Old Bay clay (Stewart et al., 2023). This has experienced significant settlement and tilting due to inadequate geological site selection and foundation design. The Tower began to settle during construction, and by approximately March 2008, settlements had exceeded the estimate in the original geotechnical report. The site, located on reclaimed land with poor soil conditions, required more robust foundation solutions, such as deeper piles or a mat foundation, to prevent the observed differential settlement.

The Hong Kong–Zhuhai–Macao Bridge (HZMB), constructed between 2009 and 2018, is the world's longest marine crossing, spanning 55 km across the Pearl River Estuary on China's southeast coast. It connects Hong Kong with Zhuhai and Macao and consists of islands, tunnels and bridges (Zhu et al., 2019). The complex marine environment, characterised by soft marine sediments, required meticulous geological site selection. Geotechnical investigations revealed soft alluvial clay, silty clay and loose marine sand overlying hard rock. To stabilise the bridge, deep cement mixing, ground improvement and large-diameter piles anchored in bedrock were employed. Approximately 130 bridge piers are supported by 1,100 rock-socketted piles, each about 100 m long, with precast pier and pile cap structures (Yeung, 2015).

1.12 SUMMARY

1. *Soils* and *rocks* are made up of small crystalline units known as minerals, and they constitute the Earth's crust (its thin outer shell). The crust is 30–35 km thick in continental regions and 5–6 km thick beneath oceans.

- 2. A mineral is basically a naturally occurring inorganic substance composed of one or more elements with a unique chemical composition and arrangement of elements (crystalline structure) and distinctive physical properties (colour, streak, hardness, cleavage, fracture, lustre, habit, tenacity, specific gravity, magnetism, odour, taste and feel). The hardness of minerals increases from 1 (for talc) to 10 (for diamond). Silica (quartz) and feldspars are the most common rock-forming minerals.
- 3. A rock is a hard, compact, naturally occurring earth material composed of one or more minerals, and is typically durable for engineering applications. Rocks generally require blasting for excavation and are classified into igneous (e.g. granite, basalt, rhyolite), sedimentary (e.g. sandstone, limestone, conglomerate) and metamorphic rocks (e.g. quartzite, slate, marble). Sedimentary rocks are generally less strong and durable compared to igneous and metamorphic rocks. In nature, one type of rock gradually transforms into another, forming the rock cycle. Rocks, whether shaped into dressed blocks or slabs (referred to as building stones) or used in other forms (known as building materials), are commonly utilised in civil engineering projects.
- 4. The strike of a plane is the direction of a line considered to be drawn along the plane so that it is horizontal. The line of maximum inclination on the inclined plane is called the line of dip. Dip direction (or dip azimuth) is the direction of the horizontal trace of the line of dip, expressed as an angle measured clockwise from north.
- 5. Folds are defined as wavy undulations developed in the rocks of the Earth's crust. Faults are fractures in crustal strata along which appreciable shear displacement of the adjacent rock blocks has occurred relative to each other, probably due to tectonic activities. Discontinuity is a collective term used for all structural breaks (e.g. bedding planes, fractures, joints) in solid geologic materials that usually have zero to low tensile strength.
- 6. Rocks exposed at the Earth's surface undergo continuous decay, disintegration and decomposition due to physical, chemical and biological agents. This process is known as weathering. Weathering increases rock porosity, weakens individual grains and breaks the bonds between mineral grains.
- 7. Soils are the result of interactions between five soil-forming factors: parent materials, topography, climate, organisms and time. Quartz that crystallises later that is, at lower temperatures during the formation of rocks from magma is the least weatherable mineral present in soils and rocks.
- 8. Earthquakes are vibrations induced in the Earth's crust that shake a part of the Earth's surface, along with all the structures and objects in that area. About 75% of all the earthquakes worldwide are shallow-focus earthquakes (with focal depths of less than 70 km). Seismic waves are categorised into two groups: surface waves (Rayleigh and Love waves) and body waves

- (P-waves and S-waves). In any given medium, P-waves always travel faster than S-waves.
- 9. The instrument used to detect and record seismic waves is called a seismograph, while the recorded data are known as seismograms. The intensity of an earthquake is a measure of the local level of ground shaking as estimated based on human perceptibility and its destructiveness. The magnitude of an earthquake is a quantitative measure of its size, based on the amplitude of elastic waves (P-waves) it generates, at known distances from the epicentre. The smallest felt earthquakes have magnitude of M = 2-2.5, the damaging earthquakes have M = 5 or more, and any earthquake greater than M = 7 is considered a major disaster.
- 10. Aquifers store large quantities of groundwater and are permeable enough to maintain a steady supply of water to wells or springs, either naturally or through pumping. Common aquifer materials include sand, gravel, sandstone, limestone, grit and conglomerate. Fault zones, shear zones, joints and similar features in igneous and metamorphic rocks can also function as aquifers.
- 11. Understanding petroleum geology is important for grasping hydrocarbon production, which involves multiphase flow through porous media. Essential factors for a reservoir include a source rock for hydrocarbon formation, a permeable carrier rock and a trap (reservoir rock) that contains and permits economic extraction of hydrocarbons. The economic viability of a reservoir is controlled by porosity, which measures fluid storage, and permeability, which measures fluid production rates. Reservoir rocks are usually sandstones and carbonates, while shales typically act as seal rocks, except in unconventional reservoirs.
- 12. A typical site investigation includes preliminary studies such as desk study and site reconnaissance, geophysical surveys, drilling of boreholes, in situ testing, sampling, laboratory testing of samples and groundwater observations and measurements. All the findings of the site investigation are presented to the client in the form of a site investigation report, which consists of a site plan, several boring logs that summarise the soil and rock properties at each test pit and borehole, and the associated laboratory and in situ test data.
- 13. Rotary drilling is the most rapid method of advancing boreholes in rock masses unless it is highly fissured. In bedrocks, core drilling to a depth of at least 3 m should be carried out. Geophysical investigations can optimise detailed exploration programmes by increasing ground coverage while reducing the need for extensive drilling and field testing.
- 14. Proper alignment of rock bedding planes is crucial for stability in dam foundations, tunnels and slopes. Rock beds dipping upstream provide ideal dam foundations, reducing the risk of sliding or failure and limiting the seepage through foundation. In tunnels along or across an anticline, favourable rock layer orientation minimises the risk of rockfalls and water ingress, lowering pressure on the roof and walls. During excavation, beds should dip away from the excavation to prevent destabilisation and reduce the risk of rockfalls.

REVIEW EXERCISES

Select the most appropriate answers to the following 15 multiple-choice questions:

- 1.1. The difference in equatorial and polar radii of the Earth is approximately
 - a. 0 km
 - b. 21 km
 - c. 42 km
 - d. 84 km
- 1.2. An acidic igneous rock has
 - a. a definite chemical composition
 - b. no definite chemical composition
 - c. silica content greater than 60%
 - d. both (b) and (c)
- 1.3. On Mohs scale, the hardness of gypsum is
 - a. 2
 - b 4
 - c. 6
 - d. 8
- 1.4. The ratio of the apparent dip to the true dip for a given bedding plane is
 - a. equal to 1
 - b. greater than 1
 - c. equal to or greater than 1
 - d. less than 1
- 1.5. Select the incorrect statement.
 - a. In anticlines, the older rock beds generally occupy a position in the interior (core) of the curvature.
 - b. The discontinuities in rocks make them anisotropic.
 - c. On a geological map, dashed lines represent the boundaries between the outcrops of rock beds.
 - d. None of the above
- 1.6. Which of the following minerals is the most weatherable?
 - a. Quartz
 - b. Olivine
 - c. Feldspar
 - d. Pyroxene
- 1.7. Which grade of the Mercalli scale of earthquake intensities corresponds roughly with the Richter earthquake magnitude M = 5?
 - a. II
 - b. IV
 - c. VI
 - d. VIII
- 1.8. S-waves pass through
 - a. solids
 - b. only solids
 - c. liquids
 - d. both solids and liquids

- 1.9. Rocks and soils having porosity but limited permeability are called
 - a. aquitards
 - b. aquifers
 - c. aquicludes
 - d. aquifuges
- 1.10. For site investigation purposes, the minimum depth of core drilling in bedrock is
 - a. 1 m
 - b. 3 m
 - c. 6 m
 - d. 9 m
- 1.11. Geohazard assessments involve
 - a. geological mapping
 - b. remote sensing
 - c. geotechnical investigation
 - d. all the above
- 1.12. Which of the following rocks is not a common hydrocarbon reservoir rock?
 - a. Sandstone
 - b. Shale
 - c. Limestone
 - d. Conglomerate
- 1.13. In an anticline trap, which one is at the bottom?
 - a. Water
 - b. Oil
 - c. Gas
 - d. Both oil and gas
- 1.14. Select the best tunnel alignment.
 - a. Tunnel axis along the axis of synclinal fold
 - b. Tunnel axis across the axis of synclinal fold
 - c. Tunnel axis along or across the axis of anticlinal fold
 - d. Tunnel axis along or across the axis of synclinal fold
- 1.15. Which of the following experienced significant settlement and tilting due to inadequate geological site selection and foundation design?
 - a. Millennium tower
 - b. Hong Kong-Zhuhai-Macao bridge
 - c. Tehri dam
 - d. Buri Khalifa
- 1.16. What is the difference between the continental crust and the oceanic crust?
- 1.17. How does the temperature vary within the Earth?
- 1.18. What are minerals? Enumerate the physical properties of minerals. Are coal and petroleum minerals?
- 1.19. How are minerals identified? Explain two common methods. How do you determine the hardness of a mineral?
- 1.20. What are the rock-forming processes? Explain the different types of rocks with some typical examples. How are rocks distinguished from each other?

1.21. What do you mean by rock cycle? Explain with the help of a neat sketch.

- 1.22. List the essential rock-forming minerals. Indicate the minerals common in igneous rocks.
- 1.23. Classify the following rock types in terms of igneous, sedimentary and metamorphic and indicate important minerals in each of them: granite, quartzite, basalt, sandstone, marble and limestone.
- 1.24. Name three metamorphic rocks and indicate the original rock prior to metamorphism in each case.
- 1.25. Define strike and dip. Also define other terms used to describe the orientation of a rock bed, discontinuity plane or sloping ground and explain them with the help of a neat sketch.
- 1.26. What are folds? Explain the different elements of a fold with the help of a neat sketch.
- 1.27. What are the differences between an anticline and a syncline? Explain briefly with the help of a neat sketch.
- 1.28. What are faults? Describe the different elements of the fault with the help of a neat sketch.
- 1.29. What are joints and how do they differ from faults and fractures?
- 1.30. What is unconformity? What does it signify? What is the most common rock type that is present at an unconformity? How is it presented in a geological map?
- 1.31. How are geological structures in rocks important in civil engineering practice? Explain briefly.
- 1.32. What is weathering? Describe the different processes of weathering.
- 1.33. Arrange the rock-forming minerals in an increasing sequence of their resistance to weathering.
- 1.34. What are the different grades of rock weathering?
- 1.35. How do soils form? What are clay minerals? Explain the different types of soil structure that affect their engineering behaviour.
- 1.36. What are the civil engineering considerations of weathering products?
- 1.37. How long would it take to completely erode Mount Everest, the highest peak in the Himalayas with a height of approximately 8,848 m above sea level, if the erosion rate is 5 mm per century?
- 1.38. What are earthquakes? Give an account of their main causes and effects. How are earthquakes classified?
- 1.39. Enumerate the different earthquake-related terms and explain them.
- 1.40. What are the differences between P-waves and S-waves? How does their ratio vary with Poisson's ratio of soils and rocks?
- 1.41. What is the difference between the intensity and magnitude of an earthquake? How are they defined and classified?
- 1.42. Consider the following for rock layer consisting of granite within the Earth's crust:

Bulk modulus of elasticity, K = 55 GPa

Shear modulus of elasticity, G = 35 GPa

Density, $\rho = 2750 \,\mathrm{kg} \,/\,\mathrm{m}^3$

Determine the P-wave and S-wave velocities.

- 1.43. If Poisson's ratio for rock mass in the oceanic crust is about 0.3, determine the ratio of P-wave velocity to S-wave velocity.
- 1.44. What are the special qualities of rocks that make them suitable for building stones and materials?
- 1.45. Define porosity. How is permeability different from porosity?
- 1.46. What are aquifers? What are their different types? Explain with the help of a neat sketch.
- 1.47. How is an aquifer different from an aquiclude, aquitard and aquifuge? Give two examples for each of them.
- 1.48. For a reservoir containing oil, water and gas phases, what is the constraint that the saturations for all three phases must satisfy?
- 1.49. Explain the basic objectives of site investigation. List the methods of site investigation.
- 1.50. What are the methods of surface and subsurface exploration for foundation rocks? Explain them briefly.
- 1.51. Explain the factors affecting the electrical resistivity of earth materials.
- 1.52. What is Archie's equation? Is it an empirical relationship? How does it define the formation resistivity of a porous medium that is partially saturated by an electrically conducting wetting phase?
- 1.53. Explain the procedure for the estimation of thickness of earth formations using the seismic refraction technique.
- 1.54. Discuss the effects of discontinuities on the selection of sites for dam projects.
- 1.55. What are the potential disadvantages of constructing dams in the Himalayan region?
- 1.56. What are the problems encountered during tunnelling in jointed rock masses?

Answers

- 1.1. b; 1.2. d; 1.3. a; 1.4. d; 1.5. c; 1.6. b; 1.7. c; 1.8. b; 1.9. a; 1.10. b; 1.11. d; 1.12. b; 1.13. d; 1.14. c; 1.15. a
- 1.37. Approximately 177 million years
- 1.42. 6 km/s, 3.568 km/s
- 143 187

REFERENCES

Adhikari, B.R. (2009). Tehri dam – an engineering marvel. *Hydro Nepal*, No. 5, pp. 26–30. Anson, R.W.W. and Hawkins, A.B. (1999). Analysis of a sample containing a shear surface from a recent landslip, south Cotswolds, UK. *Geotechnique*, Vol. 49, No. 1, pp. 33–41.

Archie, G.E. (1942). The electrical resistivity log as an aid in determining some reservoir characteristics. *Transactions of the American Institute of Mining and Metallurgical Engineers*, Vol. 146, pp. 54–62.

Bassiouni, Z. (1994). Theory, Measurement, and Interpretation of Well Logs. Society of Petroleum Engineers, Richardson, TX.

Bath, M. (1966). Earthquake seismology. Earth Science Reviews, Vol. 1, p. 69.

Bowen, N.L. (1922). The reaction principles in petrogenesis. *Journal of Geology*, Vol. 30, pp. 177–198.

Das, B.M. (2022). Principles of Geotechnical Engineering. 10th edition, Cengage Learning, Stamford.

- Das, B.M. and Ramana, G.V. (2011). Principles of Soil Dynamics. Cengage Learning, Stamford.
- Dobrin, M.B. (1976). *Introduction to Geophysical Prospecting*. McGraw-Hill Book Company, Inc., New York.
- Fanchi, J.R. and Christiansen, R.L. (2017). Introduction to Petroleum Engineering. Wiley, NJ. Gokhale, K.V.G.K. (2005). Principles of Engineering Geology. BS Publications, Hyderabad, India
- Grim, R.E. (1968). Clay Mineralogy. 2nd edition, McGraw-Hill Book Co, Inc., New York.
- Kearey, P., Brooks, M. and Hill, I. (2002). An Introduction to Geophysical Exploration. Blackwell Science Ltd., London.
- Little, A.L. (1969). The engineering classification of residual tropical soils. *Proceeding of the 7th International Conference on Soil Mechanics and Foundation Engineering*, Mexico, Vol. 1, pp. 1–10.
- Mukerjee, P.K. (1984). A Textbook of Geology. The World Press Private Limited, Kolkata.
- Poulos, H.G. and Bunce, G. (2008). Foundation design for the Burj Dubai the world's tallest building. *Proceedings of the 6th International Conference on Case Histories in Geotechnical Engineering*, Arlington, VA, Paper No. 1.47, pp. 1–16.
- Raymahashay, B.C. (1996). *Geochemistry for Hydrologists*. Allied Publishers Ltd., New Delhi. Richter, C.F. (1958). *Elementary Seismology*. W.H. Freeman, San Francisco, CA.
- Shukla, S.K. (2006). Subsoil Investigation for the Estimation of Load-Bearing Capacity of Foundation Soil at the Proposed Site for the Construction of a Coal Handling Plant (CHP), Northern Coalfields Limited, Gorbi, MP, India. A technical report dated 16 October 2006, Department of Civil Engineering, Institute of Technology, Banaras Hindu University, Varanasi, India.
- Shukla, S.K. (2007). Allowable Bearing Pressure for the Foundation Rock/Soil at km 0.080 of the Meja-Jirgo Link Canal for the Proposed Construction of a Hydraulic Structure (Head Regulator), Mirzapur, UP, India. A technical reported dated 11 June 2007, Department of Civil Engineering, Institute of Technology, Banaras Hindu University, Varanasi, India.
- Shukla, S.K. (2014). Core Principles of Soil Mechanics. ICE Publishing, London.
- Shukla, S.K. and Sivakugan, N. (2011). Site investigation and in situ tests, in *Geotechnical Engineering Handbook*, Das, B.M., editor, J. Ross Publishing, Inc., Fort Lauderdale, FL, pp. 10.1–10.78.
- Singh, A.K. (2002). Tehri Dam Project (Stage I) an overview. *ISH Journal of Hydraulic Engineering*, Vol. 8, No. 2, pp. 17–22.
- Sitharam, T.G. and Govidaraju, L. (2004). Geotechnical aspects and ground studies in Bhuj earthquake, India. *Geotechnical and Geological Engineering*, Vol. 22, pp. 439–455.
- Stewart, J.P., Wagner, N., Murphy, D., Butkovich, J., Largent, M., Nouri, H., Curran, H. Maffioli, D. and Egan, J.A. (2023). Foundation settlement and tilt of Millennium Tower in San Francisco, California. *Journal of Geotechnical and Geoenvironmental Engineering*, ASCE, Article No. 05023002, Vol. 149, No. 6, pp. 1–22.
- Tocher, D. (1958). Earthquake energy and ground breakage. *Bulletin, Seismological Society of America*, Vol. 48, No. 2, pp. 147–153.
- Waltham, T. (2002). Foundations of Engineering Geology. 2nd edition, Spon Press, London.
- Weinert, H.H. (1974). A climatic index of weathering and its application in road construction. *Geotechnique*, Vol. 24, No. 4, 475–488.
- Yeung, A.T. (2015). Geotechnical works of the Hong Kong-Zhuhai-Macao Bridge Project. Proceedings of the 15th Asian Regional Conference on Soil Mechanics and Geotechnical Engineering, Fukuoka, pp. 109–121.
- Zhu, Y., Lin, M., Meng, F. Liu, X. and Lin, W. (2019). The Hong Kong–Zhuhai–Macao bridge. *Engineering*, Vol. 5, pp. 10–14.

2 Spherical Presentation of Geological Data

2.1 INTRODUCTION

Construction activities on rocks have been reported several centuries ago. The applications include foundations, slope stability, underground excavations and so on. The early activities include structures and monuments built in Greece, Egypt, Iraq, India and China. Some of the notable examples are the Pyramids of Giza (twenty-sixth century BC), Abu Simbel temple (twelfth century BC), Hanging Gardens of Babylon (sixth century BC) and Parthenon (fifth century BC). Figure 2.1a shows the Parthenon temple on Acropolis Hill, Athens, Greece. It was built of marble on a limestone hill underlain by phyllites. Figure 2.1b shows the 6,300-m-long Corinth Canal in Greece, which has a depth varying up to 78 m. The Corinth Canal project started a few centuries BC, was abandoned, and later completed only in 1893.

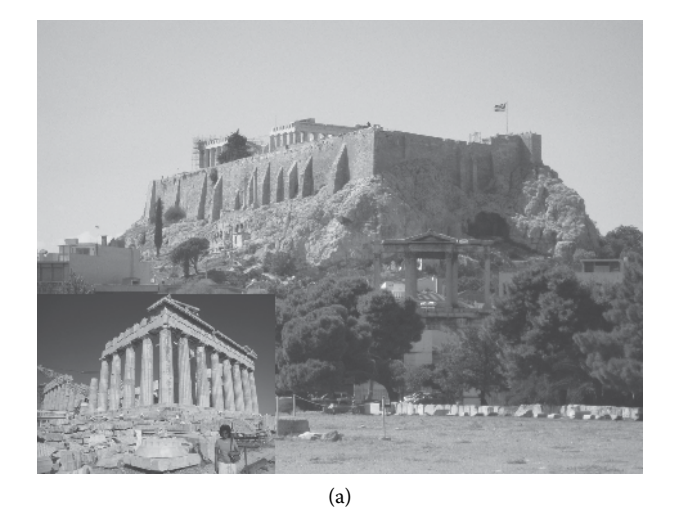
The term *rock mass* applies to a large extent of rock, from several metres to a few kilometres, which can include many *discontinuities* of different forms. The presence of discontinuities such as faults, joints and bedding planes in the rock mass, as described in Section 1.5 influences its engineering behaviour.

Our ability to present the orientations of the various discontinuities and their intersections, and to interpret them, is a prerequisite for carrying out a proper analysis of the rock mass behaviour. With the fundamentals of engineering geology covered in Chapter 1, we will continue the introduction to rock mechanics through this chapter on spherical presentation of geological data, which is a systematic method of presentation (e.g., orientation of the discontinuity planes as introduced in Section 1.5) that enables some simple stability analyses in engineering applications to be carried out.

2.2 ORIENTATIONS OF PLANES AND LINES

In rock mechanics and geology, we deal with *discontinuities*, which include bedding planes, faults and joints. It is very important to define the orientation of these planes without any ambiguity. Some of the common terms associated with the orientation of a plane are dip (ψ), dip direction (α) and strike. Dip, also known as the *true dip*, is the steepest inclination of the plane to the horizontal. Apparent dip is the inclination of any arbitrary line on the plane to the horizontal, which is always less than the true dip. When a marble is rolled down the plane, it follows the line of maximum inclination, defining the true dip. Strike is the *trace* (or intersection) of the dipping plane with the horizontal reference plane. It is also the orientation of the horizontal line drawn on the dipping plane. It is perpendicular to the dip direction.

DOI: 10.1201/9781032725161-2 57



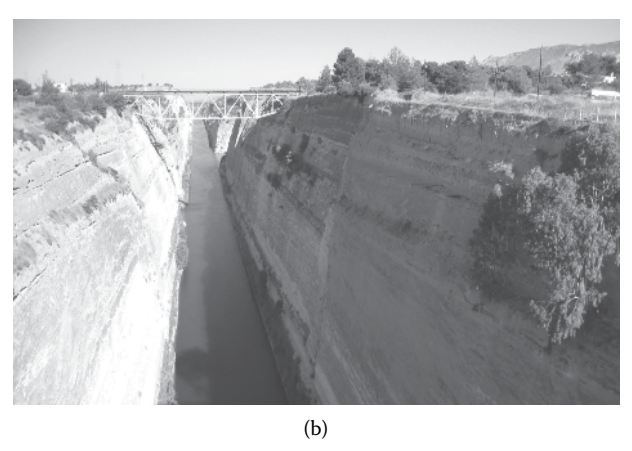


FIGURE 2.1 (a) Parthenon temple on Acropolis Hill, Athens, Greece, and (b) Corinth Canal, Greece.

Figure 2.2 shows an inclined plane (dark grey) for which we will define the dip and the dip direction. The inclined plane intersects the horizontal plane (light grey) along a horizontal line, which is known as the strike. The direction of the strike can be specified as N30E, for example, implying the line is at 30° to north on the eastern side. This is the same as S30W. If a marble is dropped from point O, it will travel along the steepest line OA on the slope, known as the *line of dip*, which is always perpendicular to the strike. Let us consider the vertical plane through OA, which intersects the horizontal plane along the line OB. The direction of OB with respect to north is the dip direction (α), which can be in the range of 0–360°. A plane dipping towards east has a dip direction of 90°. Dip direction, also known as $dip \ azimuth$, is the direction of the horizontal trace (projection) of the line of dip, measured

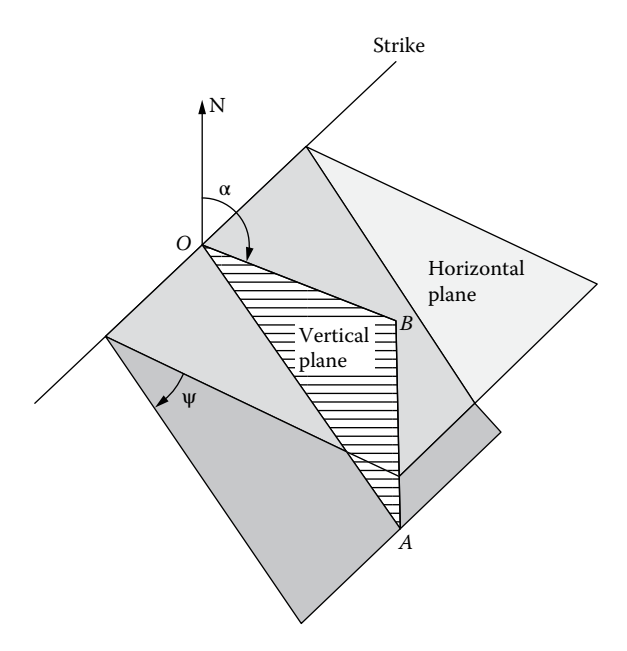


FIGURE 2.2 Definition of dip and dip direction.

clockwise from the north. Dip (ψ) is the angle the inclined plane makes with the horizontal, which is in the range of 0–90°. A horizontal plane has dip of 0° and a vertical plane has dip of 90°. A plane can be specified as 40/210, 20/080 and so on, where the angles before and after the slash denote the dip and the dip direction, respectively. The dip is specified in two digits and the dip direction in three digits to avoid confusion. Sometimes in literature, these two angles are interchanged, thus giving the dip direction first, followed by the dip.

True dip is measured perpendicularly to the strike, but when the strike is unknown, apparent dip is measured on any available vertical plane (Figure 2.3). As a consequence, apparent dip is always shallower than the true dip.

In the field, dip and dip direction of a plane can be measured by a geological compass, as shown in Figure 2.4. The measurement technique is fairly straightforward. The large horizontal dial is a compass that reads the dip direction, and the small vertical dial reads the dip.

When dealing with the axis of a borehole or a tunnel, or the intersection of two planes, we are dealing with *lines* and not planes. The orientation of a line is defined by *plunge* and *trend*. The plunge of a line (similar to the dip of a plane) is the inclination of the line to the horizontal. It is taken as positive when the line is below horizontal and negative when above horizontal. The trend (similar to dip direction) is the direction of the horizontal projection (or trace) of the line, measured clockwise from the north. The symbols (ψ and α) and the ranges are the same as before.

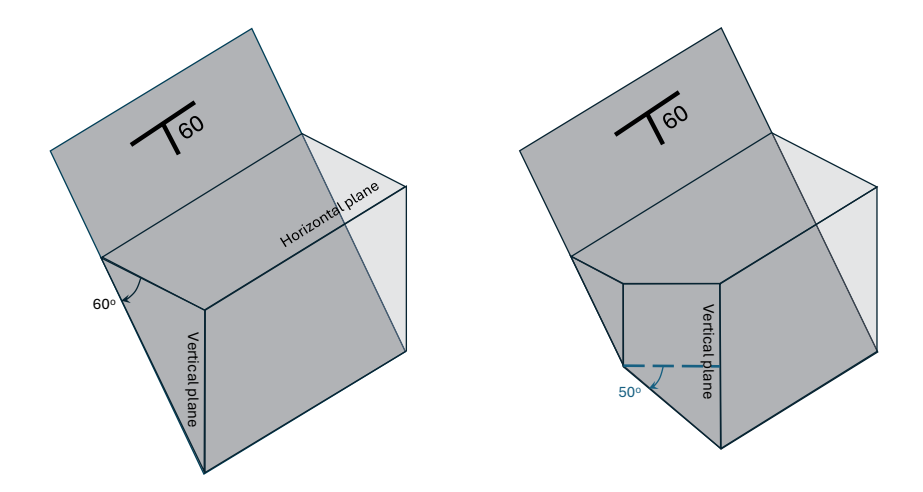


FIGURE 2.3 True dip (left) and apparent dip (right).

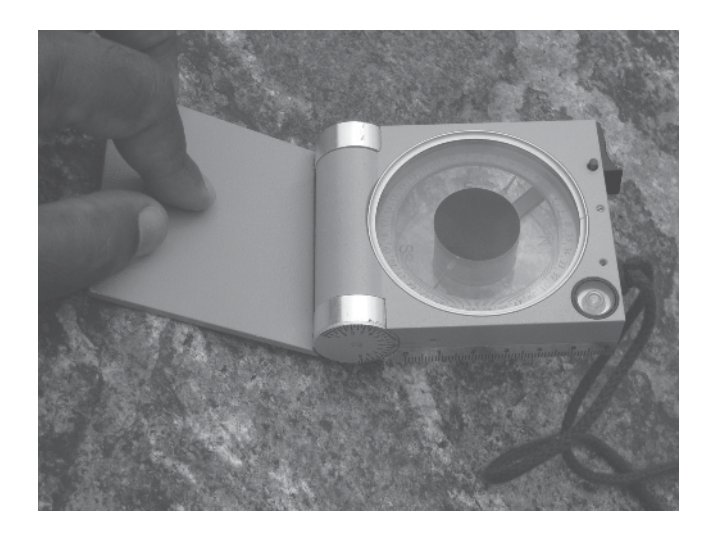


FIGURE 2.4 Geological compass.

2.3 COORDINATE SYSTEM WITH LONGITUDES AND LATITUDES

Spherical projections are used to graphically represent geological data such as the orientations of the bedding planes and other discontinuities. We look at the Earth as having *longitudes* (or *meridians*) and *latitudes* as shown in Figure 2.5, which are used to locate a point on the globe. It is, in fact, a 'coordinate system' that we will use in rock mechanics as well, but with some modifications. Meridians and latitude lines are perpendicular to each other.

Let us consider a *reference sphere*, shown in Figure 2.5, which will be used as the basis for the stereographic projection study. A peripheral circle, for which the centre

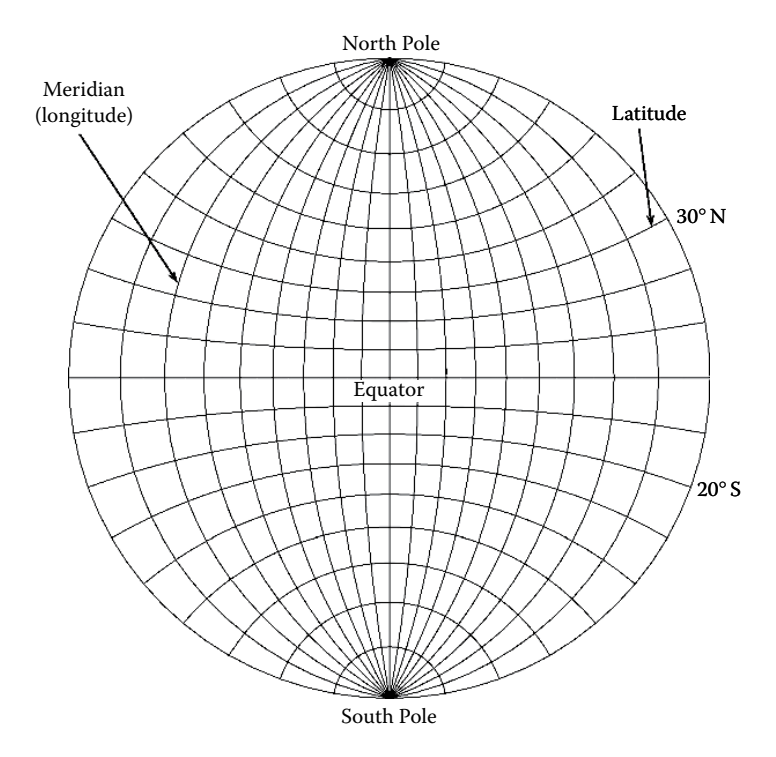


FIGURE 2.5 Reference sphere, longitudes and latitudes.

coincides with that of the reference sphere, is known as a *great circle*. It is formed at the intersection of a *diametric plane* and the sphere. It can be in any orientation, and there are thousands of great circles. Each line of longitude (or meridian) passes through the North and the South Poles and hence is part of a great circle. The *equator* is a line of latitude that divides the sphere along the *equatorial plane* into two halves – the upper and lower hemispheres. The equator is a great circle that corresponds to 0° latitude. All other lines of latitude are not great circles; they are *small circles* (see Figure 2.6). They are literally smaller than the great circles.

What does a 30°N line of latitude mean? A radial line to any point on the 30° line of latitude subtends 30° to horizontal at the centre, as shown in Figure 2.6. The equator is taken as the reference line for assigning latitudes such as 30°N, 20°S and so on. In the northern and southern hemispheres, latitudes can be in the range of 0–90°. In a similar manner, we have to select one of the longitudinal lines as the reference line and give the longitude of a point on the sphere as an angle in the range of 0–360° from this line. Remember, the longitudinal line that passes through Greenwich, England, is the reference line for defining the longitude of a city. In the global positioning system (GPS) in your car, you see these two values that define your current location on the globe.

In spherical projections, we have a simple coordinate system for locating a point (A) on a sphere. The coordinates are the latitude and the longitude, with the ranges

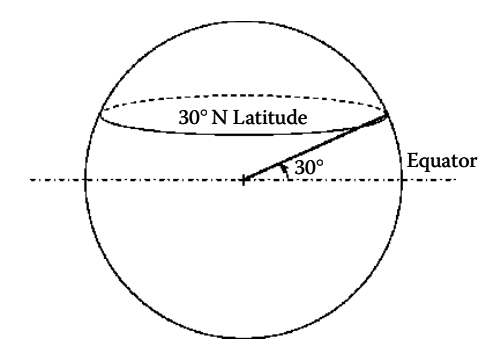


FIGURE 2.6 Definition of line of latitude.

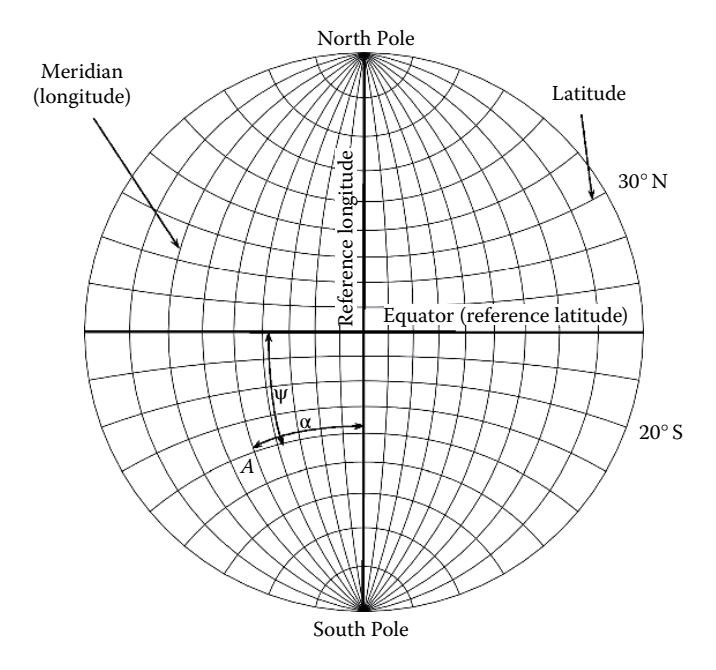


FIGURE 2.7 A simple coordinate system.

of 0– 90° (considering only one half) and 0– 360° , respectively. We have also shown that the dip (ψ) and the dip direction (α) of a plane have the same ranges. Let us see how we can use this coordinate system to represent the dip and the dip direction of a plane by the latitude and the longitude, respectively (Figure 2.7). We will be mainly using the lower half of the sphere below the equator.

2.4 INTERSECTION OF A PLANE AND A SPHERE

Figure 2.8 shows a plane passing through the centre of a *reference sphere* where the intersection is shown as a dark shaded circle. Such a circle, where the centre coincides with that of the sphere, is a great circle. The second horizontal great circle

shown as a dashed line is the one that separates the reference sphere into upper and lower halves. The lower half and the upper half of the reference sphere represent the same information about the plane, and hence, from now on, we will only refer to the *lower reference hemisphere* for simplicity. The intersection of the plane with the lower half of the reference hemisphere is shown in Figure 2.9. It can be seen that any plane with a specific dip (ψ) and dip direction (α) can be graphically presented using the lower reference hemisphere shown in Figure 2.9. For every plane, the intersection creates a unique great circle, representing the specific values of ψ and α . Let us see how we can do this more systematically and present this quantitatively.

Let us imagine that the lower reference sphere is shifted, without any rotation, to the location of the dipping plane of interest. The shifting is purely translational – that is, north remains north. The lower hemisphere is shifted until the plane passes through the centre of the hemisphere, making the plane diametrical (see Figures 2.8 and 2.9). The intersection of the plane and the *lower reference hemisphere* will define

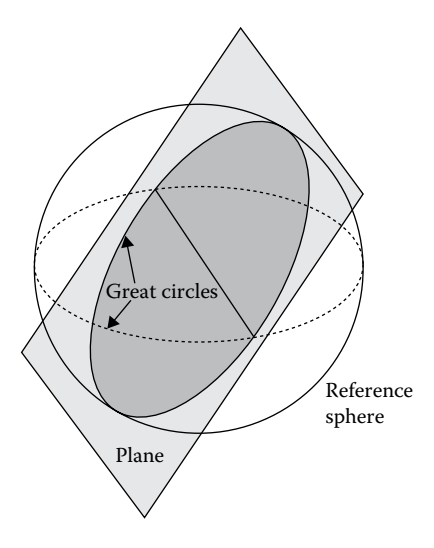


FIGURE 2.8 Intersection of a plane with reference hemisphere.

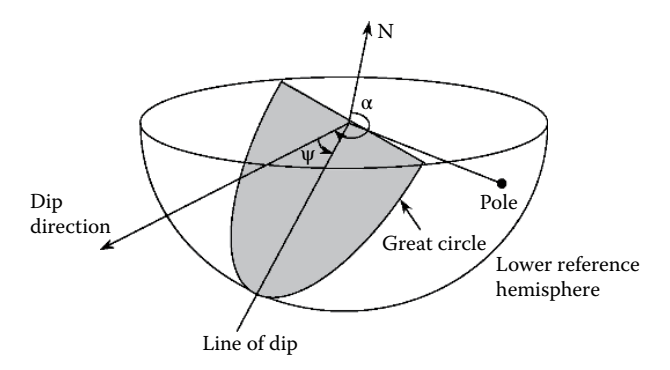


FIGURE 2.9 Intersection of the dipping plane with the lower reference hemisphere.

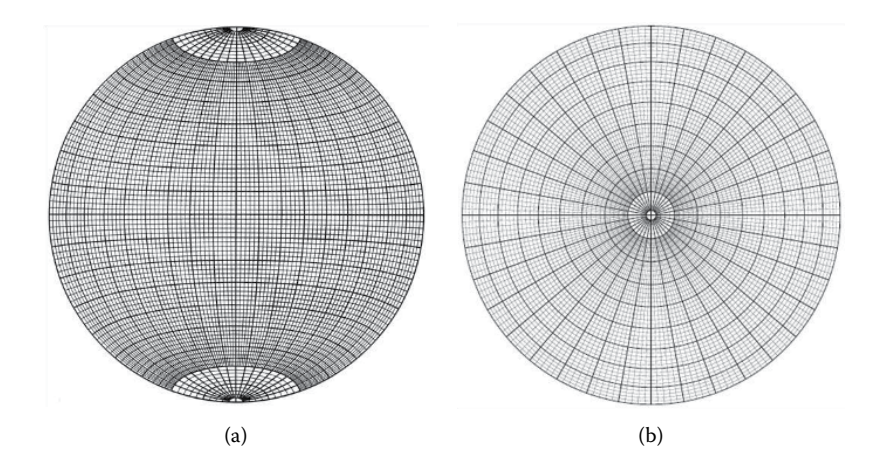


FIGURE 2.10 Stereonets: (a) front view – equatorial projection and (b) plan view – polar projection.

a unique great circle that reflects the dip and the dip direction of the plane in three-dimensional space. This also applies to lines, which are represented by points on the reference sphere through which they pierce. Here, the lower reference hemisphere is shifted without any rotation until the line of interest passes through the centre of the sphere. The intersection of the line at the surface of the lower reference hemisphere is known as the *pole of the line*. In Figure 2.9, the radial line, which is also normal to the plane, pierces the reference hemisphere at a point known as the *pole of the plane*. Every plane has a unique pole, and therefore, the pole itself can also be used to represent a plane.

Planes in three dimensions are represented in a lower reference hemisphere by a great circle or a pole. Lines are represented only by a pole. To present the three-dimensional data in two dimensions, the concept of spherical projections comes in handy.

The front view and the plan view of the reference sphere in Figure 2.5 are shown in Figure 2.10. The first (Figure 2.10a) is known as the *equatorial stereonet* or *meridional stereonet*, showing the two-dimensional projections of the longitudes and latitudes. The second (Figure 2.10b) is the *polar stereonet*, showing a series of concentric circles and radial lines, which are the same latitudes and longitudes, respectively, when projected onto a horizontal plane. The equatorial stereonet is used to present the projections of great circles, similar to the one in Figure 2.9, defining the dip (ψ) and the dip direction (α) of the corresponding plane. Poles can also be shown there. The polar stereonet is used to plot only the pole of a plane, which is adequate to fully define the plane.

2.5 SPHERICAL PROJECTIONS

We are all familiar with the plan view in engineering drawings, which we have seen in building plans, site layouts and so on. There are a few other ways of projecting the points on the surface of a sphere onto a horizontal or vertical plane. Two of the common methods of projection are (1) equal area projection and (2) equal angle

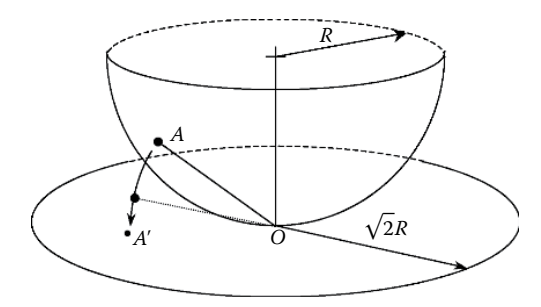


FIGURE 2.11 Equal area projection method.

projection. Both methods are good, but they should never be mixed because they are different. Analysing data originally plotted on an equal area net using an equal angle net, or vice versa, can lead to erroneous interpretations. Always note the type of projection used and avoid any confusion. From now on, we will use equal area projection.

We are gradually developing the skill of imagining the field situation in a three-dimensional space, which we can only present in two dimensions. This is a very important skill for mastering spherical projections.

2.5.1 EQUAL AREA PROJECTION

Equal area projection is sometimes called *Lambert* or *Schmidt* projection. The point A in Figure 2.11 is projected to A' on the horizontal plane at the bottom of the hemisphere by swinging an arc centred at O, the point of contact between the sphere and the horizontal plane (i.e. distance OA = OA'). In this way, every point on the lower hemisphere can be mapped onto a unique point on the horizontal plane. The furthest point from O is on the horizontal rim of the hemisphere, at a distance of $\sqrt{2}R$, and hence the projection area will have a radius of $\sqrt{2}R$. Think of peeling half an orange and leaving the skin on the table flat – it is similar. The surface area of the lower hemisphere is $2\pi R^2$. This is mapped onto an equal area on the horizontal plane in the form of a circle with a radius of $\sqrt{2}R$. An area on the lower hemisphere will have the same area when projected onto the horizontal plane, without any distortion, hence the name equal area projection. The equatorial and polar projections in Figure 2.10 are equal area projections.

2.5.2 EQUAL ANGLE PROJECTION

Equal angle projection is also known as *stereographic projection* or *Wulff projection*. The projection of a point A (or B) on the lower reference hemisphere onto the horizontal projection plane is defined as the point where the line OA (or OB) pierces the plane, as shown in Figure 2.12. Here, the point O is the top of the sphere, known as the *zenith*. An area on the lower hemisphere becomes distorted when projected onto the plane. An area of $2\pi R^2$ on the surface of the lower hemisphere is projected into an area of πR^2 on the horizontal. The extent of distortion depends on where the area

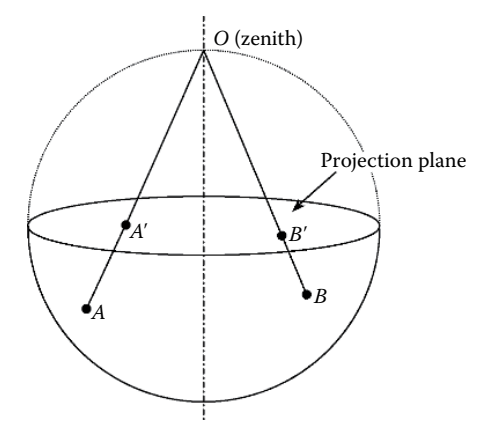


FIGURE 2.12 Equal angle projection method.

is located. The distortion is more for the regions closer to the projection plane. Computer programs usually use the following equations to convert the plunge ψ and trend α of a point to x and y Cartesian coordinates, given the radius of the stereonet is r:

$$\begin{cases} \text{Equal angle} & \begin{cases} x = r * \tan\left(\frac{\pi}{4} - \frac{\psi}{2}\right) \sin\left(\alpha\right) \\ y = r * \tan\left(\frac{\pi}{4} - \frac{\psi}{2}\right) \cos\left(\alpha\right) \end{cases} \tag{2.1a} \end{cases}$$
 Equal area
$$\begin{cases} x = \sqrt{2}r * \sin\left(\frac{\pi}{4} - \frac{\psi}{2}\right) \sin\left(\alpha\right) \\ y = \sqrt{2}r * \sin\left(\frac{\pi}{4} - \frac{\psi}{2}\right) \cos\left(\alpha\right) \end{cases} \tag{2.1c} \end{cases}$$

Equal area
$$\begin{cases} x = \sqrt{2}r * \sin\left(\frac{\pi}{4} - \frac{\psi}{2}\right) \sin(\alpha) & (2.1c) \\ y = \sqrt{2}r * \sin\left(\frac{\pi}{4} - \frac{\psi}{2}\right) \cos(\alpha) & (2.1d) \end{cases}$$

2.5.3 PROJECTIONS OF GREAT CIRCLES ON HORIZONTAL PLANES

A plane with dip ψ and dip direction α can be represented on a lower reference hemisphere by a great circle or its pole, as shown in Figure 2.9. The projections (equal area or equal angle) of this great circle and the pole onto the horizontal reference plane are shown in Figure 2.13. The two features that are important to note are as follows:

- 1. The larger/deeper the dip, the closer the projection of the great circle is to the centre.
- 2. The larger/deeper the dip, the further the pole is from the centre.

These are simple facts you will notice when looking at projections of great circles and poles.

The preceding two points are illustrated in Figure 2.14, which shows the projections of the great circles and poles representing different planes. The concept is the

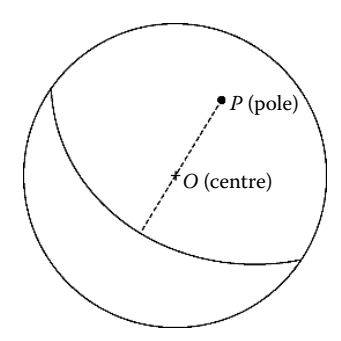


FIGURE 2.13 Projection of a great circle defining a plane.

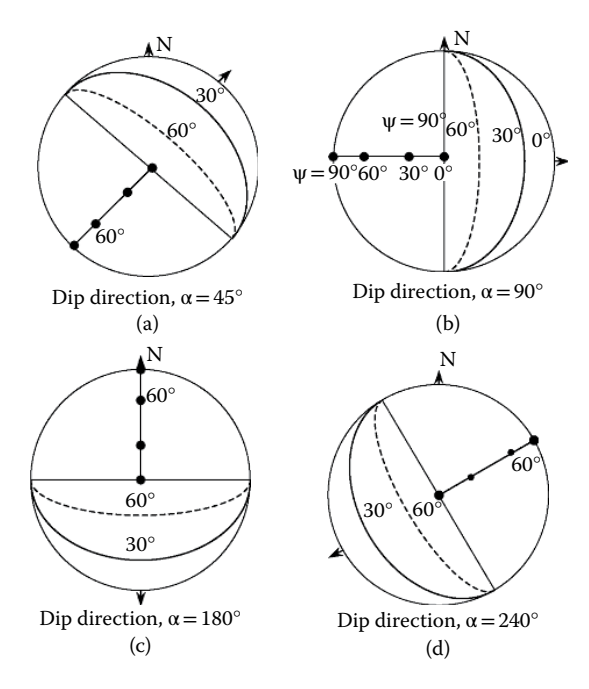


FIGURE 2.14 Projections of some great circles with different dip and dip directions: (a) $\alpha = 45^{\circ}$, (b) $\alpha = 90^{\circ}$, (c) $\alpha = 180^{\circ}$ and (d) $\alpha = 240^{\circ}$.

same for equal area or equal angle projections. Now let us see how we can use the equatorial and polar stereonets shown in Figure 2.10 (which are in fact equal area stereonets) to precisely define the orientation of a plane.

2.5.4 POLAR STEREONET

Polar stereonets are used only to plot the pole of a plane, which fully defines the orientation of the plane. A plane dipping towards the north will have its pole on a radial line towards the south, which corresponds to a dip direction of 0°. The steeper

the plane, the further the pole is from the centre. In the polar stereonet, dip (ψ) increases from 0° at the centre to 90° at the perimeter. The concentric circles and the radial lines in Figure 2.15 are at 2° intervals. The dips and the dip directions of the planes represented by poles A, B and C in Figure 2.15 are summarised in Table 2.1. When hundreds of poles representing various discontinuities are plotted, it is possible to identify their concentrations and hence simplify them into a few sets of discontinuities that may be easier to analyse. It is recommended to take at least 100 measurements of dip and dip directions in any attempt to identify the orientations of the discontinuities. If necessary, this can be increased further until a clear pattern emerges.

The types of discontinuities plotted in a *pole plot* can be distinguished by using different symbols. Hoek and Bray (1977) suggested using filled circles for faults, open circles for joints and triangles for bedding planes. These days, it is quite common to generate pole plots showing their concentrations and contours using computer programs such as DIPS developed by the University of Toronto and now available through Rocscience Inc.

Figure 2.16 shows a pole plot where 36 poles are for the bedding planes and 84 for joints. A close look at the figure clearly shows the pole concentrations and enables one to identify the approximate bedding plane orientation as 30/150, and the orientations of the two joint sets, J1 and J2, as 65/240 and 85/340, respectively. The joints in

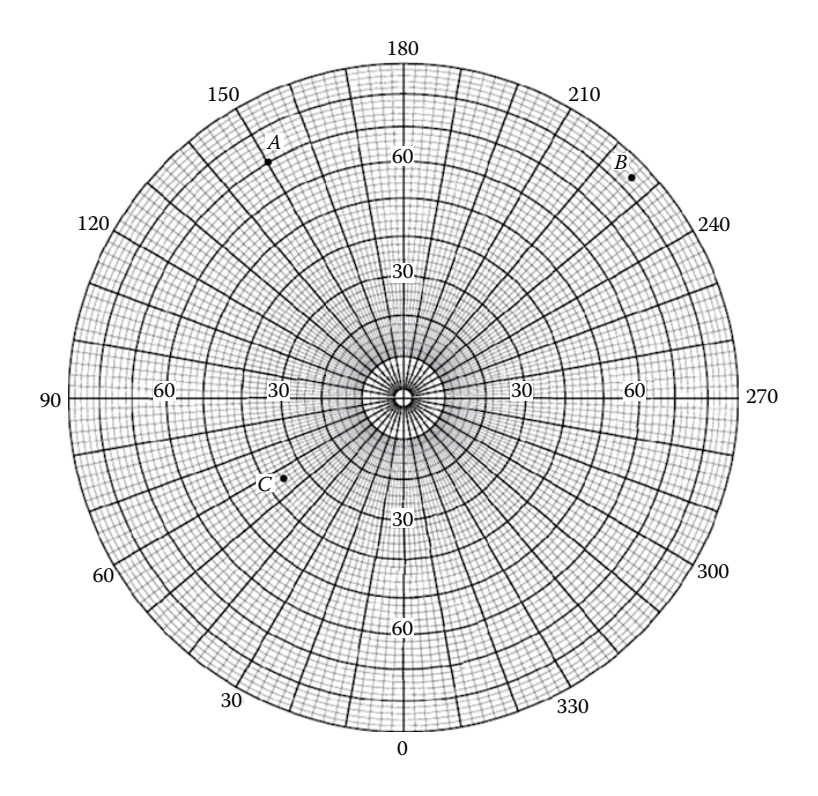


FIGURE 2.15 Equal area polar stereonet showing the poles of three planes.

TABLE 2.1

Dips and Dip Directions of the Planes
Represented by Poles A, B and C

Pole	Dip, ψ (°)	Dip direction, α (°)
A	70	150.5
В	84	226
C	35.5	56

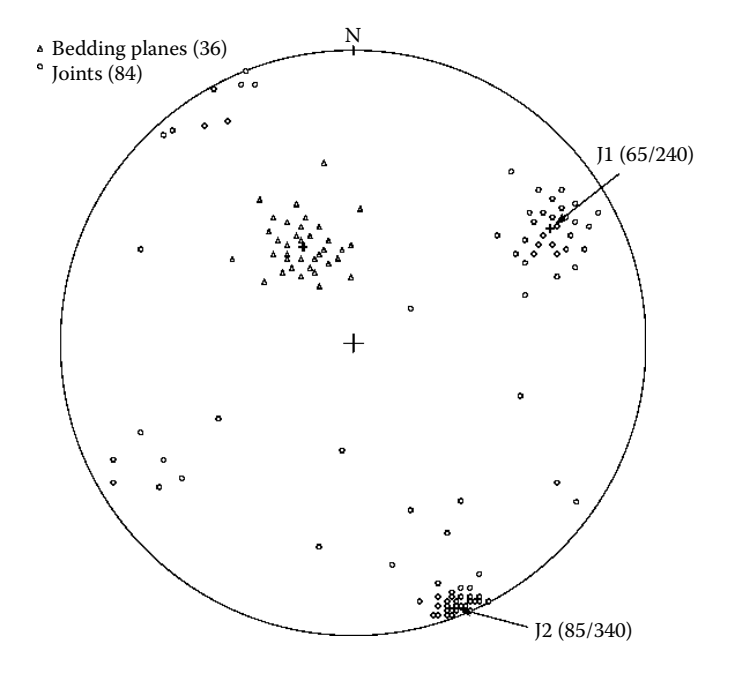


FIGURE 2.16 A pole plot.

J2 are close to being vertical and hence some of them appear on the opposite side of the pole plot. The thick crosshair shows the average orientation of the bedding plane or joint set.

Figure 2.17 shows the isometric view of the bedding plane and the two other discontinuity planes reflecting the joint sets J1 and J2 in Figure 2.16. The lines of intersection between two planes can be visualised, at least qualitatively, through such isometric views. However, pole diagrams and spherical projections make this work much simpler. When the situation is more complex, it is difficult to draw such isometric views.

As a joint set may vary its orientation slightly due to the fracture of rock, it will be plotted as a cluster of points in the pole plot. Pole concentration is calculated as the percentage of observed poles falling within a counting circle around the calculated

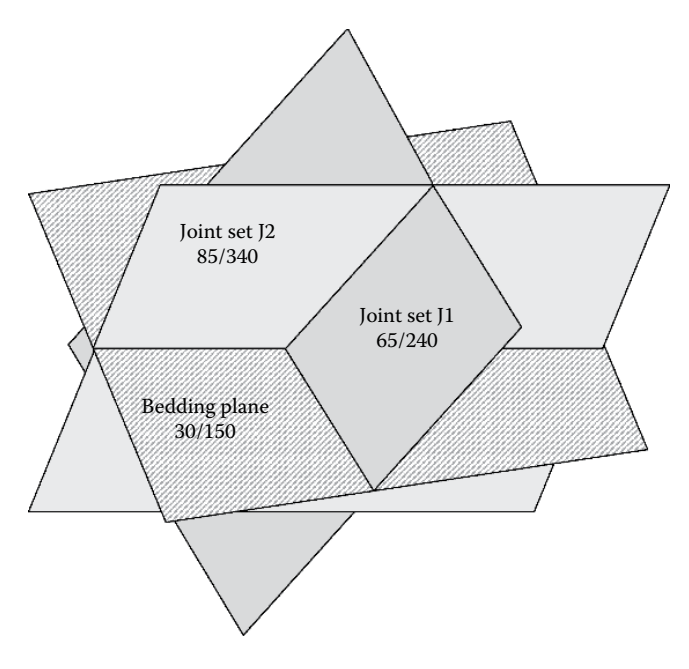


FIGURE 2.17 Isometric view of the bedding plane (30/150) and joint sets J1 (65/240) and J2 (85/340).

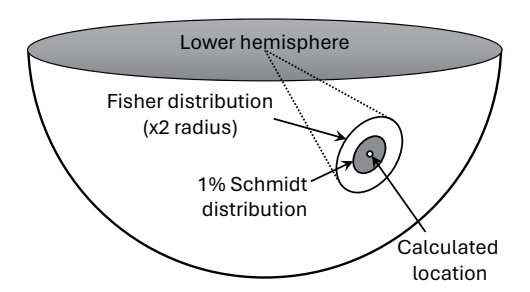


FIGURE 2.18 Counting circles for pole concentration calculation.

location. In the Schmidt distribution (Figure 2.18), the counting circle occupies 1% of the lower hemisphere surface, which is $2\pi r^2$. Therefore, the solid angle of the counting circle is 0.06282 steradians. The Fisher distribution employs a similar concept, with the radius of the counting circle being twice that in the Schmidt distribution (Goodman, 1989). Automatic detection of joint sets computes pole concentration for each point on a stereonet and marks a contour of high pole concentration around each cluster. If the clusters are distinct, these contours can be marked easily by hand.

EXAMPLE 2.1

A long cutting is to be made into a hillside with a slope of 70° to the horizontal. The strike of the slope will have an orientation of 30° from north, with the slope falling towards the east. A site investigation exercise at a weathered claystone site produced the following set of measurements for rock bedding and joint orientations.

44/052, 48/052, 48/306, 60/162, 37/130, 52/314, 32/140, 30/290, 26/123, 42/050, 32/130, 52/134, 44/048, 28/126, 68/074, 64/126, 32/124, 48/046, 40/056, 48/300, 46/308, 24/133, 34/120, 60/015, 44/242, 46/308, 52/312, 46/054, 44/208, 44/058 55/306, 46/314, 46/044, 54/305, 46/304, 44/044

Develop a pole plot showing all the above data and identify the number of joint/ bedding plane sets. Derive representative orientations for each of the discontinuity sets you have identified.

Solution

The dips and the dip directions of the 36 readings given earlier are plotted as shown in Figure 2.19.

It is quite clear that there are three sets of discontinuities J1, J2 and J3 with orientations of 30/129, 44/050 and 50/307, respectively. There is some scatter, which is always to be expected.

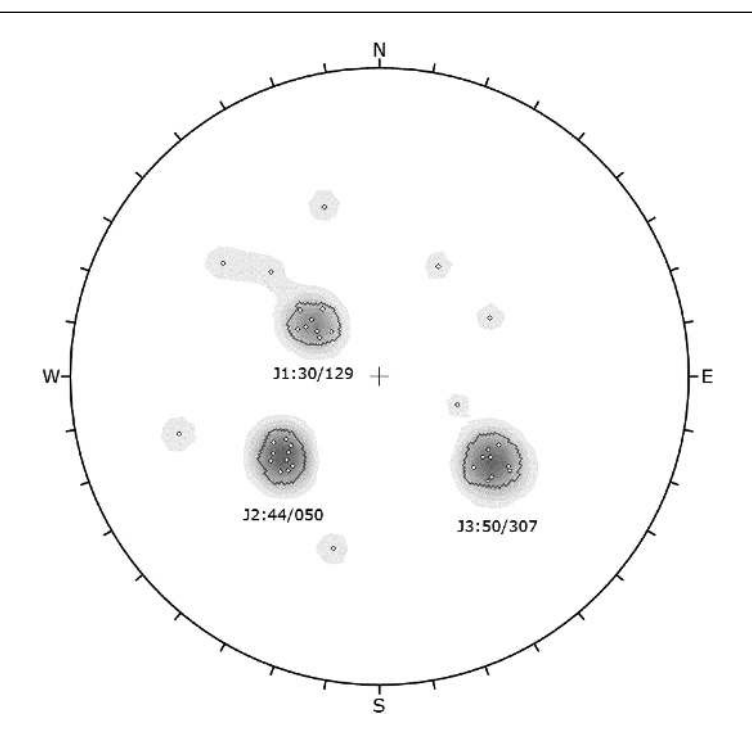


FIGURE 2.19 Pole plot for Example 2.1.

2.5.5 EQUATORIAL STEREONET

The equatorial projection of the reference sphere shown in Figure 2.10a is reused in Figure 2.20, with some additional labels. Note that we now use this in *plain view* (not front elevation), with north, south, east and west directions marked. Also shown in Figure 2.20 are the angles $0{\text -}360^\circ$, marked along the circumference, reflecting the dip direction of the plane. These are marked along the latitude lines. All meridional lines from north to south reflect the exact locations of the projections of the great circles representing planes dipping at angles of $0{\text -}90^\circ$ towards the east or west. We will use these inner meridional lines to precisely draw the projections of great circles of planes dipping at directions that are not necessarily east or west.

Equatorial stereonets can be used to represent planes and their poles. The poles plotted on a polar net fall in the same positions as those plotted on an equatorial net. Therefore, once a pole is marked on tracing paper placed on top of an equatorial stereonet, it can be verified later by overlaying it on a polar stereonet.

The great circles representing the planes (i.e. the intersection of the plane with the lower reference hemisphere) are projected onto a horizontal plane by the equal area or equal angle projection method. This is best done using a tracing paper, a pin and an equatorial stereonet. This is illustrated here through an example showing a plane with $\psi = 35^{\circ}$ and $\alpha = 135^{\circ}$.

- Step 1. Place tracing paper over an equatorial net and fix a pin (e.g. thumb tack) at the centre.
- Step 2. Trace the circumference of the net and mark north as N on the tracing paper.

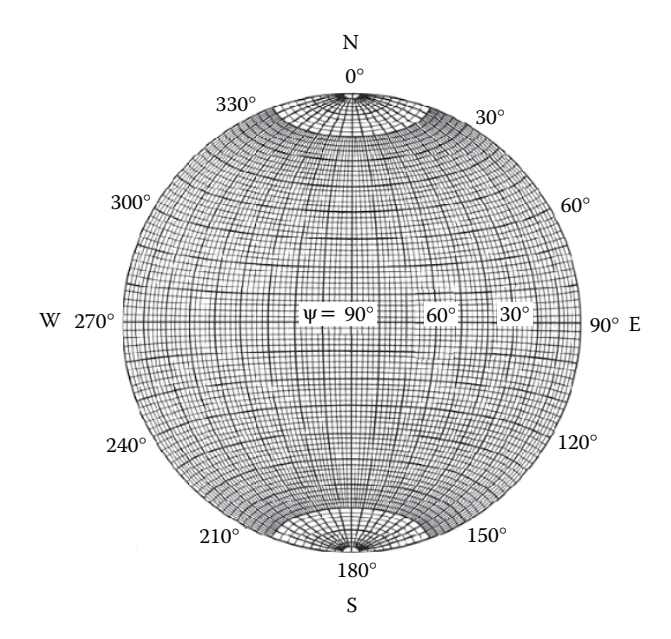


FIGURE 2.20 Equal area equatorial stereonet.

- Step 3. Count $\alpha = 135^{\circ}$ along the perimeter and mark the point X on the tracing paper. This is the line of latitude corresponding to 135° .
- Step 4. Rotate the tracing paper such that point X lies on the E–W axis, so that we can draw the projection of the great circle (that dips at 35°) precisely.
- Step 5. Trace the meridional circle corresponding to $\psi = 35^{\circ}$. Mark the pole P on the tracing paper, counting $\psi = 35^{\circ}$ from the centre. Remember, the pole of a horizontal plane is at the centre, and for a vertical plane, it is at the perimeter.
- Step 6. Rotate the tracing paper back to its original position so that the 'north mark' N on the tracing coincides with the north on the equatorial stereonet underneath. The great circle and the pole are now in their correct locations (see Figure 2.21).

Following the preceding steps, it is possible to draw on the same sheet (i.e. tracing paper) any number of great circles, representing different planes. The corresponding poles can also be marked.

A pair of decent stereonets – both polar and equatorial – is the basis for the stereographic projection studies and kinematic analysis discussed in this chapter. These are given in Appendix. A high-resolution stereonet could be printed with the following Python code:

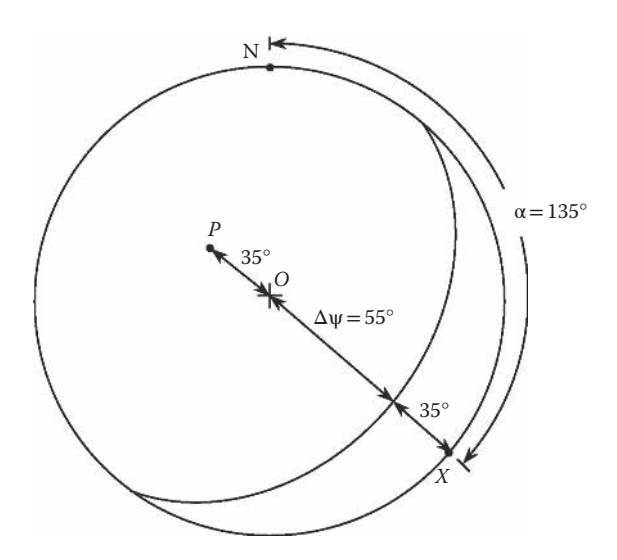


FIGURE 2.21 Representing a plane ($\psi = 35^{\circ}$, $\alpha = 135^{\circ}$) using an equatorial stereonet.

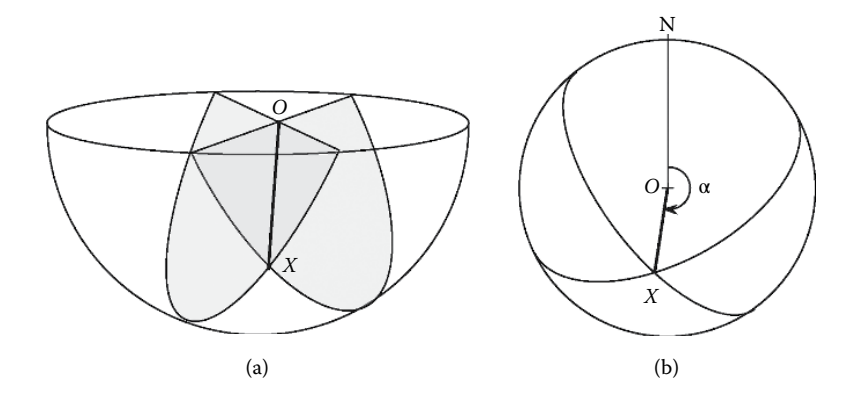


FIGURE 2.22 Line of intersection between two planes: (a) reference hemisphere and (b) projection.

2.5.6 Intersection of Two Planes

The discontinuities are often approximated as planes. These planar discontinuities, such as faults, joints and bedding planes, intersect along straight lines. Now that we have mapped these discontinuities, we should find a way to determine the orientation of the line of intersection between two planes. Figure 2.22a shows two intersecting planes on a lower reference hemisphere. O is the centre of the reference hemisphere, which also lies on both planes. The two planes intersect each other along a straight line that meets the reference hemisphere at X. Therefore, the radial line OX is the line of intersection of the two planes. By mapping the two great circles representing the planes (see Figure 2.22b), their intersection point X can be defined. The plunge (ψ) and the trend (α) of the line of intersection OX can be determined by following the same steps outlined previously. Rotating Figure 2.22b about the centre O so that OX lies on the E–W line enables determination of the plunge ψ of the line of intersection. Extending OX to intersect the circumference (i.e. the correct latitude line) enables determination of the trend α , which is measured from north, as shown in Figure 2.22b.

EXAMPLE 2.2

Find the plunge and trend of the line of intersection between the planes 40/140 and 59/250.

Solution

The steps in the graphical procedure are as follows:

- Place tracing paper on top of an equatorial stereonet with a pin at the centre O.
- Trace the circumference and mark north as 'N'. Mark A ($\alpha = 140^{\circ}$) and B ($\alpha = 250^{\circ}$) on the perimeter.
- Plot the two great circles following the procedure outlined earlier and note their intersection point X.

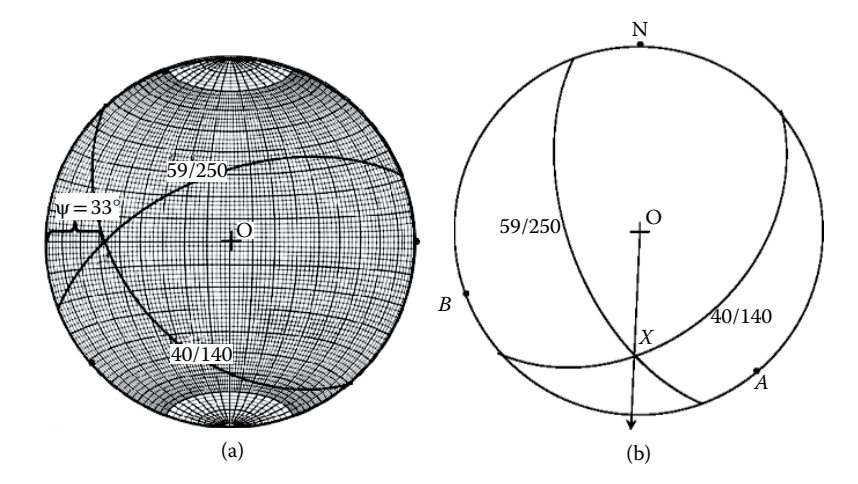


FIGURE 2.23 Solution to Example 2.2 – plunge and trend of the line of intersection: (a) determining dip and (b) determining dip direction.

- Rotate the tracing paper until the point X lies on the E–W line on the equatorial stereonet.
- Measure the plunge (ψ) as 33°, as shown in Figure 2.23a.
- Rotate the tracing paper back to its original position, ensuring that the 'N'
 mark on the tracing paper aligns with the north direction on the equatorial
 stereonet underneath.
- The line *OX* defines the trend (direction) of the line, and its intersection at the circumference defines the trend as 184°, as shown in Figure 2.23b.

2.5.7 Angle between Two Lines (Or Planes)

The angle between two planes is the same as the angle between the two radial lines connecting the poles to the centre. In spherical projection, a line is generally represented by its pole, reflecting the plunge and trend. The procedure for measuring the angle between two lines is described in the following example.

EXAMPLE 2.3

Find the angle between two intersecting lines: 20/120 and 60/230.

Solution

The steps are outlined as follows:

- 1. Define the line 20/120 (A) with $\psi = 20^{\circ}$ and $\alpha = 120^{\circ}$, following a procedure similar to that for locating the pole of a plane (see steps 2 through 6).
- 2. Place tracing paper on top of an equatorial stereonet and fix a centre pin. Trace the circumference and mark the centre as *O* and north as N (Figure 2.24a).

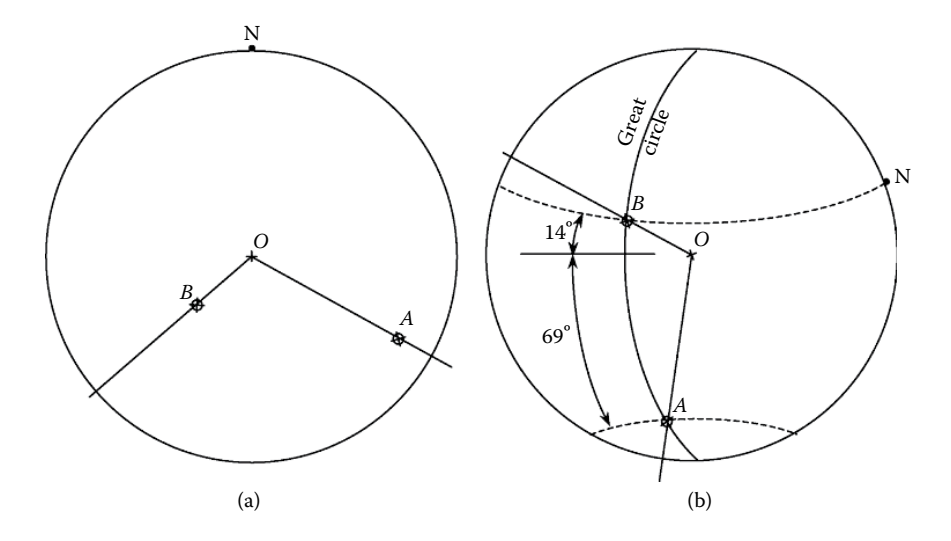


FIGURE 2.24 Solution to Example 2.3 – angle between two lines: (a) defining the lines and (b) determining the angle between the lines.

- 3. Locate $\alpha = 120^{\circ}$ on the perimeter, defining the trend of the above plane. Draw a radial line through this point.
- 4. Rotate the tracing paper anticlockwise such that the above radial line lies on the E–W line. Count $\psi = 20^{\circ}$ from the outer circle and mark the point A. Remember, the larger the plunge, the closer the point is to the centre.
- 5. Rotate the tracing paper back to its original position such that the mark 'N' coincides with north on the equatorial stereonet underneath. Now, the point *A* correctly represents the line 20/120 (see Figure 2.24a).
- 6. Repeat steps 3–5 for locating the plane 60/230, represented by point *B* (see Figure 2.24a).
- 7. Rotate the tracing paper until the two points *A* and *B* lie on the *same* meridional great circle (Figure 2.24b). Measure the angle between the two lines by counting the difference in the latitudes of *A* and *B* along the great circle. In this example, *A* is 69°S and *B* is 14°N. Therefore, the angle between the two lines *OA* and *OB* is 82°.
- 8. Rotate the tracing paper back to its original position so that the mark 'N' coincides with north on the equatorial stereonet underneath. The great circle in Figure 2.24b represents the plane that contains the two lines. The dip and the dip direction of this plane can be determined easily.

2.5.8 FAULT ESTIMATION

A frequent problem in rock mechanics is the identification of a fault plane inside a rock mass if traces are observed on rock surfaces. If the fault plane daylights onto two surfaces, two separate intersection lines could be measured and represented by two points with respective plunge and trend. The graphical solution just draws a great circle going through these two points.

EXAMPLE 2.4

Due to blasting at a copper mine, a rock fault was recently developed. Two intersections with knowns fault planes were observed at 60/225 and 45/105. Determine the new fault.

Solution

The steps are outlined as follows:

- 1. Locate the intersection lines as two points on the grid (Figure 2.25).
- 2. Rotate the tracing paper so that the two points are on the great circle. Draw this great circle.
- 3. Mark the middle line and read the dip from the reference circle.
- Rotate the tracing paper back to its original position. Read the direction of the great circle.

In general, hand-drawn solutions may have inaccuracies due to several factors. The dimension of the stereonet, transparency of the tracing paper and sharpness of the pencil have some remarkable impacts on the accuracy of the traces. Inevitably, the tack, punching through at the centre of the stereonet, may enlarge the hole after a few rotations. Therefore, a tolerance of 3° is often assumed for hand-drawn solutions (To and Sivakugan, 2023).

In underground excavation, it is frequent that only one trace is observed due to the limited exposure. However, the fault plane still could be estimated if its dip angle or direction is known with the use of geological compass.

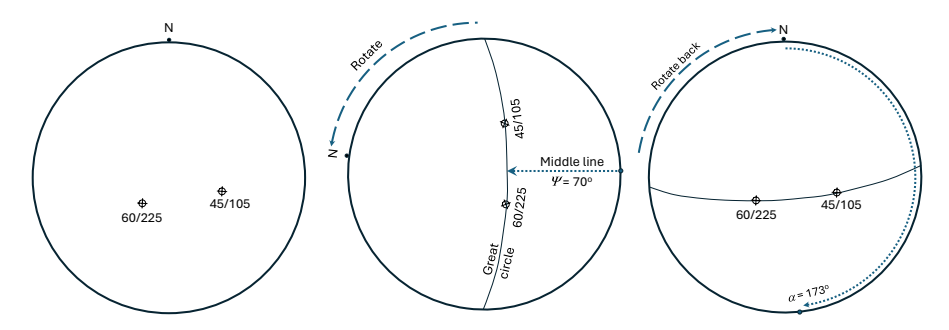


FIGURE 2.25 Solution to Example 2.4: Identifying a fault plane containing two intersection lines.

EXAMPLE 2.5

A visual investigation for an underground mine slope 60/250 showed that there might be an existing joint set. When a geo-compass was placed in the rock aperture, the dip angle was read from side inclinator at 52°. However, the dip direction could not be estimated as there was not enough space to look at the geo-compass from the top. Nevertheless, it seems that the joint set trends to the northern side. The trace on the slope has a plunge of 44° and also runs to the northern side. Identify the new joint set.

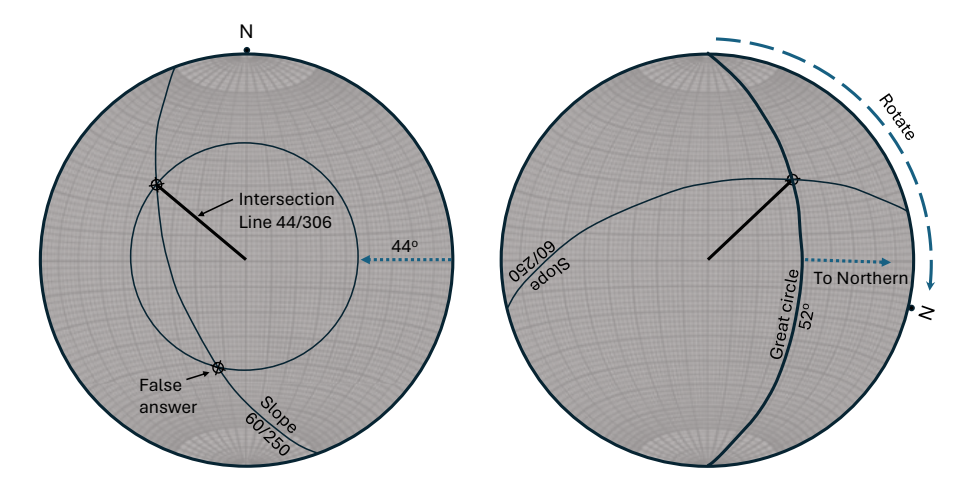


FIGURE 2.26 Solution to Example 2.5: Identify a faulty plane with missing information.

Solution

The steps are outlined as follows:

- 1. Draw a great circle to represent the mine slope 60/250 (Figure 2.26)
- 2. Using compass, draw a circle at the dip of 44°. This circle intersects the great circle of the slope at two points.
 - Hint: To avoid using a compass, mark the dip of 44° to the east on the stereonet under the tracing paper. Rotate the tracing paper until the time the point is underneath the great circle of the mine slope. Then mark the two intersection points.
- Select and mark the point in the northern half. This point represents the trace.
- 4. Rotate the tracing paper so that the point is on the great circle with a dip angle of 52°.
- 5. There will be four possible answers (85°, 167°, 265° and 347°). Two answers are just the duplication to the other side and can be eliminated. With the remaining two answers, select and draw the great circle trending to the northern half.
- Count the dip direction of the identified great circle. The fault plane should be 52/347.

2.5.8.1 Software Applications

Modern rock mechanics often deal with massive information from rock scans. Engineers often represent the entire data range with a single mean value if the range is narrow. When the values vary widely, automatic computation with software is a must. In terms of access, computer programs can be classified as open source or commercial. This chapter briefly introduces Stereonet 11 and Dips 8.0 as two representatives.

Stereonet 11 is a very popular freeware introduced in many universities as a powerful computational tool for assignments in Rock Mechanics. It was created by Prof. Richard Allmendinger and his colleagues. The installation can be downloaded from his personal website (Allmendiger, 2012):

https://www.rickallmendinger.net/stereonet

Stereonet 11 has four different formats to import files from different scanning devices. By default, Stereonet presents a plane with dip angle and strike, where the dip direction is minus 90°. This way, the dip azimuth is always to the right if one looks along the strike. After importing data, values can be converted to dip angle and direction as usual, or to any other format. Lines in Stereonet can only be imported with trend and plunge. However, there is an option to enter a line on a plane via the 'rake' option (Figure 2.27). Cones and arcs can be drawn to assist with kinematic analysis, which will be described later in this chapter. One advantage of Stereonet 11 is its 3D view, which is helpful for rock analysis with a 3D perspective.

Example 2.2 can be calculated automatically. From the *Main Menu* \rightarrow select the *Calculations* tab \rightarrow select *Two Plane Calculations* \rightarrow enter the planes' strike and dip

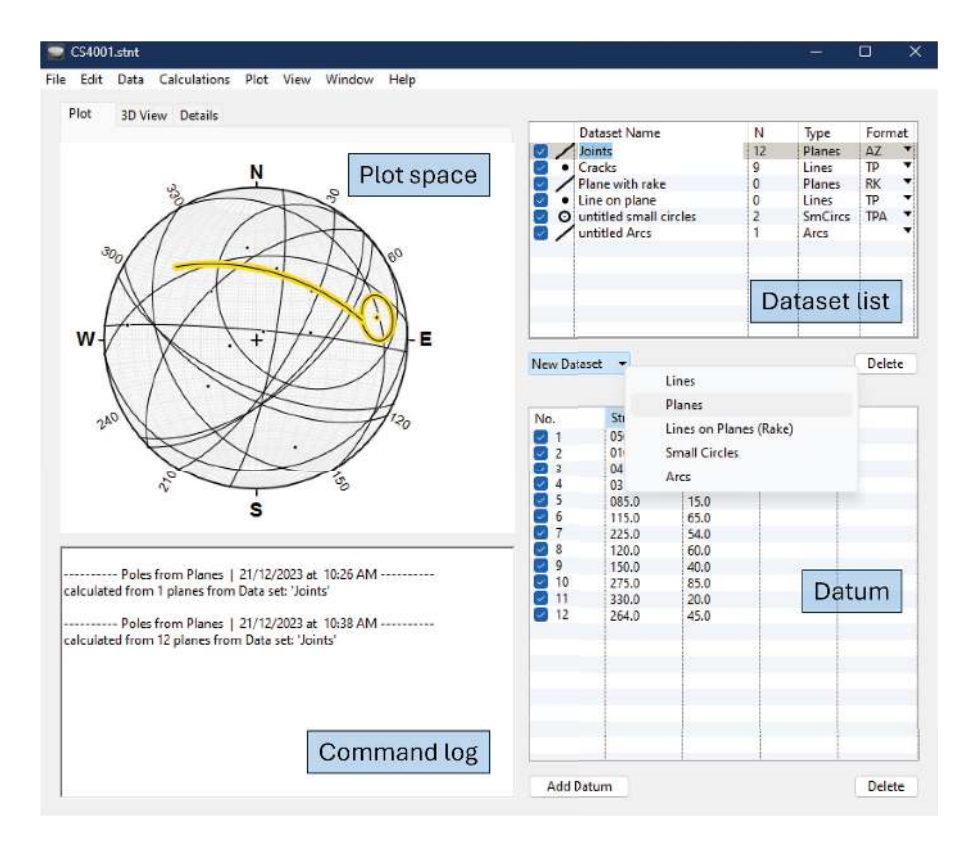


FIGURE 2.27 Interface of Stereonet 11.

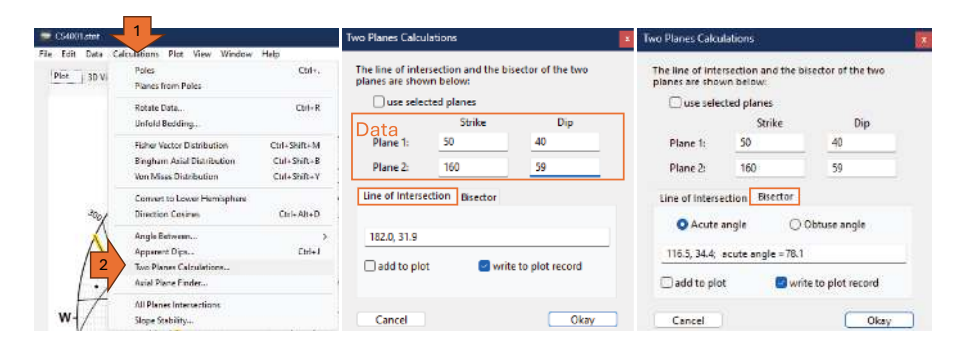


FIGURE 2.28 Solution to Example 2.2 with Stereonet 11.

(Figure 2.28). The strike and dip of the intersection line will be shown automatically when all required data is filled. It is important to repeat that, in Stereonet 11, strike is dip direction minus 90°. The angle between two planes and bisector line can also be calculated with the same data in the Bisector tab.

To calculate the intersection between all planes, go to the *Main Menu* \rightarrow select *Calculations* tab \rightarrow select *All Planes Intersections* (Figure 2.28). Then trend and plunge of all intersection lines will be calculated and stored in a new dataset named *Lines of intersection*.

Dips 8 is a popular commercial programme packed in RocScience software, which is usually used by professional rock engineers. Like Stereonet 11, Dips 8 supports several interchangeable data formats. One significant advantage of Dips 8 is its *Kinematic Analysis* feature, which will be described in the next section. Dips 8 covers four frequent types of rock failures, as detailed in the upcoming chapter. It also provides some drawing tools to aid the manual analysis in some complicated situations (Figure 2.29). Dips 8 can display data in either dip vector mode or pole vector mode, but it does not support 3D viewing.

Despite a good number of available computational tools, Dips 8 does not directly calculate the angle between two lines. It undertakes this task by computing the angle between two planes having those lines as pole lines. From the $Main\ Menu \rightarrow Select\ Tools \rightarrow Select\ Measure\ Angle\ (Figure\ 2.30)$, then click on the plot to indicate two poles of two respective planes. The click does not have to be very accurate as the data could be changed later in the new window. To access kinematic analysis, go to the $Main\ Menu \rightarrow select\ Analysis \rightarrow select\ Kinematic\ Analysis$. Then, check the box $Display\ Kinematic\ Analysis$ in the new window, select the desired $Failure\ Mode$ and input the other required information.

2.6 SUMMARY

- 1. Dip and dip direction can fully define the orientation of the plane. Similarly, the orientation of a line is defined by its plunge and trend.
- It is necessary to be able to quickly visualise the field situation (e.g. discontinuity planes daylighting on slope face) in three dimensions on every occasion.

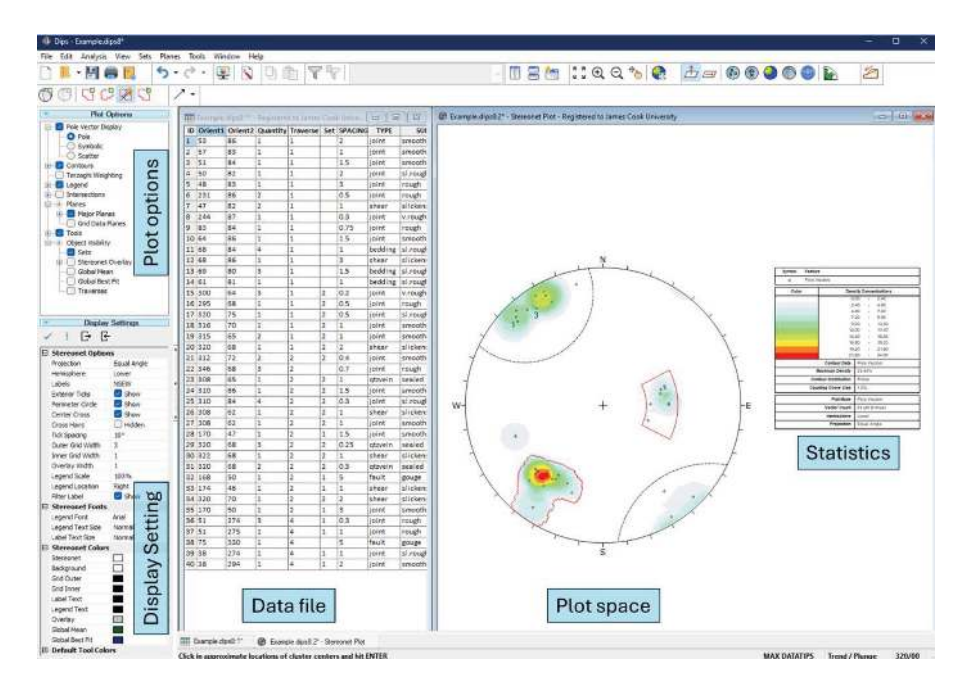


FIGURE 2.29 Interface of Dip 8 in RocScience.

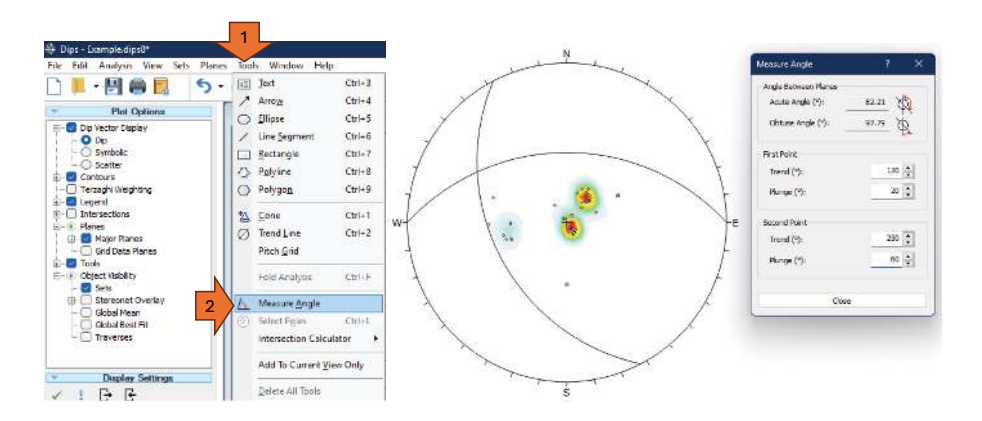


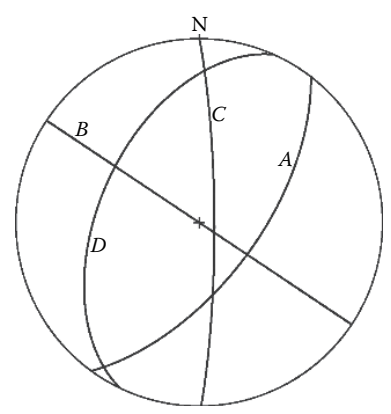
FIGURE 2.30 Solution to Example 2.3 with Dips 8.0.

- 3. In spherical projection, a line is represented by a point, and a plane is represented by a great circle. They are essentially the intersection of the line and plane, respectively, with the reference hemisphere.
- 4. In stereographic projection, a plane can be represented by a great circle or pole.
- 5. There are a few different ways to project the great circle onto a horizontal plane. Equal angle projection and equal area projection are the two common methods. They are different from the traditional projections we use in engineering drawings.

- 6. There are two separate stereonets we use: equatorial and polar.
- 7. Poles can be plotted on both equatorial and polar stereonets. The great circles can only be plotted on equatorial stereonets.
- 8. Poles can be plotted relatively fast on the polar stereonet or on tracing paper placed on top of it without any rotation.
- 9. Poles marked on an equatorial stereonet can be verified by overlaying the sheet on a polar stereonet. Remember, they fall on the same locations on both nets.
- 10. The angle between two planes is the same as the angle between the two radial lines connecting their poles.
- 11. In planar failure, sliding is possible only if the sliding surface daylights on the slope face. In addition, the dip of the sliding plane should be greater than the friction angle, and the dip direction has to be within ±20° from that of the slope face. The same applies to wedge failure as well.
- 12. In wedge failure, the line of intersection between the two discontinuity planes defines the direction of movement.

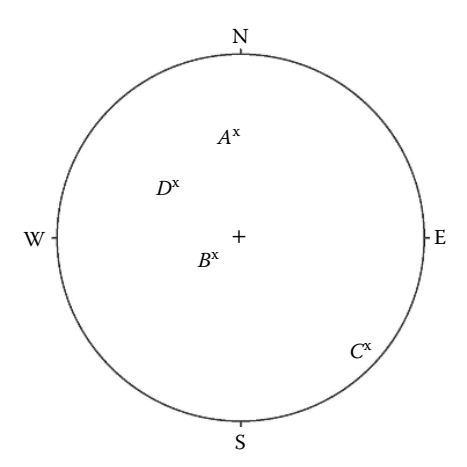
REVIEW EXERCISES

- 2.1. List 10 ancient rock-related construction marvels in chronological order, giving the important details about them very briefly.
- 2.2. List the different types of discontinuities and emphasise the differences.
- 2.3. Carry out a small research on the terms *schistosity*, *foliation* and *cleavage*, which are different forms of discontinuities, and write a 500-word essay.
- 2.4. Four great circles representing planes A, B, C and D are shown in the following figure. Answer the following.



- a. Which of the four planes has the largest dip?
 - (i) A, (ii) B, (iii) C and (iv) D
- b. Which of the four planes has the smallest dip?
 - (i) A, (ii) B, (iii) C and (iv) D
- c. Which of the four planes dips into the northwest quadrant?
 - (i) A, (ii) B, (iii) C and (iv) D

- d. Which of the following is the likely strike direction of plane A?
 - (i) N35E, (ii) S55E, (iii) N35W and (iv) S55W
- e. Which of the four planes has a dip direction of 295°?
 - (i) A, (ii) B, (iii) C and (iv) D
- 2.5. The poles of four planes A, B, C and D are shown in the following figure.



- a. Which of the four planes has the largest dip?
 - (i) A, (ii) B, (iii) C and (iv) D
- b. Which of the following is the likely dip direction of plane *A*?
 - (i) 0° , (ii) 90° , (iii) 180° and (iv) 270°
- c. Which of the four planes has the lowest dip?
 - (i) A, (ii) B, (iii) C and (iv) D
- 2.6. Photocopy the figure from the previous exercise, enlarge it to the size of the stereonets in Appendix, and draw the great circles of all four planes.
- 2.7. State whether the following are true or false.
 - a. The apparent dip of a plane can be greater than its true dip.
 - b. The pole of a plane plots at the same location in both polar and equatorial stereonets.
 - c. The pole is adequate to define a plane.
 - d. The diameter of a great circle is the same as the diameter of a reference sphere.
 - e. A strike direction of N30E is the same as S30W.
- 2.8. The orientations of two joint sets are 50/090 and 60/240. Represent the two on an equatorial stereonet, showing their great circles and poles.

Using a polar stereonet, check whether the poles you have marked are located at the right places.

What is the angle of intersection between the two planes?

What is the orientation of the line of intersection?

Answer: 77°, 20/163

2.9. The line of intersection between two joints (i.e. planes) has a plunge of 38° and trends in the northwest quadrant. The first plane has a dip and a dip direction of 50° and 256°, respectively. What is the trend (i.e. dip

direction) of the line of intersection? If the second plane strikes exactly northwest, find its dip and dip direction.

Answer: 308°; 80°, 225°

2.10. The line of intersection between two planes has a plunge of 28° and the trend line in the northeast quadrant. One of the two planes has dip and dip direction of 70° and 292°, respectively. What is the trend (i.e. dip direction) of the line of intersection? If the second plane has a strike of 120°, find its dip direction and dip angle.

Answer: 11°; 30/030

2.11. During a site investigation at some rock cuts, the following joint orientations were mapped:

25/270	82/230	80/040	90/010	70/140	70/110
80/050	62/110	58/130	90/220	90/035	85/185
85/225	88/025	15/270	75/020	90/200	90/028
80/218	85/210	50/115	90/210	90/045	70/122
30/330	20/260	15/250	88/030	58/105	22/315

Plot the joint orientations on a polar stereonet.

How many joint sets can you locate? Find the average orientation of each set.

Answer: Three sets; 20/285, 63/120, 90/210

2.12. Let us assume you are flying from Townsville, Australia (latitude 18.5° south and longitude 147° east) to either Perth (latitude 31.5° south and longitude 116° east) or Singapore (latitude 1.3° north and longitude 103.8° east). Using the equatorial net, plot the locations of the three cities. Find the distance between (a) Townsville and Perth and (b) Townsville and Singapore. Assume that the radius of the Earth is 6600 km.

Answer: 3570 km; 5300 km

- 2.13. The following question is in several parts which are related.
 - a. Using equatorial lower hemisphere projection, represent the two joint orientations J1 (150/40) and J2 (260/50) by their great circles on tracing paper. In the same plot, show the poles of the two planes as well and give the orientations of the poles.
 - b. Use a polar stereonet and verify that the poles are plotted at the right place.
 - Determine the orientation of the line of intersection between the two planes.
 - d. On the tracing paper used for the previous exercise, show the line that lies on the plane of joint J1 and is perpendicular to the line of intersection. Repeat this for joint J2. What are the orientations of these two lines? What is the angle between the two lines (and hence the two planes)?
 - e. Draw the great circle representing the plane normal to the line of intersection between the two planes. What is the orientation of this great circle? Note that the above two lines [from (d)] are lying on this plane.

f. Determine the angle between the two planes by determining the angle between the two radial lines connected to the poles of the planes. Is it the same as in (d)? Discuss.

Answer: 50/330, 40/080; 29/199; 26/094, 37/312, 109°; 61/019; 71°, same as 109°

2.14. A fire occurring at a rock engineering company destroyed all electronic devices and most documents. A report of a rock scan has been found, but some values are missing. Fill in the following table. You may have more than one answer for the angle between joint sets.

		-	-	•				
	Dip	Direction	Dip	Direction	Dip	Direction	Dip	Direction
Joint 1	43	229	65	122	25		35	
Joint 2	44	127		064	12	040	70	
Intersection			64			058	35	175
Angle					26			

2.14 answer

	Dip	Direction	Dip	Direction	Dip	Direction	Dip	Direction
Joint 1	43	229	65	122	25	122	35	170
Joint 2	44	127	70	064	12	040	70	100
Intersection	31	179	64	106	11	058	35	175
Angle	6	5 or 115	5	3 or 127	:	26/154	6	2 or 118

REFERENCES

Allmendiger, R.W., Cardozo, N. and Fisher, D.M. (2012). *Structural Geology Algorithms: Vectors and Tensors*. Cambridge University Press, Cambridge.

Goodman, R.E. (1989). *Introduction to Rock Mechanics*. 2nd edition, John Wiley & Sons, New York.

Hoek, E. and Bray, E. (1977). *Rock Slope Engineering*. 2nd edition, The Institution of Mining and Metallurgy, London.

To, P. and Sivakugan, N. (2023). *Analytical Solution for Rock Discontinuity Prediction without Stereonet*. Geotechnical and Geological Engineering.

3 Rock Properties and Laboratory Testing

3.1 INTRODUCTION

Rock mass consists of intact rock blocks separated by various discontinuities that are formed by weathering and other geological processes. Intact rock is an unjointed piece of rock. Rock fragments and rock cores used in laboratory tests are generally all intact rocks. The intact rock itself is a non-homogeneous, anisotropic and inelastic material. The presence of discontinuities on a large scale makes the situation even more complex. The engineering performance of a rock mass under external loadings is very often governed by the strength and orientation of the discontinuities rather than the properties of the intact rock. Other factors that influence rock behaviour are the presence of water and the initial stresses within the rock mass. The discontinuities make the rock mass weaker than the intact rock. In addition, the discontinuities allow access to water, thus compounding the problem. Figure 3.1 shows a relatively steep excavation in a heavily jointed rock.

3.2 ENGINEERING PROPERTIES OF INTACT ROCK

The *unconfined compressive strength*, also known as the uniaxial compressive strength (UCS), and *Young's modulus* (*E*) of concrete used in foundations are typically in the order of 30–50 MPa and 25–35 GPa, respectively. The values reported for most intact rocks are significantly greater than the above values. The UCS and *E* of intact rocks can be on the order of 1–350 MPa and 1–100 GPa, respectively. In the absence of discontinuities, there is very little need for us to worry about the adequacy of the intact rock as support for most foundations, as these values are quite high. However, the presence of discontinuities can make a significant difference and make one feel that the parameters of intact rock are irrelevant. In other words, the discontinuities will have a much greater bearing on the way the rock mass behaves under the applied loadings.

This section discusses the techniques adopted in the field for obtaining intact rock specimens and those adopted in the laboratory for preparing the specimens for specific tests. The different standards available for the laboratory testing of rocks are also briefly discussed.

3.2.1 ROTARY VERSUS PERCUSSION DRILLING

Rotary drilling and percussion drilling are two different ways of drilling into the rock overburden. In percussion drilling, the drill bit is repeatedly hammered into the rock. In rotary drilling, a sharp rotating drill bit is advanced into the ground, exerting

86 DOI: 10.1201/9781032725161-3



FIGURE 3.1 Rock mass with several discontinuities.

a downward pressure as well. To obtain good-quality rock cores for laboratory tests, rotary drilling is a better option and is more common.

3.2.2 ROCK CORING

Rock specimens from the ground are recovered through *coring*, a procedure different from sampling in soils. The high strength of the rock makes it necessary to use thick-walled core barrels (tubes or pipes) with tips made of some of the hardest materials such as diamond or tungsten carbide. The rotary drill grinds away an annular zone around the specimen and advances into the ground, while the cuttings are washed out by circulating water, in a manner similar to wash borings in soils. The central rock core is collected within the core barrel, which can typically retain cores of 0.5–3.0 m in length. The coring process subjects the cores to some torsion and significant mechanical disturbance. In addition, the core can undergo swelling and get contaminated by the drilling fluid, especially if the rock is weak or heavily fractured. These disturbances can be minimised by using *double-tube* or *triple-tube core barrels*. The cores collected are placed in sequence in a core box (Figure 3.2), with the borehole number and depth marked, for transporting to the laboratory for further testing and analysis. They also provide a tangible and accurate representation of the underlying rock formations.

The drill rod, core barrel and casing are slightly different in diameter. The early drill holes had diameters of 38 mm (1½ inches), 51 mm (2 inches), 63.5 mm (2½ inches) and 76 mm (3 inches), matching the standard steel pipes available, and they were given designations of E, A, B and N, respectively. With some standardisation worldwide in 1930, an 'X' was added. H and P are larger sizes that were introduced later.

Some of the common core sizes and their standard designations are given in Table 3.1. The first letter of the symbol (e.g. E, A, B, N, H and P) identifies the core diameter. The second letter, Q, signifies *wireline drilling*, a technique widely used for deep drilling to minimise time lost in removing and reinserting the entire length of drill rods and core barrel for recovering the cores. Instead, the core barrel is lowered



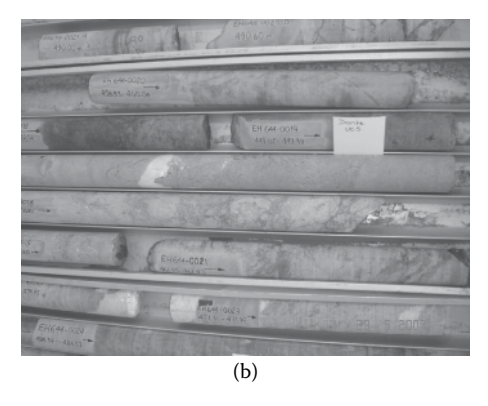


FIGURE 3.2 Intact rock cores received at James Cool University laboratory: (a) several core boxes from a large project and (b) a core box.

down a wireline inside the outer barrel, which extends to the full depth of the hole. Upon reaching the bottom of the hole, the core barrel is latched inside the outer barrel and drilling proceeds.

Single-tube core barrels are the most rugged and least expensive. They are used at the beginning of the drilling operation and are adequate in homogeneous, hard, intact rock mass or in situations where very good-quality sampling is not required. Double-tube core barrels are the most common and are often used with NX cores. While the outer barrel moves with the cutting bit, the inner barrel retains the core. In fractured or highly weathered rocks, to minimise the disturbance, triple-tube core barrels are preferred. They are also effective on brittle rocks with low strength. The outer barrel does the first cutting, while the middle one does the finer cutting. The third and the innermost barrel retains the core. This process reduces the heat

Nominal co	ore diameter	Nominal hole diameter		
(mm)	(in.)	(mm)	(in.)	
27.0	$1^{1}/_{16}$	48.0	$1^{57}/_{64}$	
36.5	17/16	60.0	$2^{23}/_{64}$	
47.6	17/8	75.8	$2^{63}/_{64}$	
63.5	$2^{1}/_{2}$	96.0	$3^{25}/_{32}$	
85.0	311/32	122.6	$4^{53}/_{64}$	
22.2	⁷ / ₈	36.5	17/16	
30.2	$1^{3}/_{16}$	47.6	17/8	
41.3	15/8	58.7	25/16	
54.0	21/8	74.6	215/16	
	(mm) 27.0 36.5 47.6 63.5 85.0 22.2 30.2 41.3	$\begin{array}{cccc} 27.0 & & & 1^{1}/_{16} \\ 36.5 & & & 1^{7}/_{16} \\ 47.6 & & & 1^{7}/_{8} \\ 63.5 & & & 2^{1}/_{2} \\ 85.0 & & & 3^{11}/_{32} \\ 22.2 & & & 7/_{8} \\ 30.2 & & & 1^{3}/_{16} \\ 41.3 & & & 1^{5}/_{8} \end{array}$	(mm)(in.)(mm) 27.0 $1^{1}/_{16}$ 48.0 36.5 $1^{7}/_{16}$ 60.0 47.6 $1^{7}/_{8}$ 75.8 63.5 $2^{1}/_{2}$ 96.0 85.0 $3^{11}/_{32}$ 122.6 22.2 $7/_{8}$ 36.5 30.2 $1^{3}/_{16}$ 47.6 41.3 $1^{5}/_{8}$ 58.7	

TABLE 3.1 Core Size Designations and Nominal Diameters

generated at the cutting edge that can otherwise damage the core. A '3' or 'TT' is added to the two-letter symbol given in Table 3.1 for triple-tube core barrels (i.e. PQ3).

3.2.3 ROCK QUALITY DESIGNATION

When attempting to obtain a rock core over a certain depth, due to the presence of joints and fractures, a significant length may be 'lost'. This can be seen as a measure of the quality of the intact rock. Two similar parameters commonly used to ascertain the quality of intact rock based on the drill record are *core recovery ratio* (CR) and *rock quality designation* (RQD). Core recovery ratio is defined as

$$CR(\%) = \frac{\text{Lenght of rock core recovered}}{\text{Total length of the core run}} \times 100$$
 (3.1)

Rock quality designation (RQD) is a modified measure of core recovery, defined as (Deere, 1964).

$$RQD(\%) = \frac{\sum Lengths \ of \ core \ pieces \ equal \ to \ or \ longer \ than \ 100 \ mm}{Total \ length \ of \ the \ core \ run} \times 100 \ \ (3.2)$$

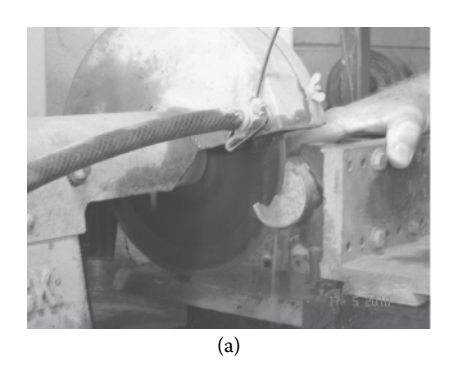
The RQD is a simple and inexpensive way to recognise low-quality rock zones that may require further investigation. The RQD, corresponding descriptions of in situ rock quality, and the allowable foundation bearing pressures as given by Peck et al. (1974) are summarised in Table 3.2. The lengths are measured along the centre line of the core. In computing the RQD, breaks that are caused by the drilling process are ignored. RQD is a parameter used in some of the popular rock mass classification systems discussed in Chapter 4.

TABLE 3.2

RQD, In Situ Rock Quality Description, and Allowable Bearing Pressure

RQD (%)	Rock quality	Allowable bearing pressure (MPa)
0–25	Very poor	1–3
25–50	Poor	3–6.5
50–75	Fair	6.5–12
75–90	Good	12–20
90–100	Excellent	20–30

Source: Peck, R.B. et al., Foundation Engineering, John Wiley & Sons, New York, 1974.



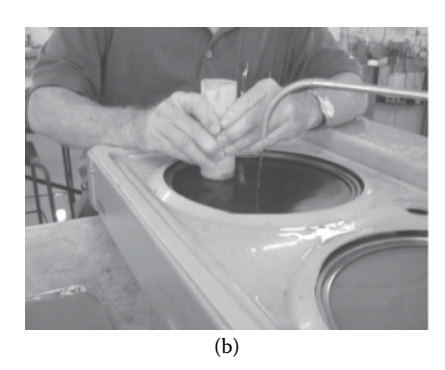


FIGURE 3.3 Specimen preparation: (a) cutting the ends using a diamond saw and (b) polishing the ends.

RQD and CR are influenced by the drilling technique and the size of the core barrel. The International Society for Rock Mechanics (ISRM) recommends that RQD be computed from double-tube NX cores of 54 mm diameter. However, ASTM D6032 permits core diameters from 36.5 mm (BQ) to 85 mm (PQ) to be used for RQD computations, while suggesting NX (54 mm) and NQ (47.6 mm) as the optimal core diameters for this purpose.

The cores recovered from the ground are tested in the laboratory to determine strength and deformation characteristics, durability and hardness. Some of the common laboratory tests on rocks are as follows:

- · Uniaxial compressive strength test
- · Brazilian indirect tensile strength test
- · Point load strength index test
- · Schmidt hammer test
- · Slake durability test
- · Triaxial test

3.2.4 Specimen Preparation

Laboratory tests such as UCS, triaxial and point load tests require good-quality cylindrical specimens that have their ends cut parallel and flat, such that they are perpendicular to the longitudinal axis of the specimen. The standard requirements are discussed in ASTM D4543. Figure 3.3a shows a specimen being cut by a diamond saw. Then the ends are further smoothed using a surface grinder and polished (Figure 3.3b) to minimise friction during loading. Non-parallel ends can induce eccentricity in the applied loads. Roughness at the ends can mean that the applied stresses are no longer principal stresses. Applying capping materials (e.g. sulphur) to the ends is not generally recommended with rock specimens.

3.2.5 STANDARDS

Similar to the International Society of Soil Mechanics and Geotechnical Engineering (ISSMGE) that looks after the research and professional practice in soil mechanics and geotechnical engineering, there is a society for rock mechanics too. The ISRM is a non-profit scientific organisation that has more than 5,000 members representing 46 national groups (http://www.isrm.net). It was founded in 1962 at Karlsruhe University by Professor Leopold Mueller. It appointed the Commission on Standardization of Laboratory and Field Tests on Rock in 1967, which later became the Commission on Testing Methods. The commission proposed 'Suggested Methods' for various rock tests that have been adopted worldwide and were published from time to time in the International Journal of Rock Mechanics and Mining Sciences & Geomechanics Abstracts, Pergamon Press, United Kingdom. These were compiled by Professor Ted Brown (1981) of the University of Queensland, Australia, as the ISRM 'Yellow Book'. This was later updated by Professor Ulusay of Hacettepe University, Turkey, and Professor Hudson, formerly of Imperial College, United Kingdom, in 2007 as the 'Blue Book', which is a one-stop shop for all relevant ISRM-suggested methods for rock testing. The test procedures for rocks described in this chapter are mainly based on the ISRM-suggested methods, with references to ASTM (American Society for Testing Materials) and Australian Standards as appropriate. The United States, United Kingdom, Canada, South Africa and Australia are some of the countries that played pioneering roles in the development of rock mechanics, including the laboratory test methods.

3.3 UNIAXIAL COMPRESSIVE STRENGTH TEST

The UCS test is also known as the *uniaxial compressive strength* test. Here, a cylindrical rock specimen is subjected to an axial load without any lateral confinement. The axial load is increased gradually until the specimen fails. The vertical normal stress on the specimen, when failure occurs, is known as the unconfined compressive strength or uniaxial compressive strength, fondly known as UCS. By monitoring the vertical deformations, the vertical normal strains can be computed. By plotting the stress–strain curve, Young's modulus (*E*) can be determined. By monitoring the lateral or circumferential deformation, Poisson's ratio can be computed too.

3.3.1 Soils versus Rocks

What is the dividing line between hard soil and soft rock? When do we call a material a rock rather than a soil? A commonly used but rather arbitrary cut-off is the uni-axial compressive strength of 1 MPa. Soils have their UCS and *E* generally quoted in kPa and MPa, respectively. In rocks, they are orders of magnitude greater and are given in MPa and GPa respectively.

Saturated clays under undrained conditions are generally analysed using the total stress parameters $c_{\rm u}$ and $\phi_{\rm u}$. Here, $c_{\rm u}$ is the undrained shear strength and $\phi_{\rm u}$ is the friction angle in terms of total stresses. In saturated clays, the Mohr–Coulomb failure envelope in terms of total stresses is horizontal, and hence $\phi_{\rm u}=0$. The unconfined compression test is one of the many ways of deriving the undrained shear strength of a clay. The UCS of a clay, denoted often by $q_{\rm u}$ in geotechnical literature, is twice the undrained shear strength $c_{\rm u}$ when $\phi_{\rm u}=0$.

The same principle holds in rocks too. Uniaxial compressive strength, often denoted by σ_c in rock mechanics literature, is the most commonly used rock strength parameter in rock mass classification and rock engineering designs. Unlike saturated undrained clays, the friction angle of a rock specimen is not zero, and hence the Mohr–Coulomb failure envelope is not horizontal. It can be shown from the Mohr circle that

$$\sigma_{\rm c} = \frac{2c\cos\phi}{1-\sin\phi} \tag{3.3}$$

where c and ϕ are the cohesion and friction angles of the rock, respectively.

3.3.2 Test Procedure

The test is quite simple, and the interpretation is fairly straightforward. A cylindrical core of at least 54 mm in diameter (NX core) and a length-to-diameter ratio of 2.0–3.0 (ISRM suggests 2.5–3.0 and ASTM D 7012 suggests 2.0–2.5) is subjected to an axial load that is increased until failure. The specimen is loaded axially using spherical seating, at a constant rate of strain or stress such that it fails in 5–15 minutes. Alternatively, the stress rate shall be in the range of 0.5–1.0 MPa/s. The axial loads



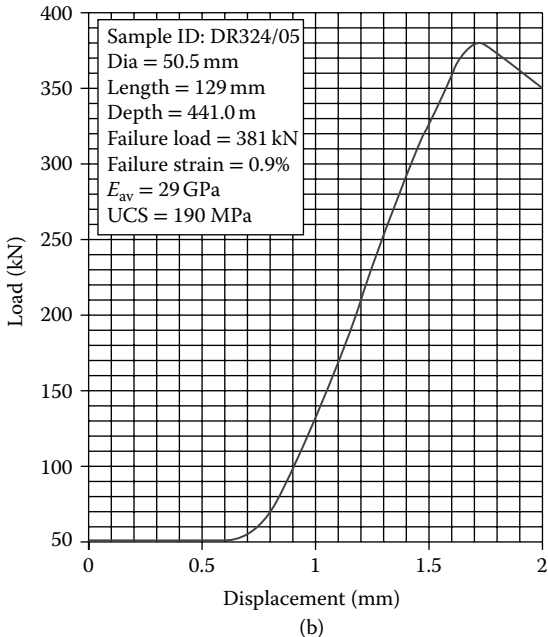


FIGURE 3.4 (a) UCS test on an MTS universal testing machine and (b) load–displacement plot.

at failure can be very large for large diameter cores in good-quality intact igneous rocks. Uniaxial compressive strength is the maximum load carried by the specimen divided by the cross-sectional area.

The change in the specimen length is measured throughout the test using a dial gauge or an LVDT (linear variable differential transformer). These days, it

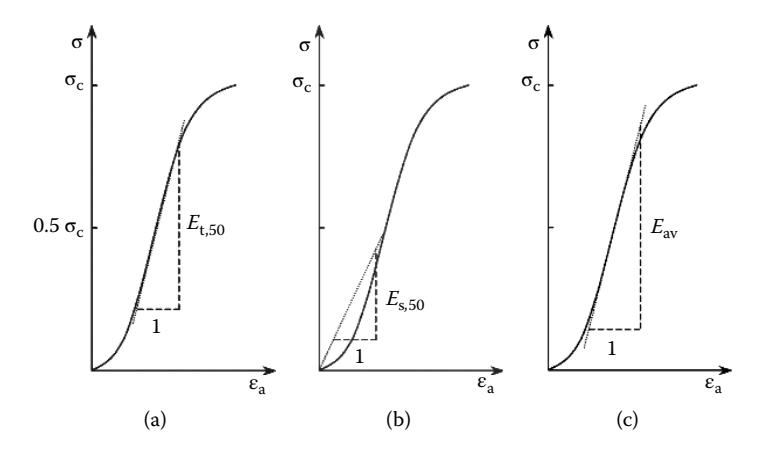


FIGURE 3.5 Young's modulus: (a) tangent modulus, (b) secant modulus and (c) average modulus.

is common to use sophisticated data acquisition systems that would keep track of the load–deformation data. Figure 3.4a shows a UCS test in progress on an MTS universal testing machine with axial load capacity of 1,000 kN and a data acquisition system. To prevent injury from flying rock fragments upon failure, a protective shield should be placed around the test specimen, as shown in the figure. The load–displacement plot generated from the MTS machine for a rock specimen is shown in Figure 3.4b.

From the load and displacement measured throughout the loading, the stressstrain plot can be generated. From the stress–strain plot, Young's modulus (E) can be computed. Young's modulus is a measure of the rock stiffness, which is required for modelling the rock and for computing deformations, where the rock is assumed to be an elastic continuum. You may recall Hooke's law from the study of the strength of materials, which states that stress is proportional to the strain in a linear elastic material. Young's modulus is the slope of the stress-strain plot. In reality, rocks are not linearly elastic, and the stress-strain plot is not a straight line. There are a few different ways of defining Young's modulus here. The tangent modulus (E_i) is defined as the slope of a tangent to the stress-strain plot (Figure 3.5a). The secant modulus (E_s) is defined as the slope of a line joining a point on the stress-strain plot to the centre (Figure 3.5b). When the stress-strain plot is not linear, the tangent and secant moduli can vary depending on the stress level. It is common to measure the tangent and secant Young's modulus at 50% of σ_c . Alternatively, an average Young's modulus (E_{av}) can be determined as the slope of the straight line portion of the stress-strain plot (Figure 3.5c).

By measuring diametrical or circumferential strains during loading, Poisson's ratio can be measured. Poisson's ratio v is defined as

$$v = -\frac{\text{Lateral strain}}{\text{Axial strain}} = -\frac{\varepsilon_d}{\varepsilon_a}$$
 (3.4)

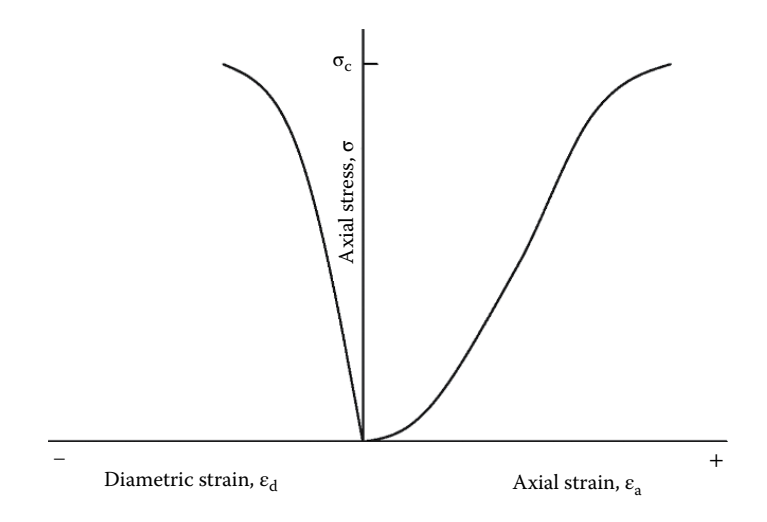


FIGURE 3.6 Variation of axial and diametrical strains with the applied axial stress.

TABLE 3.3					
Typical Values of Poisson's Ratio for Rocks					
Rock type	v				
Andesite	0.20-0.35				
Basalt	0.10-0.35				
Conglomerate	0.10-0.40				
Diabase	0.10-0.28				
Diorite	0.20-0.30				
Dolerite	0.15-0.35				
Dolomite	0.10-0.35				
Gneiss	0.10-0.30				
Granite	0.10-0.33				
Granodiorite	0.15-0.25				
Greywacke	0.08-0.23				
Limestone	0.10-0.33				
Marble	0.15-0.30				
Marl	0.13-0.33				
Norite	0.20-0.25				
Quartzite	0.10-0.33				
Rock salt	0.05-0.30				
Sandstone	0.05-0.40				
Shale	0.05-0.32				
Siltstone	0.05-0.35				
Tuff	0.10-0.28				

Source: Gercek, H., Int. J. Rock Mech. Min. Sci., 44, 1-13, 2007.

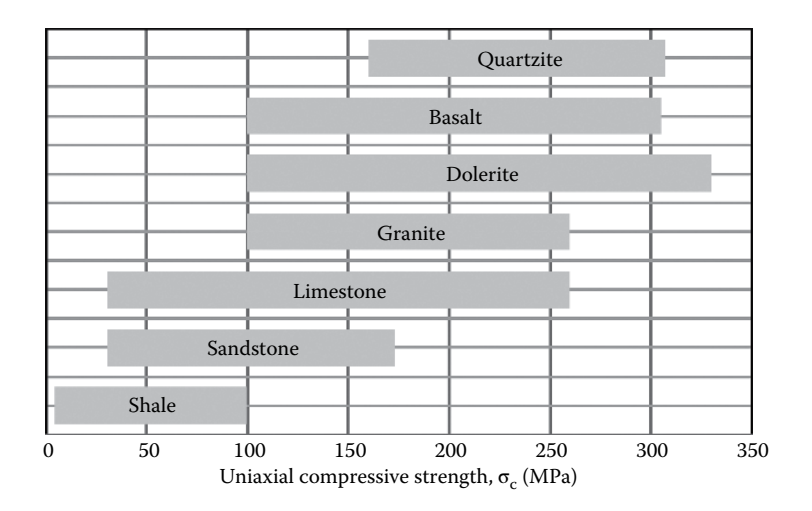


FIGURE 3.7 Typical values for uniaxial compressive strengths of common rock types. (Adapted from Hudson, J.A., *Rock Mechanics Principles in Engineering Practice*, Butterworths, London, 1989.)

Typical variation of the axial (ε_a) and diametrical (ε_d) strains with the applied axial stress in a UCS test on a rock specimen is shown in Figure 3.6. Here, diametrical strain is the same as the circumferential strain, defined as the ratio of the change in diameter (or circumference) to the original diameter (or circumference). The volumetric strain (ε_{vol}) of the specimen is given by

$$\varepsilon_{\rm vol} = \varepsilon_{\rm a} + 2\varepsilon_{\rm d} \tag{3.5}$$

Poisson's ratio for a common engineering material varies in the range of 0–0.5. Typical values of Poisson's ratio for common rock types are given in Table 3.3. Hawkes and Mellor (1970) discussed various aspects of the UCS laboratory test procedure in great detail. Typical values of the uniaxial compressive strength for some major rock types, as suggested by Hudson (1989), are given in Figure 3.7. As seen here, the UCS values are in the range of 0–350 MPa for most rocks. The axial strain at failure is a measure of the ductility of the intact rock. Qualitative descriptions of materials as ductile, brittle and so on, based on failure strains, as suggested by Handin (1966), are given in Table 3.4.

Young's modulus and Poisson's ratio are the two crucial parameters in defining the rock behaviour when it is assumed to behave as a linear elastic material, obeying Hooke's law. They are related to the bulk modulus, K, and shear modulus, G, by

$$K = \frac{E}{3(1 - 2v)} \tag{3.6}$$

and

$$G = \frac{E}{2(1+\nu)} \tag{3.7}$$

TABLE 3.4
Relative Ductility Based on Axial Strain at Peak Load

Classification	Axial strain (%)
Very brittle	<1
Brittle	1–5
Moderately brittle ^a (transitional)	2–8
Moderately ductile	5–10
Ductile	>10

Source: Handin, J., Handbook of Physical Contacts, Geological Society of America, New York, 1966.

EXAMPLE 3.1

A 50.5-mm-diameter, 129-mm-long rock specimen is subjected to a uniaxial compression test. The load–displacement plot is shown in Figure 3.4b. Determine the uniaxial strength and Young's modulus of the intact rock specimen.

Solution

Noting that there was no load for displacement up to 0.6 mm, the origin (i.e. the load axis) is shifted to a displacement of 0.6 mm. The cross-sectional area, A, of the specimen is given by

$$A = \pi \times 25.25^2 = 2003.0 \text{ mm}^2$$

The failure load = 381 kN

 \therefore UCS = 381,000/2003 MPa = 190.2 MPa

Considering the linear segment of the load–displacement plot between displacements of 1.0 and 1.5 mm in Figure 3.4b,

$$E = \frac{\Delta P \times L}{\Delta L \times A} = \frac{22,5000 \times 129}{0.5 \times 2003} = 28,982 \text{ MPa} = 29.0 \text{ GPa}$$

A semi-quantitative classification of rocks, based on the uniaxial compressive strength and Young's modulus, proposed by Hawkes and Mellor (1970), is shown in Figure 3.8. Here, the *modulus ratio* is the ratio of Young's modulus, E, to the uniaxial compressive strength, σ_c . In concrete, this ratio is about 1,000, which is well above the upper end of the values for rocks. The cut-off values used for the UCS in Figure 3.8 were later revised by ISRM (1978c), which are discussed later in Chapter 4 (see Table 4.1). Typical values of modulus ratios of various rock types, suggested by Hoek and Diederichs (2006), are summarised in Table 3.5.

^a Note the overlap.

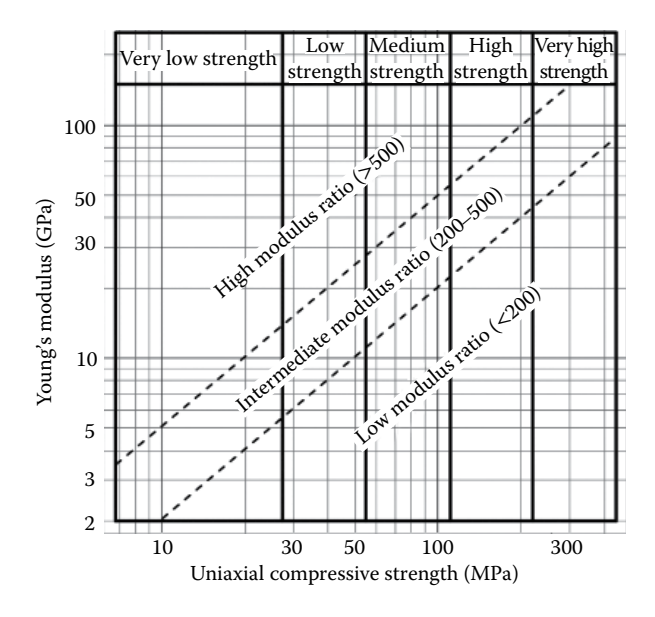


FIGURE 3.8 Rock classification based on UCS and Young's modulus. (Adapted from Hawkes, I. and M. Mellor, *Eng. Geol.*, 4, 179–285, 1970 and Deere, D.U. and R.P. Miller, Engineering classification and index properties of intact rock. *Report AFWL-TR-65–116, Air Force Weapon Laboratory (WLDC)*, Kirtland Airforce Base, New Mexico, 1966.)

TABLE 3.5 Typical Values of Modulus Ratios

		Texture	2	
	Coarse	Medium	Fine	Very fine
	Conglomerates	Sandstones	Siltstones	Claystones
	300–400 200–350		350-400	200-300
ij	Breccias 230-350		Greywackes 350	Shales 150-250a
Sedimentary				Marls 150-200
Hi.	Crystalline limestone	Sparitic limestone	Micritic limestone	Dolomite
Sec	400-600	600-800	800-1000	350-500
		Gypsum	Anhydrite	Chalk
		$(350)^{c}$	(350) ^c	1000^{b}
	Marble	Hornfels	Quartzite	
	700-1000	400-700	300-450	
hic		Metasandstone		
orp		200-300		
Metamorphic	Migmatite	Amphibolites	Gneiss	
Me	350-400	400-500	$300-750^{a}$	
		Schists	Phyllites/mica schist	Slates
		250-1100 ^a	$300-800^a$	$400-600^{a}$

Table 3.5 (Continued)

Typical Values of Modulus Ratios

	Texture			
Coarse Medium		Fine	Very fine	
Granite ^b	Diorite ^b			
300-550	300-350			
Granodior	ite 400–450			
Gabro 400-500	Dolerite 300-400			
Norite 350-400				
Porphyries		Diabase	Peridotite	
$(400)^{c}$		300-350	250-300	
	Rhyolite 300-500	Dacite 350-450		
	Andesite 300-500	Basalt 250-450		
Agglomerate	Volcanic breccia	Tuff		
400-600	(500) ^c	200-400		

Source: Hoek, E. and M.S. Diederichs, Int. J. Rock Mech. Min. Sci., 43, 203-215, 2006.

^c No data available; estimated on the basis of geological logic.

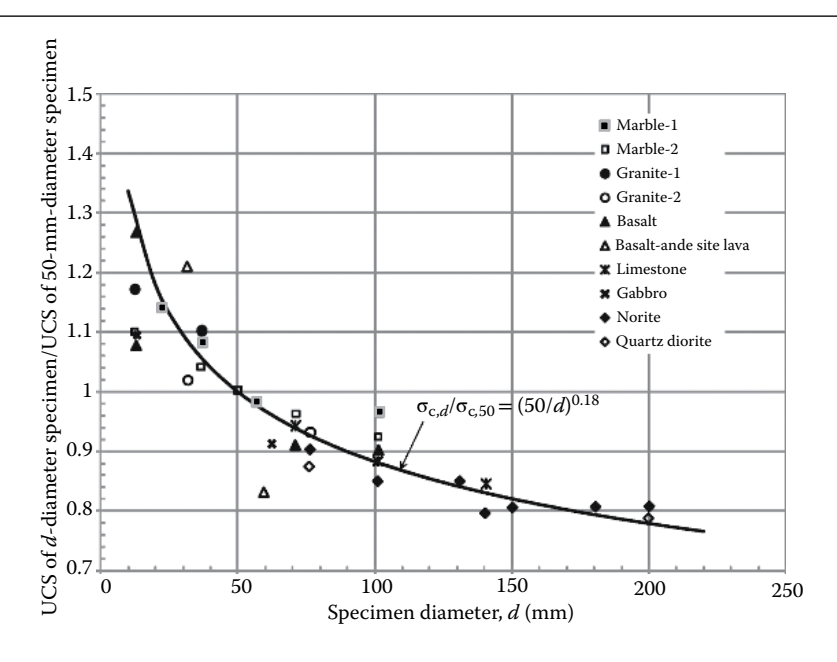


FIGURE 3.9 Influence of specimen size on UCS. (After Hoek, E. and E.T. Brown, *Underground Excavations in Rock*, Institution of Mining and Metallurgy, London, 1980.)

a Highly anisotropic rocks: the modulus ratio will be significantly different if normal strain and/or loading occurs parallel (high modulus ratio) or perpendicular (low modulus ratio) to a weakness plane. The uniaxial test loading direction should be equivalent to field application.

^b Felsic granitoids: coarse-grained or altered (high modulus ratio), fine-grained (low modulus ratio).

In clays, the ratio of undrained Young's modulus to the undrained shear strength is expressed as a function of the over-consolidation ratio and the plasticity index, and this varies in the range of 100–1,500. Note that undrained shear strength is half of UCS. Therefore, similar modular ratios for clays are in the range of 50–750.

Generally, there is a significant reduction in the uniaxial compressive strength with increasing specimen size, as evident from Figure 3.9 (Hoek and Brown, 1980).

TABLE 3.6 Typical Values of σ_c , E, Modulus Ratio and V

7.				
Rock description	$\sigma_{\rm c}$ (MPa)	E (GPa)	$\mathbf{E}/\sigma_{\mathrm{c}}$	v
Fine-grained, slightly porous Berea sandstone	73.8	19.3	261	0.38
Fine- to medium-grained, friable Navajo sandstone	214.0	39.2	183	0.46
Calcite cemented, medium-grained Tensleep sandstone	72.4	19.1	264	0.11
Argillaceous Hackensack siltstone, cemented with hematite	122.7	26.3	214	0.22
Monticello Dam greywacke - Cretaceous sandstone	79.3	20.1	253	0.08
Very fine crystalline limestone from Solenhofen, Bavaria	245.0	63.7	260	0.29
Slightly porous, oolitic, bioclastic limestone, Bedford, Indiana	51.0	28.5	559	0.29
Fine-grained, cemented and interlocked crystalline Tavernalle limestone	97.9	55.8	570	0.30
Fine-grained, Oneota dolomite with interlocking granular texture	86.9	43.9	505	0.34
Very fine-grained Lockport dolomite, cemented granular texture	90.3	51.0	565	0.34
Flaming Gorge shale, Utah	35.2	5.5	157	0.25
Micaceous shale with kaolinite clay mineral, Ohio	75.2	11.1	148	0.29
Dworshak Dam granodiorite gneiss, fine- to medium- grained, with foliation	162.0	53.6	331	0.34
Quartz mica schist ⊥ schistosity	55.2	20.7	375	0.31
Fine-grained, brittle, massive Baraboo quartzite, Wisconsin	320.0	88.3	276	0.11
Uniform, fine-grained, massive Taconic white marble with sugary texture	62.0	47.9	773	0.40
Medium- to coarse-grained, massive Cherokee marble	66.9	55.8	834	0.25
Coarse-grained granodiorite granite, Nevada	141.1	73.8	523	0.22
Fine- to medium-grained, dense Pikes Peak granite, Colorado	226.0	70.5	312	0.18
Cedar City tonalite, Utah – somewhat weathered quartz monzonite	101.5	19.2	189	0.17
Medium-grained Palisades diabase, New York	241.0	81.7	339	0.28
Fine olivine basalt, Nevada	148.0	34.9	236	0.32
John Day basalt, Arlington, Oregon	355.0	83.8	236	0.29
Nevada tuff - welded volcanic ash with 19.8% porosity	11.3	3.6	323	0.29

Source: Goodman, R.E., Introduction to Rock Mechanics, John Wiley & Sons, New York, 1980.

The uniaxial compressive strength of a *d*-diameter specimen, $\sigma_{c,d}$ and a 50-mm-diameter specimen, $\sigma_{d,50}$ are related by

$$\sigma_{c,50} = \sigma_{c,d} \left(\frac{d}{50}\right)^{0.18} \tag{3.8}$$

The reduction is probably due to the fact that the larger specimens include more grains, thus enabling greater tendency to fail around these grain surfaces.

Some typical values of the uniaxial compressive strength, Young's modulus, modulus ratio and Poisson's ratio are given in Table 3.6 (Goodman, 1980). It may be useful to cross-check your laboratory data against these values.

3.4 INDIRECT TENSILE STRENGTH TEST

Unlike soils, rocks can carry some tensile stresses. The tensile strength of a rock is required in most designs, analyses and numerical modelling of excavation, tunnelling, slope stability and so on. On rock specimens, it is difficult to carry out a direct tensile strength test in the same way we test steel specimens. The main difficulties are (1) in gripping the specimens without damaging them and applying stress concentrations at the loading grips and (2) in applying the axial load without eccentricity. The *indirect tensile strength test*, also known as the *Brazilian test*, is an indirect way of measuring the tensile strength of a cylindrical rock specimen having the shape of a disc. The rock specimen, with a thickness-to-diameter ratio of 0.5, is subjected to a load that is spread over the entire thickness of the disc, applying a uniform vertical *line load* diametrically (Figure 3.10). The load is increased to failure, where the sample generally splits along the vertical diametrical plane. The fracture should ideally initiate at the centre and progress vertically towards the loading points. From the

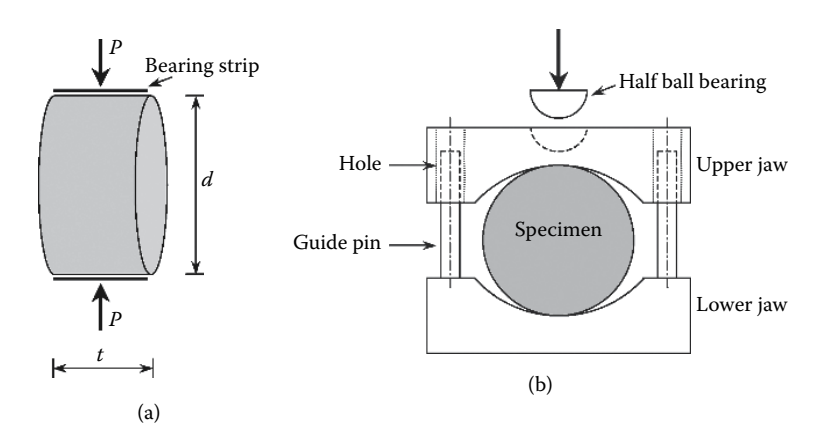


FIGURE 3.10 Indirect tensile strength test: (a) schematic diagram and (b) loading arrangement.

theory of elasticity, and assuming the material to be isotropic, the tensile strength of the rock, σ_i , is given by

$$\sigma_{t} = \frac{2P}{\pi dt} \tag{3.9}$$

where P = the load at failure, d = specimen diameter and t = specimen thickness (Timoshenko, 1934; Hondros, 1959). It can be shown that, at the centre of the specimen, the minor and the major principal stresses are horizontal and vertical, respectively, at failure. The vertical compressive stress is three times the horizontal tensile stress σ_{t} , as given by Equation 3.9.

Mellor and Hawkes (1971) discussed the test procedure in detail. The standard procedure is discussed in ISRM (1978a) and ASTM D3967. The test works better for brittle materials and has been adopted for concrete, ceramics, cemented soils and asphalt. Note that the recommended *t/d* ratio can be different for other materials. In the case of concrete, a length-to-diameter ratio of 2.0 is recommended for the test specimens. A schematic diagram and the loading arrangement are shown in Figure 3.10a and b, respectively.

3.4.1 Test Procedure

The test specimen diameter should be at least NX core size (54 mm), and the thickness should be approximately half the diameter (ISRM, 1978a). ASTM D3967 allows a *t/d* ratio between 0.20 and 0.75. The loading arrangement suggested by ISRM (1978a) is shown in Figure 3.10b, where the two steel jaws will be in contact with the specimen over an arc length that subtends 10° at the centre, when failure occurs. It is suggested that the radius of the jaws be 1.5 times the specimen radius. The upper jaw has a spherical seating formed by a 25-mm-diameter half ball bearing.

The state of stress at the *centre* of the specimen is given by a horizontal tensile stress, σ_t , and a vertical compressive stress that is three times greater in magnitude, both of which are principal stresses (Hondros, 1959). The theoretical basis for Equation 3.9 is that the specimen splits along the vertical diameter. If the fracture plane deviates significantly from being vertical, the test results are questionable.

Indirect tensile strength can be assumed to be approximately equal to the direct tensile strength. Goodman (1980) noted that the Brazilian indirect tensile strength test gives a higher value for σ_t than the direct tensile strength test, sometimes by as many as 10 times, especially when there are internal fissures. The fissures in the specimens weaken them in direct tension more than in the Brazilian test.

TABLE	3.7		
Typical	σ /σ.	va	lues

Rock type	$\sigma_{\rm c}$ (MPa)	$\sigma_{\rm t}$ (MPa)	$\sigma_{\rm c}/\sigma_{\rm t}$
Coarse-grained Nevada granodiorite	141.1	11.7	12.1
Cedar City tonalite, somewhat weathered quartz monzonite	101.5	6.4	15.9
Fine olivine Nevada basalt	148.0	13.1	11.3
Nevada tuff – welded volcanic ash with 19.8% porosity	11.3	1.1	10.0

Source: Goodman (1989).

In the absence of any measurements, σ_t is sometimes assumed to be a small fraction of the uniaxial compressive strength, σ_c . A wide range of values from 1/5 to 1/20 has been suggested in the literature, and 1/10 is a good first estimate. The σ_c/σ_t ratios reported by Goodman (1989), along with the σ_c values of several rock types, are given in Table 3.7. All σ_t values reported herein are from the Brazilian indirect tensile test. Further descriptions of the rock specimens are given in Goodman (1989).

3.5 POINT LOAD STRENGTH TEST

The origins of the *point load test* can be traced back to the pioneering work of Reichmuth (1968), which was simplified into its present form by Broch and Franklin (1972). It is an index test for strength classification of rocks, where a piece of rock is held between two conical platens of a portable lightweight tester, shown in Figure 3.11. The historical development of the point load test and the theoretical background were discussed by Broch and Franklin (1972). The test is rather quick and can be conducted on regular rock cores or irregular rock fragments. The test specimen can be any of the four forms shown in Figure 3.12. The load is increased to failure, and the point load strength index, I_s , is calculated based on the failure load and the distance, D, between the cone tips. The *uncorrected point load strength index*, I_s , is defined as

$$I_{\rm s} = \frac{P}{D_{\rm e}^2} \tag{3.10}$$

where $D_{\rm e}$ is the equivalent diameter of the specimen and $I_{\rm s}$ generally given in MPa. In the diametrical test (Figure 3.12a), $D_{\rm e}=D$. In axial, block or irregular lump tests (Figures 3.12b, c and d, respectively), the minimum cross-sectional area A of the plane through the platen contact points is computed as A=WD. Equating this area to that of a circle, the equivalent diameter $D_{\rm e}$ is computed as

$$D_{\rm e} = \sqrt{\frac{4A}{\pi}} = \sqrt{\frac{4WD}{\pi}} \tag{3.11}$$

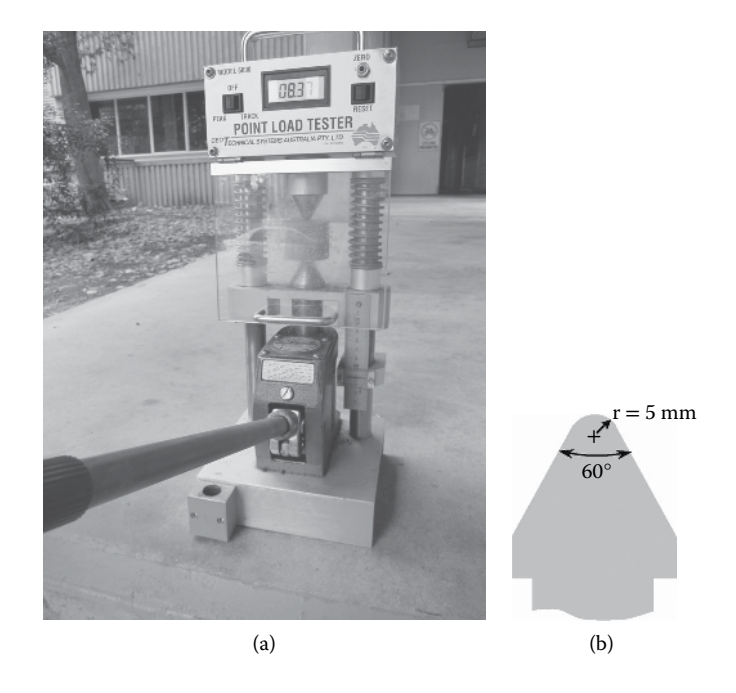


FIGURE 3.11 (a) Point load tester and (b) conical platen.

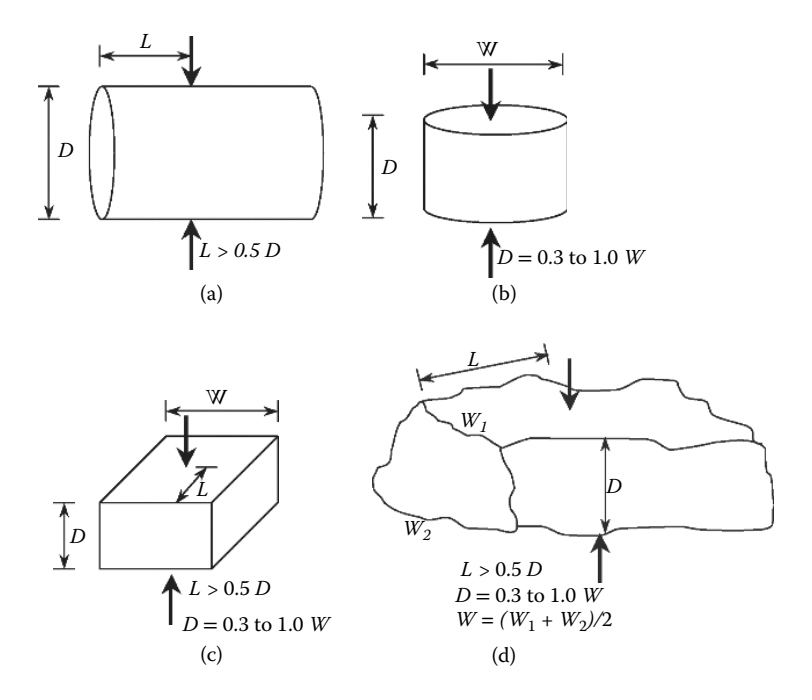


FIGURE 3.12 Possible specimen shapes and loading directions: (a) diametrical, (b) axial, (c) block and (d) irregular.

It has been observed that I_s increases with D_e , and therefore it is desirable to have a unique point load index for the rock sample that can be used in rock strength classification. The *size-corrected* point load strength index, $I_{s(50)}$, is defined as the value of I_s obtained if D_e is 50 mm. It can be computed as

$$I_{s(50)} = I_s \times \left(\frac{D_e}{50}\right)^{0.45}$$
 (3.12)

where D_e is in millimetres.

 $I_{\rm s(50)}$ is used to classify rocks and is correlated to the strength parameters such as uniaxial compressive strength, $\sigma_{\rm c}$, or the tensile strength, $\sigma_{\rm t}$. A key advantage of the point load test is that it can be carried out on an irregular rock fragment, which is not the case with most other tests where the specimens have to be machined and significant effort is required for preparation. This makes it possible to do the tests at the site on several samples in a relatively short time. Especially during the exploration stage, point load tests are very valuable in making informed decisions and can help in selecting the correct samples for the more sophisticated laboratory tests.

The ratio of uniaxial compressive strength, $\sigma_{c.}$ to $I_{s(50)}$ can be taken as 20–25, but it can vary in the range of 15–50, considering extreme possibilities including anisotropic rocks. Bieniawski (1975) and Broch and Franklin (1972) suggested that $\sigma_{c} = 24I_{s(50)}$. In spite of the similarities between the point load test and the Brazilian indirect tensile strength test, any attempt to derive $\sigma_{t.}$ from $I_{s(50)}$ should be discouraged (Russell and Wood, 2009). Nevertheless, a crude estimate of Brazilian indirect tensile strength can be obtained as $\sigma_{t.} = 1.25I_{s(50)}$. Point load tests are unreliable for rocks that have uniaxial compressive strength less than 25 MPa (Hoek and Brown, 1997). The test can also be used to quantify the strength anisotropy by the *point load strength anisotropy index*, $I_{a(50)}$, defined as the ratio of $I_{s(50)}$ obtained when testing perpendicular and parallel to the planes of weakness. This index is greater than unity when there is anisotropy.

3.5.1 Test Procedure

The standard test procedure is described in ISRM (1985) and ASTM D5731. The test is carried out on a specimen that can be of any of the four forms shown in Figure 3.12, with an *equivalent diameter*, $D_{\rm e}$, of 30–85 mm. It is held between the two conical ends of the point load tester, and the load is applied to failure. The loading is rather quick so that the specimen fails in 10–60 seconds. It is recommended that the test be carried out on at least 10 specimens (more if anisotropic or heterogeneous), where the highest two and the lowest two values are discarded, and the average value of the remaining specimens is reported as the point load index. Any specific test where the failure does not extend to the full depth should be rejected. A typical point load test datasheet is shown in Table 3.8.

TABLE 3.8
Point Load Test Data

No.	Туре	W (mm)	D (mm)	P (kN)	D _e (mm)	I _s (MPa)	$I_{s(50)}$ (MPa)
1.	i⊥	30.4	17.2	2.687	25.8	4.04	3.00
2.	i⊥	16.0	8.0	0.977	12.8	5.99	3.24
3.	i⊥	19.7	15.6	1.962	19.8	5.01	3.30
4.	i⊥	35.8	18.1	3.641	28.7	4.41	3.44
5.	i⊥	42.5	29.0	6.119	39.6	3.90	3.51
6.	i⊥	42.0	35.0	7.391	43.3	3.95	3.70
7.	b⊥	44	21	4.600	34.3	3.91	3.30
8.	b⊥	40	30	5.940	39.1	3.89	3.48
9.	b	19.5	15	2.040	19.3	5.48	3.57
10.	b⊥	33	16	2.870	25.9	4.27	3.18
11.	d//	-	49.93	5.107	49.93	2.05	2.05
12.	d//	-	49.88	4.615	49.88	1.85	1.85
13.	d//	-	49.82	5.682	49.82	2.29	2.29
14.	d//	-	49.82	4.139	49.82	1.67	1.66
15.	d//	-	49.86	4.546	49.86	1.83	1.83
16.	d//	-	25.23	1.837	25.23	2.89	2.12
17.	d//	-	25.00	1.891	25	3.03	2.21
18.	d//	-	25.07	2.118	25.07	3.37	2.47
19.	d//	-	25.06	1.454	25.06	2.32	1.70
20.	d#	-	25.04	1.540	25.04	2.46	1.80

a = axial

^{//=} loaded parallel to plane of weakness

Mean $I_{s(50) \perp}$	3.38 MPa
Mean $I_{s(50)/\!\!/}$	1.98 MPa
$I_{a(50)}$	1.71

Source: Adapted from ISRM, Int. J. Rock Mech. Min. Sci. & Geomech. Abstr., 22, 51-60, 1985.

3.6 SLAKE DURABILITY TEST

Rocks are generally weaker when wet than dry due to the presence of water in the cracks and its subsequent reaction to the applied loads during the tests. Repeated wetting and drying, which happens often in service, can weaken the rock significantly. *Slaking* is a process of disintegration of an aggregate when in contact with water. The

b = block

d = diametrical

i = irregular lump

 $[\]perp$ = loaded perpendicular to plane of weakness

slake durability index quantifies the resistance of a rock to wetting and drying cycles and is seen as a measure of the durability of the rock. This is mainly used for weak rocks such as shales, mudstones, claystones and siltstones. The slake durability test is an index test that was first proposed by Franklin and Chandra (1972), during their PhD and MSc work, respectively, at London University in 1970.

Figure 3.13 shows the slake durability apparatus, which consists of two rotating sieve mesh drums immersed in a water bath. Ten rock lumps, each weighing 40–60 g, are placed in the drum and rotated for 10 minutes, allowing for disintegrated fragments to leave the drum through the 2 mm sieve mesh. The remaining fragments in the drum are dried and weighed. Gamble (1971), a PhD student at University of Illinois, United States, suggested that this be repeated over a second cycle of slaking. The dry mass of the sample remaining in the drum at the end of the second cycle, expressed as a percentage of the *original dry mass* in the drum at the beginning of the test, is known as the *second-cycle slake durability index*, $I_{\rm d2}$, which varies in the range of 0–100%. For samples that are highly susceptible to slaking, $I_{\rm d2}$, is close to zero, and for very durable rocks, it is close to 100%.

The first-cycle slake durability index, I_{d1} , is defined as

$$I_{\rm d1} = \frac{m_2}{m_1} \times 100 \tag{3.13}$$

The second-cycle slake durability index, I_{d2} , is defined as

$$I_{\rm d2} = \frac{m_3}{m_1} \times 100 \tag{3.14}$$

Here m_1 = dry mass of the original lumps in the drum, m_2 = dry mass of the material retained in the drum after the first cycle and m_3 = dry mass of the material retained after the second cycle.

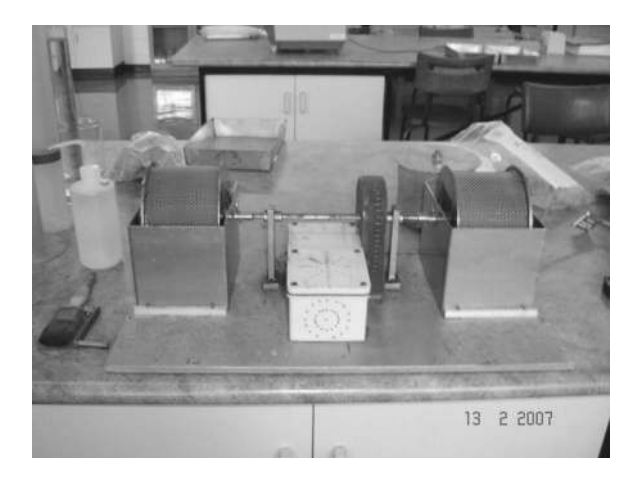


FIGURE 3.13 Slake durability apparatus.

TABLE 3.9					
Durability	Classification	Based on	Slake	Durability	Index

Durability	\mathbf{I}_{d1}	I_{d2}
Very high	>99	98-100
High	98–99	95–98
Medium high	95–98	85–95
Medium	85–95	60-85
Low	60-85	30-60
Very low	<60	0-30

Source: Gamble, J.C., Durability – Plasticity classification of shales and other argillaceous rocks, PhD thesis, University of Illinois at Urbana-Champaign, IL, 1971

The second-cycle slake durability index, $I_{\rm d2}$, is the one that is commonly used as a measure of rock durability. Only in rocks that are classified as very low in durability, with $I_{\rm d2} < 10\%$, it is recommended to include $I_{\rm d1}$ as well. A durability classification of rocks based on the slake durability index, as proposed by Gamble (1971), is given in Table 3.9. This is slightly different from what is proposed by Franklin and Chandra (1972), who did not distinguish between the two cycles and used a single slake durability index, $I_{\rm d}$, based on the first cycle. ASTM D4644 and ISRM (1979) suggest reporting $I_{\rm d2}$ as the slake durability index. For rocks of higher durability, three or more cycles (i.e. $I_{\rm d3}$, $I_{\rm d4}$ and so on) may be appropriate.

3.6.1 Test Procedure

The standard procedure for the slake durability test is described in ISRM (1979) and ASTM D4644. A representative sample of 10 rock lumps, each with a mass of 40-60 g, giving a total mass of 450-550 g, is dried and placed within the drum. The corners of the lumps should be rounded off so that they are approximately spherical. The drum is partly submerged in the slaking fluid (see Figure 3.13), which can be tap water, seawater and so on, to simulate the service environment. For each cycle, the drum is rotated at a standard rate of 20 rev/min for 10 minutes. Generally, only $I_{\rm d2}$ is reported to the nearest 0.1%. Only when $I_{\rm d2}$ is less than 10% is it suggested to report $I_{\rm d1}$ as well. A typical slake durability test datasheet is shown in Table 3.10.

The usefulness of the slake durability test is limited to relatively weak rocks such as shales, mudstones and other highly weathered rocks.

3.7 SCHMIDT HAMMER TEST

The Schmidt (1951) hammer (Figure 3.14) was originally developed in 1948 for testing the hardness of concrete. It is a simple, portable and inexpensive device that gives the rebound hardness value, R, for an intact rock specimen in the laboratory or the rock mass in situ. The test is generally non-destructive for rocks of at least moderate strength, and therefore, the same specimen can be used for other tests. ASTM

TABLE 3.10 Slake Durability Test Datasheet

Sample no.	Porcellanite2	Porcellanite7	Claystone1	Claystone3	Claystone8
Mass of drum + dry sample (m_1) , g	1476	1457	1464	1493	1503
Mass of drum + dry sample after first cycle (m_2) , g	1472	1452	1125	1114	1103
Mass of drum + dry sample after second cycle (m_3) , g	1467	1446	1013	1004	1009
Mass of drum (m_4) , g	971	970	968	969	968
Second-cycle slake durability index, I_{d2}	98.2	97.7	9.1	6.7	7.7
First-cycle slake durability index, $I_{\rm d1}$	99.2	99.0	31.7	27.7	25.2
Mass of drum + dry sample after third cycle, g (only if required)	1464	1443	_	_	_
Duration of third cycle (if not 10 minutes)					
Third-cycle slake durability index, I_{d3}	97.6	97.1	-	-	-
Mass of drum + dry sample after fourth cycle, g (only if required)	1468.0	1447.0			
Duration of fourth cycle (if not 10 minutes)	30 minutes	30 minutes			
Fourth-cycle slake durability index, I_{d4}	98.4	97.9			
Slaking fluid	Seawater		Tap water		
Temperature of slaking fluid	26°C	26°C	27°C	27°C	27°C

D5873 and ISRM (1978b) recommend this test for rocks with UCS of 1–100 MPa and 20–150 MPa, respectively. This is a popular index test on rocks, and the rebound hardness, *R*, has been correlated with rock properties such as UCS and *E*. The ISRM suggested method was revised by Aydin (2009).

The hammer consists of a spring-loaded metal piston that is released when the plunger is pressed against the rock surface. The impact of the piston on the plunger transfers the energy to the rock. How much of this energy is recovered depends on the hardness of the rock and is measured by the rebound height of the piston. The harder the surface, the shorter the penetration time (i.e. smaller impulse and less energy loss), and hence the greater the rebound. Rebound hardness R is a number that varies in the range of 0–100.



FIGURE 3.14 Schmidt hammer test.

Two types of Schmidt hammers are commonly used. They are L-type with an impact energy of 0.735 N·m and N-type with an impact energy of 2.207 N·m. The measured rebound hardness is denoted by $R_{\rm L}$ and $R_{\rm N}$, respectively. Other few notations used in the literature for rebound hardness are $H_{\rm R}$, N, SRH and so on. Prior to 2009, ISRM recommended only L-type hammers; now both types are allowed (Aydin, 2009). N-type hammers were mostly used for concrete. However, they are less sensitive to surface irregularities and are suited for field applications. ASTM does not specify the type of hammer.

3.7.1 Test Procedure

A Schmidt hammer must be calibrated first, using a calibration test anvil supplied by the manufacturer, based on the average of 10 readings. A correction factor (CF) is computed as

$$CF = \frac{Specified standard value of the anvil}{Average of the 10 readings on the anvil}$$
(3.15)

and it has to be applied to all future readings. This factor is to account for the spring losing its stiffness with time. For L-type hammers, the test specimen must be of at least NX (54 mm) core size, with length greater than 100 mm (ISRM). ASTM suggests a minimum length of 150 mm. For N-type hammers, ISRM suggests 84 mm diameter or larger cores (Aydin, 2009). The hammer should be used vertically

upwards, horizontally or vertically downwards, with a ±5° tolerance. ISRM recommends 20 readings at different locations, with an option to stop when the subsequent 10 readings differ by less than 4. ASTM recommends 10 readings. ISRM (1978b) suggests using the average of the top 10 readings. ASTM recommends discarding the readings that differ from the average by more than 7 and averaging the rest. The revised ISRM (Aydin, 2009) suggests not discarding any data and presenting the values as a histogram with the mean, median, mode and range.

3.8 TRIAXIAL TEST

As a first approximation, it can be assumed that rocks, like most geomaterials, follow the *Mohr–Coulomb* failure criterion, given by

$$\tau_{\rm f} = c + \sigma \tan \phi \tag{3.16}$$

where τ_f = shear strength (or shear stress at failure on the failure plane), σ = normal stress on the failure plane, c = cohesion and ϕ = friction angle. Cohesion and friction angle are the shear strength parameters of the rock and are constants. Thus, it can be seen from Equation 3.16 that τ_f is proportional to σ . In terms of major and minor principal stresses at failure, Equation 3.16 can be written as

$$\sigma_1 = \left(\frac{1+\sin\phi}{1-\sin\phi}\right)\sigma_3 + 2c\left(\frac{1+\sin\phi}{1-\sin\phi}\right)^{0.5}$$
(3.17)

There are also other *failure criteria* for rocks such as Hoek-Brown, where the failure envelope is non-linear.

Similar to the triaxial tests on soils, here too cylindrical rock specimens are subjected to different confining pressures and loaded axially to failure (Figure 3.15a and b). The only difference is that the loads and pressures are much higher. The test procedure suggested by ISRM (1983) does not have a provision for pore water pressure or drainage measurements. It is similar to an unconsolidated undrained triaxial test on a clay specimen. Only the procedure for an individual test is described here. The procedures for a multiple failure state test, similar to staged test and a continuous failure state test, are given in ISRM (1983).

3.8.1 Test Procedure

The test specimen diameter should be at least of NX core size (54 mm), and the length should be approximately equal to two to three times the diameter. The test specimens should be cut and prepared using clean water. The ends of the test specimens shall be flat to ± 0.01 mm and be parallel to each other and at right angles to the longitudinal axis. The sides of the specimens shall be smooth and free of abrupt irregularities and straight within 0.3 mm over the full length of the specimen. The diameter of the specimen should be at least 10 times larger than the largest mineral grain present. The use of capping material or end surface treatment is not permitted.

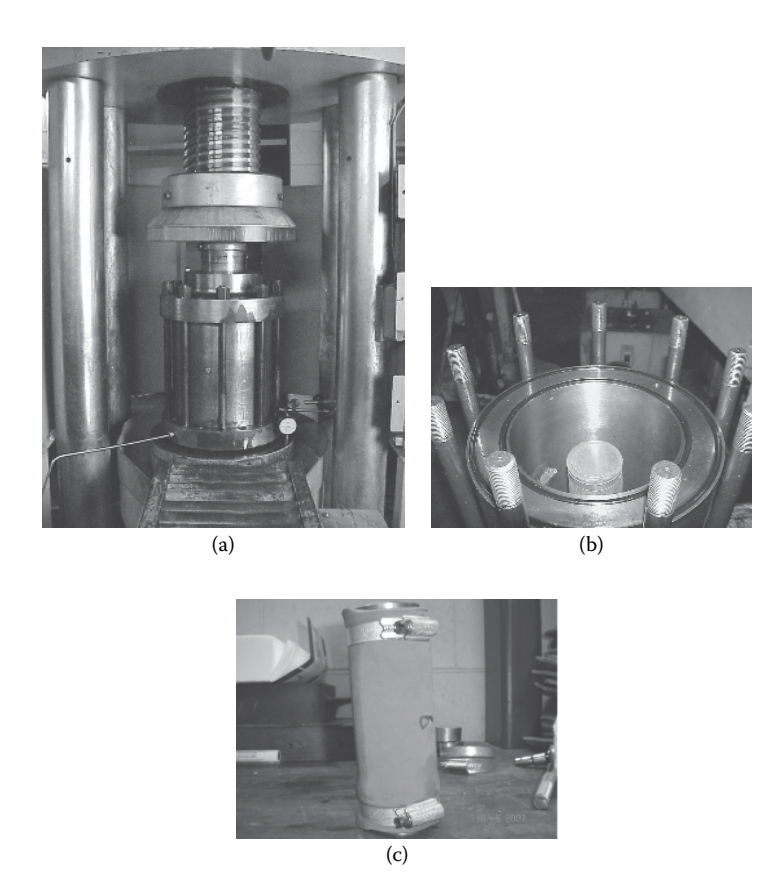


FIGURE 3.15 Rock triaxial test: (a) triaxial test in progress, (b) triaxial cell interior with specimen and (c) rock specimen enclosed in membrane.

The specimen is enclosed in a flexible, impervious membrane (Figure 3.15c) to prevent the confining fluid from entering the specimen pores. Sometimes, it is required to make customised membranes that suit the different core diameters. Oil is generally used as the confining fluid and the confining pressure (σ_3) is increased to desired levels. The vertical stress ($\Delta\sigma$) on the specimen is increased at a constant stress or strain rate (e.g. 0.5–1.0 MPa/s) until failure occurs, ideally within 5–15 minutes. The vertical stress at failure (σ_1) is given by $\sigma_3 + \Delta\sigma$.

3.9 EMPIRICAL CORRELATIONS

There are several empirical correlations interrelating the intact rock parameters such as uniaxial compressive strength σ_c , indirect tensile strength σ_t , point load strength index $I_{s(50)}$ and so on. Some of the correlations between the uniaxial compressive strength and the indirect tensile strength are summarised in Table 3.11. Correlations between the uniaxial compressive strength and the point load strength index are summarised in Table 3.12.

TABLE 3.11

$\sigma_c - \sigma_t$ Correlations

Correlation	Reference	Comments
$\sigma_c = 10.5\sigma_t + 1.2$	Hassani et al. (1979)	
$\sigma_{c} = 3.6\sigma_{t} + 15.2$	Szlavin (1974)	United Kingdom; 229 tests
$\sigma_c = 2.84\sigma_t - 3.34$	Hobbs (1964)	Mudstone, sandstone and limestone
$\sigma_c = 12.4\sigma_t - 9.0$	Gunsallus and Kulhawy (1984)	Dolostone, sandstone and limestone from the United States
$\sigma_{\rm c} = 10\sigma_{\rm t}$	Broch and Franklin (1972)	

TABLE 3.12

$\sigma_c - I_{s(50)}$ Correlations

Correlation	Reference	Comments
$\sigma_{\rm c} = 24I_{\rm s(50)}$	Broch and Franklin (1972)	
$\sigma_{\rm c} = 24I_{\rm s(50)}$	Bieniawski (1975)	Sandstone, South Africa
$\sigma_{c} = 29I_{s(50)}$	Hassani et al. (1980)	Sedimentary rocks, United Kingdom
$\sigma_{\rm c} = 14.5 I_{\rm s(50)}$	Forster (1983)	Dolerite and sandstone
$\sigma_{\rm c} = 12.5 I_{\rm s(50)}$	Chau and Wong (1996)	Hong Kong rocks
$\sigma_{\rm c} = 16I_{\rm s(50)}$	Read et al. (1980)	Basalt
$\sigma_{c} = 20I_{s(50)}$	Read et al. (1980)	Sedimentary rocks, Australia
$\sigma_{c} = 23.4 I_{s(50)}$	Singh and Singh (1993)	Quartzite, India
$\sigma_{c} = 15.3I_{s(50)} + 16.3$	D'Andrea et al. (1964)	Range of rock types
$\sigma_{c} = 16.5I_{s(50)} + 51.0$	Gunsallus and Kulhawy (1984)	Dolostone, sandstone and limestone from the United States
$\sigma_{\rm c} = 9.3I_{\rm s(50)} + 20.04$	Grasso et al. (1992)	
$\sigma_{c} = 23I_{s(54)} + 13$	Cargill and Shakoor (1990)	Mostly from the United States and some from Canada; 54-mm-diameter cores

Gunsallus and Kulhawy (1984) carried out these tests on rock specimens of dolostones (predominantly dolomite), sandstones and limestones in the United States, representing eight different rock types, and assessed the different correlations reported in the literature to find that the two popular correlations, $\sigma_c = 10\sigma_t$ and $\sigma_c = 24I_{s(50)}$, work quite well.

3.10 SUMMARY

- 1. A UCS of 1 MPa is the cut-off between soils and rocks.
- 2. Laboratory tests are generally carried out on intact rock specimens, which will not reflect the discontinuities present within the rock mass.
- 3. UCS is the most used strength parameter in the design and analysis of rocks.

4. It is difficult to carry out a proper tensile strength test on rocks. The Brazilian indirect tensile test is a simple way around this problem. How close the estimated tensile strength is to the real value is the million-dollar question.

- 5. In the Brazilian indirect tensile test, tensile failure is induced in the rock specimen by applying a vertical compressive load diametrically.
- 6. The advantage of point load test is that it can be tested on irregular-shaped specimens and gives a quick estimate of the point load strength index. The simple apparatus can be taken to the site where several specimens can be tested within a few minutes, which will be of good value in preliminary assessments.
- 7. The Schmidt hammer test is not recommended for very weak or very hard rocks. It is a non-destructive test that can be carried out on rock cores in the laboratory or in the field outcrops. It gives a dimensionless empirical relative hardness number in the range of 0–100.
- 8. Triaxial tests are effective for assessing the strength variation with confining pressures.

REVIEW EXERCISES

- 3.1. State whether the following are true or false.
 - i. Uniaxial compressive strength is the same as UCS.
 - ii. The point load strength index is a dimensionless number.
 - iii. The larger the slake durability index, the higher the durability of the rock in wetting and drying.
 - iv. In the slake durability test, $I_{\rm d2}$ is always less than $I_{\rm d1}$.
 - v. In a UCS test, the larger the specimen diameter, the greater the strength.
 - vi. In a UCS test, the faster the rate of loading, the lower the strength.
 - vii. The larger the core size, the greater the uniaxial compressive strength.
- 3.2. Circle the correct answer.
 - i. Which of the following rock cores is larger in diameter?
 - a. AQ
 - b. BO
 - c. HQ
 - d. NQ
 - ii. Which of the following rock core diameters is the minimum recommended size for most laboratory tests?
 - a. AX
 - b. BX
 - c. EX
 - d. NX
 - iii. The typical range for the uniaxial compressive strength of rocks is
 - a. 1-400 kPa
 - b. 1-400 MPa

- c 1-400 GPa
- d. None of these
- iv. Which of the following can be a typical value for the E/UCS ratio of a rock?
 - a. 3
 - b. 30
 - c. 300
 - d. 3000
- v. Which of the following tests require the most sample preparation?
 - a. Slake durability test
 - b. Point load test
 - c. UCS test
 - d. Schmidt hammer test
- vi. Which of the following tests require the least sample preparation?
 - a. UCS test
 - b. Indirect tensile strength test
 - c. Point load test
 - d. Direct tensile strength test
- vii. Which of the following is the preferred aspect (length/diameter) ratio for a Brazilian indirect tensile strength test specimen?
 - a. 3
 - b. 2
 - c. 1
 - d. 0.5
- viii. Which one of the following tensile strengths does the Brazilian indirect tensile strength test measure?
 - a. At the centre
 - b. At the top of the diameter
 - c. At the bottom of the diameter
 - d. Average value for the entire specimen volume
 - ix. Which of the following parameters (in MPa) would be the smallest?
 - a. σ_c from a UCS test
 - b. σ, from a Brazilian indirect tensile strength test
 - c. $I_{s(50)}$ from a point load strength test
- 3.3. In a 1500-mm rock core run, the following rock pieces were recovered from a borehole: 53 mm, 108 mm, 125 mm, 75 mm, 148 mm, 320 mm, 68 mm, 145 mm, 35 mm and 134 mm. Find the RQD and the core recovery ratio.

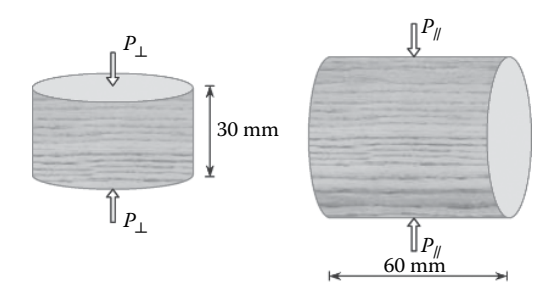
Answer: 65%, 81%

3.4. For a cylindrical rock specimen subjected to an axial load (e.g. UCS), neglecting higher-order terms of strains, show that the volumetric strain, ε_{vol} , is given by

$$\varepsilon_{\rm vol} = \varepsilon_{\rm a} + 2\varepsilon_{\rm d}$$

where $\varepsilon_a = axial$ strain and $\varepsilon_d = diametral$ strain.

3.5. Point load tests were carried out on two sedimentary rock specimens of 54 mm diameter (NX core), as shown in the following figure. The loads P_{\perp} and P_{\parallel} at failure are 6.28 kN and 4.71 kN, respectively. Find the point load strength index $I_{s(50)}$ in the two directions and compute the point load strength anisotropy index $I_{a(50)}$.



Answer: 2.92 MPa, 1.68 MPa; 1.74

- 3.6. Surf the web and do a research on the following and explain them in less than 100 words each.
 - a. Wire line drilling
 - b. Triple-tube sampling
 - Types of drilling in rocks

REFERENCES

ASTM D3967-16. Standard test method for splitting tensile strength of intact rock core specimens.

ASTM D4543-19. Standard practices for preparing rock core as cylindrical test specimens and verifying conformance to dimensional and shape tolerances.

ASTM D4644-16. Standard test method for slake durability of shales and similar weak rocks.

ASTM D5731-16. Standard test method for determination of the point load strength index and application to rock strength classifications.

ASTM D5873-14. Standard test method for determination of rock hardness by rebound hammer method.

ASTM D6032-17. Standard test method for determining rock quality designation (RQD) of rock core.

ASTM D7012-14e1. Standard test method for compressive strength and elastic moduli of intact rock core specimens under varying states of stress and temperatures.

Aydin, A. (2009). ISRM suggested method for determination of the Schmidt hammer rebound hardness: Revised version. *International Journal of Rock Mechanics and Mining Sciences*, Vol. 46, No. 3, pp. 627–634.

Bieniawski, Z.T. (1975). The point load test in geotechnical practice. *Engineering Geology*, Vol. 9, No. 1, pp. 1–11.

Broch, E. and Franklin, J.A. (1972). The point load strength test. *International Journal of Rock Mechanics and Mining Sciences*, Vol. 9, No. 6, pp. 669–697.

Brown, E.T. (Ed.) (1981). Rock Chracterisation Testing and Monitoring – ISRM Suggested Methods. Pergamon Press, Oxford, 211pp.

Cargill, J.S. and Shakoor, A. (1990). Evaluation of empirical methods for measuring the uniaxial strength of rock. *International Journal of Rock Mechanics and Mining Sciences & Geomechanics Abstracts*, Vol. 27, No. 6, pp. 495–503.

- Chau, K.T. and Wong, R.H.C. (1996). Uniaxial compressive strength and point load strength. *International Journal of Rock Mechanics and Mining Sciences & Geomechanics Abstracts*, Vol. 33, No. 2, pp. 183–188.
- D'Andrea, D.V., Fisher, R.L. and Fogelson, D.E. (1964). Prediction of compression strength from other rock properties. *Colorado School of Mines Quarterly*, Vol. 59, No. (4B), pp. 623–640.
- Deere, D.U. (1964). Technical description of rock cores for engineering purposes. *Rock Mechanics and Engineering Geology*, Vol. 1, pp. 17–22.
- Deere, D.U. and Miller, R.P. (1966). Engineering classification and index properties of intact rock. *Report AFWL-TR-65–116*, *Air Force Weapon Laboratory (WLDC)*, Kirtland Airforce Base, New Mexico, 308pp.
- Forster, I.R. (1983). The influence of core sample geometry on the axial pointload test. *International Journal of Rock Mechanics and Mining Science & Geomechanics Abstracts*, Vol. 20, No. 6, pp. 291–295.
- Franklin, J.A. and Chandra, J.A. (1972). The slake durability test. *International Journal of Rock Mechanics and Mining Sciences*, Vol. 9, No. 3, pp. 325–341.
- Gamble, J.C. (1971). *Durability Plasticity Classification of Shales and Other Argillaceous rocks*, PhD thesis, University of Illinois at Urbana-Champaign, IL, 159pp.
- Gercek, H. (2007). Poisson's ratio values for rocks. *International Journal of Rock Mechanics* and Mining Sciences, Vol. 44, No. 1, pp. 1–13.
- Goodman, R.E. (1980). *Introduction to Rock Mechanics*. 1st edition, John Wiley & Sons, New York.
- Goodman, R.E. (1989). Introduction to Rock Mechanics. 2nd edition, John Wiley & Sons, New York.
- Grasso, P., Xu, S. and Mahtab, A. (1992). Problems and promises of index testing of rocks. *Proceedings of the 33rd US Symposium of Rock Mechanics*, Santa Fe, New Mexico, A.A. Balkema, Rotterdam, pp. 879–888.
- Gunsallus, K.L. and Kulhawy, F.H. (1984). A comparative evaluation of rock strength measures. *International Journal of Rock Mechanics and Mining Sciences & Geomechanics Abstracts*, Vol. 21, No. 5, pp. 233–248.
- Handin, J. (1966). Strength and ductility, in *Handbook of Physical Contacts*, Clark, S.P., editor, Geological Society of America, New York, pp. 223–289.
- Hassani, F.P., Scoble, M.J. and Whittaker, B.N. (1980). Application of point load index test to strength determination of rock and proposals for new size-correction chart, in *Proceedings of 21st US Symposium on Rock Mechanics*, Summers, D.A., editor, University of Missouri Press, Rolla, MO, pp. 543–564.
- Hassani, F.P., Whittaker, B.N. and Scoble, M.J. (1979). Strength characteristics of rocks associated with opencast coal mining in UK. *Proceedings of 20th U.S. Symposium on Rock Mechanics*, Austin, TX, pp. 347–356.
- Hawkes, I. and Mellor, M. (1970). Uniaxial testing in rock mechanics laboratories. *Engineering Geology*, Vol. 4, No. 3, pp. 179–285.
- Hobbs, D.W. (1964). Simple method for assessing uniaxial compressive strength of rock. *International Journal of Rock Mechanics and Mining Sciences & Geomechanics Abstracts*, Vol. 1, No. 1, pp. 5–15.
- Hoek, E. and Brown, E.T. (1980). *Underground Excavations in Rock*. Institution of Mining and Metallurgy, London, 527pp.
- Hoek, E. and Brown, E.T. (1997). Practical estimates of rock mass strength. *International Journal of Rock Mechanics and Mining Sciences & Geomechanics Abstracts*, Vol. 34, No. 8, pp. 1165–1186.
- Hoek, E. and Diederichs, M.S. (2006). Empirical estimation of rock mass modulus. *International Journal of Rock Mechanics and Mining Sciences*, Elsevier, Vol. 43, No. 2, pp. 203–215.

Hondros, G. (1959). The evaluation of Poisson's ratio and the modulus of materials of a low tensile resistance by the Brazilian (indirect tensile) test with particular reference to concrete. *Australian Journal of Applied Science*, Vol. 10, No. 3, pp. 243–268.

- Hudson, J.A. (1989). Rock Mechanics Principles in Engineering Practice. Butterworths, London.
- ISRM (1978a). International Society of Rock Mechanics, Commission on Standardisation of Laboratory and Field Tests. Suggested methods for determining tensile strength of rock materials. *International Journal of Rock Mechanics and Mining Sciences & Geomechanics Abstract*, Vol. 15, No. 3, pp. 99–103.
- ISRM (1978b). International Society of Rock Mechanics, Commission on Standardisation of Laboratory and Field Tests. Suggested methods for determining hardness and abrasiveness of rocks. *International Journal of Rock Mechanics and Mining Sciences & Geomechanics Abstract*, Vol. 15, No. 3, pp. 89–97.
- ISRM (1978c). International Society of Rock Mechanics, Commission on Standardisation of Laboratory and Field Tests. Suggested methods for the quantitative description of rock discontinuities in rock masses. *International Journal of Rock Mechanics and Mining Sciences & Geomechanics Abstracts*, Vol. 15, No. 6, pp. 319–368.
- ISRM (1979). International Society of Rock Mechanics, Commission on Standardisation of Laboratory and Field Tests. Suggested methods for determining water content, porosity, density, absorption and related properties and swelling and slake durability index properties. *International Journal of Rock Mechanics and Mining Sciences & Geomechanics Abstracts*, Vol. 16, No. 2, pp. 143–156.
- ISRM (1983). International Society of Rock Mechanics, Commission on Testing Methods. Suggested method for determining the strength of rock materials in triaxial compression. *International Journal of Rock Mechanics and Mining Sciences & Geomechanics Abstract*, Vol. 20, No. 6, pp. 285–290.
- ISRM (1985). International Society of Rock Mechanics, Commission on Testing Methods. Suggested method for determining point load strength. *International Journal of Rock Mechanics and Mining Sciences & Geomechanics Abstract*, Vol. 22, No. 2, pp. 51–60.
- Mellor, M. and Hawkes, I. (1971). Measurement of tensile strength by diametral compression of discs and annuli. *Engineering Geology*, Vol. 5, No. 3, pp. 173–225.
- Peck, R.B., Hanson, W.E. and Thornburn, T.H. (1974). *Foundation Engineering*. 2nd edition, John Wiley & Sons, New York.
- Read, J.R.L., Thornten, P.N. and Regan, W.M. (1980). A rational approach to the point load test. *Proceedings of ANZ Geomechanics Conference*, Vol. 2, pp. 35–39.
- Reichmuth, D.R. (1968). Point load testing of brittle materials to determine tensile strength and relative brittleness, Status of Practical Rock Mechanics. *Proceedings of 9th Symposium of Rock Mechanics, Colorado School of Mines*, Boulder, CO, pp. 134–159.
- Russell, A.R. and Wood, D.M. (2009). Point load tests and strength measurements for brittle spheres. *International Journal of Rock Mechanics and Mining Sciences*, Vol. 46, No. 2, pp. 272–280.
- Schmidt, E. (1951). A non-destructive concrete tester. *Concrete*, Vol. 59, No. 8, pp. 34–35.
- Singh, V.K. and Singh, D.P. (1993). Correlation between point load index and compressive strength for quartzite rocks. *Geotechnical and Geological Engineering*, Vol. 11, pp. 269–272.
- Szlavin, J. (1974). Relationship between some physical properties of rock determined by laboratory tests. *International Journal of Geomechanics and Mining Sciences & Geomechanics Abstracts*, Vol. 11, No. 2, pp. 57–66.
- Timoshenko, S. (1934). Theory of Elasticity. McGraw Hill, New York.

4 Rock Mass Classification

4.1 INTRODUCTION

When a site investigation is carried out, cylindrical rock cores are collected from boreholes for their identification, laboratory tests and classification. What we learn from these rock cores is only part of the story; the situation can be very different in the larger rock mass in situ, thanks to the discontinuities present in the rock mass in the form of joints, faults and bedding planes. These are the planes of weakness, which become the weakest links and can cause instability.

The rock cores are intact rock specimens that are so small that they are often free of discontinuities. Even when they break along discontinuities, we trim them further to have a 'joint-free' core for the laboratory tests. On the other hand, the larger rock mass may have one or more sets of discontinuities that can have a significant influence on stability, which is not reflected in the intact rock specimen. The strength of the intact rock is only one of the key parameters used in classifying the rock mass. The different laboratory tests discussed in Chapter 3 are for intact rock specimens, with no reflection on the extent of discontinuities present within the rock mass. The laboratory test data are used only here to get the big picture relating to the much larger rock mass. It is important to understand the difference between the rock mass and the intact rock.

As we discussed when looking at kinematic analysis in Chapter 2, the orientations of the discontinuities can play a significant role in the stability of rock slopes and underground openings. In the same rock mass, the orientation of the discontinuity sets can be favourable or unfavourable, depending on how the facility (e.g. tunnel) is located with respect to the orientations of the discontinuities. There are several variables (e.g. orientation, spacing and so on) associated with the discontinuities in a rock mass, all of which are relevant in rock mass classification. This chapter discusses the different ways of classifying the rock mass with due consideration to the above variables, including the intact rock strength.

4.2 INTACT ROCK AND ROCK MASS

Figure 4.1a shows a schematic diagram of a rock mass with two sets of discontinuities and an intact rock specimen that is typically tested in the laboratory. The stability of the rock mass under a specific loading condition (e.g. foundation or tunnelling) can be very different from the stability of the intact rock specimen, thanks to the discontinuities. Due to the presence of discontinuities, the rock mass is weaker than the intact rock specimen, showing lower strength and stiffness (see Figure 4.1b). In

DOI: 10.1201/9781032725161-4

addition, the rock mass is more permeable, with the discontinuities allowing greater access to water, which can make the rock mass even weaker. Water reduces the friction along the discontinuities, and the increased pore water pressure reduces the effective stresses and hence the shear strength.

The stability of the rock mass is thus governed by the properties of the intact rock as well as the relative ease at which the rock pieces (or blocks) can slide, rotate or topple. This in turn is influenced by the dimensions of the individual blocks and the frictional characteristics at the joints that separate the blocks. We will see in the following sections that the rock mass is generally characterised based on the properties of the intact rock, block size and the frictional characteristics of the joint. The frictional characteristics include the roughness profile of the joint surface and the quality of the infill material.

Discontinuity is a generic term used to describe a fault, joint, bedding plane, foliation, cleavage or schistosity. A fault is a planar fracture along which noticeable movement has taken place. Joints are filled or unfilled fractures within the rock mass that do not show any sign of relative movement (Figure 4.2). Bedding planes are formed when the sediments are deposited during the rock formation process, creating planes of weakness, which are not necessarily horizontal. They are common in sedimentary rocks. Foliation occurs in metamorphic rocks where the rock-forming minerals exhibit a platy structure or banding, thus developing planes of weakness. Cleavages are planes of weaknesses that occur often as parallel layers and are formed in a metamorphic process. Schistosity is a type of cleavage seen in metamorphic rocks such as schists and phyllites, where the rocks tend to split along parallel planes of weakness.

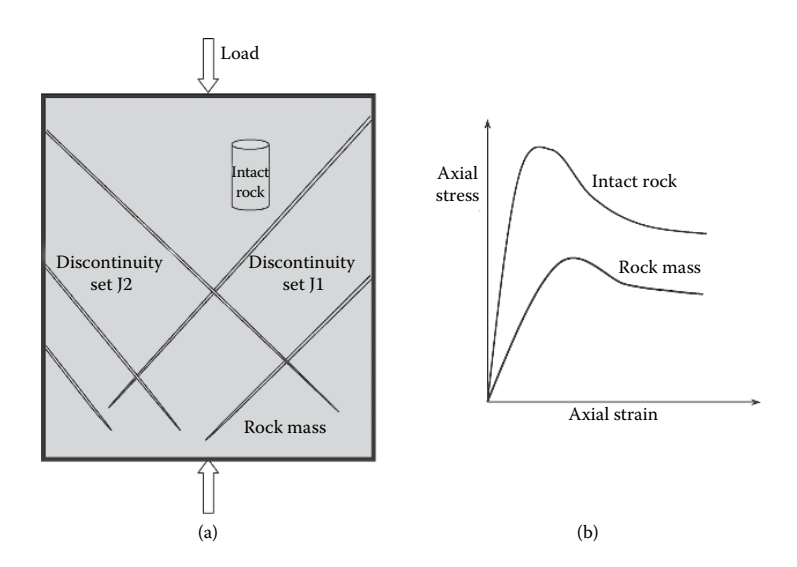


FIGURE 4.1 (a) Rock mass and intact rock and (b) stress-strain plot.

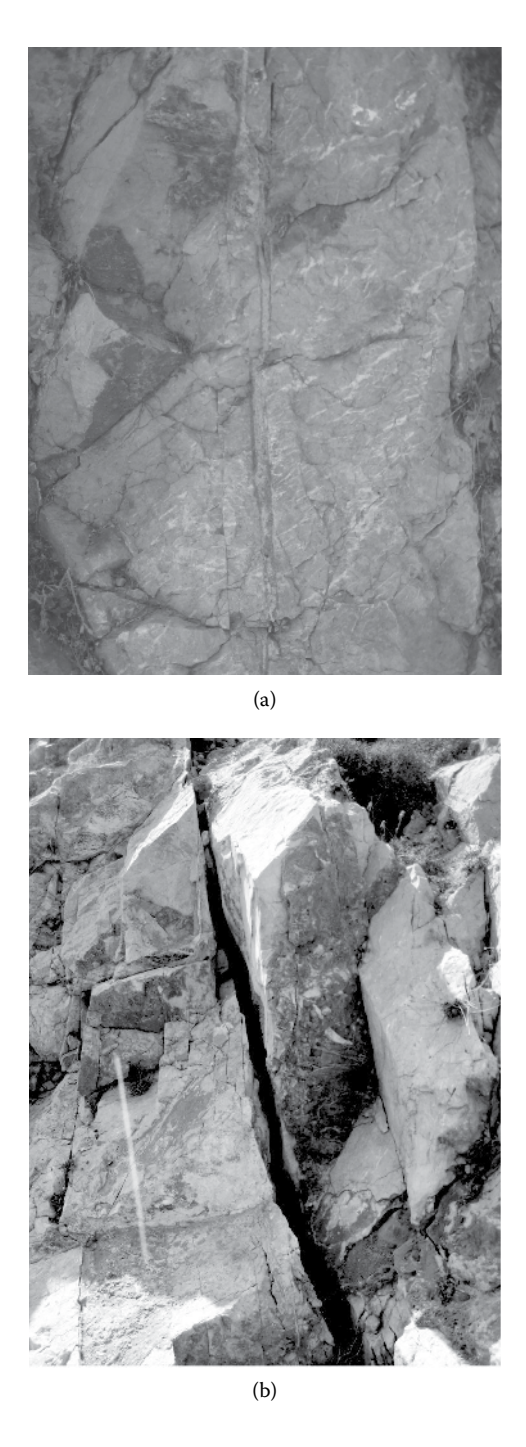


FIGURE 4.2 Joints: (a) filled and (b) unfilled.

TABLE 4.1 Classification of Soil and Rock Strengths

Grade	Description	Field identification	σ_{c} or q_{u} (MPa)	Rock types
S1	Very soft clay	Easily penetrated several inches by fist.	<0.025	
S2	Soft clay	Easily penetrated several inches by thumb.	0.025-0.05	
S 3	Firm clay	Can be penetrated several inches by thumb with moderate effort.	0.05-0.10	
S4	Stiff clay	Readily indented by thumb, but penetrated only with great effort.	$0.1-0.25^{a}$	
S5	Very stiff clay	Readily indented by thumbnail.	0.25^{a} -0.50^{a}	
S6	Hard clay	Indented with difficulty by thumbnail.	>0.5ª	
R0	Extremely weak rock	Indented by thumbnail.	0.25-1.0	Stiff fault gouge
R1	Weak rock	Crumbles under firm blows with point of geological hammer; can be peeled by pocketknife.	1–5	Highly weathered or altered rock
R2	Weak rock	Can be peeled by a pocketknife with difficulty; shallow indentations made by firm blow with a point of geological hammer.	5–25	Chalk, rock salt, potash
R3	Medium strong rock	Cannot be scraped or peeled with a pocketknife; specimen can be fractured with a single firm blow of a geological hammer.	25–50	Claystone, coal, concrete, schist, shale, siltstone
R4	Strong rock	Specimen requires more than one blow by geological hammer to fracture it.	50–100	Limestone, marble, phyllite, sandstone, schist, shale
R5	Very strong rock	Specimen requires many blows of geological hammer to fracture it.	100–250	Amphibiolite, sandstone, basalt, gabbro, gneiss, granodiorite, limestone, marble, rhyolite, tuff
R6	Extremely strong rock	Specimen can only be chipped by a geological hammer.	>250	Fresh basalt, chert, diabase, gneiss, granite, quartzite

Source: Hoek, E. and Brown, E.T., Int. J. Rock Mech. Min. Sci. Geomech. Abstr., 34, 1165, 1997. Source: ISRM, Int. J. Rock Mech. Min. Sci. Geomech. Abstr., 15, 319, 1978.

^a Slightly different to classification in geotechnical context.

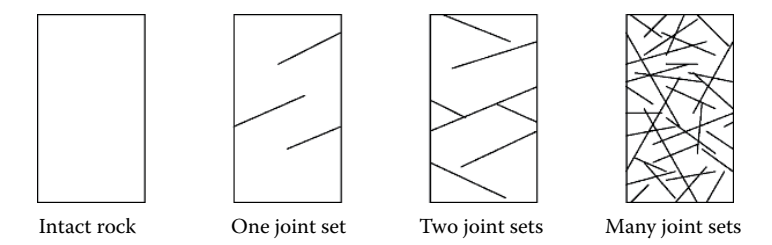


FIGURE 4.3 Number of joint sets.

Table 4.1 shows the classification of soils and rocks on the basis of the uniaxial compressive strength, as recommended by the International Society for Rock Mechanics (ISRM) (1978). Also shown in the table are the rock types that fall into each group and simple index tests that can be carried out in the field to classify them.

The rock mass can have any number of joints. When there are no joints, ideally, the rock mass and the intact rock should have the same properties, provided the rock is homogeneous. Joints within a joint set are approximately parallel. One can even define an average spacing for a joint set. This is simply the distance between the two adjacent joints in the same set. An increasing number of joints and joint sets make the rock mass more and more fragmented, thus increasing the degrees of freedom of the individual pieces. In addition, the block sizes become smaller. This is evident in Figure 4.3, showing a diagrammatic representation of intact rock and rock masses with one or more joint sets.

4.3 FACTORS AFFECTING DISCONTINUITIES

There are several parameters that are used to describe discontinuities and the rock mass. They are as follows:

- Orientation
- Spacing
- Persistence
- · Roughness
- Wall strength
- Aperture
- Filling
- Seepage
- Number of joint sets
- Block size and shape

TABLE 4.2

Rock Classification Based on the Spacing of Discontinuities

Description	Spacing (mm)
Extremely close spacing	<20
Very close spacing	20-60
Close spacing	60-200
Moderate spacing	200-600
Wide spacing	600-2000
Very wide spacing	2000-6000
Extremely wide spacing	>6000

Source: ISRM, Int. J. Rock Mech. Min. Sci. Geomech. Abstr., 15, 319, 1978.

TABLE 4.3

Description for Persistence

Description	Trace length (m)
Very low persistence	<1
Low persistence	1–3
Medium persistence	3–10
High persistence	10–20
Very high persistence	>20

Source: ISRM, Int. J. Rock Mech. Min. Sci. Geomech. Abstr., 15, 319, 1978.

4.3.1 ORIENTATION

The orientation of the discontinuity, measured by the dip and dip direction, is very critical to stability, as we observed during the discussion of kinematic analysis in Chapter 2. By locating and/or aligning the structure (e.g. tunnel) in the right direction, the stability can be improved significantly.

4.3.2 SPACING

Spacing is the perpendicular distance between two adjacent discontinuities of the same set. It affects the hydraulic conductivity of the rock mass and the failure mechanism. Closely spaced joints can imply highly permeable rock. Spacing determines the intact rock block sizes within the rock mass, with closer spacing implying smaller blocks. The spacing can be used to describe the rock mass, as shown in Table 4.2.

4.3.3 Persistence

Persistence is a measure of the extent to which the discontinuity extends into the rock. In other words, what is the surface area of the discontinuity? This is the area that takes part in any possible sliding and hence is an important parameter in determining stability. Although this is an important parameter in characterising the rock mass, it is quite difficult to determine. The trace length of the discontinuity on the exposed surface is often taken as a crude measure of the persistence. The persistence of a rock mass can be described on the basis of Table 4.3. Spacing and persistence are two parameters that control the sizes of the blocks of intact rocks that make up the rock mass. They are both measured by a measuring tape.

4.3.4 ROUGHNESS

The roughness of a rock joint refers to the large-scale surface undulations (waviness) observed over several metres and the small-scale unevenness of the two sides relative to the mean plane, observed over several centimetres (see Figure 4.4). The large-scale undulations can be called stepped, undulating or planar; the small-scale unevenness can be called rough, smooth or slickensided. Figure 4.4 shows the three major large-scale undulations. Close-up views in Figure 4.4 show two (rough and smooth) of the three small-scale unevenness profiles. Slickenside is a standard term used for smooth and slick, shiny surfaces that look polished. Combining the

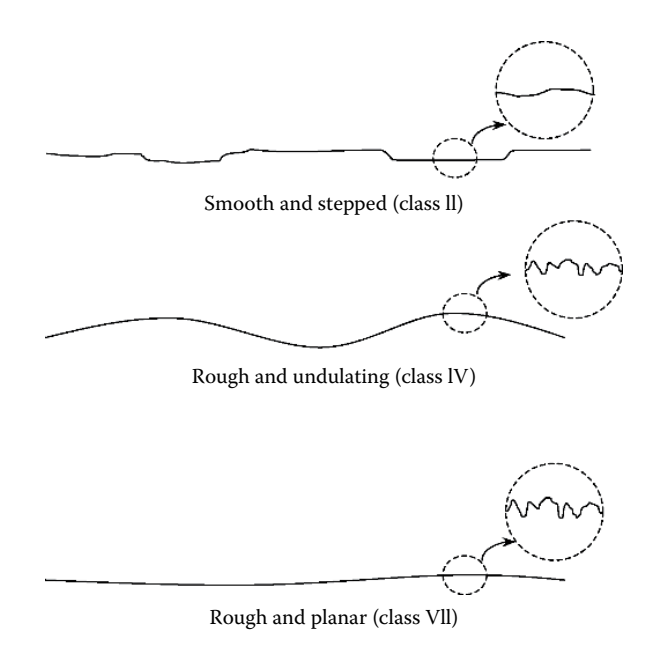


FIGURE 4.4 Three different roughness profiles.

TABLE 4.4 Roughness Classification

Class	Unevenness and undulations	J_r	
I	Rough, stepped	4 ^a	
II	Smooth, stepped	3^a	
III	Slickensided, stepped	2ª	•
IV	Rough, undulating	3	= SSS
V	Smooth, undulating	2	roughness
VI	Slickensided, undulating	1.5	rouş
VII	Rough, planar	1.5	ing
VIII	Smooth, planar	1	Increasing
IX	Slickensided, planar	0.5	Inc

Source: ISRM, Int. J. Rock Mech. Min. Sci. Geomech. Abstr., 15, 319, 1978. Note: Slickenside = polished and striated surface.

large-scale undulations and small-scale unevenness, the roughness of a joint can be classified as shown in Table 4.4, where the roughness decreases (in a broad sense) from Class I to IX. Large-scale surface undulations have a greater influence on the roughness than the small-scale unevenness, and this is reflected in Table 4.4. Although it is clear that when it comes to roughness, I > II > III, IV > V > VI, VII > VIII > IX and I > IV > VII, II > V > VIII, III > VI > IX, it is not always the case that class III is rougher than VII.

Roughness is an important factor governing the shear strength of the joint, especially when the discontinuity is undisplaced or interlocked. When displaced or the joints are infilled, the interlock is lost and the roughness is less important. Under such circumstances, the shear strength characteristics of the infill material govern the shear strength along the joint. Figure 4.4 shows three of the possible nine roughness profiles suggested in Table 4.4. The large-scale undulations and small-scale unevenness are shown separately. The joint roughness number J_r given in the table is used later in rock mass classification using the Q-system, which is discussed in more detail in Section 4.6.

There are special techniques such as the linear profiling method, compass and disc-clinometer method and photogrammetric method, available for measuring roughness. It is measured along the dip direction. Barton (1973) defined the term *joint roughness coefficient* (JRC), a value ranging from 0 for smooth or slickensided planar surfaces to 20 for rough, stepped or undulating surfaces. Roughness profiles with corresponding JRC values, as suggested by Barton and Choubey (1977) are also reproduced in ISRM (1978). JRC can be estimated visually by comparing the surface profiles with these standard ones.

 $^{^{\}rm a}$ $J_{\rm r}$ values for I, II and III as suggested by Barton (1987) and others by Hoek et al. (2005).

4.3.5 WALL STRENGTH

Wall strength refers to the compressive strength of the rock that makes up the walls of the discontinuity. Barton (1973) introduced the term joint wall compressive strength (JCS) to describe wall strength, which was later refined by Barton and Choubey (1977). This is an important factor that governs the shear strength and deformability. In unaltered joints, the uniaxial compressive strength (UCS) can be taken as JCS. When the joint surface is weathered, JCS can conservatively (i.e. lower bound) be taken as 25% of UCS.

The point load test or Schmidt hammer test are other possibilities here that can be used for estimating the UCS. JCS can be determined from the Schmidt hammer rebound number as follows (Franklin and Dusseault, 1989):

$$\log_{10} JCS(MPa) = 0.00088 \gamma R + 1.01$$
 (4.1)

where γ = unit weight of the rock (kN/m³) and R = Schmidt hammer rebound number on the joint surface.

The peak friction angle ϕ_{peak} of an unfilled joint can be in the range from 30° to 70°. When the joint walls are not weathered, the residual friction angle ϕ_r is typically in the range of 25° to 35°. In the case of weathered joint walls, ϕ_r can be as low as 15°.

The friction angle of a rough discontinuity surface has two components: basic friction angle of the rock material ϕ_b , and the roughness angle due to interlocking of the surface irregularities or asperities *i*. Therefore, when cohesion is neglected, the shear strength can be written as (remember the Mohr–Coulomb failure criterion from soil mechanics):

$$\tau = \sigma_{\rm n} \tan \left(\phi_{\rm b} + i \right) \tag{4.2}$$

where σ_n is the effective normal stress on the discontinuity plane. The basic friction angle ϕ_b is approximately equal to the residual friction angle ϕ_r . The roughness angle i (in degrees) can be estimated by

$$i = \operatorname{JRClog}\left(\frac{\operatorname{JCS}}{\sigma_{n}}\right) \tag{4.3}$$

At low values of effective normal stresses, the roughness angle estimated from Equation 4.3 can be unrealistically large. For designs, it is suggested that $\phi_b + i$ should be limited to 50° and JCS/ σ_n should be in the range of 3–100 (Wyllie and Mah, 2004). Substituting Equation 4.3 into Equation 4.2, we can express the shear strength as

$$\tau = \sigma_{\rm n} \tan \left[\phi_{\rm b} + JRC \log \left(\frac{JCS}{\sigma_{\rm n}} \right) \right]$$
 (4.4)

An average value of ϕ_b can be taken as 30° (ISRM, 1978). The roughness angle i can be as high as 40°. At the very early stages of movement along the discontinuity planes, there is relatively high interlocking due to the surface roughness, with a friction angle of $\phi + i$. When the asperities are sheared off, the roughness angle i decreases to zero, and the friction angle reaches the residual friction angle. In Equation 4.4, ϕ_b can be replaced by ϕ_r .

4.3.6 APERTURE

A discontinuity can be closed, open or filled. Aperture is the perpendicular distance between the two adjacent rock walls of an open discontinuity (Figure 4.2b), where the space is filled by air or water. The joint is called tight or open, depending on whether the aperture is small or large. Aperture is generally greater near the surface due to stress relief and becomes less with depth. Apertures can be described using terms given in Table 4.5. When the space between the walls is filled (Figure 4.2a) with sediments, we will not use the term *aperture* – we call it the width of the infill. A measuring tape or a feeler gauge can be used for measuring aperture.

4.3.7 FILLING

TABLE 4.5

>1000

Filling is the term used to describe the material (e.g. calcite, chlorite, clay and silt) that occupies the space between the adjacent rock walls of a discontinuity (Figure 4.2a). Its properties can differ significantly from those of the rocks on either side. It affects the permeability and the deformability of the rock mass. A complete description of the filling may include the width, mineralogy, grain size, water content, permeability and strength (see Table 4.1). Depending on the nature of the project, relevant laboratory tests may be carried out on the fillings to assess their characteristics.

Descriptions Associated with Apertures			
Aperture (mm)		Description	
< 0.1	Very tight		
0.1-0.25	Tight	Closed features	
0.25-0.5	Partly open		
0.5-2.5	Open		
2.5-10	Moderately wide	Gapped features	
>10	Wide		
10-100	Very wide		
100-1000	Extremely wide	Open features	

Source: ISRM, Int. J. Rock Mech. Min. Sci. Geomech. Abstr., 15, 319, 1978.

Cavernous

TABLE 4.6						
Classification	Based	on	Number	of	loint	Sets

Group	Joint sets
I	Massive, occasional random joints
II	One joint set
III	One joint set plus random
IV	Two joint sets
V	Two joint sets plus random
VI	Three joint sets
VII	Three joint sets plus random
VIII	Four or more joint sets
IX	Crushed rock, similar to soils

Source: ISRM, Int. J. Rock Mech. Min. Sci. Geomech. Abstr., 15, 319, 1978.

4.3.8 SEEPAGE

In a rock mass, seepage occurs mainly through discontinuities (secondary permeability), as the permeability of the intact rock (primary permeability) is generally very low. The observation is generally visual and hence subjective. An excavation can range from being literally dry to one that has a heavy inflow of water. ISRM (1978) has separate ratings from I (no seepage) to VI (heavy flow) for unfilled and filled discontinuities. It also gives ratings from I (no seepage) to V (exceptionally high inflow) for tunnel walls on the basis of seepage. The presence of water can reduce the shear strength along the joint and can have adverse effects on the stability.

4.3.9 Number of Joint Sets

The number of joint sets in the system of discontinuities is one of the factors used in classifying the rock mass. It determines the ability of the rock mass to deform without actually undergoing any failure within the intact rock. As the number of joint sets increases, the individual block size decreases and their degrees of freedom to move increase. The rock mass can be classified based on the number of joint sets as given in Table 4.6. About 100–150 joints must be located, and their dip and dip directions be measured for generating a pole plot (see Chapter 2). These can be used to identify the number of joint sets present.

4.3.10 BLOCK SIZE

The rock mass consists of blocks formed by intersections of several joints. Block size in a rock mass depends on the number of discontinuity sets, spacing and persistence that separates the blocks. It is similar to grain size in soils. The blocks can be in the form of cubes, tetrahedrons, sheets and so on. The block size and the interblock shear

strength at the face of the discontinuities play a key role in the stability of the rock mass in rock slopes and underground openings. It is a key parameter in rock mass classification.

Block size is defined as the average diameter of an equivalent sphere of the same volume. It is quantified by block size index I_b , the average dimension of a typical block, or volumetric joint count J_v , the total number of joints intersecting a unit volume of rock mass. Rock quality designation (RQD) is also a measure of the block size – the larger the RQD, the larger the blocks. In the case of an orthogonal joint system of three sets with spacing of S_1 , S_2 and S_3 , the block size index is defined as follows:

$$I_{\rm b} = \frac{S_1 + S_2 + S_3}{3} \tag{4.5}$$

There are $1/S_1$, $1/S_2$ and $1/S_3$ joints per metre along the three orthogonal directions, where S_1 , S_2 and S_3 are in metres. The volumetric joint count (in joints/m³) is defined as the sum of the number of joints per metre for each joint set present, and is given as follows:

$$J_{v} = \frac{1}{S_{1}} + \frac{1}{S_{2}} + \dots + \frac{1}{S_{n}}$$

$$\tag{4.6}$$

ISRM (1978) suggests that RQD and J_y can be related by

$$ROD = 115 - 3.3J_{..} \tag{4.7}$$

For $J_v < 4.5$, RQD is taken as 100% and for $J_v > 30$, RQD is taken as 0%. ISRM (1978) suggests some standard descriptions for the block sizes based on J_v (Table 4.7).

EXAMPLE 4.1

A rock mass consists of four joint sets. The following joint counts are made normal to each set: joint set 1 = 12 per 10 m, joint set 2 = 17 per 5 m, joint set 3 = 16 per 5 m and joint set 4 = 13 per 10 m. Find the volumetric joint count. How would you describe the block size?

Estimate the RQD.

Solution

The joint spacings are given by $S_1 = 10/12$ m, $S_2 = 5/17$ m, $S_3 = 5/16$ m and $S_4 = 10/13$ m. Applying Equation 4.6, we get

$$J_{\rm v} = \frac{12}{10} + \frac{17}{5} + \frac{16}{5} + \frac{13}{10} = 9.1 \,\text{joints per m}^3 \to \text{Medium-sized blocks}$$

From Equation 4.7, RQD = $115 - (3.3 \times 9.1) = 85$

The rock mass is described by one of the following adjectives, reflecting the block size and shape (ISRM, 1978).

- Massive few joints or very wide spacing
- Blocky approximately equidimensional
- Tabular one dimension considerably smaller than the other two
- Columnar one dimension considerably larger than the other two
- Irregular wide variations of block size and shape
- Crushed heavily jointed to sugar cubes

The common methods of measurements of the 10 parameters listed at the beginning of this section and their relative merits are summarised in Table 4.8. The relative presence of these parameters is illustrated in Figure 4.5.

4.4 ROCK MASS CLASSIFICATION

In soils, we have been using different soil classification systems, such as the Unified Soil Classification System (USCS), American Association of State Highway Transportation Officials (AASHTO), British Standards (BS) and Australian Standards (AS). The main objective has been to group soils of similar behaviour and to develop some systematic ways to describe soils without any ambiguity. This is not any different with rocks.

A rock mass is classified on the basis of three factors: (1) intact rock properties, (2) joint characteristics and (3) boundary conditions. When it comes to intact rock properties, the strength and stiffness (Young's modulus) are the two parameters that are used in designs. In rock mass classification, it is the UCS that is commonly used as a measure of strength. The stability of the jointed rock mass is severely influenced by the frictional resistance along the joint between the adjacent blocks. The joint surface can be stepped or undulated (macroscopically) and very rough at the contact points, implying very high shear strength. However, when the joints are filled, the aperture width and the characteristics of the filling become more important than the

TABLE 4.7		
Block Sizes	and J_{v}	Values

J _v (Joints/m³)	Description
<1	Very large blocks
1–3	Large blocks
3–10	Medium-sized blocks
10–30	Small blocks
30–60	Very small blocks
>60	Crushed rock

Source: Franklin, J.A. and Dusseault, M.B., Rock Engineering, McGraw Hill, New York, p. 600, 1989.

Source: ISRM, Int. J. Rock Mech. Min. Sci. Geomech. Abstr., 15, 319, 1978.

TABLE 4.8
Methods of Measurements of Discontinuity Parameters

Parameter Method of measurement		Core	Borehole via TV camera	Exposure
Orientation	Compass-inclinometer	M	G	G
Spacing	Measuring tape	G	G	G
Persistence	Measuring tape	В	В	G/M
Roughness	Against reference chart	M	В	G
Wall strength	Schmidt hammer	M	В	G
Aperture	Scale or feeler gauge	В	M	G
Filling	Visual	В	В	G
Seepage	Timed observations	В	B/M	G
Number of sets	Stereographic projections	M	G	G
Block size	3D fracture frequency	В	В	G

G = Good, M = Medium, B = Bad.

Source: Hudson, J.A., Rock Mechanics Principles in Engineering Practice, Butterworths, London, 1989.

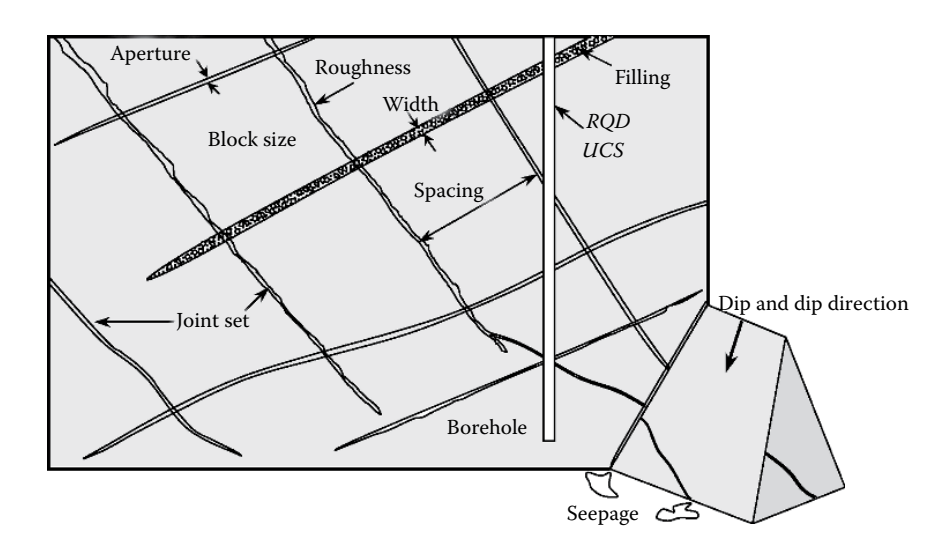


FIGURE 4.5 Diagrammatic representations of parameters describing discontinuities. (Adapted from Hudson, J.A., *Rock Mechanics Principles in Engineering Practice*, Butterworths, London, 1989.)

characteristics of the rock wall roughness. The third factor is the boundary conditions, which include the in-situ stresses present within the rock mass and the groundwater conditions. Groundwater has adverse effects on the stability by increasing the pore water pressure; it reduces the effective stress and therefore reduces the shear strength.

With a wide range of strength values for the intact rock cores and so many different parameters to describe the discontinuities and the rock mass, there is certainly a need to have some classification systems for rocks too. The classification systems ensure that we all speak the same language when referring to a specific rock mass. Some of the common rock mass classification systems are as follows:

- Rock mass rating (RMR)
- Q-system
- Geological strength index (GSI)

These are discussed in detail in the following sections. They are commonly used for designing the underground openings such as tunnels and excavations.

4.5 ROCK MASS RATING

Rock mass rating (RMR), also known as the Geomechanics Classification System, was originally proposed by Bieniawski in 1973 at the Council for Scientific and Industrial Research in South Africa. It was slightly modified in 1989, based on the analysis of data from 268 tunnel sites in hard rock areas. RMR is a rating out of a maximum of one hundred, based on the following five parameters:

- Strength of intact rock (Table 4.9) maximum score of 15
- RQD (Table 4.10) maximum score of 20
- Mean spacing of the discontinuities (Table 4.11) maximum score of 20
- Condition of discontinuities (Table 4.12) maximum score of 30
- Groundwater conditions (Table 4.14) maximum score of 15
- Orientation of discontinuities (Table 4.15)

The ratings of the first five factors are added to make up the RMR, which lies in the range of 0–100. The last one is an adjustment to the RMR, considering how favourable or unfavourable the joint orientations are with respect to the project. These values are negative, ranging from 0 to -60, and are different for tunnels, foundations and slopes.

The strength of intact rock can be quantified by UCS or the point load strength index $I_{s(50)}$. The corresponding rating increments are given in Table 4.9. Hoek and Brown (1997) noted that point load tests are unreliable when UCS is less than 25 MPa. For weaker rocks, it is recommended that the point load strength index is not used when assigning ratings for classification. Deere and Miller's (1966) strength classification was used as the basis in assigning these rating increments, and UCS and $I_{s(50)}$ values in Table 4.9 are related by UCS = $25I_{s(50)}$.

The rating increments for the drill core quality (represented by RQD) are given in Table 4.10. RQD can vary depending on the direction of the borehole.

The rating increments based on the mean spacing of discontinuities are given in Table 4.11. Very often, there are more than one set of discontinuities is present within the rock mass. The set of discontinuities that is the most critical for the specific project must be considered in assigning the rating increment. The wider the joint

TABLE 4.9
Rating Increments for Uniaxial Compressive Strength

Point load strength index, $I_{s(50)}$ (MPa)	UCS (MPa)	Rating
Not applicable; use UCS only	<1	0
	1–5	1
	5–25	2
1–2	25–50	4
2–4	50–100	7
4–10	100-250	12
>10	>250	15

Source: Bieniawski, Z.T., Engineering Rock Mass Classification, Wiley Interscience, New York, p. 251, 1989.

TABLE 4.10

Rating Increments for RQD

RQD (%)	<25	25-50	50–75	75–90	90-100
Rating	3	8	13	17	20

Source: Bieniawski, Z.T., Engineering Rock Mass Classification, Wiley Interscience, New York, p. 251, 1989.

TABLE 4.11

Rating Increments for Joint Spacing

Spacing (mm)	<60	60-200	200-600	600-2000	>2000
Rating	5	8	10	15	20

Source: Bieniawski, Z.T., Engineering Rock Mass Classification, Wiley Interscience, New York, p. 251, 1989.

spacing, the lesser the deformation within the rock mass, and hence the higher the rating increments. When there are joint sets with spacing of S_1 , S_2 , S_3 and so on, the average spacing can be computed as follows:

$$\frac{1}{S_{\text{avg}}} = \frac{1}{S_1} + \frac{1}{S_2} + \frac{1}{S_3} \dots \tag{4.8}$$

Hudson and Priest (1979) analysed 7,000 joint spacing values measured in chalk at Chinnor tunnel in England and proposed the following relationship between RQD and the mean joint frequency λ per unit length (m):

$$RQD = 100e^{-0.1\lambda} (0.1\lambda + 1)$$
 (4.9)

where λ is the number of joints per metre. In the absence of measurements of joint spacing, Equation 4.9 can be used to estimate the joint frequency and thus joint spacing.

EXAMPLE 4.2

Estimate the joint spacing of a rock mass where RQD = 81%.

Solution

```
From Equation 4.9, for RQD = 81%, \lambda = 8 per m.
Therefore, the joint spacing = 1/8 m = 0.125 m = 125 mm.
```

The rating increments for the condition of the discontinuities are given in Table 4.12. Here too, the joint set that is the most critical to the project should be considered in assigning the rating. In general, the weakest and smoothest joint set should be considered.

Gouge is a fine filling material between the joint walls that is formed by the grinding action between the two walls. It can be in the form of silt, clay, rock flour and the like, and can be a few centimetres in thickness. Table 4.12 is adequate when there is little information about the joints. In the presence of more detailed information about the joint, the guidelines in Table 4.13 can be used for a more thorough classification of the joint conditions.

EXAMPLE 4.3

A joint with slightly rough and weathered walls has a separation less than 1 mm. What would be the rating increment for the joint conditions?

Solution

From Table 4.12, the rating increment is 25.

TABLE 4.12

Rating Increments for the Joint Condition

Condition of joint	Rating
Open joint infilled with soft gouge >5 mm thickness OR separation >5 mm, and continuous extending several metres	0
Smooth surfaces OR 1–5 mm gouge infilling OR 1–5 mm aperture, and continuous joint extending several metres	10
Slightly rough surfaces, aperture <1 mm, and highly weathered walls	20
Slightly rough surfaces, <1 mm separation, slightly weathered walls	25
Very rough surfaces, not continuous joints, no separation, unweathered wall	30

Source: Bieniawski, Z.T., Engineering Rock Mass Classification, Wiley Interscience, New York, p. 251, 1989.

TABLE 4.13
Guidelines for Classifying the Condition of Discontinuity

Persistence (m)	<1	1–3	1–3 3–10 10–20		>20
Rating	6	4	2	1	0
Aperture (mm)	None	< 0.1	0.1-1.0	1–5	>5
Rating	6	5	4	1	0
Roughness	Very rough	Rough	Slightly rough	Smooth	Slickensided
Rating	6	5	3	1	0
Infilling (gouge)	None	Hard filling	Hard filling	Soft filling	Soft filling
		<5 mm	>5 mm	<5 mm	>5 mm
Rating	6	4	2	2	0
Weathering	Unweathered	Slightly	Moderately	Highly	Decomposed
		weathered	weathered	weathered	
Rating	6	5	3	1	0

Source: Bieniawski, Z.T., Engineering Rock Mass Classification, Wiley Interscience, New York, p. 251, 1989. Source: Hoek, E., et al., Support of Underground Excavations in Hard Rock, A.A. Balkema, Rotterdam, 2005.

EXAMPLE 4.4

In Example 4.3, if the following information is available, how would you modify the rating increment for the joint condition?

Persistence = 2 m, aperture = 0.1–0.5 mm, roughness = slightly rough, infilling = none, weathering = slight

Solution

From Table 4.13, the rating increment = 4 + 4 + 3 + 6 + 5 = 22.

The presence of groundwater in the joints can severely influence the shear strength and the deformability of the rock mass. The rating increment for the groundwater conditions is based on (1) inflow (L/min) per 10 m of tunnel length, (2) ratio of joint water pressure to major principal stress or (3) the general wetness condition of the joint. The general condition (e.g. damp) of the joint can be determined qualitatively from the drill cores and bore logs, in the absence of exploratory audits or pilot tunnels. These rating increments are given in Table 4.14.

Although it is not possible to do much about the intact rock strength, discontinuities, and the groundwater conditions in the rock mass, it is certainly possible to improve the stability of the proposed structure by orienting it in the best possible way. Bieniawski (1989) assigned negative rating increments depending on how favourable or unfavourable the orientations of the discontinuities are with respect to the project. These rating increments, given in Table 4.15, often called rating adjustments, are different for tunnels, foundations and slopes.

None

15

TABLE	4.14			
Rating	Increments	for Grou	ndwater (Conditions

O			
Inflow (L/min) per 10-m tunnel length	Joint water pressure/ major principal stress	General conditions	Rating increment
>125	>0.5	Flowing	0
25–125	0.2-0.5	Dripping	4
10–25	0.1-0.2	Wet	7
<10	< 0.1	Damp	10

Source: Bieniawski, Z.T., Engineering Rock Mass Classification, Wiley Interscience, New York, p. 251, 1989.

Completely dry

TABLE 4.15
Rating Adjustments for Discontinuity Orientations

0

Orientation of joints with	Rating increments				
respect to the project	Tunnels and mines	Foundations	Slopes		
Very unfavourable	-12	-25	-60		
Unfavourable	-10	-15	-50		
Fair	-5	– 7	-25		
Favourable	-2	-2	-5		
Very favourable	0	0	0		

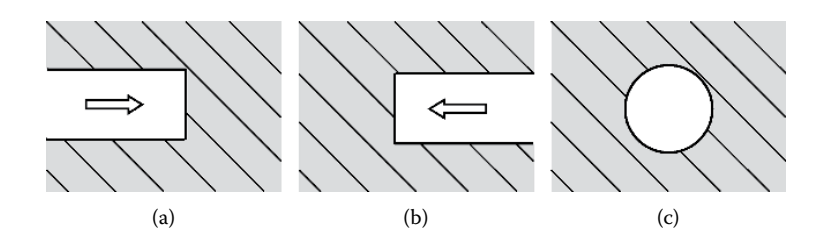


FIGURE 4.6 Tunnelling: (a) drive with dip, (b) drive against dip and (c) tunnel axis parallel to strike.

Rating adjustments in Table 4.15 are rather subjective. It requires some sound judgement in assigning the rating adjustments for the discontinuity orientations. Consultation with an engineering geologist familiar with the rock formation and the project is very valuable here.

Let us consider some tunnelling work. The strike of the discontinuity plane can be perpendicular (Figure 4.6a and b) or parallel (Figure 4.6c) to the tunnel axis. When it is perpendicular, depending on whether the tunnel is driven with (Figure 4.6a)

TABLE 4.16	
Effects of Discontinuity	Orientation in Tunnelling

Strike perpendicular to tunnel axis				Strike parallel to tunnel axis		Dip 0-20°
Drive with dip Drive against dip		irrespective of strike				
Dip 45–90°	Dip 20–45°	Dip 45–90°	Dip 20–45°	Dip 45–90°	Dip 20–45°	
Very favourable	Favourable	Fair	Unfavourable	Very unfavourable	Fair	Fair

or against (Figure 4.6b) the dip, the rating adjustments should be different. Some guidelines for choosing the appropriate adjective in the first column of Table 4.15 in tunnelling work are given in Table 4.16.

Adding up all five empirical rating increments and the negative rating adjustments for orientations, a total score out of 100 is obtained. This is known as the RMR value.

EXAMPLE 4.5

Determine the RMR value for tunnelling work in a rock formation with the following details:

- The point load strength index $I_{s(50)} = 6$ MPa
- ROD = 80%
- Mean spacing of discontinuities = 500 mm
- Joint walls are slightly rough and weathered surfaces, with less than 1-mm separation
- Groundwater condition = Damp
- Discontinuity orientation with respect to the project = Fair

Solution

From Tables 4.9, 4.10, 4.11, 4.12 and 4.14, the score = 12 + 17 + 10 + 25 + 10 = 74. Taking the discontinuity orientation into consideration (Table 4.15), with the rating adjustment of -5, the RMR becomes 69.

Based on the RMR value, including the adjustment for the discontinuity orientation, the rock mass can be classified and described as given in Table 4.17 (Bieniawski, 1989).

Tunnelling is common in mining engineering when accessing the mineral deposits from deep inside the Earth. Tunnels are also used for transportation by trains and vehicles. Furthermore, tunnels are used to carry water, sewage and gas lines over

|--|

Rock Mass Classes Based on RMR

RMR	81–100	61–80	41–60	21–40	0–20
Class number	I	II	III	IV	V
Description	Very good rock	Good rock	Fair rock	Poor rock	Very poor rock

TABLE 4.18

Meaning of Rock Mass Class

Class number	1	II	III	IV	V
Average stand-up time of tunnel	20 years for 15-m span	1 year for 10-m span	1 week for 5-m span	10 hours for 2.5-m span	30 minutes for 1-m span
Cohesion of rock mass (kPa)	>400	300–400	200–300	100–200	<100
Friction angle of rock mass (°)	>45	35–45	25–35	15–25	<15

Source: Bieniawski, Z.T., Engineering Rock Mass Classification, Wiley Interscience, New York, p. 251, 1989.

long distances. In tunnelling work, stand-up time is the time that an open excavation can stand unsupported before it caves in. Of course, it depends on the length of the tunnel. This is an important consideration in tunnelling work. The approximate relationship between the rock mass class (Table 4.17) and stand-up time in a tunnel, along with the cohesion and friction angle of the rock mass, is given in Table 4.18.

Bieniawski (1989) suggested guidelines for selecting the excavation and support procedures (e.g. rock bolt and shotcrete) for underground openings such as tunnels on the basis of the rock mass class derived from the RMR. Noting the fact that RMR was originally developed for tunnelling based on civil engineering case studies, Laubscher (1977) extended it to mining as mining rock mass rating (MRMR). The MRMR has further adjustments for in situ and mining-induced stresses, effects of blasting and weathering of the parent rock.

4.6 TUNNELLING QUALITY INDEX: Q-SYSTEM

Barton et al. (1974) of the Norwegian Geotechnical Institute proposed the Tunnelling Quality Index, known as Q, a new rock mass classification system. The system was developed based on several case histories, and the objective was to characterise the rock mass and determine the tunnel support requirements. Similar to RMR, the Tunnelling Quality Index Q is derived based on the following six parameters:

- RQD (0-100)
- Joint set number, $J_{\rm p}$ (1–20)

- Joint roughness number, J_r (1–4)
- Joint alteration number, J_a (1–20)
- Joint water reduction factor, J_{w} (0.1–1.0)
- Stress reduction factor, SRF (1–20)

It is defined as follows:

$$Q = \left(\frac{\text{RQD}}{J_{\text{n}}}\right) \left(\frac{J_{\text{r}}}{J_{\text{a}}}\right) \left(\frac{J_{\text{w}}}{\text{SRF}}\right) \tag{4.10}$$

The numerical value of Q ranges on a logarithmic scale from 0.001 to over 1000, covering the whole spectrum of rock mass from a heavily jointed weak rock mass to sound, unjointed rock. The higher the value of Q, the better the rock mass quality. The three numerators in the quotients – RQD, $J_{\rm r}$ and $J_{\rm w}$ – are assigned values such that their higher values reflect better quality rock mass. The three denominators, $J_{\rm n}$, $J_{\rm a}$ and SRF, are assigned values such that their lower values reflect better quality rock mass. Barton (2002) suggested slight modifications to the original Q-system, particularly to $J_{\rm a}$ and SRF.

RQD and J_n are both reflections of the number of joints present within the rock mass. The higher the RQD, the lower the J_n and vice versa. As a result, the first quotient RQD/ J_n in Equation 4.10 can take a wide range of values from 0.5 to over 200. These values are seen crudely as the block sizes in centimetres (Barton et al., 1974). The RQD values and rock classifications (Table 4.19) are quite similar to those used in the RMR classification. The joint set number J_n is assigned on the basis of Table 4.20. J_n is 1.0 for rock with no joints and is assigned the maximum possible value of 20 when it is crushed. J_n increases with the increasing number of joint sets, reflecting lower values of Q in Equation 4.10.

The second quotient, J_r/J_a , in Equation 4.10 is a measure of shear strength. The joint roughness number J_r is a measure of the joint roughness and lies in the range of 0.5–4, with larger numbers representing rougher joints, implying greater shear strength. Rocks with discontinuous joints (i.e. low persistence) are assigned the maximum value of 4, and those with continuous slickensided planar joints are assigned the minimum value of 0.5. Suggested values of J_r are given in Table 4.21. It can be seen that Table 4.21 correlates with the ISRM-suggested roughness classes given in Table 4.4.

TABLE 4.19
RQD Values in Q-System

Class	Α	В	C	D	E
Designation	Very poor	Poor	Fair	Good	Excellent
RQD	0-25	25-50	50-75	75–90	90-100

Source: Barton, N.R., et al., Rock Mech., 6, 189, 1974. Notes: (1) When RQD <10, use 10 in computing Q; (2) ROD rounded off to 5 (i.e. 80 and 85) is adequate.

TABLE 4.20

Joint Set Number J_n for Q-System

Class	Description	\boldsymbol{J}_n
A	Massive; none or few joints	0.5-1.0
В	One joint set	2
C	One joint set plus random joints	3
D	Two joint sets	4
E	Two joint sets plus random joints	6
F	Three joint sets	9
G	Three joint sets plus random joints	12
H	Four or more joint sets; random; heavily jointed; sugar cubes and so on.	15
J	Crushed rock; earth-like	20

Source: Barton, N.R., et al., Rock Mech., 6, 189, 1974. Notes: (1) For tunnel intersections, use $3.0 \times J_n$; (2) for portals, use $2.0 \times J_n$.

TABLE 4.21

Joint Roughness Number J_r

Class	Description	J_r
(a) Rock-wall	contact, and (b) Rock-wall contact before 10 cm of shear	
A	Discontinuous joints	4
В	Rough or irregular, undulating	3
C	Smooth, undulating	2
D	Slickensided, undulating	1.5
E	Rough or irregular, planar	1.5
F	Smooth, planar	1.0
G	Slickensided, planar	0.5
(c) No rock-w	all contact when sheared	
Н	Zone containing clayey minerals thick enough to prevent rock-wall contact	1.0
J	Sandy, gravelly or crushed zone thick enough to prevent rock-wall contact	1.0

Source: Barton, N.R., et al., Rock Mech., 6, 189, 1974.

Notes: (1) Add 1.0 if the mean spacing of the relevant joint set is greater than 3 m and (2) $J_r = 0.5$ for planar slickensided joints having lineations if the lineations are favourably oriented.

Joint alteration number, J_a , is a measure of the degree of alteration of the joint wall or infill material, which is quantified in terms of residual friction angle ϕ_r . Tan⁻¹ (J_r/J_a) is a fair approximation of the residual friction angle. Noting that there is no cohesion at the residual state, the residual shear strength is given by $\tau \approx \sigma_n (J_r/J_a)$. The weakest joint set (i.e. with the lowest J_r/J_a value), with due consideration to its orientation with

IABLE 4.22	
Joint Alteration	Number J_a

Class	Description	φ _r (°)	J _a		
(a) Rock-	(a) Rock-wall contact (no mineral fillings, only coatings)				
A	Tightly healed, hard, nonsoftening, impermeable filling, that is, quartz or epidote		0.75		
В	Unaltered joint walls, surface staining only	25-35	1.0		
С	Slightly altered joint walls, nonsoftening mineral coatings, sandy particles, clay-free disintegrated rock and so on.	25–30	2.0		
D	Silty- or sandy-clay coatings, small clay fraction (nonsoftening)	20-25	3.0		
Е	Softening or low-friction clay mineral coatings, that is, kaolinite or mica; also chlorite, talc, gypsum, graphite and so on, and small quantities of swelling clays	8–16	4.0		
(b) Rock	-wall contact before 10-cm shear (thin mineral fillings)				
F	Sandy particles, clay-free disintegrated rock and so on.	25-30	4.0		
G	Strongly over-consolidated nonsoftening clay material fillings (continuous but <5-mm thickness)	16–24	6.0		
Н	Medium or low over-consolidation, softening clay mineral fillings (continuous but <5-mm thickness)	12–16	8.0		
J	Swelling clay fillings, that is, montmorillonite (continuous but <5-mm thickness); value of J_a depends on % of swelling clay-size particles and access to water and so forth.	6–12	8–12		
(c) No ro	ck-wall contact when sheared (thick mineral fillings)				
K, L, M	Zones or bands of disintegrated crushed rock and clay (see G, H and J for description of clay condition)	6–24	6, 8 or 8–12		
N	Zones or bands of silty- or sandy-clay, small clay fraction (nonsoftening)	-	5.0		
O, P, R	Thick continuous zones or bands of clay (see G, H and J for description of clay condition)	6–24	10, 13 or 13–20		
Source: Barton, N., Int. J. Rock Mech. Min. Sci., 39, 185, 2002.					

Source: Barton, N.R., et al., Rock Mech., 6, 189, 1974.

Note: ϕ_r values are approximate.

respect to stability should be used in computing the Q-value. The suggested values of J_a are given in Table 4.22. It can be seen that the rough and unaltered joint sets get larger values of J_i/J_a than the smooth, slickensided joints with clay fillings. Surface staining on rocks occurs due to moisture and the presence of chemicals.

Rough and unaltered joints that are in direct contact have undergone very low strains, and hence the shear strength along such a surface is closer to the peak value than the residual values. These surfaces will dilate when sheared, which favours the stability of the tunnels. When the joints are filled or have thin mineral coatings, the shear strength would be significantly lower. In some situations where the mineral filling is rather thin, the rock-wall contact takes place after some shear (case b in Table 4.22), which minimises further slide. When the filling is thick, there will be no

TABLE 4.23 Joint Water Reduction J_w

Class	Description	Approx. water pressure (kPa)	$J_{\rm w}$
A	Dry excavation or minor inflow (i.e. <5 L/min locally)	<100	1.0
В	Medium inflow or pressure, occasional outwash of joint fillings	100–250	0.66
С	Large inflow or high pressure in competent rock with unfilled joints	250–1000	0.5
D	Large inflow or high pressure, considerable outwash of joint fillings	250–1000	0.33
E	Exceptionally high inflow or water pressure at blasting, decaying with time	>1000	0.2-0.1
F	Exceptionally high inflow or water pressure, continuing without noticeable decay	>1000	0.1-0.05

Source: Barton, N., Int. J. Rock Mech. Min. Sci., 39, 185, 2002.

Source: Barton, N.R., et al., Rock Mech., 6, 189, 1974.

Notes: (1) C to F are crude estimates; increase J_{w} if drainage measures installed; (2) special problems

formed by ice formation are not considered.

contact even after some shear (case c in Table 4.22), enabling the residual strength to be reached. Such situations are unfavourable in tunnelling work.

The third quotient in Equation 4.10, $J_{\rm w}/{\rm SRF}$, is something Barton et al. (1974) referred to as an 'active stress' term. It is well known that water can reduce the effective normal stress (σ'), which in turn reduces the shear strength. Further, water can soften and possibly wash out the infill. The joint water reduction factor $J_{\rm w}$, which ranges from 0.05 to 1.0, accounts for such reduction in shear strength due to the presence of water in the rock mass. A dry excavation is assigned a factor of 1.0 and a situation with exceptionally high inflow of water is assigned a factor of 0.05. The joint water reduction factors are given in Table 4.23.

SRF, the stress reduction factor, is a total stress parameter that ranges from 1 to 400, with 1 being most favourable (e.g. rock with unfilled joints) and 400 being most unfavourable (e.g. rock burst). The suggested values of SRF are given in Table 4.24. When the rock mass contains clay, SRF is used to account for the stress relief in excavations and hence loosening of the rock mass (case a in Table 4.24). In competent rock, SRF is a measure of the in-situ stress conditions (case B, Table 4.24). SRF is also used to account for the squeezing (case C in Table 4.24) and swelling (case D in Table 4.24) loads in plastic-incompetent rocks.

EXAMPLE 4.6

It is proposed to construct an underground tunnel 500 m below the ground. The drilled cores have an RQD of 85% and the number of joint sets is estimated to be 2.

TABLE 4.24

Stress Reduction Factor SRF

(a) Weakness zones intersecting excavations, which may cause loosening of rock mass when tunnel is excavated

Class	Description	SRF		
A	Multiple occurrences of weakness zones containing clay or chemically disintegrated rock, very loose surrounding rock (any depth)	10		
В	Single-weakness zone containing clay or chemically disintegrated rock (depth of excavation ≤50 m)	5.0		
С	Single-weakness zones containing clay or chemically disintegrated rock (depth of excavation >50 m)	2.5		
D	Multiple-shear zones in competent rock (clay-free), loose surrounding rock (any depth)	7.5		
Е	Single-shear zones in competent rock (clay-free) (depth of excavation ≤50 m)	5.0		
F	Single-shear zones in competent rock (clay-free) (depth of excavation >50 m)	2.5		
G	Loose, open joints, heavily jointed or sugar cube and so on (any depth)	5.0		
(b) Con	npetent rock, rock stress problems			
Class	Description	σ_c/σ_1	$\sigma_{\theta}/\sigma_{c}$	SRF
H	Low stress, near surface, open joints	>200	< 0.01	2.5
J	Medium stress, favourable stress condition	200-10	0.01 - 0.3	1
K	High stress, very tight structure. Usually favourable to stability; may be unfavourable to wall stability	10–5	0.3-0.4	0.5–2
L	Moderate slabbing after >1 h in massive rock	5–3	0.5 - 0.65	5-50
M	Slabbing and rock burst after a few minutes in massive rock	3–2	0.65-1.0	50-200
N	Heavy rock burst (strain-burst) and dynamic deformations in massive rock	<2	>1	200–400
(c) Squ	eezing rock: plastic flow of incompetent rock under the influ	ence of hig	gh rock pres	sure
Class	Description		$\sigma_{\theta}/\sigma_{c}$	SRF
O	Mild squeezing rock pressure		1–5	5-20
P	Heavy squeezing rock pressure		>5	10-20
(d) Swe	lling rock: chemical swelling activity depending on presence	of water		
Class	Description			SRF
R	Mild swelling rock pressure			5-10
S	Heavy swelling rock pressure			10-15

Source: Barton, N., Int. J. Rock Mech. Min. Sci., 39, 185, 2002.

Source: Barton, N.R., et al., Rock Mech., 6, 189, 1974.

Notes: (1) σ_{θ} = maximum tangential stress (estimated from elastic theory), σ_{c} = unconfined compressive strength, σ_{1} = major principal stress. (2) Reduce SRF by 25–50% if relevant shear zones only influence but do not intersect the excavation. (3) Barton et al. (1974) have a maximum SRF of 20. (4) In strongly anisotropic stress fields (when measured), when σ_{1}/σ_{3} = 5 to 10, reduce σ_{c} by 25%, and for σ_{1}/σ_{3} > 10, reduce σ_{c} by 50%.

The joints are rough, undulating and unweathered with minor surface staining. The average uniaxial compressive strength of the cores is 190 MPa. The major principal stress acts horizontally and is twice the vertical stress. The unit weight of the rock is approximately 30 kN/m³. The excavation is relatively dry, with some dampness and negligible inflow. Estimate the *Q*-value.

Solution

No. of joint sets = 2. Therefore, $J_n = 4$.

Rough and undulating joints $\rightarrow J_r = 3$

Unaltered joint walls with minor surface staining $\rightarrow J_a = 1$

Some dampness and negligible inflow $\rightarrow J_{w} = 1$

Overburden stress (also, the minor principal stress σ_3) = 30 × 500 kPa = 15 MPa

$$\therefore \sigma_1 = 2 \times 15 = 30 \text{ MPa}$$

Uniaxial compressive strength $\sigma_c = 190 \text{ MPa}$

 $\sigma_{c}/\sigma_{1} = 190/30 = 6.3$

From Table 4.24, SRF = 1.5

Applying Equation 4.10,

$$Q = \left(\frac{85}{4}\right)\left(\frac{3}{1}\right)\left(\frac{1}{1.5}\right) = 42.5$$

On the basis of the Q-value, the rock mass can be classified as shown in Table 4.25. RMR and Q can be approximately related by

Bieniawski (1976, 1989): RMR
$$\approx 9 \ln Q + 44$$
 (4.11)

Barton (1995): RMR
$$\approx 15 \ln Q + 50$$
 (4.12)

TABLE 4.25
Rock Mass Classification for Tunnelling Work Based on Q-System

Q-value	Class	Rock mass quality
400-1000	A	Exceptionally good
100–400	A	Extremely good
40–100	A	Very good
10–40	В	Good
4–10	C	Fair
1–4	D	Poor
0.1-1.0	E	Very poor
0.01-0.1	F	Extremely poor
0.001-0.01	G	Exceptionally poor

The Q-value in Equation 4.10 is derived as the product of three quotients. The first one is a measure of the block size. The second is a measure of the joint roughness. The third is a tricky one; it is a stress parameter reflecting the water effects and in situ stresses.

4.7 GEOLOGICAL STRENGTH INDEX

We have looked at the two popular rock mass classification systems, the RMR and Q-systems, which use similar parameters reflecting the intact rock properties and the joint characteristics. They were developed primarily for tunnelling work but are being used for other applications too. The main difference is in the weightings of the relative factors. Uniaxial compressive strength is not a parameter in the Q-system; however, it has some influence through the SRF.

The Hoek-Brown failure criterion is quite popular for studying stability of rock mass in underground excavations. In its general form, the failure criterion is expressed as follows:

$$\sigma'_{1f} = \sigma'_{3f} + \sigma_{ci} \left(m_m \frac{\sigma'_{3f}}{\sigma_{ci}} + s \right)^a$$
 (4.13)

where $\sigma_{1f}^{'}$ = effective major principal stress at failure, $\sigma_{3f}^{'}$ = effective minor principal stress at failure, and σ_{ci} = uniaxial compressive strength of the intact rock. The constants s and a depend on the rock mass characteristics. The constant s ranges between 0 for poor-quality rock and 1 for intact rock. The constant a ranges between 0.5 for good-quality rock and 0.65 for poor-quality rock. The Hoek–Brown constant m takes separate values of m_i for intact rock and m_m for the rock mass. These are discussed in more detail in Chapter 5. Typical values of m_i for different rock types are given in Table 4.26.

Before 1994, the parameters in the Hoek–Brown criterion were derived from RMR, assuming dry conditions at the excavation (rating increment = 15), with no adjustment for discontinuity orientations with respect to the project (very favourable; rating increment = 0). Noting the fact that relating RMR to Hoek–Brown parameters is not reliable for poor-quality rock masses of low RMR, the GSI was introduced in 1994 by Dr Evert Hoek (Hoek, 1994). It is a number ranging from about 10 for extremely poor-quality rock mass to 100 for extremely strong unjointed rock mass. Around the time of its introduction, GSI was estimated from RMR as follows:

$$GSI \approx RMR_{76} \approx RMR_{89} - 5 \tag{4.14}$$

where RMR₈₉ is the value computed according to Bieniawski (1989) as discussed in Section 4.5, and RMR₇₆ is the value computed using the older system (Bieniawski, 1976), where the maximum rating increment for groundwater conditions was 10.

GSI is a recent rock mass classification system that was introduced by Hoek (1994), with a heavy reliance on geological observations and less on numerical values. The two major parameters are (1) the surface condition of the discontinuity and

TABLE 4.26 m. Values for Rocks

Texture Coarse Medium Fine Very fine Sedimentary Conglomerates Sandstones, 17 ± 4 Siltstones, 7 ± 2 Claystones, 4 ± 2 (21 ± 3) Breccias (19 ± 5) Greywackes (18 ± 3) Shales (6 ± 2) Marls (7 ± 2) Crystalline Sparitic limestone Micritic limestone Dolomite (9 ± 3) limestone (12 ± 3) (10 ± 2) (9 ± 2) Gypsom, 8 ± 2 Anhydrite, 12 ± 2 Chalk, 7 ± 2 Metamorphic Marble, 9 ± 3 Hornfels (19 ± 4) Ouartzite, 20 ± 3 Metasandstone (19 ± 3) Amphibiolites, Gneiss, 28 ± 5 Migamatite (29 ± 3) 26 ± 6 Schists, 12 ± 3 Phyllites (7 ± 3) Slates, 7 ± 4 Diorite (25 ± 5) Igneous Granite (32 ± 3) Granodiorite (29 ± 3) Gabro, 27 ± 3 Dolerite (16 ± 5) Norite, 20 ± 5 Porphyries (20 ± 5) Diabase (15 ± 5) Peridotite (25 ± 5) Dacite (25 ± 3) Obsidian (19 ± 3) Rhyolite (25 ± 5) Andesite, 25 ± 5 Basalt (25 ± 5) Breccia (19 ± 5) Tuff (13 ± 5) Agglomerate (19 ± 3)

Source: Hoek, E., and Brown, E.T., Int. J Rock Mech. Min. Sci. Geomech. Abstr., 34, 1165, 1997. Source: Wyllie, D.C., and Mah, C.W., Rock Slope Engineering, 4th edition, Spon Press, London, 2004. Note: The values in parenthesis are estimates. The others are measured.

(2) interlocking among the rock blocks. The surface condition can vary from 'very good' for fresh, unweathered surface to 'very poor' for highly weathered or slickensided surfaces with clay infill. The interlocking blocks can be literally massive at the upper end of the scale to crushed or laminated at the lower end. From these two qualitative parameters, a GSI value is assigned using Figure 4.7.

GSI is one of the parameters used in assessing the strength and deformability of the rock mass using the Hoek–Brown failure criterion. It has been related to m, s and a in Equation 4.13 empirically. The Hoek–Brown parameters for the rock mass and the intact rock are related by

$$m_{\rm m} = m_{\rm i} \exp\left(\frac{{\rm GSI} - 100}{28}\right) \text{ for } {\rm GSI} > 25$$
 (4.15)

GEOLOGICAL STRENGTH INDEX FOR JOINTED ROCKS (Hoek and Marinos, 2000) From the lithology, structure and surface conditions of the discontinuities, estimate the average value of GSI. Do not try to be too precise. Quoting a range from 33 to 37 is more realistic than stating that GSI = 35. Note that the table does not apply to structurally controlled failures. Where weak planar structural planes are present in an unfavorable orientation with respect to the excavation face, these will dominate the rock mass behavior. The shear strength of surfaces in rocks that are prone to deterioration as a result of changes in moisture content will be reduced if water is present. When working with rocks in the fair to very poor categories, a shift to the right may be made for wet conditions. Water pressure is dealt with by effective stress analysis. STRUCTURE	DELY GOOD DELY FORM THE SHORT THE SULFACES DELY FORM THE SHORT T	GOOD OR Rough, slightly weathered, iron stained surfaces	FAIR D Smooth, moderately weathered and altered surfaces	G POOR Slickensided, highly weathered surfaces with C compact coatings or fillings or angular fragments	VERY POOR Slickensided, highly weathered surfaces with soft clay coatings or fillings
INTACT OR MASSIVE – intact rock specimens or massive in situ rock with few widely spaced discontinuities	90			N/A	N/A
BLOCKY – well interlocked undisturbed rock mass consisting of cubical blocks formed by three intersecting discontinuity sets		70 60			
VERY BLOCKY – interlocked, partially disturbed mass with multi-faceted angular blocks formed by 4 or more joint sets		5	40-		
BLOCKY – well interlocked undisturbed rock mass consisting of cubical blocks formed by three intersecting discontinuity sets VERY BLOCKY – interlocked, partially disturbed mass with multi-faceted angular blocks formed by 4 or more joint sets BLOCKY/DISTURBED/ SEAMY – olded with angular blocks formed by many intersecting discontinuity sets. Persistence of bedding planes or schistosity				60	
DISINTEGRATED – poorly interlocked, heavily broken rock mass with mixture of angular and rounded rock pieces				20	
LAMINATED/SHEARED – lack of blockiness due to close spacing of weak schistosity or shear planes	N/A	N/A			10

FIGURE 4.7 Geological strength index for jointed rocks.

Here m_i is specific to the rock type, and typical values suggested in the literature are given in Table 4.26 (Hoek and Brown, 1997; Wyllie and Mah, 2004). For good-quality rock mass (GSI > 25),

$$a = 0.5$$
 (4.16)

$$s = \exp\left(\frac{\text{GSI} - 100}{9}\right) \tag{4.17}$$

Here the original Hoek–Brown criterion can be used, where GSI is estimated from RMR using Equation 4.14. For very poor-quality rock masses, it is difficult to estimate RMR, and hence the modified Hoek–Brown criterion (Hoek et al., 1992) should be used, where GSI has to be estimated from geological observations related to the interlocking of the individual blocks and joint surface conditions, as summarised in Table 4.26. For such poor-quality rocks (GSI < 25),

$$a = 0.65 - \frac{\text{GSI}}{200} \tag{4.18}$$

$$s = 0 \tag{4.19}$$

In Chapter 5, you will note that the most recent modification of the Hoek–Brown criterion uses the same expressions for a and s, irrespective of the GSI value. Both approaches give approximately the same values for a and s.

When using the Q-value to derive GSI, as in the case with RMR, it should be assumed that the excavation is dry. A modified Tunnel Quality Index Q' is defined as follows (Hoek et al., 2005):

$$Q' = \left(\frac{\text{RQD}}{J_{\text{n}}}\right) \left(\frac{J_{\text{r}}}{J_{\text{a}}}\right) \tag{4.20}$$

Here $J_{\rm w}$ and SRF in Equation 4.10 are both taken as 1. Similar to Equation 4.12, GSI can be estimated as follows:

$$GSI = 9 \ln Q' + 44 \tag{4.21}$$

Descriptions of rock mass quality, given on the basis of GSI, are shown in Table 4.27.

١RI		

Rock Mass Quality and GSI

GSI	<20	21–40	41–55	56–75	76–95
Rock mass quality	Very poor	Poor	Fair	Good	Very good

EXAMPLE 4.7

A granite rock mass has three joint sets, an RQD of 85%, and an average joint spacing of 250 mm. Joint surfaces are stepped and rough, unweathered with some stains and have no separations. The average uniaxial strength of the intact rock cores is 190 kPa and the excavation area is slightly damp. The excavation is at a depth of 200 m where no unusual in situ stresses are expected. Find the RMR, *Q* and GSI values. Assume a density of 2.8 t/m³ and that the vertical in situ stress is the major principal stress.

Assuming dry conditions in the excavation (i.e. maximum rating of 15), compute RMR_{89} and estimate GSI from Equation 4.14

Solution

(a) RMR

UCS = 190 MPa → Rating increment = 12

 $RQD = 85\% \rightarrow Rating increment = 17$

Joint spacing = $250 \text{ mm} \rightarrow \text{Rating increment} = 10$

Joint conditions = Very rough, unweathered and no separation → Rating increment = 30

Groundwater = Damp \rightarrow Rating increment = 10

$$\therefore$$
 RMR = 12 + 17 + 10 + 30 + 10 = 79

(b) Q

RQD = 85 and
$$J_{n} = 9$$

Rough and stepped $\rightarrow J_r = 3$

Unweathered, no separations and some stains $\rightarrow J_a = 1$

Excavation is damp (i.e. minor inflow) $\rightarrow J_w = 1$

$$\sigma_{c} = 190 \text{ MPa}, \ \sigma_{v} = 200 \times 28/1000 = 5.6 \text{ MPa} \approx \sigma_{1}$$

$$\sigma_{c}/\sigma_{1} = 190/5.6 = 33.9 \rightarrow SRF = 1$$

$$Q = \frac{85}{9} \times \frac{3}{1} \times \frac{1}{1} = 28$$

- (c) Rock mass structure = Blocky Joint surface condition = Very good GSI = 75 ± 5
- (d) Assuming dry conditions in the excavation, $RMR_{89} = 84$. From Equation 4.11, GSI $\approx 84-5 = 79$, which matches the value computed in (c).

EXAMPLE 4.8

Check the empirical correlations (Equations 4.11 and 4.12) relating RMR and Q, in light of the RMR and Q values in Example 4.7.

Solution

Substituting Q = 28 from Example 4.7 in Equations 4.11 and 4.12, Bieniawski (1989): RMR $\approx 9\ln 28 + 44 = 74$ Barton (1995): RMR $\approx 15\ln 28 + 50 = 100$

The actual RMR from Example 4.7 is 79. This is in good agreement with the estimate from Equation 4.11 (Bieniawski, 1989).

4.8 SUMMARY

- 1. The rock mass is weaker and more permeable than the intact rock, mainly due to the discontinuities present.
- Although all laboratory tests (discussed in Chapter 3) are carried out on the intact rock, it is the strength and deformability of the rock mass that governs the stability.
- 3. Intact rock strength is only one of the parameters that govern rock mass behaviour.
- 4. RQD is a reflection of joint spacing or volumetric joint count.
- 5. The rock mass is classified based on intact rock properties (intact rock strength), joint characteristics (e.g. spacing and roughness) and the boundary conditions (stress field and water).
- 6. The friction angle ϕ at the joint is derived from two components: the basic friction angle ϕ_b and the joint roughness angle i, that is, $\phi = \phi_b + i$.
- 7. The basic friction angle ϕ_b is approximately equal to the residual friction angle ϕ_c .
- 8. RMR and the Tunnelling Quality Index (*Q*) are the two popular rock mass classification systems. They both rely on similar parameters, with a slight difference in the weightings of these parameters. These were developed for tunnelling but are used in other applications as well.
- 9. The first two quotients in Equation 4.10 for computing the *Q*-value are measures of the block size and joint roughness, respectively. The third quotient is a stress ratio that reflects the effects of water and in situ stresses.
- 10. GSI is useful in determining the parameters in the Hoek–Brown failure criterion. It is obtained from two qualitative parameters (Table 4.26) describing the interlocking of the rock pieces and the surface quality. It can also be derived indirectly from RMR or Q'.
- 11. RMR and GSI are numbers that range from 0 to 100. *Q* ranges from 0.001 to 1000+, similar to grain sizes. The larger the value, the better the rock mass characteristics.

REVIEW EXERCISES

- 4.1. State whether the following are true or false:
 - a. The larger the RQD, the larger the joint spacing.
 - b. The joint roughness is governed more by the large-scale undulations than by the small-scale unevenness.
 - c. The peak friction angle along a discontinuity can be as high as 70°.
 - d. The term aperture applies to both open and filled joints.
- 4.2. Carry out a thorough literature review and summarise the empirical correlations relating RMR, *Q* and GSI, including the limitations of the specific correlations.
- 4.3. A granite rock formation consists of three sets of discontinuities where the average joint spacing is 320 mm. The RQD of the rock cores obtained from the boreholes is 82%. The joint surfaces are rough, stepped and unweathered, with no separation. The average uniaxial compressive strength of the intact rock cores is 200 MPa. The surface of the excavation is found to be damp. Determine the RMR value, disregarding the rating adjustment for discontinuity orientation. What values would you use for cohesion and friction angle in analysis of the rock mass?

Answer: 79; 390 kPa, 44

4.4. A tunnel is to be constructed 160 m below ground level, through a highly fractured rock mass where the RQD is 35% and the uniaxial compressive strength of the intact rock cores ranges from 60 to 80 MPa. The joints are separated by 3–4 mm, filled with some clayey silt, and are continuous, extending to several metres. The joint surfaces are smooth and undulating. Some preliminary measurements show that the groundwater pressure is about 140 m of water and that the overburden pressure can be taken as 160 m of rock. In the absence of any knowledge about the in-situ stress ratio, the vertical overburden stress can be taken as the major principal stress. The average unit weight of the rock can be taken as 27 kN/m³. Estimate the RMR value, without the adjustment for the discontinuity orientation.

(Hint: No joint spacing is given. Use RQD in Equation 4.5.)

Answer: 34

4.5. It is proposed to drive a tunnel through a granite rock formation, against the main joint set dipping at 50°. The uniaxial compressive strength of the rock cores tested in the laboratory ranges from 180 to 230 MPa. The RQD of the rock cores is 80%. The joints are spaced at 500 mm with less than 1 mm separation, and the surfaces are rough and slightly weathered. It is expected that the tunnelling conditions will be wet. Estimate the RMR value with due consideration of the adjustment for discontinuity orientation. In the same location, if the tunnel is driven with the dip, what would be the RMR value?

Answer: 66; 71

4.6. A sandstone rock mass with RQD of 70% has two joint sets and some random fractures. The joints, spaced at 130 mm, are generally in contact, with less than a 1-mm aperture. The joint surfaces are slightly rough

and highly weathered, with no clay found on the surface. The uniaxial compressive strength is 95 MPa. The excavation is being carried out at a depth of 110 m below the ground level, and the water table is at a depth of 15 m below the ground level. Estimate RMR, *Q* and GSI. Assume a unit weight of 28 kN/m³ for the rock mass.

Answer: 52, 4.4, 55 ± 5

4.7. During an excavation for a tunnel, 250 m below ground level, a highly fractured siltstone rock mass with two major joint sets and many random fractures is encountered. The RQD from the rock cores is 40%, and the average UCS is 70 MPa. The joints, with average spacing of 75 mm, are rather continuous with high persistence, with apertures of 3–5 mm, and they are filled with silty clay. The joint surface walls are highly weathered, undulating and slickensided. There is some water inflow into the tunnel, estimated as 15 L/min per 10 m of tunnel length, with some outwash of joint fillings. Estimate RMR, *Q* and GSI. Assume a unit weight of 28 kN/m³ for the rock mass.

Answer: 40, 1.7, 20 ± 5

REFERENCES

- Barton, N.R. (1973). Review of a new shear strength criterion for rock joints. *Engineering Geology*, Vol. 7, pp. 287–322.
- Barton, N.R. (1987). Predicting the Behaviour of Underground Openings in Rock. Manuel Rocha Memorial Lecture, Lisbon, NGI Publication 172, Oslo, p. 21.
- Barton, N. (1995). The influence of joint properties in modelling jointed rock masses. *Keynote Lecture*, 8th ISRM Congress. Tokyo, Balkema, Rotterdam.
- Barton, N.R. (2002). Some new Q-value correlations to assist in site characterisation and tunnel design. *International Journal of Rock Mechanics & Mining Sciences*, Vol. 39, No. 2, pp. 185–216.
- Barton, N.R. and Choubey, V. (1977). The shear strength of rock joints in theory and practice. *Rock Mechanics*, Vol. 10, pp. 1–54.
- Barton, N.R., Lien, R. and Lunde, J. (1974). Engineering classification of rock masses for the design of tunnel support. *Rock Mechanics*, Vol. 6, No. 4, pp. 189–239.
- Bieniawski, Z.T. (1973). Engineering classification of jointed rock masses. *Transactions, South African Institution of Civil Engineers*, Vol. 15, No. 12, pp. 335–344.
- Bieniawski, Z.T. (1976). Rock mass classification in rock engineering, in *Proceedings of Symposium on Exploration for Rock Engineering*, Bieniawski, Z.T., editor, A.A. Balkema, Rotterdam, Vol. 1, pp. 97–106.
- Bieniawski, Z.T. (1989). *Engineering Rock Mass Classification*. Wiley Interscience, New York, p. 251.
- Deere, D.U. and Miller, R.P. (1966). Engineering classification and index properties of intact rock. *Report AFWL-TR-65–116*, *Air Force Weapon Laboratory (WLDC)*, Kirtland Airforce Base, p. 308.
- Franklin, J.A. and Dusseault, M.B. (1989). *Rock Engineering*. McGraw Hill, New York, p. 600. Hoek, E. (1994). Strength of rock and rock masses. *ISRM News Journal*, Vol. 2, No. 2, pp. 4–16.
- Hoek, E. and Brown, E.T. (1997). Practical estimates of rock mass strength. *International Journal of Rock Mechanics and Mining Sciences & Geomechanics Abstracts*, Vol. 34, No. 8, pp. 1165–1186.

Hoek, E., Kaiser, P.K. and Bawden, W.F. (2005). Support of Underground Excavations in Hard Rock, A.A. Balkema. Rotterdam.

- Hoek, E. and Marinos, P. (2000). Predicting tunnel squeezing. *Tunnels and Tunnelling International*, Part 1, 32/11, pp. 45–51, November 2000; Part 2, 32/12, pp. 33–36, December 2000.
- Hoek, E., Wood, D. and Shah, S. (1992). A modified Hoek-Brown criterion for jointed rock masses, in *Proceedings of Rock Characterization Symposium*, Hudson, J., editor, ISRM, Eurock '92, pp. 209–213.
- Hudson, J.A. (1989). Rock Mechanics Principles in Engineering Practice. Butterworths, London.
- Hudson, J.A. and Priest, S.D. (1979). Discontinuities and rock mass geometry. *International Journal of Rock Mechanics and Mining Sciences & Geomechanics Abstracts*, Vol. 16, No. 6, pp. 339–362.
- International Society for Rock Mechanics (ISRM) (1978). Suggested methods for quantitative description of discontinuities in rock masses. *International Journal of Rock Mechanics* and Mining Sciences & Geomechanics Abstracts, Vol. 15, No. 6, pp. 319–368.
- Laubscher, D.H. (1977). Geomechanics classification of jointed rock masses mining applications. *Transactions of Institution of Mining and Metallurgy*, Vol. 86, Section A, pp. A1–A8.
- Wyllie, D.C. and Mah, C.W. (2004). Rock Slope Engineering. 4th edition, Spon Press, London.

5 Strength and Deformation Characteristics of Rocks

5.1 INTRODUCTION

Although soils and rocks are both geomaterials, their behaviour under applied loads can be quite different. When it comes to strength and deformation, some of the major differences between rocks and soils are as follows:

- Soils are classic particulate media, and rocks can be seen as a disjointed continuum. There is a significant scale effect in rocks, which is not present in soils. The intact rock, with no structural defects (Figure 5.1a), can be treated as homogeneous and isotropic. On the contrary, the rock mass will often be heterogeneous and anisotropic due to the presence of discontinuities (Figure 5.1b). It can be seen in Figure 5.1b that the stability is better when the loads are applied vertically than horizontally. A highly disjointed or fractured rock (Figure 5.1c) can again be treated as an isotropic material, with a large number of randomly oriented discontinuities. In the case of soils, we generally treat them as homogeneous and isotropic. There are no scale effects in soils; irrespective of the extent considered, the behaviour is the same.
- While the intact rock can show significant tensile strength, the rock mass will have little or no tensile strength due to the presence of discontinuities. We never rely on the tensile strength of soils. However, in good-quality rocks with no discontinuities, it is possible to rely on some of its tensile strength.
- Intact rocks have very low porosity with no free water present. Therefore,
 the permeability is often extremely low. In the rock mass, the discontinuities
 can contain substantial free water and can lead to high permeabilities. This
 is known as secondary permeability. The presence of water in the discontinuities can lead to high pore water pressures and hence reduce the effective
 stresses and shear strength along the discontinuities.
- The strength of the intact rock increases with the confining pressure, but not linearly, and it does not follow the Mohr–Coulomb failure criterion very well. The failure stresses are better related by the Hoek–Brown failure criterion, where the failure envelope is parabolic.

5.2 IN SITU STRESSES AND STRENGTH

The overburden stresses within a rock mass are computed the same way as with soils. The unit weight of rocks can be assumed to be 27 kN/m³ when computing the overburden stresses. This value is more than what we normally see in compacted soils or concrete. In situ measurements worldwide, at various depths up to 2,500 m,

DOI: 10.1201/9781032725161-5 **155**

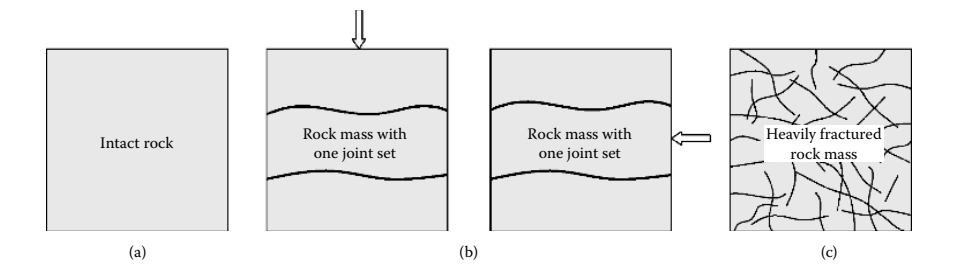


FIGURE 5.1 Isotropic and anisotropic behaviours: (a) intact rock – isotropic, (b) rock mass with one set of joints – anisotropic and (c) heavily fractured rock mass – isotropic.

show clearly that the vertical normal stress varies linearly with depth, as shown in Figure 5.2a (Hoek and Brown, 1980b). The average in situ vertical overburden stress (σ_{v}) can be estimated at any depth as

$$\sigma_{v}(MPa) = 0.027 z(m)$$
 (5.1)

where z is the depth in metres.

In normally consolidated and slightly over-consolidated soils, the vertical normal stress is generally the major principal stress and the horizontal stress is the minor principal stress. Here, the *coefficient of earth pressure at rest*, K_0 , defined as the ratio of horizontal to vertical effective stress, is less than 1. Only in highly over-consolidated soils can K_0 become greater than 1, making the horizontal stresses larger than the vertical stresses. The situation is quite different in rocks, where horizontal stresses are often larger than the vertical stress, especially at depths that are of engineering interest.

In addition to the in-situ stresses within the rock mass, stresses are also induced by tectonic activities, erosion and other geological factors. The ratio (K_0) of horizontal normal stress σ_h to vertical normal stress σ_v is generally larger than 1 and can be as high as 3 at shallow depths, where most of the civil engineering works are being carried out. With such a wide variability, horizontal stress should never be estimated. The value of K_0 gets smaller with increasing depth. The variations of K_0 values derived from in situ measurements worldwide are plotted against depth in Figure 5.2b. The two dashed lines show the lower and upper bounds for K_0 at any depth. They can be represented by the following equations:

Lower bound:
$$K_0 = 0.3 + \frac{100}{z(m)}$$
 (5.2a)

Upper bound:
$$K_0 = 0.5 + \frac{1500}{z(m)}$$
 (5.2b)

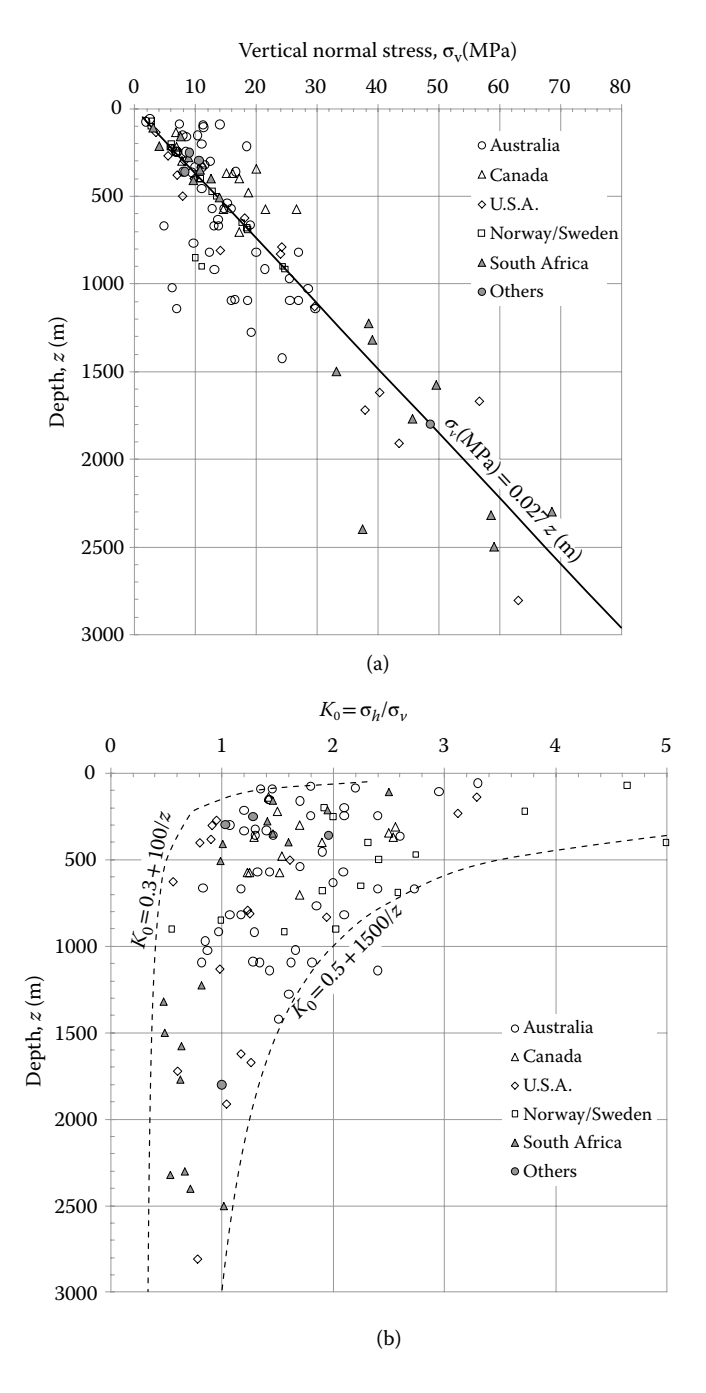


FIGURE 5.2 In situ measurement data: (a) σ_v with depth and (b) K_0 with depth. (After Hoek and Brown, 1980b.)

Shorey (1994) incorporated the horizontal deformation modulus ($E_{\rm h}$) and proposed Equation 5.3 for K_0 . The trend and the estimates fit well with those from Hoek and Brown (1980b).

$$K_0 = 0.25 + 7 E_h \left(\text{GPa} \right) \times \left(0.001 + \frac{1}{z(\text{m})} \right)$$
 (5.3)

5.3 STRESS-STRAIN RELATIONS

The stress-strain relationship of an engineering material is generally specified through a *constitutive relationship* or *constitutive model*. Some of the common constitutive models used to describe the stress-strain behaviour of geomaterials are linear elastic, non-linear elastic, elastoplastic, elastic-plastic, rigid-plastic, strain hardening, strain softening, Mohr-Coulomb, Cam clay, Drucker-Prager, visco-elastic, visco-plastic and so on. These constitutive models specify how strains are related to stresses.

The simplest analysis of a rock mass is often carried out assuming that it behaves as a *linear isotropic elastic material*, following Hooke's law, which states that strain is proportional to stress. The interrelationships between the six stress components and the six strain components of an isotropic linear elastic material can be written as

$$\varepsilon_{x} = \frac{1}{E} \left[\sigma_{x} - \nu \left(\sigma_{y} + \sigma_{z} \right) \right] \tag{5.4a}$$

$$\varepsilon_{y} = \frac{1}{E} \left[\sigma_{y} - \nu \left(\sigma_{x} + \sigma_{z} \right) \right]$$
 (5.4b)

$$\varepsilon_{z} = \frac{1}{E} \left[\sigma_{z} - \nu \left(\sigma_{x} + \sigma_{y} \right) \right]$$
 (5.4c)

$$\gamma_{xy} = \frac{1}{G} \tau_{xy} \tag{5.4d}$$

$$\gamma_{yz} = \frac{1}{G} \tau_{yz} \tag{5.4e}$$

$$\gamma_{x} = \frac{1}{G} \tau_{x} \tag{5.4f}$$

where σ = normal stress, τ = shear stress, ε = normal strain and γ = shear strain. x, y and z are the three mutually perpendicular directions in the Cartesian coordinate system. E and G are Young's modulus and the shear modulus (or modulus of rigidity), respectively. ν is Poisson's ratio (see Table 3.3 for typical values), which varies between 0 and 0.5. E and G are related by

$$G = \frac{E}{2(1+\nu)} \tag{3.7}$$

In matrix form, Equation 5.4 can be represented as

$$\begin{bmatrix}
\varepsilon_{x} \\
\varepsilon_{y} \\
\varepsilon_{z} \\
\gamma_{xy} \\
\gamma_{yz} \\
\gamma_{zx}
\end{bmatrix} = \frac{1}{E} \begin{bmatrix}
1 & -\nu & -\nu & 0 & 0 & 0 \\
-\nu & 1 & -\nu & 0 & 0 & 0 \\
-\nu & -\nu & 1 & 0 & 0 & 0 \\
0 & 0 & 0 & 2(1+\nu) & 0 & 0 \\
0 & 0 & 0 & 0 & 2(1+\nu) & 0 \\
0 & 0 & 0 & 0 & 0 & 2(1+\nu)
\end{bmatrix} \begin{bmatrix}
\sigma_{x} \\
\sigma_{y} \\
\sigma_{z} \\
\tau_{xy} \\
\tau_{yz} \\
\tau_{zx}
\end{bmatrix} (5.5)$$

or

$$\begin{bmatrix}
\sigma_{x} \\
\sigma_{y} \\
\sigma_{z} \\
\tau_{xy} \\
\tau_{zx}
\end{bmatrix} = \frac{E}{(1+\nu)(1-2\nu)}
\begin{bmatrix}
1-\nu & \nu & \nu & 0 & 0 & 0 \\
\nu & 1-\nu & \nu & 0 & 0 & 0 \\
\nu & \nu & 1-\nu & 0 & 0 & 0 \\
0 & 0 & 0 & \frac{(1-2\nu)}{2} & 0 & 0 \\
0 & 0 & 0 & 0 & \frac{(1-2\nu)}{2} & 0 \\
0 & 0 & 0 & 0 & \frac{(1-2\nu)}{2} & 0
\end{bmatrix}
\begin{bmatrix}
\varepsilon_{x} \\
\varepsilon_{y} \\
\varepsilon_{z} \\
\gamma_{xy} \\
\gamma_{yz} \\
\gamma_{zx}
\end{bmatrix} (5.6)$$

The volumetric strain ϵ_{vol} is the ratio of volume change to the initial volume and is given by

$$\varepsilon_{\text{vol}} = \varepsilon_x + \varepsilon_y + \varepsilon_z \tag{5.7}$$

Substituting the expressions for strains from Equation 5.5,

$$\varepsilon_{\text{vol}} = \frac{1 - 2\nu}{E} \left[\sigma_x + \sigma_y + \sigma_z \right]$$

$$\varepsilon_{\text{vol}} = \frac{3(1 - 2\nu)}{E} \left[\frac{\sigma_x + \sigma_y + \sigma_z}{3} \right] = \frac{1}{E} \left[\frac{\sigma_x + \sigma_y + \sigma_z}{3} \right]$$
(5.8)

where K is the bulk modulus given by Equation 3.6 in Chapter 3. In some numerical modelling applications, G and K are used as input parameters rather than E and v. They are related by

$$E = \frac{9KG}{3K + G} \tag{5.9}$$

$$\nu = \frac{3K - 2G}{2(3K + G)} \tag{5.10}$$

EXAMPLE 5.1

When the applied normal stresses in the x, y and z directions are principal stresses, express the principal strains in terms of principal stresses, and then the principal stresses in terms of the principal strains.

Solution

Substituting $\tau_{xy} = 0$, $\tau_{yz} = 0$ and $\tau_{zx} = 0$ in Equation 5.5:

$$\begin{cases} \varepsilon_1 \\ \varepsilon_2 \\ \varepsilon_3 \end{cases} = \frac{1}{E} \begin{bmatrix} 1 & -\nu & -\nu \\ -\nu & 1 & -\nu \\ -\nu & -\nu & 1 \end{bmatrix} \begin{bmatrix} \sigma_1 \\ \sigma_2 \\ \sigma_3 \end{bmatrix}$$

Substituting $\gamma_{xy} = 0$, $\gamma_{yz} = 0$ and $\gamma_{zx} = 0$ in Equation 5.6,

$$\begin{bmatrix} \sigma_1 \\ \sigma_2 \\ \sigma_3 \end{bmatrix} = \frac{E}{(1+\nu)(1-2\nu)} \begin{bmatrix} 1-\nu & \nu & \nu \\ \nu & 1-\nu & \nu \\ \nu & \nu & 1-\nu \end{bmatrix} \begin{bmatrix} \varepsilon_1 \\ \varepsilon_2 \\ \varepsilon_3 \end{bmatrix}$$

5.3.1 Plane Strain Loading

In geotechnical engineering, when the structure (e.g. retaining wall, embankment and strip footing) is long in one direction, the deformation or strain in this direction can be neglected, and the situation can be assumed as a plane strain problem. This is also true in rock mechanics. For a plane strain loading, where the strains are limited to the *x-y* plane, Equations 5.5 and 5.6 become

$$\begin{cases}
\varepsilon_{x} \\
\varepsilon_{y} \\
\gamma_{xy}
\end{cases} = \frac{1}{E} \begin{bmatrix}
1 - \nu^{2} & -\nu(1 + \nu) & 0 \\
-\nu(1 + \nu) & 1 - \nu^{2} & 0 \\
0 & 0 & 2(1 + \nu)
\end{bmatrix} \begin{bmatrix}
\sigma_{x} \\
\sigma_{y} \\
\tau_{xy}
\end{cases} (5.11)$$

and

$$\begin{bmatrix} \sigma_{x} \\ \sigma_{y} \\ \tau_{xy} \end{bmatrix} = \frac{E}{(1+\nu)(1-2\nu)} \begin{bmatrix} 1-\nu & \nu & 0 \\ \nu & 1-\nu & 0 \\ 0 & 0 & \frac{(1-2\nu)}{2} \end{bmatrix} \begin{bmatrix} \varepsilon_{x} \\ \varepsilon_{y} \\ \gamma_{xy} \end{bmatrix}$$
(5.12)

Plane strain loading does not mean that there are no normal stresses in the direction perpendicular to the plane. It is the normal *strains* that are zero in that direction. The normal stress in the direction perpendicular to the plane (in the direction of zero normal strain) is given by

$$\sigma_z = \nu \left(\sigma_x + \sigma_y \right) \tag{5.13}$$

In plane strain loading, the non-zero stresses are σ_x , σ_y , σ_z and τ_{xy} . The non-zero strains are ε_x , ε_v and γ_{xy} .

EXAMPLE 5.2

In plane strain loading, when the applied normal stresses in x and y directions are principal stresses, derive the expressions for the major and the minor principal strains.

In a rock mass subjected to plane strain loading, $\sigma_1 = 2$ MPa and $\sigma_3 = 1$ MPa. Assuming a Young's modulus of 20 GPa and Poisson's ratio of 0.2, determine the principal strains and the normal stress perpendicular to the plane.

Solution

Substituting $\sigma_x = \sigma_1$, $\sigma_y = \sigma_3$ and $\tau_{xy} = 0$ in Equation 5.11, the major and the minor principal strains ε_1 and ε_3 are given by

$$\begin{cases} \varepsilon_1 \\ \varepsilon_3 \end{cases} = \frac{1}{E} \begin{bmatrix} 1 - \nu^2 & -\nu(1 + \nu) \\ -\nu(1 + \nu) & 1 - \nu^2 \end{bmatrix} \begin{bmatrix} \sigma_1 \\ \sigma_3 \end{bmatrix}$$

The principal stress in the direction of zero normal strain is given by

$$\sigma_2 = \nu (\sigma_1 + \sigma_3)$$

This is not necessarily the intermediate principal stress. Depending on the values of v, σ_1 and σ_3 , this can be the minor or intermediate principal stress.

Substituting the values,

$$\varepsilon_1 = \frac{1}{20} \{ (1 - 0.2^2) \times 2 - 0.2 \times (1 + 0.2) \times 1 \} = 0.084$$

$$\varepsilon_3 = \frac{1}{20} \left\{ -0.2 \times (1 + 0.2) \times 2 + (1 - 0.2^2) \times 1 \right\} = 0.024$$

For plane strain loading, $\varepsilon_2 = 0$. For principal planes, the shear strains are zero as well. The normal stress in the direction of zero normal strain is given by

$$\sigma_2 = 0.2 \times (2+1) = 0.6 \text{ MPa}$$

5.3.2 PLANE STRESS LOADING

Plane stress loading is not very common in geotechnical or rock engineering applications. Let us think of a thin plate being loaded along its plane. When the stresses are confined to *x-y* plane, the stresses and strains are related by

$$\begin{cases}
\varepsilon_{x} \\
\varepsilon_{y} \\
\gamma_{xy}
\end{cases} = \frac{1}{E} \begin{bmatrix}
1 & -\nu & 0 \\
-\nu & 1 & 0 \\
0 & 0 & 2(1+\nu)
\end{bmatrix} \begin{cases}
\sigma_{x} \\
\sigma_{y} \\
\tau_{xy}
\end{cases}$$
(5.14)

or

The dimension in the z-direction is very small. Here, the non-zero stresses are σ_x , σ_y and τ_{xy} . There can be strains perpendicular to the x-y plane. The non-zero strains are ε_x , ε_y , ε_z and γ_{xy} . The normal strain in the direction of zero normal stress is given by

$$\varepsilon_{z} = \frac{\nu}{1 - \nu} \left(\varepsilon_{x} + \varepsilon_{y} \right) = -\frac{\nu}{F} \left(\sigma_{x} + \sigma_{y} \right) \tag{5.16}$$

5.3.3 AXISYMMETRIC LOADING

Axisymmetric loading is quite common in geotechnical and rock engineering. For example, along the vertical centre line of a uniformly loaded circular footing, the lateral stresses are the same in all directions. If σ_1 and σ_3 are the axial and the radial normal stresses, respectively, they are related to the normal strains in the same directions, ϵ_1 and ϵ_3 , by

$$\begin{cases} \varepsilon_1 \\ \varepsilon_3 \end{cases} = \frac{1}{E} \begin{bmatrix} 1 & -2\nu \\ -\nu & 1-\nu \end{bmatrix} \begin{cases} \sigma_1 \\ \sigma_3 \end{cases}$$
(5.17)

$$\begin{cases}
 \sigma_1 \\
 \sigma_3
 \end{cases} = \frac{E}{(1+\nu)(1-2\nu)} \begin{bmatrix} 1-\nu & 2\nu \\ \nu & 1 \end{bmatrix} \begin{bmatrix} \varepsilon_1 \\ \varepsilon_3 \end{bmatrix}$$
(5.18)

5.3.4 STRAIN-DISPLACEMENT RELATIONSHIPS

The strains in the elastic body are caused by displacements. The displacements in the three mutually perpendicular directions, u, v and w, and strains are related by

$$\begin{bmatrix}
\varepsilon_{x} \\
\varepsilon_{y} \\
\varepsilon_{z} \\
\gamma_{xy} \\
\gamma_{yz} \\
\gamma_{zx}
\end{bmatrix} = \begin{bmatrix}
\frac{\partial}{\partial x} & 0 & 0 \\
0 & \frac{\partial}{\partial y} & 0 \\
0 & 0 & \frac{\partial}{\partial z} \\
\frac{\partial}{\partial y} & \frac{\partial}{\partial x} & 0 \\
0 & \frac{\partial}{\partial z} & \frac{\partial}{\partial y} \\
0 & \frac{\partial}{\partial z} & \frac{\partial}{\partial z}
\end{bmatrix} \begin{bmatrix} u \\ v \\ w \end{bmatrix}$$

$$(5.19)$$

5.4 MOHR-COULOMB FAILURE CRITERION

Mohr–Coulomb is the most popular failure criterion that works quite well for geomaterials, especially soils, where the failure generally takes place in shear. The shear strength on the failure plane, τ_f , is proportional to the normal stress, σ , on the plane and is expressed as

$$\tau_{\rm f} = c + \sigma \tan \phi \tag{5.20}$$

where c is the cohesion and ϕ is the friction angle. It can be seen in Equation 5.20 that the shear strength has two separate components: cohesive (c) and frictional $(\sigma \tan \phi)$. While the frictional component is proportional to the normal stress, the cohesive component is a constant, which is independent of the normal stress. Let us apply the same Mohr–Coulomb failure criterion to rocks as well.

Uniaxial compression is a very common test that is carried out on soils, rocks and concrete. The uniaxial compressive strength, fondly known as UCS, is denoted as σ_c here. When the specimen fails, $\sigma_1 = \sigma_c$ and $\sigma_3 = 0$. Here, σ_1 and σ_3 are the major and the minor principal stresses, respectively. Uniaxial tensile tests are common on steel

specimens but are uncommon for geomaterials or concrete. When testing steel specimens in tension, it is common to use dog-bone-shaped specimens that will prevent slip when the specimen is being pulled axially. This is not possible with rocks. Here, the problem is to hold a specimen without any slippage while the tensile load is applied and increased to failure. Holding the specimen too tightly in a chuck would fail the specimen. Further, any misalignment can induce eccentricity and hence a moment, in addition to the axial load. Nevertheless, let us consider a uniaxial tensile strength test, where the magnitude of the tensile strength is σ_i . At failure, $\sigma_i = 0$ and $\sigma_3 = -\sigma_i$.

The Mohr circles at failure in a uniaxial tensile strength test and a uniaxial compressive strength test are shown in Figure 5.3a and b, respectively. Here, it is assumed that the Mohr–Coulomb failure criterion (Equation 5.20) is valid in the tensile region too. By simple trigonometry and algebra, it can be shown that

$$x = \frac{c\cos\phi}{1+\sin\phi}$$

and

$$y = \frac{c\cos\phi}{1-\sin\phi}$$

Noting that the magnitudes of the uniaxial tensile strength, σ_t , and the uniaxial compressive strength, σ_c are given by 2x and 2y, respectively,

$$\sigma_{t} = \frac{2c\cos\phi}{1+\sin\phi} \tag{5.21}$$

and

$$\sigma_{\rm c} = \frac{2c\cos\phi}{1-\sin\phi} \tag{5.22}$$

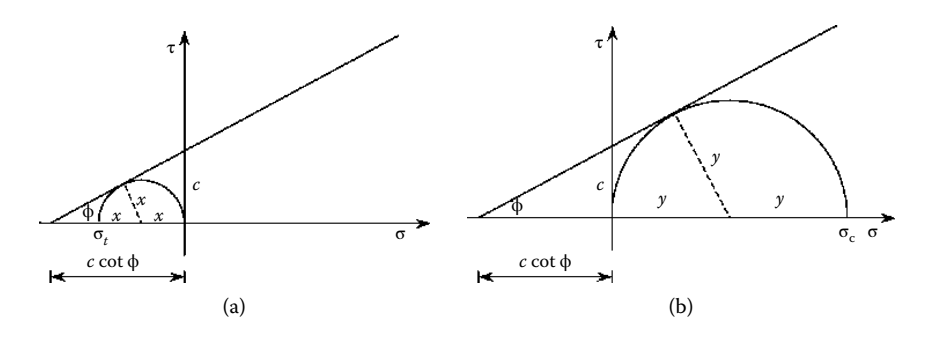


FIGURE 5.3 Mohr circles at failure: (a) uniaxial tensile strength test and (b) uniaxial compressive strength test.

Therefore, the theoretical ratio of σ_c to σ_t for a Mohr–Coulomb material is given by $(1 + \sin\phi)/(1 - \sin\phi)$. For a friction angle of 30–60°, this ratio is in the range of 3–14.

The Brazilian indirect tensile strength test was introduced for rocks and concrete due to the difficulty in carrying out a direct tensile strength test for determining σ_t . In a Brazilian indirect tensile strength test, an intact rock specimen with a thickness-to-diameter ratio of 0.5 is subjected to a diametrical load, P, applied along the entire length of the core, which is increased until failure occurs by splitting (see Chapter 3 for details). Ideally, the disc splits vertically along the diameter into two halves. At failure, the vertical normal stress at the centre of the specimen is compressive, and the horizontal normal stress is tensile, as shown in the inset in Figure 5.4. These are also principal stresses. Hondros (1959) showed that the horizontal and the vertical normal stresses at the centre of the core are given by

$$\sigma_{\text{horizontal}} \left(\text{tensile} \right) = -\frac{2P}{\pi Dt}$$
 (5.23)

for the element at the centre of the specimen during failure in a Brazilian indirect tensile strength test.

$$\sigma_{\text{vertical}} \left(\text{compressive} \right) = \frac{6P}{\pi Dt}$$
 (5.24)

where P = failure load, D = specimen diameter and t = specimen thickness. The horizontal normal stress at failure, at the centre of the specimen, is known as the indirect tensile strength, denoted here as σ_t . The million-dollar question is how close it is to the uniaxial tensile strength, σ_t of the intact rock.

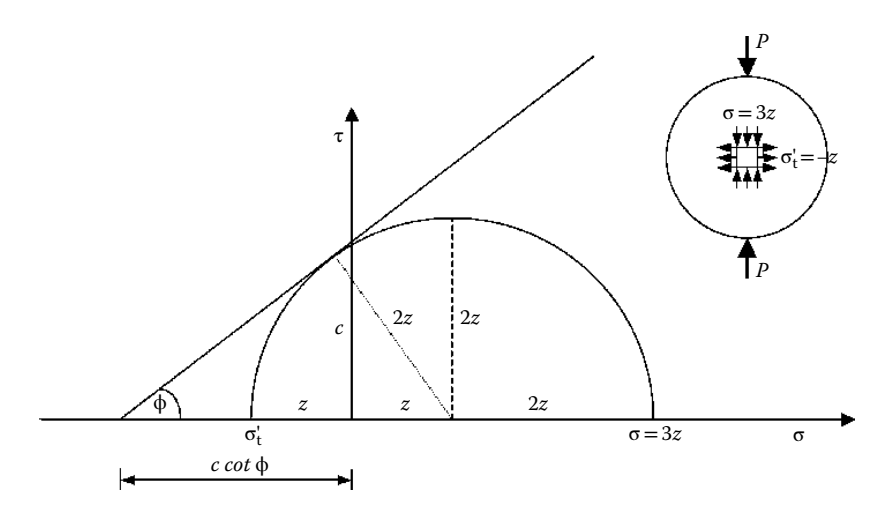


FIGURE 5.4 Mohr circle.

From the Mohr circle shown in Figure 5.4, and by simple trigonometric and algebraic manipulations, it can be shown that

$$z = \frac{c\cos\phi}{2-\sin\phi}$$

and therefore the magnitude of the indirect tensile strength is given by

$$\sigma_{t}' = \frac{c\cos\phi}{2-\sin\phi} \tag{5.25}$$

which is different from the expression derived for the uniaxial tensile strength, σ_{t_i} in Equation 5.21. It can be seen here that, theoretically, the magnitude of σ_t' is less than that of σ_t , provided the Mohr–Coulomb criterion is valid in the tensile region as well. The theoretical ratio of σ_c to σ_t' of a Mohr–Coulomb material is given by $2(2-\sin\phi)/(1-\sin\phi)$. For a friction angle of $30-60^\circ$, this ratio is in the range of 6-17.

The frictional component in Equation 5.20 is meaningless when the normal stress, σ , is tensile. Therefore, Equation 5.20 is valid essentially when the normal stress is positive (i.e. compressive). Therefore, in soils, the Mohr–Coulomb failure criterion is used mainly for $\sigma \ge 0$. Unlike soils, rocks can carry some tensile stresses, and therefore the Mohr–Coulomb failure criterion requires some adjustment in the tensile region. There are better failure theories (e.g. Griffith theory) for rocks under tensile stresses.

Figure 5.5 shows a simple extrapolation of the Mohr–Coulomb failure criterion into the tensile region, for situations where the minor principal stress can be negative. Figure 5.5 also shows the three Mohr circles corresponding to (a) a uniaxial compressive strength test, (b) a Brazilian indirect tensile strength test and (c) a uniaxial tensile strength test. It is assumed that the tensile strength derived from the

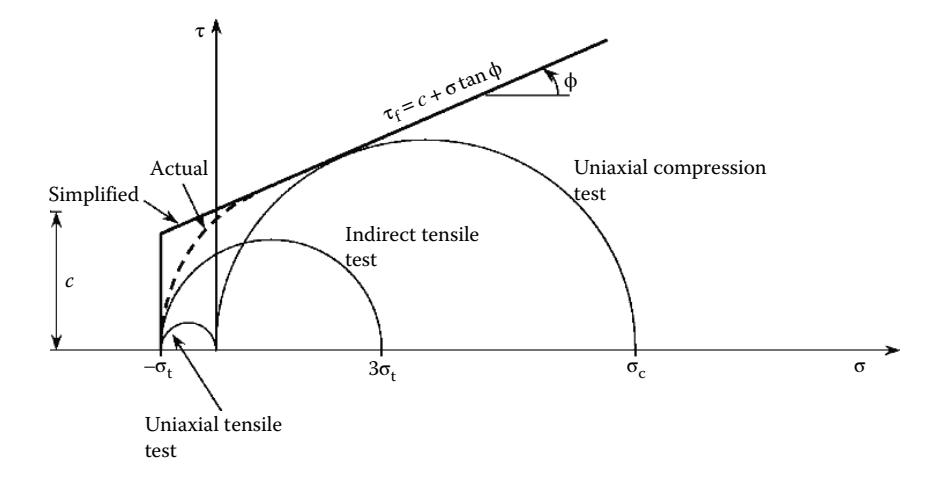


FIGURE 5.5 Mohr–Coulomb failure criterion with adjustment for tensile normal stresses.

uniaxial tensile test is the *same* as the one from the Brazilian indirect tensile test. σ_c and σ_t are the uniaxial (or unconfined) compressive and tensile strength values of the rock. The curved dashed line shows the actual envelope in the tensile region, implying that the simplified Mohr–Coulomb extrapolation can overestimate the strength in the tensile region. Therefore, it is prudent to use lower values of c and σ_t when using this simplification (Goodman, 1989). Remember, we are reasonably confident about the Mohr–Coulomb envelope on the right side of the τ -axis; it is the left side that is a concern.

It can be shown from Figure 5.5 that

$$\sigma_c = 2c \tan\left(45 + \frac{\phi}{2}\right) = 2c \frac{\cos\phi}{1 - \sin\phi} = 2c \sqrt{\frac{1 + \sin\phi}{1 - \sin\phi}}$$
 (5.26)

and, at failure, σ_1 can be related to σ_3 by

$$\sigma_1 = 2c \tan\left(45 + \frac{\phi}{2}\right) + \sigma_3 \tan^2\left(45 + \frac{\phi}{2}\right) = \sigma_c + \sigma_3 \tan^2\left(45 + \frac{\phi}{2}\right)$$
 (5.27)

EXAMPLE 5.3

Triaxial tests were carried out on 50-mm-diameter limestone cores and the following data were obtained for the principal stresses at failure.

$\overline{\sigma_{3f}(MPa)}$	0	5.0	10.0	20.0	30.0	40.0
$\sigma_{1f}(MPa)$	78.0	124.5	145.5	196.0	230.5	262.5

Plot σ_{lf} against σ_{3f} and determine the uniaxial compressive strength, σ_{c} , and friction angle, ϕ , of the limestone.

Solution

From the plot shown in Figure 5.6, $\sigma_c = 95.2$ MPa and

$$\tan^2\left(45 + \frac{\phi}{2}\right) = 4.4337 \rightarrow \phi = 39.2^{\circ}$$

EXAMPLE 5.4

It is proposed to excavate a horseshoe-shaped tunnel at a depth of 1,000 m below ground level into sound unjointed fresh granite with c = 0.5 MPa and $\phi = 40^{\circ}$. The average unit weight of the overburden is 27 kN/m³. Once the tunnel is excavated, it is expected that the lateral normal stress near the tunnel walls will be close to zero. Will the rock fail ('burst') into the excavated tunnel?

What level of prestressing (i.e. σ_3) in the form of struts, rock bolting and so on, is required to ensure that the tunnel can just resist the failure?

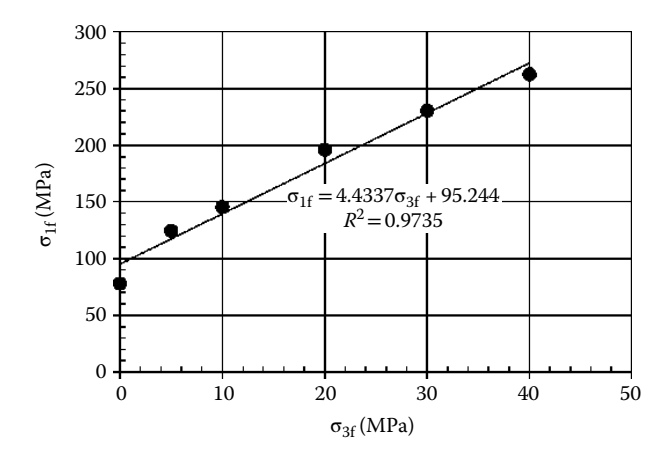


FIGURE 5.6 Plot of σ_{1f} against σ_{3f} .

Solution

 $\sigma_v = \sigma_1 = 100 \times 27 \text{ kPa} = 2.7 \text{ MPa}$ $\sigma_h = \sigma_3 \approx 0$ (i.e. more like unconfined compression) $\phi = 40^\circ$ and c = 0.5 MPa

Substituting these values of σ_3 , ϕ and c in Equation 5.27, the maximum vertical normal stress the rock can withstand is given by

$$\sigma_{1f} = 2 \times 0.5 \tan \left(45 + \frac{40}{2}\right) + 0 \times \tan^2 \left(45 + \frac{40}{2}\right) = 2.14 \text{ MPa}$$

Since the vertical overburden stress of 2.7 MPa exceeds the available strength of 2.14 MPa, the tunnel wall will fail.

To resist failure, we require some confining pressure σ_3 that would increase the shear strength of the rock. This can be estimated from Equation 5.27 as

2.70 = 2×0.5 tan
$$\left(45 + \frac{40}{2}\right)$$
 + σ_3 × tan² $\left(45 + \frac{40}{2}\right)$
∴ σ_3 = 0.121 MPa

As in the case of soils, the shear strength of a rock mass can be defined in terms of peak or residual stresses. *Peak shear strength* is the maximum shear stress that can be carried by the element; *residual shear strength*, which is less than the peak shear strength (Figure 5.7a), is the shear stress when the element has undergone significant strain. Using the shear stress values at peak or residual states, Mohr–Coulomb failure envelopes can be developed on the τ – σ plane, as shown in Figure 5.7b. Here, the peak and residual friction angles are denoted by ϕ_p and ϕ_r , respectively. In soils and rocks,

at residual states, where the strains are large, the cohesive bonds are broken and there is little or no cohesion contributing towards the shear strength. Therefore, $c_r \approx 0$ and the failure envelope at the residual state passes through the origin in the τ - σ plane. In a rock mass, at large strains, the surface irregularities are further smoothened, and therefore ϕ_r is significantly less than ϕ_p . The difference between the peak friction angle and the residual friction angle can be quite substantial and is approximately equal to the roughness angle i, introduced in Equation 4.2. This roughness angle is the result of the surface irregularities or asperities in the rock. The residual friction angle is approximately equal to the basic friction angle of the rock material, ϕ_b .

While the intact rock is relatively impervious, the discontinuities present within the rock mass allow easy access to water. With the pore water pressures within the joints, Terzaghi's effective stress theory can be applied to the rock mass. It simply states that the total stress σ is distributed between the rock and the pore water, as effective stress σ' and pore water pressure

$$\sigma = \sigma' + u \tag{5.28}$$

Applying the Mohr–Coulomb failure criterion to the *rock mass* in terms of effective stresses, Equation 5.27 becomes

$$\sigma'_{1f} = \sigma_{cm} + \sigma'_{3f} \tan^2 \left(45 + \frac{\phi'}{2} \right) = 2c' \tan \left(45 + \frac{\phi'}{2} \right) + \sigma'_{3f} \tan^2 \left(45 + \frac{\phi'}{2} \right)$$
(5.29)

where σ'_{1f} = effective major principal stress at failure within the rock mass, σ'_{3f} = effective minor principal stress at failure within the rock mass, σ_{cm} = uniaxial compressive strength of the rock mass, c' = effective cohesion of the rock mass and ϕ' = effective friction angle of the rock mass.

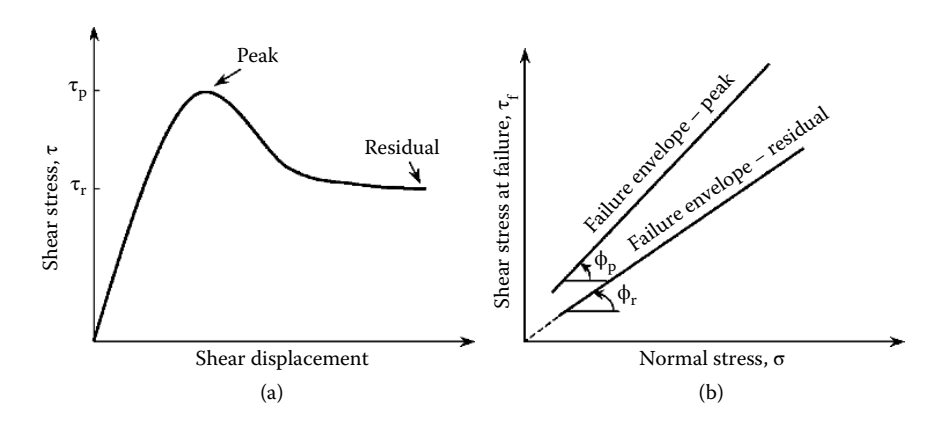


FIGURE 5.7 Peak and residual shear strengths: (a) stress–strain plot and (b) failure envelopes.

We can carry out triaxial tests and determine c' and ϕ' of the intact rock, which is a fairly straightforward exercise. How does one determine c' and ϕ' of the *rock mass*? Ideally, we should test a very large rock mass that includes discontinuities as well. It is a difficult problem. This is discussed further in Section 5.6.

5.5 HOEK-BROWN FAILURE CRITERION

In geotechnical engineering, where the failure within the soil mass occurs in shear, it is common to present the failure criterion in terms of shear and normal stresses on the failure plane. In rock mechanics, however, the common practice is to present the failure criterion in terms of the principal stresses σ_1 and σ_3 , having them on the *x*- and *y*-axes, respectively.

5.5.1 INTACT ROCK

Noting the deficiencies of the Mohr–Coulomb failure criterion, Hoek and Brown (1980a, 1980b) proposed that the effective major and minor principal stresses within an *intact rock* at failure, $\sigma_{1f}^{'}$ and $\sigma_{3f}^{'}$, respectively, can be related by

$$\sigma'_{1f} = \sigma'_{3f} + \sigma_{ci} \left(m_i \frac{\sigma'_{3f}}{\sigma_{ci}} + s \right)^{0.5}$$
 (5.30)

where s=1 (for intact rocks only). Here, σ_{ci} is the uniaxial compressive strength of the intact rock, and m_i is the Hoek–Brown parameter for the intact rock, both of which can be determined from a series of triaxial tests. In the past, we used the notation σ_c for uniaxial compressive strength – now we have to separate intact rock and the rock mass and hence give the notation σ_{ci} for the intact rock and σ_{cm} for the rock mass.

For intact rocks, assuming s = 1, Equation 5.30 can be written as

$$\left(\sigma'_{1f} - \sigma'_{3f}\right)^2 = m_i \sigma_{ci} \sigma'_{3f} + \sigma_{ci}^2$$
 (5.31)

Plotting the triaxial test data as $\left(\sigma_{1f}^{'} - \sigma_{3f}^{'}\right)^{2}$ against $\sigma_{3f}^{'}$, it is possible to determine m_{i} and σ_{ci} (see Example 5.5). Alternatively, m_{i} can be estimated from Table 4.26. It is simply a petrographic constant that is analogous to the friction angle. The strength increases with increasing m_{i} . The variation of $\sigma_{1f}^{'}$ against $\sigma_{3f}^{'}$ as per the Hoek–Brown criterion is shown in Figure 5.8a, where the failure envelope is parabolic. The variation as per the Mohr–Coulomb failure criterion, as deduced from Equation 5.27, is shown in Figure 5.8b, where the failure envelope is a straight line. The intercepts of the $\sigma_{1f}^{'}$ -axis and the $\sigma_{3f}^{'}$ -axis are the uniaxial compressive strength σ_{ci} and uniaxial tensile strength σ_{ci} , respectively.

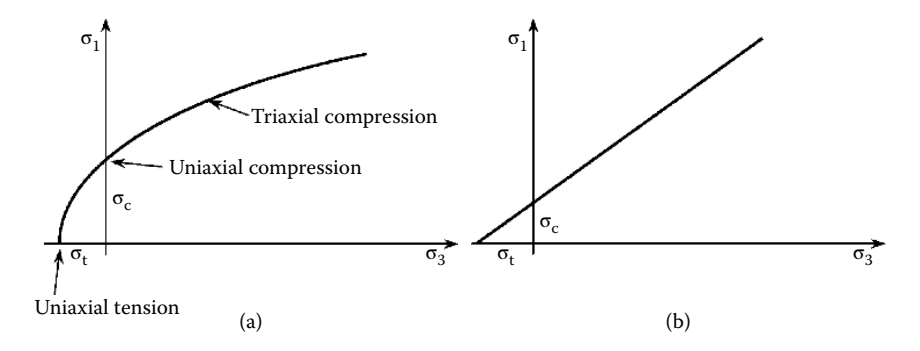


FIGURE 5.8 A comparison: (a) Hoek–Brown failure criterion and (b) Mohr–Coulomb failure criterion.

Substituting $\sigma'_{3f} = -\sigma_{ti}$ and $\sigma'_{1f} = 0$ in Equation 5.30,

$$0 = -\sigma_{ti} + \sigma_{ci} \left(-m_i \frac{\sigma_{ti}}{\sigma_{ci}} + s \right)^{0.5}$$

$$\left(\frac{\sigma_{ti}}{\sigma_{ci}}\right)^{2} + m_{i}\left(\frac{\sigma_{ti}}{\sigma_{ci}}\right) - s = 0$$

Therefore,

$$\left(\frac{\sigma_{ti}}{\sigma_{ci}}\right) = -\frac{\sqrt{m_i^2 + 4s} - m_i}{2} \tag{5.32}$$

Equation 5.32 shows that the ratio of compressive strength to tensile strength of an intact rock depends only on m_i . This ratio σ_{ci}/σ_{ti} increases with m_i . For the range of $m_i = 5-35$, σ_{ci}/σ_{ti} lies within 5 and 35. As a first approximation, σ_{ci}/σ_{ti} can be taken as m_i .

EXAMPLE 5.5

Triaxial tests were carried out on 50-mm-diameter limestone cores and the following data were obtained for the principal stresses at failure (same data as in Example 5.3).

σ_{3f} (MPa)	0	5.0	10.0	20.0	30.0	40.0
σ_{lf} (MPa)	78.0	124.5	145.5	196.0	230.5	262.5

Neglect the pore water pressures. Plot $(\sigma_{1f} - \sigma_{3f})^2$ versus σ_{3f} and determine m_i and σ_{ci} for the limestone.

Using the preceding values of m_i and σ_{ci} , plot the theoretical failure envelope in σ_{3f} versus σ_{1f} space.

Show the test data along with the theoretical failure envelope and see how well they match.

Solution

The plot of $(\sigma_{1f} - \sigma_{3f})^2$ versus σ_{3f} is shown in Figure 5.9. From the line of best fit,

$$\sigma_{ci}^2 = 7835 \rightarrow :: \sigma_{ci} = 88.5 \text{ MPa}$$

The gradient $m_i \sigma_{ci} = 1070.4 \rightarrow m_i = 12.1$

Substituting $m_i = 12.1$, $\sigma_{ci} = 88.5$ MPa and s = 1 in Equation 5.30, the theoretical Hoek–Brown failure envelope can be derived.

The theoretical envelope derived here is shown along with the experimental data in Figure 5.10.

EXAMPLE 5.6

In Example 5.5, estimate the tensile strength of the rock.

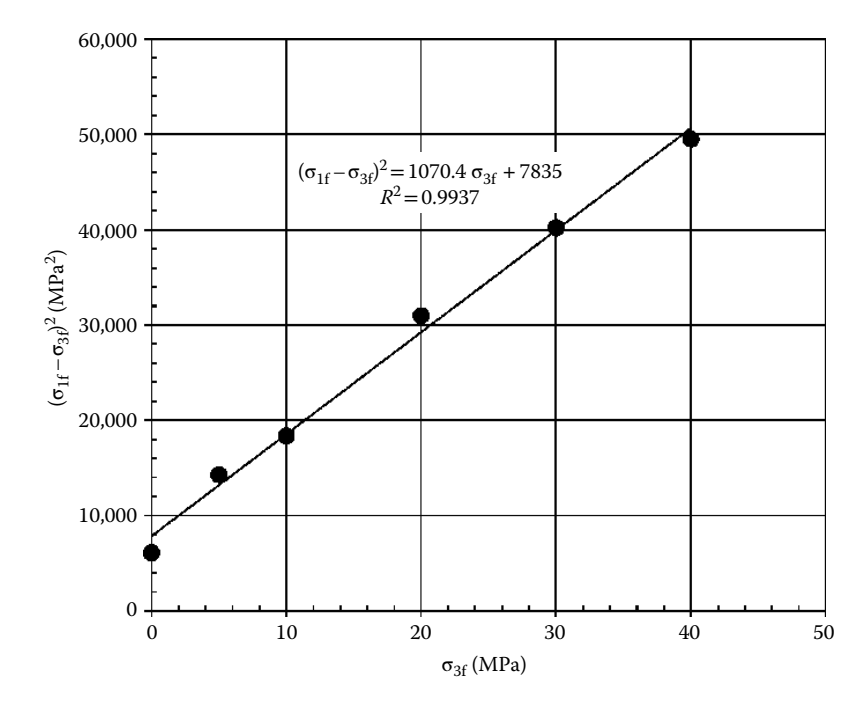


FIGURE 5.9 Determination of σ_{ci} and m_i .

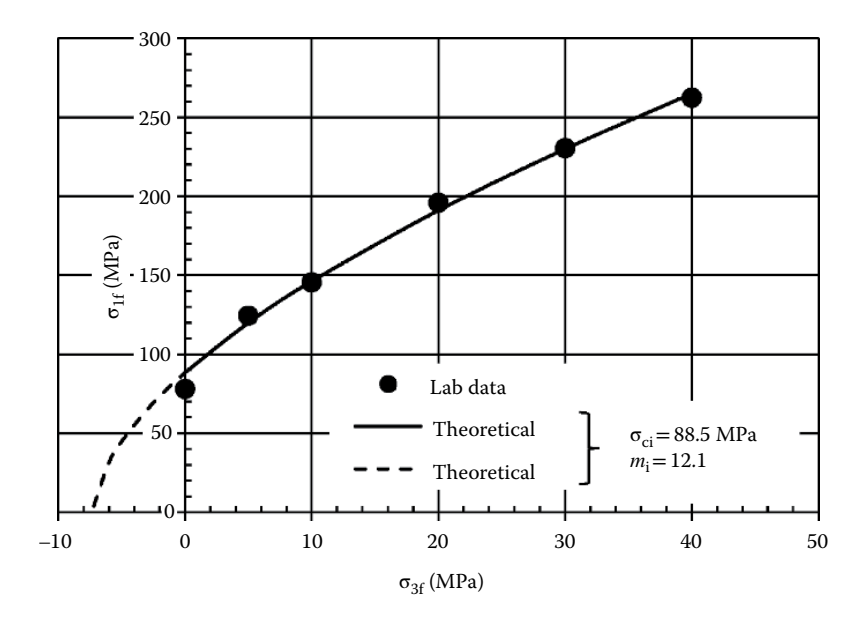


FIGURE 5.10 Theoretical Hoek–Brown failure envelope.

Solution

From the triaxial test data, it was determined in Example 5.5 that $m_i = 12.1$ and $\sigma_{ci} = 88.5$ MPa. Assuming s = 1 and substituting in Equation 5.32,

$$\begin{pmatrix} \sigma_{ti} \\ \sigma_{ci} \end{pmatrix} = -\frac{\sqrt{m_i^2 + 4s} - m_i}{2} = -\frac{\sqrt{12.1^2 + 4 \times 1} - 12.1}{2} = -0.082$$

$$\therefore \sigma_{ti} = -7.3 \text{ MPa}$$

5.5.2 ROCK MASS

The Hoek–Brown failure criterion has evolved over the years into a more *generalised* Hoek–Brown criterion that can also be applied to the rock mass as well as intact rocks. This was discussed briefly in Chapter 4. For the jointed *rock mass*, Equation 5.30 was modified to (Hoek and Brown, 1997)

$$\sigma'_{1f} = \sigma'_{3f} + \sigma_{ci} \left(m_m \frac{\sigma'_{3f}}{\sigma_{ci}} + s \right)^a$$
 (4.13)

where $m_{\rm m}$ is the *m*-parameter for the rock mass (sometimes denoted as $m_{\rm b}$ in the literature, with subscript b referring to *broken rock*), which is derived from the value for the intact rock $m_{\rm i}$ as (Hoek et al., 2002)

$$m_{\rm m} = m_{\rm i} \exp\left(\frac{\text{GSI} - 100}{28 - 14D}\right) \tag{5.33}$$

where D is a factor to account for the disturbance in the rock mass due to blasting and stress relief, introduced by Hoek et al. (2002). It varies in the range of 0–1; 0 for undisturbed and 1 for highly disturbed rock mass. Note that we still use σ_{ci} in Equation 4.13, which is essentially for the rock mass.

The constant $m_{\rm m}$ can take a positive value in the range of 0.001–25, with highly disturbed poor-quality rock masses falling in the lower end and the hard and almost intact rocks at the upper end. It can be seen from Equation 5.33 that $m_{\rm m}$ is less than $m_{\rm i}$, which is expected intuitively. Yes, the rock mass is weaker than the intact rock. Typically, $m_{\rm i}$ varies in the range of 2–35. The difference between the two becomes larger with poorer-quality rock mass with low GSI. The uniaxial compressive strength of the rock mass, $\sigma_{\rm cm}$, is less than that of the intact rock, $\sigma_{\rm ci}$, due to the presence of discontinuities.

The constants s and a for the rock mass are given by (Hoek et al., 2002):

$$s = \exp\left(\frac{\text{GSI} - 100}{9 - 3D}\right) \tag{5.34}$$

and

$$a = \frac{1}{2} + \frac{1}{6} \left(e^{-GSI/15} - e^{-20/3} \right)$$
 (5.35)

Generally, s varies in the range of 0–1, mostly at the lower end of the range, with 0 for very poor-quality rock and 1 for intact rock. It is a petrographic constant that is similar to cohesion in the Mohr–Coulomb failure criterion. The constant a varies between 0.50 for good-quality rock (or intact rock) and 0.65 for poor-quality rock. D is a factor to account for the disturbance within the rock mass due to blasting, stress relief and so on. It varies in the range of 0–1; 0 for undisturbed and 1 for highly disturbed rock mass.

The Hoek–Brown failure criterion is developed assuming isotropic behaviour of the intact rock and rock mass. Therefore, it works well for intact rock specimens as well as closely spaced, heavily jointed rock masses where isotropy can be assumed. In situations where the structure being analysed and the block sizes are of the same order in size, or in situations with specific weak discontinuities, the Hoek–Brown failure criterion should not be applied.

Substituting $\sigma_{3f} = 0$ and $\sigma_{1f} = \sigma_{cm}$ in Equation 4.13, the uniaxial compressive strength of the rock mass can be calculated as

$$\sigma_{\rm cm} = \sigma_{\rm ci} s^a \tag{5.36}$$

where σ_{ci} is the UCS of the intact rock. Marinos and Hoek (2001) proposed an empirical equation for σ_{cm} in terms of m_i , σ_{ci} and GSI as

$$\sigma_{\rm cm} = \sigma_{\rm ci} \times 0.0034 \, m_{\rm i}^{0.8} \times \left\{ 1.029 + 0.025 e^{-0.1 m_{\rm i}} \right\}^{\rm GSI}$$
 (5.37)

The ratio $\sigma_{\rm cm}/\sigma_{\rm ci}$ approaches unity when GSI increases to 100. There are empirical equations reported in the literature that relate $\sigma_{\rm cm}/\sigma_{\rm ci}$ to RMR or Q.

Assuming a = 0.5, Equation 5.32 can be extended to the rock mass, where the uniaxial tensile strength can be expressed as (Hoek and Brown, 1997)

$$\sigma_{\rm tm} = -\sigma_{\rm ci} \frac{\sqrt{m_{\rm m}^2 + 4s} - m_{\rm m}}{2} \tag{5.38}$$

Hoek (1983) noted that for brittle materials, the uniaxial tensile strength is the same as the biaxial tensile strength. Therefore, substituting $\sigma'_{3f} = \sigma'_{1f} = \sigma_{tm}$ in Equation 4.13, the tensile strength of the rock mass is given by Hoek et al. (2002).

$$\sigma_{\rm tm} = -\frac{s\sigma_{\rm ci}}{m_{\rm m}} \tag{5.39}$$

Some typical values of the Hoek–Brown parameters of the intact rock and the rock mass, the GSI of the rock mass and the deformation modulus of the rock mass from a few larger projects worldwide, as documented by Hoek (2007), are summarised in Table 5.1.

TABLE 5.1

Some Typical Values of Hoek–Brown Parameters from Case Histories

	Intact R	ock	Rock Mass				
Description	σ _{ci} (MPa)	mi	GSI	m _m	s	a	E _m (GPa)
Massive (almost intact) but weak cemented breccias – similar to weak concrete	51	16.3	75	6.68	0.062	0.501	15.0
Massive strong rock gneiss, with very few joints	110	28	75	11.46	0.062	0.501	45.0
Average quality rock mass: jointed quartz mica schist	30	15	65	4.3	0.02	0.5	10.0
Poor-quality rock mass at shallow depth: Athenian schist	5–10	9.6	20	0.55	0.0001	0.544	0.60
Poor-quality rock mass under high stress: 25-km-long water supply tunnel 1200 m below surface; graphitic phyllite, squeezing ground	50	10	25	0.48	0.0002	0.53	1.0

Source: Hoek, E., Practical Rock Engineering, http://www.rocscience.com/hoek/corner/practical_rock_engineering.pdf, 2007.

EXAMPLE 5.7

For the massive strong rock gneiss with very few joints in Table 5.1, with GSI = 75, $m_{\rm i} = 28$ and $\sigma_{\rm ci} = 110$ MPa, estimate the rock mass parameters $m_{\rm m}$, s and a. How do they compare with the values given in Table 5.1?

Estimate the uniaxial compressive strength of the rock mass, σ_{cm} .

Solution

Assuming D = 0,

From Equation 5.33 $\rightarrow m_m = 11.46$.

From Equation $5.34 \rightarrow s = 0.062$.

From Equation $5.35 \rightarrow a = 0.501$.

The values match those in Table 5.1 very well.

Substituting in Equation 5.36, $\sigma_{cm} = \sigma_{ci} s^a = 110 \times 0.062^{0.501} = 27.3$ MPa.

5.6 MOHR–COULOMB c' AND φ' FOR ROCK MASS FROM THE HOEK–BROWN PARAMETERS

We have seen in Section 5.5 that deriving the Hoek–Brown parameters for the rock mass from those of an intact rock is a straightforward exercise. For the intact rock, the parameters are m_i and σ_{ci} (s=1 and a=0.5). For the rock mass, the parameters are m_m , σ_{cm} , s and a. These two sets of parameters are related through GSI and D that reflect the quality of the rock mass and the degree of disturbance it has undergone during excavation, blasting and so on.

The Mohr–Coulomb failure criterion is quite popular among geotechnical engineers, and there is a tendency to apply this to rocks too. The main difficulty here is to derive the shear strength parameters c' and ϕ' in terms of effective stresses for the *rock mass*. It is not practical to test a representative rock mass in a triaxial cell. It can only be carried out through a simulation exercise.

Hoek and Brown (1997) simulated a series of triaxial test data for the rock masses of different GSI, $m_{\rm i}$ and $\sigma_{\rm ci}$ values, in the confining pressure $\sigma_{\rm 3f}'$ range of $0-\sigma_{\rm ci}/2$. Mohr–Coulomb envelopes were drawn with these simulated data from which c' and ϕ' for the rock masses were determined. The values of c' and ϕ' thus determined are presented graphically in Figures 5.11 and 5.12. It should be noted that the synthetic data were generated to follow a parabolic failure envelope in $\sigma_{\rm i}' - \sigma_{\rm 3}'$ space. The linear Mohr–Coulomb envelope fitted to these data will vary depending on the stress range covered $\left(\sigma_{\rm tm} < \sigma_{\rm 3f}' < \sigma_{\rm 3,max}'\right)$. Therefore, the Mohr–Coulomb parameters c' and ϕ' will vary depending on the range of values selected for $\sigma_{\rm 3f}'$. A simple simulation exercise is shown through Examples 5.8 and 5.9.

Hock et al. (2002) reported that the curve fitting exercise gives the following expressions for determining ϕ' and c'.

$$\sin \phi' = \frac{6am_{\rm m} \left(s + m_{\rm m} \sigma'_{3\rm n}\right)^{a-1}}{2(1+a)(2+a) + 6am_{\rm m} \left(s + m_{\rm m} \sigma'_{3\rm n}\right)^{a-1}}$$
(5.40)

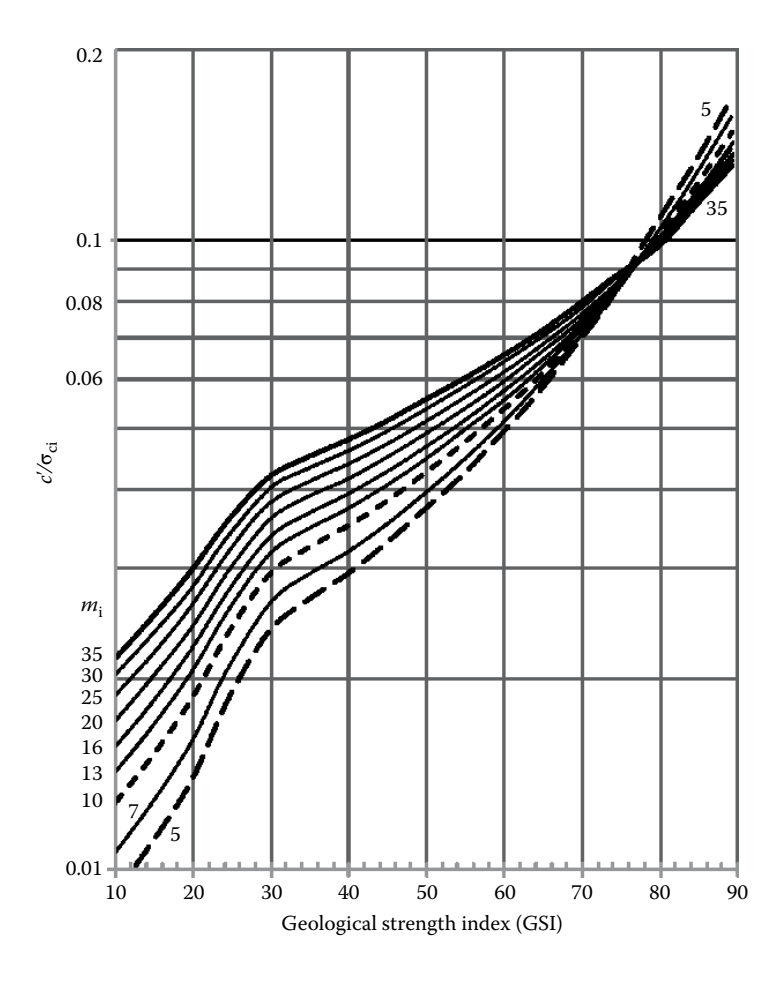


FIGURE 5.11 Mohr–Coulomb envelope in the $\sigma_{1f}^{'}$ – $\sigma_{3f}^{'}$ plane.

$$\frac{c'}{\sigma_{ci}} = \frac{\left[(1+2a)s + (1-a)m_{m}\sigma'_{3n} \right] \left(s + m_{m}\sigma'_{3n}\right)^{a-1}}{(1+a)(2+a)\sqrt{1 + \left(6am_{m}\left(s + m_{m}\sigma'_{3n}\right)^{a-1}\right)/\left((1+a)(2+a)\right)}}$$
(5.41)

where $\sigma_{3n}^{'} = \sigma_{3,max}^{'} / \sigma_{ci}$. They also suggested that $\sigma_{3,max}^{'}$, the upper limit of $\sigma_{3f}^{'}$, should be selected depending on the project and stress levels. As a general guide, $\sigma_{3,max}^{'}$ can be estimated from the following equation for tunnels and underground excavations (Hoek et al., 2002):

$$\frac{\sigma'_{3,\text{max}}}{\sigma'_{\text{cm}}} = 0.47 \left(\frac{\sigma'_{\text{cm}}}{\gamma H}\right)^{-0.94}$$
 (5.42)

where *H* is the depth below the surface and γ is the unit weight of the rock mass. σ'_{cm} is what Hoek and Brown (1997) refer to as the *global rock mass strength*, determined

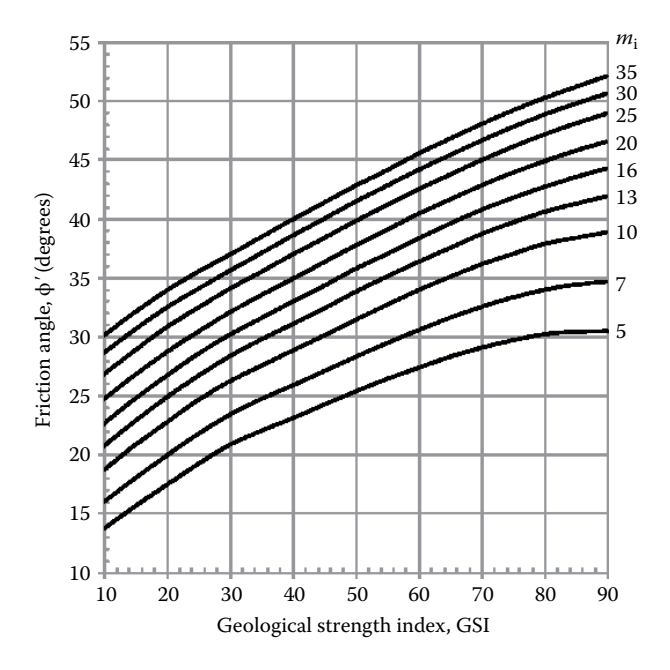


FIGURE 5.12 $c'/\sigma_{ci}-m_i$ —GSI relationship for the rock mass. (After Hoek, E. and E.T. Brown, *Int. J. Rock Mech. Min. Sci.*, 34, 1165–1186, 1997.)

from the Mohr–Coulomb failure envelope fitted to the simulated data. It is a better representation of the average uniaxial compressive strength of the rock mass. This is simply the uniaxial compressive strength determined from the Mohr–Coulomb failure criterion, which is generally larger than the rock mass strength σ_{cm} (Equation 5.36) determined from the Hoek–Brown criterion. For slopes, $\sigma_{3,max}$ can be estimated from (Hoek et al., 2002)

$$\frac{\sigma'_{3,\text{max}}}{\sigma'_{\text{cm}}} = 0.72 \left(\frac{\sigma'_{\text{cm}}}{\gamma H}\right)^{-0.91} \tag{5.43}$$

where H = height of the slope. Equation 5.43 was developed assuming two-dimensional failure surfaces in the form of circular arcs and Bishop's method of slices.

From the Mohr–Coulomb envelope,

$$\sigma'_{\rm cm} = \frac{2c'\cos\phi'}{1-\sin\phi'} \tag{5.44}$$

where c' and ϕ' are the shear strength parameters for the rock mass in terms of effective stresses. In the normal stress range of $\sigma_{\rm t} < \sigma_{\rm 3f}^{'} < 0.25\sigma_{\rm ci}$ (Hoek et al., 2002),

$$\sigma'_{cm} = \sigma_{ci} \frac{\left[m_b + 4s - a(m_b - 8s)\right] (0.25m_b + s)^{a-1}}{2(1+a)(2+a)}$$
(5.45)

EXAMPLE 5.8

Let us carry out a simple simulation exercise. Generate a set of triaxial data for the *rock mass* in Example 5.7, by determining the values of σ'_{1f} for $\sigma'_{3f} = 0$, 10, 20, 40 and 60 MPa.

Solution

For the rock mass,

$$\sigma'_{1f} = \sigma'_{3f} + \sigma_{ci} \left(m_b \frac{\sigma'_{3f}}{\sigma'_{ci}} + s \right)^a$$

$$\sigma'_{1f} = \sigma'_{3f} + 110 \left(11.46 \frac{\sigma'_{3f}}{110} + 0.062 \right)^{0.501}$$

Substituting for $\sigma_{3f}^{'}$ in the preceding equation, the following values are obtained for $\sigma_{1f}^{'}$.

$\sigma_{3f}^{'}$ (MPa)	0	10	20	40	60
σ _{1f} (MPa)	27.3	125.6	181.3	266.5	336.9

EXAMPLE 5.9

Use the synthetic triaxial data for the rock mass from Example 5.8 and draw the Mohr–Coulomb envelope in the $\sigma_{1f}^{'} - \sigma_{3f}^{'}$ plane. Determine c' and ϕ' and check whether the values match those estimated from Figures 5.11 and 5.12.

Solution

The experimental data and the Mohr-Coulomb envelope are shown in Figure 5.13.

From Equation 5.29,
$$\tan^2\left(45 + \frac{\phi'}{2}\right) = 4.9045 \rightarrow \phi' = 41.4^\circ$$
 and $2c' \tan\left(45 + \frac{\phi'}{2}\right) = 60.003 \rightarrow c' = 13.5 \text{ MPa}$

For GSI = 75 and m_i = 28 (see Example 5.7). From Figure 5.11, c'/σ_{ci} = 0.086 $\rightarrow c'$ = 9.5 MPa; from Figure 5.12, ϕ' = 47°.

There are some difference between the computed values and those estimated from Figures 5.11 and 5.12.

Note that fitting a straight line envelope to satisfy the Mohr–Coulomb criterion gives a global rock mass strength $\sigma_{cm}^{'}$ of 60 MPa, which is greater than the σ_{cm} estimated as 27.3 MPa in Example 5.7.

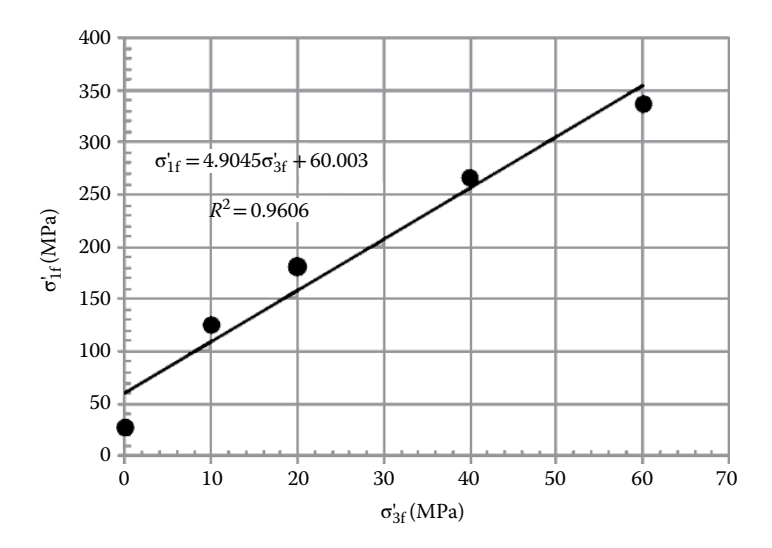


FIGURE 5.13 ϕ' - m_i -GSI relationship for the rock mass. (After Hoek, E. and E.T. Brown, *Int. J. Rock Mech. Min. Sci.*, 34, 1165–1186, 1997.)

5.7 DEFORMATION MODULUS

The deformation modulus of the rock mass is a very important parameter in computing the strains or deformations. Young's modulus of the intact rock (E_i) is generally derived from uniaxial compression tests on the intact cores. In the absence of laboratory measurements, E_i can be estimated from an assumed value of σ_c and the modulus ratio (E/σ_c) , which varies in the range of 150–1000. Typical values of modulus ratio and σ_c are given in Tables 3.5 and 3.6, respectively. The rock mass modulus can be determined from empirical correlations discussed in this section.

Young's modulus (E_i) of an intact rock is generally 150–1000 times the uniaxial compressive strength. It is generally measured at low stress levels where the rock behaves elastically. The stiffness (i.e. Young's modulus) is fairly consistent for a rock type even though there can be some scatter in the strength data. It can vary from less than 1 GPa to more than 100 GPa (see Figure 3.8 and Table 3.6).

The deformation modulus can be estimated from the tunnel quality index Q as (Grimstad and Barton, 1993)

$$E_{\rm m} = 25 \log Q \quad \text{for } Q > 1$$
 (5.46)

Bieniawski (1978) suggested that the in-situ deformation modulus of a rock mass can be related to the RMR by

$$E_{\rm m}$$
 (GPa) = 2 RMR - 100 for RMR > 55 (5.47)

Serafim and Pereira (1983) suggested that

$$E_{\rm m}({\rm GPa}) = 10^{\frac{{\rm RMR} - 10}{40}}$$
 (5.48)

Hoek et al. (2002) modified Equation 5.48 and suggested that the deformation modulus of the rock mass can be expressed as

$$E_{\rm m} \left({\rm GPa} \right) = \left(1 - \frac{D}{2} \right) \sqrt{\frac{\sigma_{\rm ci}}{100}} \times 10^{\frac{{\rm GSI} - 10}{40}} \quad {\rm for} \ \sigma_{\rm ci} < 100 \, {\rm MPa}$$
 (5.49a)

$$E_{\rm m} \left(\text{GPa} \right) = \left(1 - \frac{D}{2} \right) \times 10^{\frac{\text{GSI} - 10}{40}} \quad \text{for } \sigma_{\rm ci} > 100 \,\text{MPa}$$
 (5.49b)

Hoek and Diederichs (2006) reviewed several empirical relationships that are used to estimate the deformation modulus of the rock mass. Based on a large number of in situ measurements from China and Taiwan, they proposed the following two equations:

$$E_{\rm m} (\text{GPa}) = 100 \left(\frac{1 - D/2}{1 + e^{(75 + 25D - \text{GSI})/11}} \right)$$
 (5.50)

$$E_{\rm m} = E_{\rm i} \left[0.02 + \frac{1 - D/2}{1 + e^{(60 + 15D - GSI)/11}} \right]$$
 (5.51)

From Equation 5.50, it is evident that the ratio $E_{\rm m}/E_{\rm i}$ approaches unity with GSI increasing towards 100.

5.8 STRENGTH OF ROCK MASS WITH A SINGLE PLANE OF WEAKNESS

Let us consider the simple situation shown in Figure 5.14a, where the rock mass consists of a single joint, inclined at an angle β to the major principal plane. The major and the minor principal stresses are σ_1 and σ_3 , respectively. The discontinuity planes are often weaker than the intact rock with a lower cohesion and friction angle (Figure 5.14b).

The Mohr circle representing the state of stress at the intact rock (Figure 5.14a) is shown in Figure 5.15. The shear and normal stresses at the discontinuity plane (i.e. joint) are represented by point *A* and given by

$$\sigma_{j} = \sigma_{3} + \left(\frac{\sigma_{1} - \sigma_{3}}{2}\right) \left(1 + \cos 2\beta\right) \tag{5.52}$$

$$\tau_{j} = \left(\frac{\sigma_{1} - \sigma_{3}}{2}\right) \sin 2\beta \tag{5.53}$$

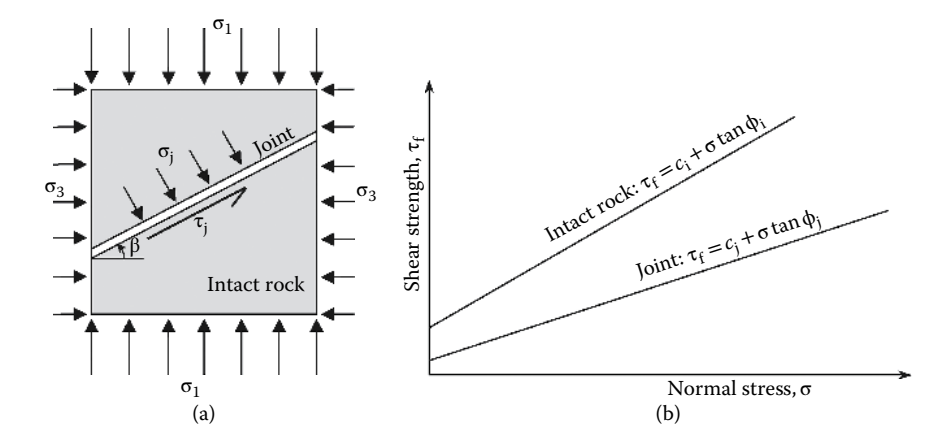


FIGURE 5.14 Strength of rock mass with a single discontinuity: (a) state of stress and (b) failure envelopes.

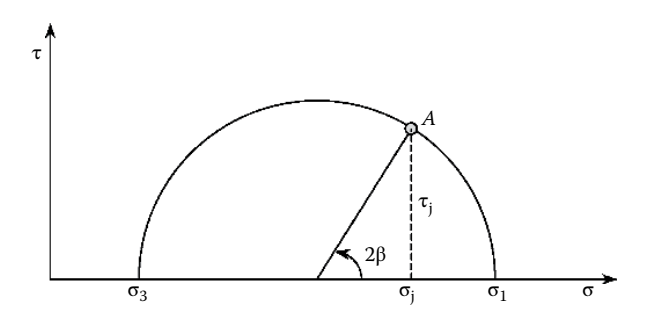


FIGURE 5.15 Mohr circle representing the state of stress shown in Figure 5.14a.

For failure to take place along the joint, these two values of σ_j and τ_j should satisfy the equation representing the Mohr–Coulomb failure envelope given by

$$\tau_{i} = c_{i} + \sigma_{i} \tan_{i} \phi_{i} \tag{5.54}$$

Substituting the expressions for σ_j (Equation 5.52) and τ_j (Equation 5.53) in Equation 5.54, it can be shown that when slip occurs along the joint

$$(\sigma_1 - \sigma_3) = \frac{2(c_j + \sigma_3 \tan \phi_j)}{\sin 2\beta \left(1 - \frac{\tan \phi_j}{\tan \beta}\right)}$$
(5.55)

It can be seen from Equation 5.55 that when $\beta = \phi_j$ or 90°, $\sigma_1 - \sigma_3 = \infty$. Under such circumstances, the rock mass will not fail by slip along the discontinuity; failure can only take place in the intact rock.

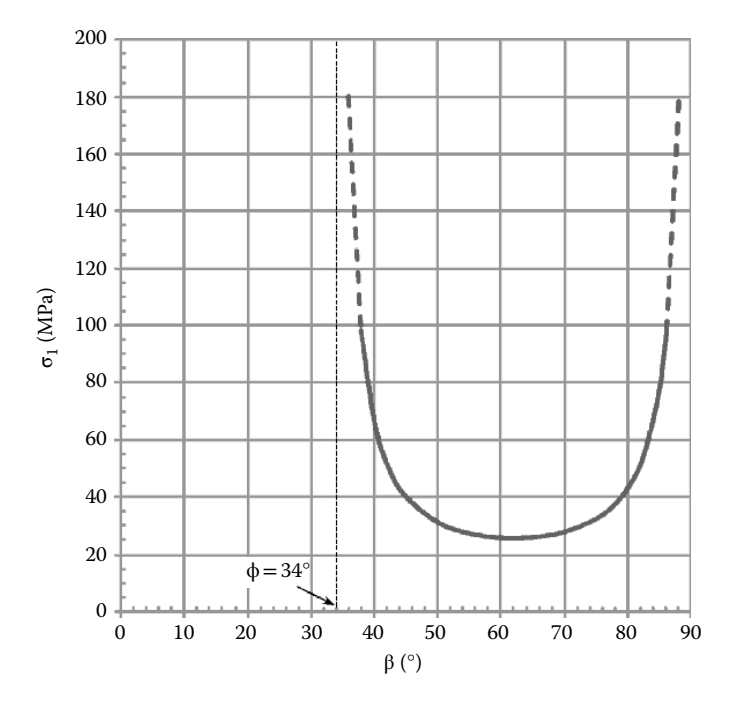


FIGURE 5.16 The variation of σ_1 against β .

EXAMPLE 5.10

A large extent of rock mass has a single plane of discontinuity, where the aperture is filled. The shear strength parameters for this fill material are c = 4.0 MPa and $\phi = 34^{\circ}$. For $\sigma_3 = 3$ MPa, find the values of σ_1 for different values of β and plot the variation of σ_1 against β .

Solution

The variation of σ_1 against β is shown in Figure 5.16. For $\beta < \phi$, slip is not possible. When the discontinuity is oriented at an angle less than ϕ (= 34° in this case) to the principal plane, failure can only take place in the intact rock.

5.9 SUMMARY

- 1. The presence of discontinuities makes the rock mass behave anisotropically. However, when there are too many discontinuities (e.g. joints), the block size is reduced, and with increased degrees of freedom for movement, the rock mass becomes isotropic and acts like soil.
- 2. In rocks, the horizontal stress is often larger than the vertical stress. This is the opposite of what we see in soils.

 Rock overburden pressure can be estimated using an average unit weight of 27 kN/m³.

- 4. The isotropic linear elastic constitutive model is the simplest of all the models presented. The stresses and the strains can be related by two constants: Young's modulus *E* and Poisson's ratio *v*.
- 5. Plane strain, plane stress and axisymmetric loadings are three special situations that we encounter when solving engineering problems.
- 6. The Mohr–Coulomb failure criterion is freely used for soils. In rocks, it does not work very well in the tensile region. σ_c, σ_t and σ_t can be related to c and φ based on the Mohr–Coulomb criterion.
- 7. The peak shear strength can be significantly larger than the residual one ($\phi_p > \phi_r$, $c_r \approx 0$).
- 8. The Hoek–Brown failure criterion is more popular than the Mohr–Coulomb criterion for rock mechanics applications. It can be applied to both the intact rock and the rock mass.
- 9. The Hoek–Brown constant m_i is analogous to the friction angle ϕ in the Mohr–Coulomb failure criterion. The constant s is analogous to cohesion.
- 10. The Hoek–Brown constant m_i of an intact rock is approximately equal to the ratio σ_{ci}/σ_{ii} .
- 11. Typical values: m = 0 (weak) to 35 (strong); s = 0 (weak) to 1 (strong); a = 0.50 (strong) to 0.65 (weak).
- 12. In the Hoek–Brown model, the parameters for the rock mass and the intact rock are related through GSI, which accounts for the quality (interlocking of the blocks and joint surfaces) of the rock mass.
- 13. When the failure envelope is drawn on the σ_1/σ_3 space, the intercepts of the failure envelope on the two axes give the uniaxial compressive and tensile strengths. This is true for both Mohr–Coulomb and Hoek–Brown failure criteria (see Figure 5.7).
- 14. For massive rock mass with widely spaced discontinuities, with GSI or RMR approaching 100, the rock mass will have the same strength and modulus as the intact rock.

REVIEW EXERCISES

- 5.1. State whether the following are true or false.
 - a. In rocks, K_0 is larger at shallower depths.
 - Generally, in rocks, the horizontal stress is greater than the vertical stress.
 - c. The tensile strength of an intact rock is greater than its Brazilian indirect tensile strength.
 - d. In the Hoek–Brown failure criterion, the larger the *m*, the larger is the strength.
 - e. m_i is always greater than m_m .
 - f. The larger the GSI, the larger is the strength of a rock mass.

- 5.2. What are the non-zero stress components in (a) plane strain loading and (b) plane stress loading?
- 5.3. What are the non-zero strain components in (a) plane strain loading and (b) plane stress loading?
- 5.4. Carry out a literature survey and list the empirical equations relating σ_{cm}/σ_{ci} to (a) RMR and (b) Q.
- 5.5. In plane strain loading, show that the principal strains in terms of principal stresses are given by

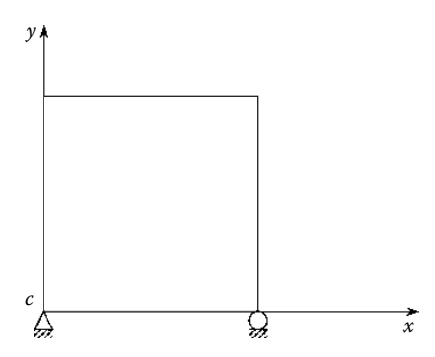
$$\sigma_{1} = \frac{E}{(1+\nu)(1-2\nu)} \{ (1-\nu)\varepsilon_{1} + \nu\varepsilon_{2} \}$$

$$\sigma_{3} = \frac{E}{(1+\nu)(1-2\nu)} \{ \nu\varepsilon_{1} + (1-\nu)\varepsilon_{2} \}$$

5.6. Using Equation 5.6, show that for one-dimensional consolidation, the normal stress and the normal strain are related by $\sigma = D\varepsilon$, where *D* is the *constrained modulus* given by

$$D = \frac{E(1-\nu)}{(1+\nu)(1-2\nu)}$$

5.7. In a plane strain situation, express the strains in terms of displacements. The square object shown in the following figure is subjected to plane strain loading where the displacements u and v are given by $u = x^2y$ and $v = xy^3$. Determine the strain components in terms of x and y.



- 5.8. The same square object shown in the figure in the previous exercise is subjected to plane strain loading where the strains are given by $\varepsilon_x = 2xy$, $\varepsilon_y = 3xy^2$ and $\gamma_{xy} = x^2 + y^3$. Applying appropriate boundary conditions, develop the expressions for the displacements.
- 5.9. Based on the Mohr–Coulomb failure criterion and assuming that it holds in the tensile region as well, what is the ratio of tensile strength to indirect tensile strength for typical values of the friction angle?

5.10. Triaxial tests were carried out on 54-mm-diameter (NX core) intact rock specimens. The applied confining pressures and the principal stress differences at failure are summarised in the following table.

Confining pressure (MPa)	0	5.0	10.0	15.0	20.0	25.0
Principal stress difference (MPa)	59.5	87.5	116.0	139.5	167.5	192.5

Plot σ_1 against σ_3 at failure and determine the uniaxial compressive strength and the friction angle of the intact rock.

- 5.11. The intact rock that follows the Mohr–Coulomb failure criterion has c=15 MPa and $\phi=27^\circ$. Estimate the uniaxial compressive strength σ_c , the uniaxial tensile strength σ_t and the Brazilian indirect tensile strength σ_t . Give an estimate of the point load strength index $I_{s(50)}$ and suggest a realistic range for Young's modulus E.
 - Answer: 49.0 MPa, 18.4 MPa, 8.6 MPa, 2.0 MPa and 14.7-49.0 GPa
- 5.12. The rock mass at a hydroelectric powerhouse project in Himachal Pradesh, India, consists of jointed quartz mica schist with average GSI of about 65 (Hoek and Brown, 1997). Triaxial tests on intact rock cores showed $\sigma_{ci} = 30$ MPa and $m_i = 15.6$.
 - a. Estimate the rock mass parameters m_m , s and a.
 - b. Estimate c' and ϕ' of the rock mass.
 - Estimate the uniaxial compressive and tensile strengths of the rock mass.

Answer: 4.47, 0.021, 0.502 and 1.9 MPa, 39°

- 5.13. Using the values in Exercise 12 (i.e. $\sigma_{ci} = 30$ MPa, $m_{m} = 4.47$, s = 0.021 and a = 0.502) in the generalised Hoek–Bray failure criterion for rock mass, generate the values of σ_{lf} corresponding to $\sigma_{3f} = 0, 2.5, 5, 7.5, 10, 12.5$ MPa.
- 5.14. Undisturbed specimens of the gouge material filling a rock joint was tested in the laboratory, and the cohesion and friction angles are determined as 5 MPa and 35°, respectively. If the minor principal stress at the joint is 2 MPa, determine the value of σ_1 that is required to cause shear failure along the joint that is inclined to the major principal plane by (a) 45°, (b) 55° and (c) 65°.

Answer: 44.7, 28.7 and 26.8 MPa

REFERENCES

- Bieniawski, Z.T. (1978). Determining rock mass deformability Experience from case histories. *International Journal of Rock Mechanics and Mining Sciences*, Vol. 15, No. 5, pp. 237–248.
- Goodman, R.E. (1989). Introduction to Rock Mechanics. 2nd edition, John Wiley & Sons, New York.
- Grimstad, E. and Barton, N. (1993). Updating the Q-system for NMT. Proceedings of the International Symposium on Sprayed Concrete, Fagernes, Norway, Norwegian Concrete Association, Oslo, 20pp.

- Hoek, E. (1983). Strength of jointed rock masses, 23rd Rankine lecture. *Geotechnique*, Vol. 33, No. 3, pp. 187–223.
- Hoek, E. (2007). Practical Rock Engineering. http://www.rocscience.com/hoek/corner/practical_rock_engineering.pdf.
- Hoek, E. and Brown, E.T. (1980a). Empirical strength criterion for rock masses. *Journal of Geotechnical Engineering Division*, ASCE, Vol. 106, No. GT9, pp. 1013–1035.
- Hoek, E. and Brown, E.T. (1980b). *Underground Excavation in Rock*. Institute of Mining and Metallurgy, London.
- Hoek, E. and Brown, E.T. (1997). Practical estimates of rock mass strength. *International Journal of Rock Mechanics and Mining Sciences*, Vol. 34, No. 8, pp. 1165–1186.
- Hoek, E., Carranza-Torres, C.T. and Corkum, B. (2002). Hoek-Brown failure criterion 2002 edition. *Proceedings of the 5th North American Rock Mechanics Symposium*, Toronto, Canada, Vol. 1, pp. 267–273.
- Hoek, E. and Diederichs, M.S. (2006). Empirical estimation of rock mass modulus. *International Journal of Rock Mechanics and Mining Sciences*, Vol. 43, No. 2, pp. 203–215.
- Hondros, G. (1959). The evaluation of Poisson's ratio and the modulus of materials of a low tensile resistance by the Brazilian (indirect tensile) test with particular reference to concrete. *Australian Journal of Applied Science*, Vol. 10, No. 3, pp. 243–268.
- Marinos, P. and Hoek, E. (2001). GSI: A geologically friendly tool for rock mass strength estimation. *Proceedings of the International Conference on Geotechnical & Geological Engineering, GeoEng2000*, Technomic Publications, Melbourne, Australia, pp. 1422–1442.
- Serafim, J.L. and Pereira, J.P. (1983). Consideration of the geomechanical classification of Bieniawski. *Proceedings of the International Symposium on Engineering Geology and Underground Construction*, Lisbon, 1(II), pp. 33–44.
- Shorey, P.R. (1994). A theory for in situ stresses in isotropic and transversely isotropic rock. *International Journal of Rock Mechanics and Mining Sciences & Geomechanics Abstracts*, Vol. 31, No. 1, pp. 23–34.

6 Rock Slope Stability

6.1 INTRODUCTION

Rock slopes occur either naturally (Figure 6.1a) or are engineered through excavation to create space for structures such as buildings, highways, railways, powerhouses, dams and mine pits (Figure 6.1b). The analysis for the estimation of stability of rock slopes has been a challenging task for engineers, especially under hydraulic and seismic conditions. In most civil and mining engineering projects, the main purpose of slope stability analysis is to contribute to the safe and economic design of rock slopes. This chapter describes the basic modes/mechanisms of rock slope failures and presents the fundamental concepts and methods of rock slope stability analysis. In field situations, many rock slopes are unstable, or they require an improvement in their stability. Such slopes need to be stabilised as per the specific needs of the project. Therefore, this chapter introduces some common rock slope stabilisation techniques.

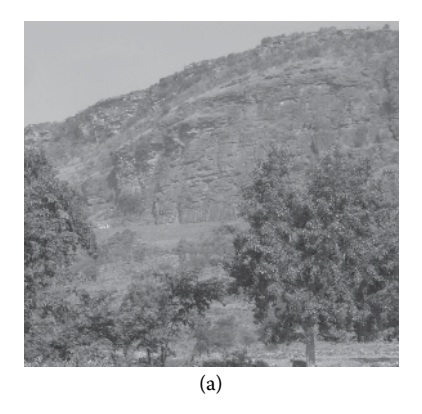
6.2 MODES OF ROCK SLOPE FAILURE

The modes of rock slope failure depend mainly on the geometric interaction of existing discontinuities (jointing and bedding patterns) and free space/excavation surfaces in the rock mass constituting the slope. For safe and economic design of rock slopes, it is important to recognise the modes/mechanisms in which slopes in rock masses can fail. This task requires sound engineering judgement, which is developed through effective engineering practices that address rock slopes in diverse geological conditions. The spherical presentation of geological data (dip and strike) helps identify the most likely basic potential modes of rock slope failure (see Section 2.6). The measurement of piezometric levels and springs throughout the slope, and measurements of slope deformations (with slope inclinometers and precise surveying of fixed surficial targets), are other basic tools to judge the most likely potential failure modes of rock slope failure. The idealised, simple, basic modes of rock slope failure that are considered in practice are the following (Hoek and Bray, 1981; Goodman, 1989; Goodman and Kieffer, 2000; Wyllie and Mah, 2004):

- 1. Plane failure
- Wedge failure
- 3. Circular failure
- 4. Toppling failure

In *plane failure* mode, the rock block slides on a single face that can be a joint plane or bedding plane striking parallel to the slope face and dipping into free space/excavation at an angle greater than the angle of internal friction of the joint

DOI: 10.1201/9781032725161-6



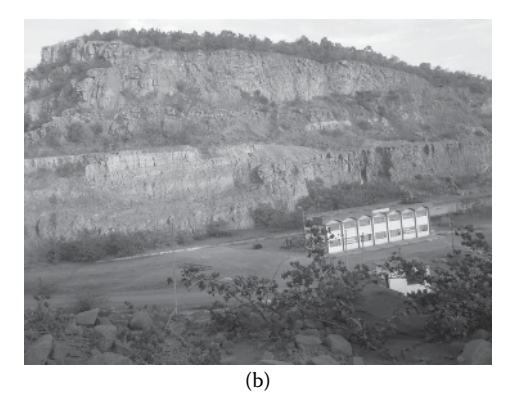


FIGURE 6.1 Rock slopes: (a) natural rock slope; (b) engineered (excavated) rock slope.

or bedding material (Figure 6.2a). *In wedge* failure mode, the wedge of rock slides simultaneously on two discontinuity planes, striking obliquely across the slope face, along their line of intersection daylighting into the slope face, provided that the inclination of this line is significantly greater than the average angle of internal friction of the two joint or bedding materials (Figure 6.2b). In the *circular failure* mode, the heavily jointed and weathered rock mass, similar to a waste dump rock, slides on a single cylindrical face into free space/excavation (Figure 6.2c). In *toppling failure* mode, the multiple rock columns or layers caused by a steeply dipping joint set rotate about their bases into the free space/excavation (Figure 6.2d). Plane and wedge failures are more common than circular and toppling failures. Toppling failure can be very significant, if not dominant, in some rock types of steep mountain slopes or open pit mines. Table 6.1 describes these failure modes and gives examples of typical materials in which they are realised.

A rock fall is a type of slope failure where individual rock fragments or blocks detach from a steep slope or cliff and fall freely due to gravity. This often occurs in areas with highly fractured rock or along weathered surfaces and can be triggered by processes such as freeze-thaw cycles, seismic activity or erosion. Once detached, the

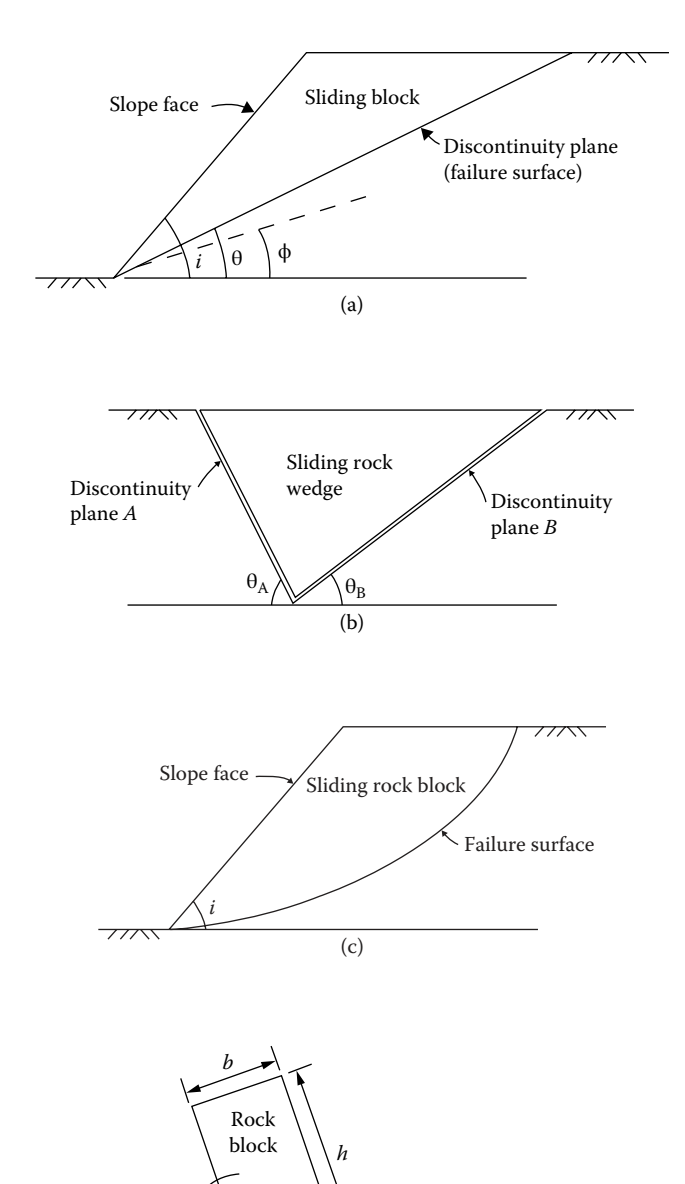


FIGURE 6.2 Basic modes of rock slope failure: (a) plane failure ($i > \theta > \phi$; i is slope inclination to the horizontal, θ is inclination of the discontinuity plane/failure plane and ϕ is angle of internal friction of the joint/bedding material); (b) wedge failure (θ_A and θ_B are the inclinations of discontinuity planes A and B, respectively); (c) circular failure; (d) direct toppling failure (b is width and b is height of the rock block).

(d)

Discontinuity plane

TABLE 6.1
Basic Modes of Rock Slope Failure

Mode of rock failure	Description	Typical materials
Plane failure	Sliding without rotation along a face; single or multiple blocks	Hard or soft rocks with well-defined discontinuities and jointing, e.g. layered sedimentary rocks, volcanic flow rocks, block-jointed granite, foliated metamorphic rocks
Wedge failure	Sliding without rotation on two non-parallel planes, parallel to their line of intersection; single or multiple blocks	Blocky rocks with at least two continuous and non-parallel joint sets, e.g. cross-jointed sedimentary rocks, regularly faulted rocks, block-jointed granite and especially foliated or jointed metamorphic rocks
Circular failure	Sliding on a cylindrical face	Heavily jointed and weathered rock masses similar to the soils
Flexural toppling failure	Interlayer friction and bending; multiple blocks/columns	Soft rock with anticlinal bedding structures. Each rock layer works like an independent cantilever beam at the free end, where the interlayer friction keeps them together at the fixed end.
Direct toppling failure	Forward rotation about an edge/base; single or multiple blocks	Hard rocks with regular, parallel joints dipping away from the free space/excavation, that is, dipping into the hillside, with or without crossing joints; foliated metamorphic rocks and steeply dipping layered sedimentary rocks; also in block-jointed granites

Source: Adapted from Goodman, R.E., and Kieffer, D.S., J. Geotech. Geoenviron. Eng., 126, 675-684, 2000.

falling rocks may bounce, roll or slide down the slope, posing significant hazards in mountainous or cliffside areas. Rock falls are common in steep, exposed rock formations and can lead to rapid, unpredictable movements.

It is important to note that if a rock slope is large and comprises a mix of rock types and structures, multiple basic failure modes may occur. Conversely, within a single sliding mass, it is not uncommon to observe more than one basic failure mode at a site.

6.3 SLOPE FAILURE MECHANISMS AND KINEMATIC ANALYSIS

In principles, slopes are unstable if a rock mass can move. As rocks possess high stiffness, the movement often goes along rock discontinuities to avoid crashing through the whole rock mass. A discontinuity is said to 'daylight' onto the face of the rock slope where the two planes intersect. Figure 6.3 shows a rock slope with three sets of discontinuities A, B and C, shown as dashed lines. Here, the discontinuities A and C daylight on the slope face. While the discontinuity A is of concern due to sliding instability, discontinuity C is quite stable. The core conditions for instability are: (1)

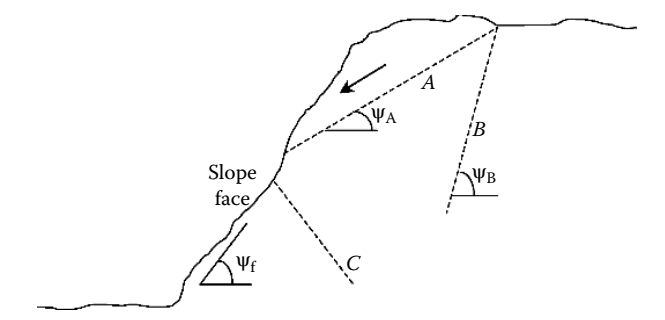


FIGURE 6.3 Plane failure of a rock slope.

at least a discontinuity set must daylight or tend to daylight on the rock slope surface, and (2) a rock mass could move with gravity along the discontinuity, outwards from the slope. Therefore, how the discontinuity is oriented has significant influence on the stability.

6.3.1 SLOPE FAILURE MECHANISMS

It can be seen that the rock mass above the discontinuity A can slide down, leading to plane failure, one of the four failure mechanisms suggested by Hoek and Bray (1981). For the plane failure to occur, the dip of the planar discontinuity has to be less than that of the slope face (e.g. $\psi_A < \psi_f$); otherwise, the discontinuity will not daylight on the slope face. In addition, for sliding to take place, the dip directions of both planes must not differ by more than 20° (i.e. $|\alpha_A - \alpha_f| < 20^\circ$), and the dip of the sliding surface has to be greater than the friction angle ϕ .

In the case of discontinuity B, since the dip ψ_B is greater than the dip of the slope face ψ_B it will not daylight onto the slope face and therefore plane failure is not possible. Discontinuity C does not pose any threat even though it daylights on the slope face because the rock mass cannot move along it and outwards from the slope with gravity.

Two intersecting planes of discontinuities A and B can daylight on the slope face, as shown in Figure 6.4a, where the line of intersection is shown by a dashed line. Here, failure can occur when the wedge enclosed between the two planes slides towards the slope face. This type of failure is known as *wedge failure*, which is one of the four failure mechanisms suggested by Hoek and Bray (1981). Plane failure is a special case of wedge failure where the two planes have the same dip and dip directions.

The spherical representation of the two discontinuities and the slope face is shown in Figure 6.4b. The line of intersection (i) between the two discontinuities defines the direction of sliding, which is shown by the arrow OX in Figure 6.4b. The plunge (ψ_i) and the trend (α_i) of this line can be determined as demonstrated earlier. The angle between the two planes of discontinuity can also be determined using the procedure discussed earlier. Generally, larger angles are associated with greater likelihood of wedge failure. In Figure 6.4b, the great circle representing the slope face is shown slightly darker. The arrow OY shows the dip direction of the slope face.

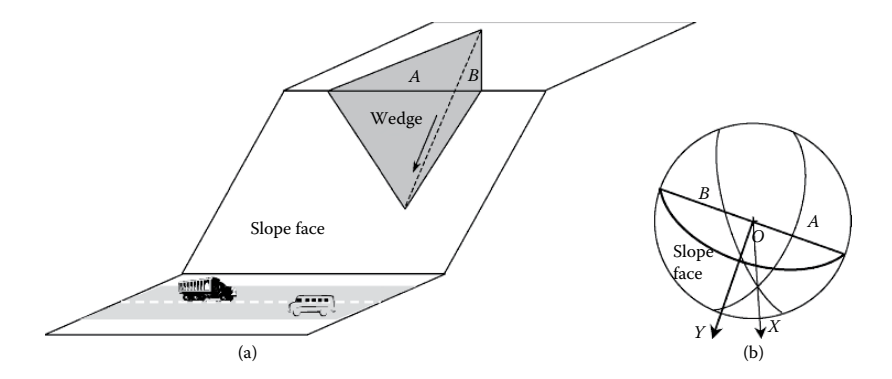


FIGURE 6.4 Wedge failure of a rock slope: (a) schematic diagram and (b) spherical representation.

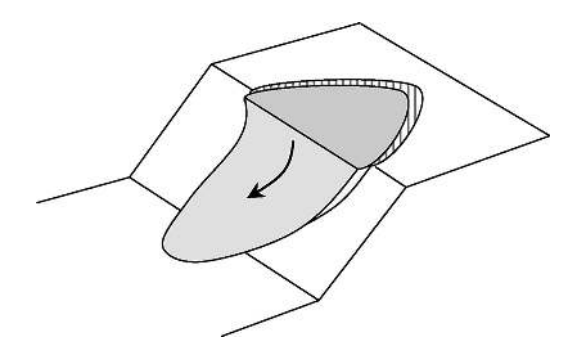


FIGURE 6.5 Circular failure.

For wedge failure to occur, the trend of the intersection line must be within 20° of the dip direction of the face of the slope (i.e. $|\alpha_i-\alpha_f|<20^\circ$) as in plane failure. However, several current computer programs, including Dips 8, removed this lateral limit if the frictional angle of the rock is known. This chapter will show examples with both traditional and updated theories. The plunge (ψ_i) of this line must be less than the dip (ψ_f) of the slope face so that the line of intersection daylights on the slope face. In addition, the plunge of the line of intersection (ψ_i) has to be greater than the friction angle (ϕ) so that the wedge can slide. These three conditions are the same as the ones for plane failure. The only difference is that here we are looking at the orientation of the line of intersection (along which the slide takes place) rather than a discontinuity plane.

The circular slope failure shown in Figure 6.5 occurs mainly in rock fills, weathered rocks or rocks with closely spaced, randomly oriented discontinuities. This three-dimensional slope failure is similar to those occurring in soils. The fourth failure mechanism suggested by Hoek and Bray (1981) is *toppling failure*, which takes place in hard rocks of columnar structure separated by discontinuities that dip steeply into the slope face. Two frequent types of toppling are *direct toppling* and *flexural toppling*. Direct toppling occurs when a rock mass is overturned because the centre of gravity lies outside the base. The condition of direct toppling for a

rectangular block is b/h<tan(ψ_i) so that the centre of gravity fall outside the outline of the base. Meanwhile, flexural toppling occurs when the principal stress induces interlayer slip. To overcome the friction, the dip must satisfy that $\psi_i < 90^\circ + \psi_f - \phi$. In general, the toppling takes lateral limit of 30° from the direction of the rock slope but to the opposite side of the centre O, $|(\alpha_i - 180^{\infty}) - \alpha_f| < 30^\circ$.

The spherical projections are valuable tools for identifying the failure mechanisms and carrying out a *kinematic analysis* of the slope stability. Kinematic analysis is a geometric approach that examines the orientations of the discontinuities and the slope face, possible modes of failures and direction of movement in the case of instability. These methods are widely used in structural geology and rock mechanics. While offering a clear picture of the spatial arrangements of the discontinuities, they enable a simple and quantitative analysis of the stability. These are discussed in more detail by Goodman (1989), Hoek and Bray (1981) and Wyllie and Mah (2004). A summary of the failure mechanisms and conditions can be found in Table 6.2. All dip analyses employ slope of 70/120 as instance. More descriptions and worked examples will be depicted in the upcoming section.

6.3.2 KINEMATIC ANALYSIS

6.3.2.1 Planar Failure

Figure 6.6a shows the great circle representing the face of a slope, which has a dip of ψ_f and a dip direction of $\alpha_f = 270^\circ$, facing west. The dip and dip direction of a discontinuity A are ψ_A and α_A , respectively. For plane failure to occur along the discontinuity A, the following conditions must be satisfied:

- $\psi_A < \psi_f$
- $\psi_A > \phi$
- $\alpha_{\rm f} 20^{\circ} \le \alpha_{\rm A} \le \alpha_{\rm f} + 20^{\circ}$

These three conditions are satisfied only if the dip vector (i.e. the line defining the dip and dip direction) of the discontinuity falls within the hatched region in Figure 6.6a. In other words, the lowest point of the great circle representing the discontinuity should lie within the hatched zone for plane failure to occur. For simplicity, the slope is assumed to be facing west. The same procedure applies to slopes facing any direction. By overlaying tracing paper and rotating about the centre, as in the previous examples, the hatched zone can be defined, and the kinematic analysis can be carried out.

6.3.2.2 Wedge Failure

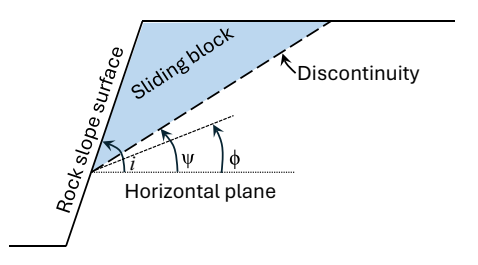
Figure 6.6b shows two great circles corresponding to planes of discontinuities A and B, which intersect at X. The line OX defines the plunge (ψ_i) and trend (α_i) of the line of intersection between these two planes. Any possible sliding will occur along this line. Wedge failure can occur when all the following conditions are satisfied:

1.a $\psi_i < \psi_f$ 1.b $\psi_i > \phi$ (slide on both planes)

TABLE 6.2

Kinematic Analyses of Typical Failures in Rock

Failure Planar



Illustration

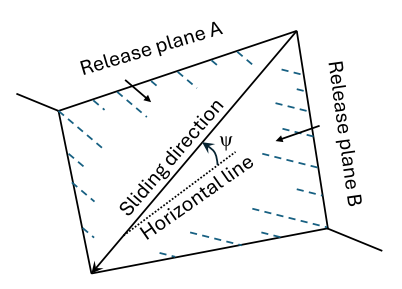
Dip:

 $i > \psi > \phi$ Direction:

 $|\alpha - \alpha_{\rm f}| < 20^{\circ}$

Conditions

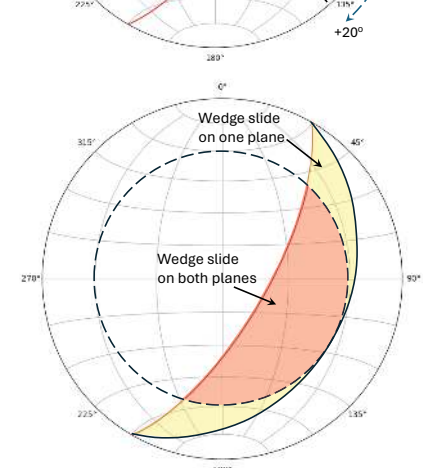
Wedge



Dip:

 $i > \psi > \phi$ Direction:

No lateral limits



Kinematic analysis

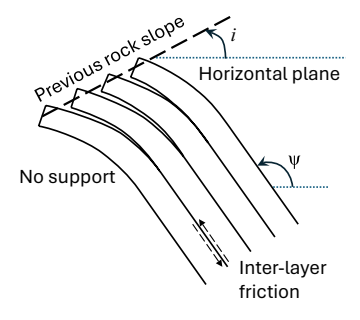
Slope plane

Friction circle

TABLE 6.2 (Continued)

Kinematic Analyses of Typical Failures in Rock

Flexural toppling



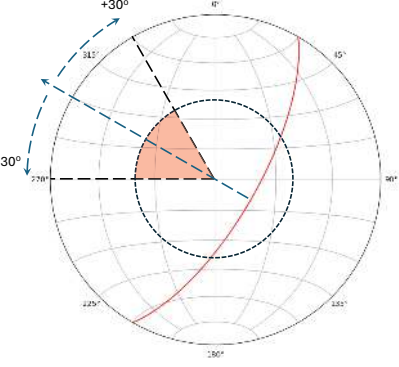
Dip:

Has pole on the slip limit plane

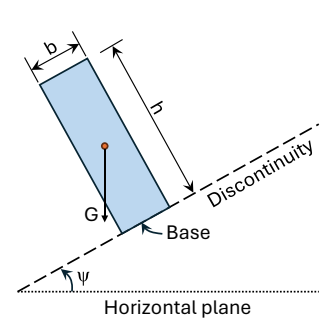
$$90^{\circ_0} < \psi < 90^{\circ} + i - \phi$$

Direction:

$$I(\alpha - 180^\circ) - \alpha_f I < 30^\circ$$



Direct toppling



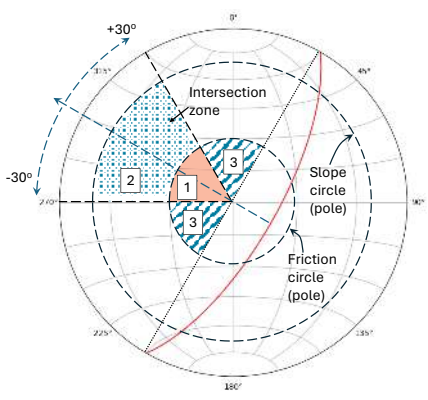
 $b/h < tan(\psi)$

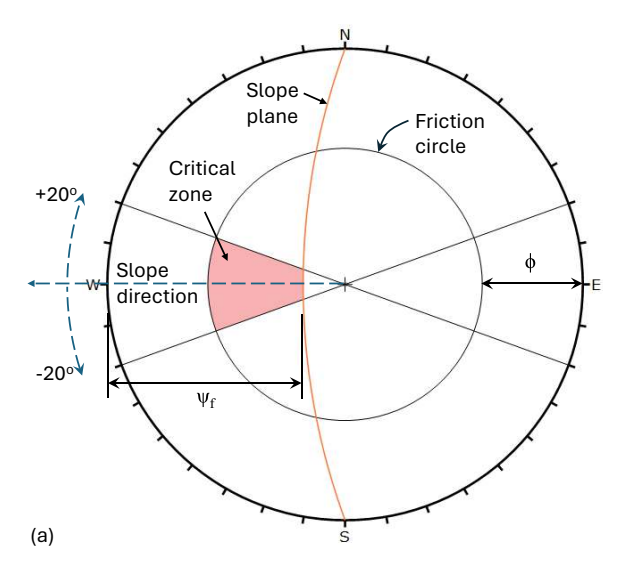
Dip:

 $i > \psi$

Direction:

$$|\alpha - \alpha_{\rm f}| < 30^{\circ}$$





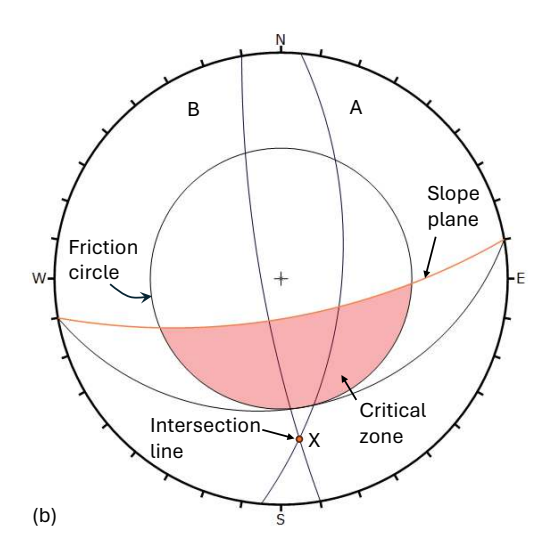


FIGURE 6.6 Identification of rock slope failure modes: (a) plane failure and (b) wedge failure.

These conditions are satisfied only when X lies within the hatched zone. If the intersection falls into the critical zone, the wedge block can slide on either one plane or both. When the intersection is plotted in the secondary zone, the wedge block can slide on one plane. In the illustration in Figure 6.6b, the condition is not satisfied (i.e. OX is quite shallow), and hence wedge failure is unlikely to occur.

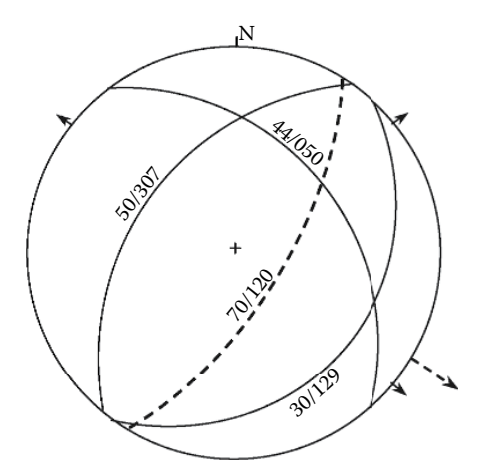


FIGURE 6.7 Great circles of the three discontinuity sets and the cut slope in Example 6.1.

EXAMPLE 6.1

Draw the spherical projections of the great circles representing the three joint sets identified in Example 2.1 and the proposed cut on the hillside.

Solution

The great circles of the three joint sets J1 (30/129), J2 (44/050) and J3 (50/307) are shown in Figure 6.7 as continuous lines, along with the cut slope (70/120) shown as a dashed line. The short arrows marked along the perimeter show the dip directions of these four planes.

EXAMPLE 6.2

Check whether planar or wedge failure is likely in Example 6.1. Disregard the friction angle consideration in this exercise. However, there is a lateral limit of 20° for both modes of failure.

Solution

Let us check the possibilities for a planar failure. The dotted region in Figure 6.8 shows the region in which the dip vector of the discontinuity should fall for planar failure to occur. The discontinuity set J1 (30/129) certainly appears to have potential to slide and cause a plane failure; the other two joint sets have no possibilities of planar slides. The dip direction of J1 (30/129) and the dip direction of the cut slope (70/120) are very close – within $\pm 20^{\circ}$ – and the dip of J1 is less than the dip of the slope. This is a recipe for planar failure if the friction angle is less than 30° .

Let us now check the possibilities of wedge failure. The intersection of joint sets J1 (30/129) and J2 (44/050) lies within the dotted region in Figure 6.8. Therefore, there is a possibility of wedge failure. The line of intersection (between J1 and J2)

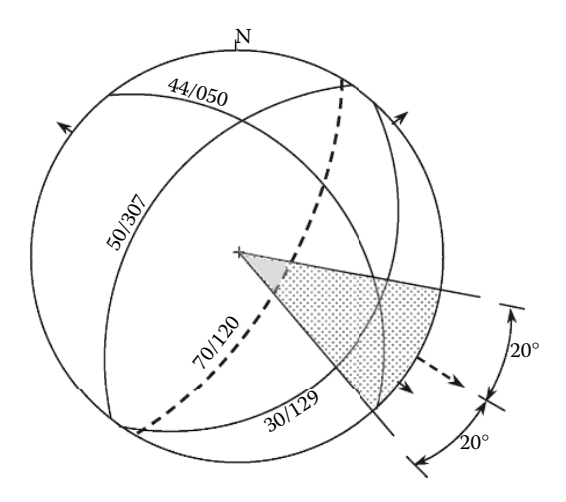


FIGURE 6.8 Kinematic analysis in Example 6.2.

is shallower than the face of the rock slope and hence would daylight on the slope face. The dip direction of this line is within $\pm 20^{\circ}$ of the dip direction of the cut slope (70/120).

6.3.2.3 Flexural Toppling Failure

For the slip to occur, the bedding normal must be inclined at a smaller angle than the friction angle above the slope. Hence, the poles of the discontinuities must have a higher plunge than the slip limit plane, with the dip $\psi_{\rm limit}$ at slope dip (i) minus the friction angle (ϕ) of the rock. The dips of the dangerous discontinuities must fall within the dip limit oval, which is to the other side. For a simplified assumption, it can be assumed safely that dangerous dip ψ must satisfy $90^{\circ} < \psi < 90^{\circ} + i - \varphi$, as shown in Table 6.2. The kinematic analysis for flexural toppling failure should proceed with the following steps:

- 1. Construct slip limit plane with dip $\psi_{limit} = i \phi$. The dip direction is the same as the slope direction.
- 2. From each point on the plane, count 90° towards the opposite direction of the circle to build an oval of dip limit.
- Construct two lines for lateral limits, which depart 30° from the slope direction.

Figure 6.9 shows a discontinuity which is prone to flexural toppling.

6.3.2.4 Direct Toppling Failure

Flexural toppling failure requires only one set of discontinuities to form rock layers. However, direct toppling failure needs three sets of discontinuities. The first two sets dip into the slope to form discrete rock columns. The third set daylights on the rock

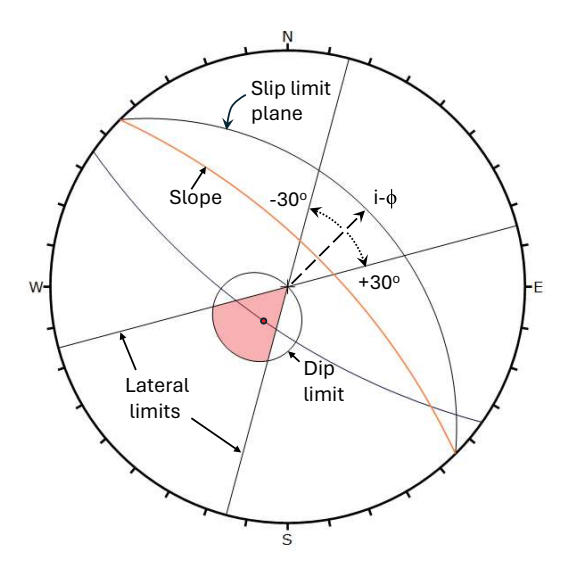


FIGURE 6.9 Flexural toppling analysis.

slope, divides columns into blocks and acts as a release plane, allowing the blocks to topple (Figure 6.2d). In addition, the blocks must be tall enough so that the line of gravity falls outside their base. Therefore, kinematic analysis has several criteria and cannot be done simply with stereonet. A simplified version is described in this chapter.

Figure 6.10 shows three discontinuities J1 (45/315), J2 (50/215) and J3 (25/060) found at a rock slope (70/045). The first two sets of discontinuities, J1 and J2, form rock columns and go into the slope. The last discontinuity J3 daylights onto the slope and may act as a release plane allowing blocks to topple. Zones 1 and 2 are limited by lateral limits $\pm 30^{\circ}$ from the slope direction. Zone 2 is limited by a circle going through the pole of the slope. The boundary between zone 1 and zone 2 is the friction circle in pole analysis, which is 90° - ϕ . The kinematic analysis has two separate conditions for the intersection and the base, respectively.

- 1.a If the intersection of J1 and J2 falls in zones 1 or 2, the rock columns formed by J1 and J2 may have high potential for direct toppling. Zone 1 is considered to have higher risk than zone 2.
- 1.b If the intersection falls in zone 3, rock columns may have oblique toppling as they are almost vertical.
- 2.a If the pole of base J3 falls in zone 1, J3 could release the block.
- 2.b If the pole of J3 falls in zone 2, there may be a combined failure of toppling and planar sliding.
- 2.c If the pole of J3 falls in zone 3, the risk is lower, but the rock may still have oblique toppling.

As the intersection is plotted outside the lateral limits, the rock does not have high risk of toppling, even though the pole of J3 is in the critical zone.

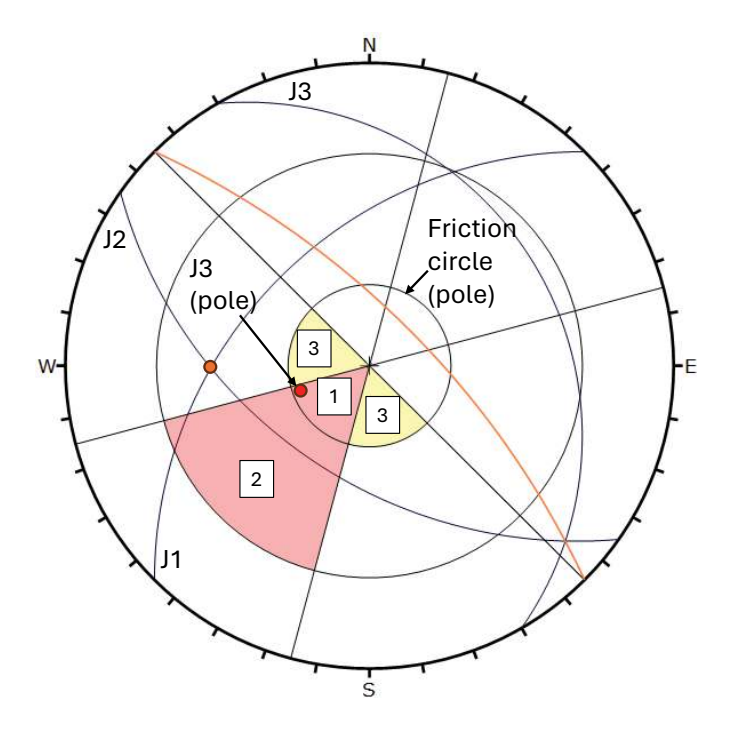


FIGURE 6.10 Pole analysis for direct toppling.

6.4 SLOPE STABILITY ANALYSIS

The stability of rock slopes is primarily governed by the shear strength along joints and interfaces between the unstable rock block or wedge and the surrounding intact rock. Additionally, the geometric interaction between jointing and bedding patterns within the rock mass plays a crucial role in influencing slope stability. Determining the magnitude of available shear strength along joints and interfaces is highly challenging due to the inherent variability of the material and the difficulties associated with sampling and laboratory testing. Depending on the critical nature of the project, field direct shear tests are performed on joints to determine reliable strength parameters. Factors that directly or indirectly influence the strength include the following (Bromhead, 1992; Abramson et al., 2002):

- 1. The planarity and smoothness of the joint surfaces. A smooth planar surface will have a lower strength than an irregular and rough surface.
- 2. The inclination of the discontinuity plane with respect to the slope.
- 3. The openness of the discontinuity, which can range from a small fissure to a readily visible joint.
- 4. The extent of the weathering along the surfaces and the possible infill of the joint with weaker material such as clays and calcareous materials. A calcareous infill may potentially increase the strength of the joint, whereas a soft

clay infill may reduce the strength of the joint to the same level as the clay material itself. Such infills may also change the seepage pattern, improving or degrading the drainage, which will be manifested by an increase or decrease in pore water pressures within the joints.

Once the failure modes have been recognised and the joint strengths have been determined, the factor of safety can be estimated using the principles of statics, with free-body diagrams deduced from the geological map that describes the geological structures, and water/seepage forces calculated from the piezometric measurements. Limit equilibrium methods have been useful in developing the fundamental understanding of rock slope stability analysis for simple modes of failure. Numerical methods help analyse the rock slopes, especially failing in a combination of basic modes and/or other known failure modes (erosion, ravelling, slumping, block torsion, sheet failure, buckling, bursting and so on, as listed by Goodman and Kieffer (2000)). This section discusses the fundamentals of limit equilibrium methods for rock slope stability analysis and presents analytical expressions for both static and seismic loading conditions.

6.4.1 FACTOR OF SAFETY

The engineer's task in analysing rock slope stability is to determine the factor of safety. Generally, the *factor of safety* (FS) against the sliding of a rock block is defined as

$$FS = \frac{F_{r}}{F_{i}} \tag{6.1}$$

where F_r is the total force available to resist the sliding of the rock block and F_i is the total force tending to induce sliding. For a slope on the point of failure, a condition of limiting equilibrium exists in which $F_r = F_i$, and thus FS = 1. For stable slopes, $F_r > F_i$, and therefore FS > 1. In practice, temporary rock slopes with minimal risk of damage require FS \geq 1.3, and permanent slopes with significant risk of damage require FS \geq 1.5. Computation for special loads, such as earthquake and wind, could take a multiplier \geq 1.1.

6.4.2 PLANE FAILURE

Figure 6.11 shows a rock slope of height H inclined to the horizontal at an angle i. The sliding rock block $A_1A_2A_3$ is separated by the joint/bedding/failure plane A_2A_3 , which is inclined to the horizontal at an angle θ . A_1A_3 (= B) is the top width of the sliding rock block, and W is its weight. The stability of the rock block $A_1A_2A_3$ is analysed as a two-dimensional limit equilibrium problem, considering a slice of unit thickness through the slope. Only the force equilibrium is considered, neglecting any resistance to sliding at the lateral boundaries of the sliding block. The joint/bedding plane material is assumed to be a $c-\phi$ soil material, with c and ϕ as cohesion and angle of internal friction (also called angle of shearing resistance), respectively, obeying the Mohr–Coulomb failure criterion.

The total force available to resist the sliding block is

$$F_{r} = sA \tag{6.2}$$

where s is the shear strength of the sliding failure plane and A is the area of the base A_2A_3 of the sliding rock block. It is given as

$$A = \frac{H}{\sin \theta} \tag{6.3}$$

The top width B is calculated as

$$B = H(\cos\theta - \cot i) = \frac{H\sin(i - \theta)}{\sin i \sin \theta}$$
(6.4)

The Mohr–Coulomb failure criterion provides:

$$s = c + \sigma_n \tan \phi \tag{6.5}$$

where σ_n is the normal stress on the failure plane. From Equations 6.2 and 6.5,

$$F_{\rm r} = cA + F_{\rm n} \tan \phi \tag{6.6}$$

where $F_n = \sigma_n A$ is the normal force on the failure plane. Considering equilibrium of forces acting on the rock block in a direction normal to the slope face, F_n is obtained as

$$F_{n} = W \cos \theta \tag{6.7}$$

The weight W is calculated as

$$W = \frac{1}{2} \gamma BH$$

or, using Equation 6.4, we get

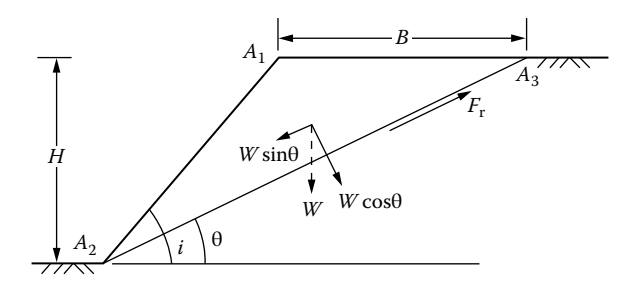


FIGURE 6.11 A rock slope in plane failure.

$$W = \frac{1}{2} \left[\frac{\sin(i - \theta)}{\sin i \sin \theta} \right] \gamma H^2$$
 (6.8)

Substituting values from Equations 6.3, 6.7 and 6.8 into Equation 6.6, we arrive at

$$F_{\rm r} = \frac{cH}{\sin\theta} + \frac{1}{2} \left[\frac{\sin(i-\theta)\cos\theta}{\sin i \sin\theta} \right] \gamma H^2 \tan\phi \tag{6.9}$$

From Figure 6.11, the total force tending to induce sliding is calculated as

$$F_{\rm i} = W \sin \theta$$

or, using Equation 6.8, we get

$$F_{i} = \frac{1}{2} \left[\frac{\sin(i - \theta)}{\sin i} \right] \gamma H^{2} \tag{6.10}$$

Substituting $F_{\rm r}$ and $F_{\rm i}$ from Equations 6.9 and 6.10, respectively, into Equation 6.1, the factor of safety is obtained as

$$FS = \frac{2c\sin i}{\gamma H\sin\theta\sin(i-\theta)} + \frac{\tan\phi}{\tan\theta}$$
 (6.11)

or

$$FS = \frac{2c^* \sin i}{\sin \theta \sin (i - \theta)} + \frac{\tan \phi}{\tan \theta}$$
(6.12)

where $c^* = c/\gamma H$ is a nondimensional parameter that may range between 0 and 1, although c, γ and H vary over wide ranges. From Equation 6.11, it is noted that the factor of safety is a function of six parameters $(c, \gamma, H, i, \theta, \phi)$, whereas Equation 6.12 states that it is a function of only four parameters (c^*, i, θ, ϕ) , which are nondimensional. Therefore, Equation 6.12 can be conveniently used for preparing design charts for the design of simple rock slopes against plane failure. The authors recommend calculation of the factor of safety using Equation 6.11 or Equation 6.12 in the MS Excel spreadsheet in place of using developed design charts or a pocket calculator, to save design time, especially when several rock slopes have to be analysed and designed.

EXAMPLE 6.3

For the rock slope shown in Figure 6.11, consider that the joint or bedding material is cohesionless. What is the expression for the factor of safety? Under what condition can the slope fail?

Solution

For cohesionless joint/bedding material, c = 0, and Equation 6.12 reduces to

$$FS = \frac{\tan \phi}{\tan \theta} \tag{6.13}$$

For failure of the slope,

FS < 1

or

 $\tan \theta > \tan \phi$

or

It should be noted that Figure 6.11 presents a simple case of plane failure, which is not a very common field situation; however, this case is very useful in understanding how the variation in basic factors can govern the stability of rock slopes against plane failure. In reality, some or all of the following factors or physical situations can be present at many field sites (Shukla et al., 2009; Hossain and Shukla, 2010; Shukla and Hossain, 2010, 2011a, 2011b):

- Tension crack in slope with no water
- Tension crack in rock slope filled with water partially or fully
- Seepage pressure at the joint/bedding plane
- Surcharge at the top of the slope
- · Horizontal and vertical seismic loads
- Stabilising force through reinforcing system such as rock bolts, anchors and cables

Figure 6.12 shows an anchored rock slope of height H with an inclination i to the horizontal. The joint/bedding plane A_2A_3 , inclined to the horizontal at an angle θ , and a vertical tension crack A_3A_4 of depth z, separate a portion of the rock mass as the block $A_1A_2A_3A_4$ having a weight W. The tension crack is filled with water having a unit weight γ_w to a depth z_w . The stabilising tensile force T, inclined at an angle α to the normal at the joint/bedding plane A_2A_3 , simulates the effect of a rock-anchoring system, which is commonly used to stabilise rock slopes. The horizontal and vertical seismic inertial forces, k_hW and k_vW with k_h and k_v [\downarrow + and \uparrow -] as horizontal and vertical seismic coefficients, respectively, are shown acting on the sliding block. A surcharge placed at the top of the slope A_1A_4 (= B) applies a vertical pressure q, along with horizontal and vertical seismic inertial forces, k_hqB and k_vqB , respectively. The horizontal force due to water pressure in the tension crack is U_1 . The water in the tension crack seeps through the joint/bedding plane and applies an uplift force U_2 . Under a critical combination of forces, the rock mass block $A_1A_2A_3A_4$ can slide along the joint/bedding plane A_2A_3 as a failure plane.

The expression for the factor of safety of the slope shown in Figure 6.12 against plane failure can be derived by following the steps described for the simple slope

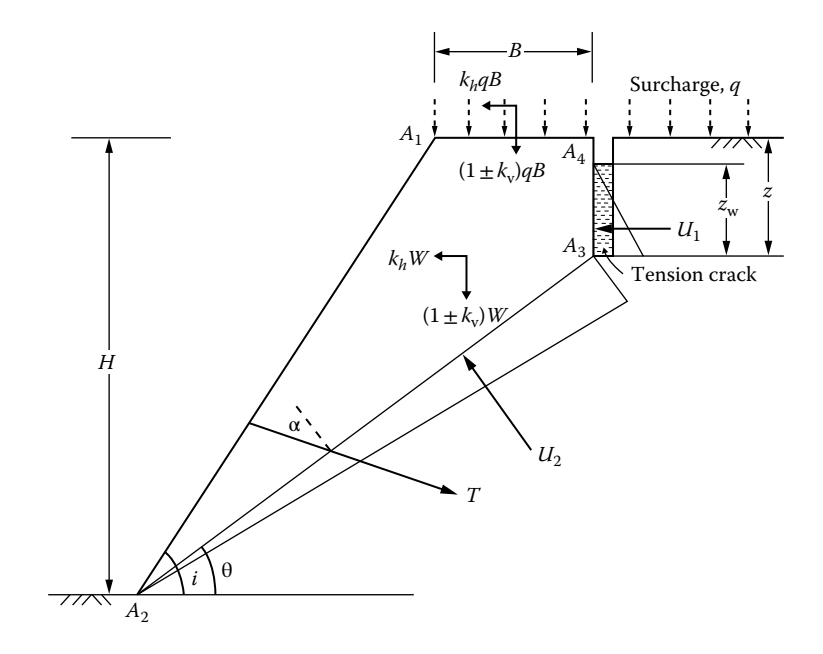


FIGURE 6.12 Anchored rock slope with a water-filled tension crack subjected to surcharge and seismic loads in plane failure along the joint/bedding plane. (Adapted from Shukla, S.K. and Hossain, M.M., *Int. J. Geotech. Eng.*, 5, 181–187, 2011.)

shown in Figure 6.11. The readers can find the complete derivation in the research article by Shukla and Hossain (2011a), where the factor of safety is given as

$$\mathrm{FS} = \frac{2c^{*}P + \left[(1 \pm k_{\mathrm{v}}) \left(Q + 2q^{*}R \right) \left\{ \frac{\cos\left(\theta + \Psi\right)}{\cos\Psi} \right\} - \left(\frac{z_{\mathrm{w}}^{*2}}{3^{*}} \right) \sin\theta - \left(\frac{z_{\mathrm{w}}^{*}}{3^{*}} \right) P + 2T^{*}\cos\alpha \right] \tan\phi}{(1 \pm k_{\mathrm{v}}) \left(Q + 2q^{*}R \right) \left\{ \frac{\sin\left(\theta + \Psi\right)}{\cos\Psi} \right\} + \left(\frac{z_{\mathrm{w}}^{*2}}{3^{*}} \right) \cos\beta - 2T^{*}\sin\alpha}$$
 (6.14)

in terms of the following nondimensional parameters:

$$c^* = \frac{c}{\gamma H} \tag{6.15a}$$

$$z^* = \frac{z}{H} \tag{6.15b}$$

$$z_{\rm w}^* = \frac{z_{\rm w}}{H} \tag{6.15c}$$

$$\gamma^* = \frac{\gamma}{\gamma_w} \tag{6.15d}$$

$$q^* = \frac{q}{\gamma H} \tag{6.15e}$$

$$T^* = \frac{T}{\gamma H^2} \tag{6.15f}$$

$$P = (1 - z^*) \operatorname{cosec} \theta \tag{6.15g}$$

$$Q = \left(1 - z^{*2}\right)\cot\theta - \cot i \tag{6.15h}$$

$$R = (1 - z^*)\cot\theta - \cot i \tag{6.15i}$$

and

$$\Psi = \tan^{-1} \left(\frac{k_{\rm h}}{1 \pm k_{\rm v}} \right) \tag{6.15j}$$

Equation 6.14 is a general expression for the factor of safety of the rock slope against plane failure. It can be used to investigate the effect of any individual parameter on the factor of safety of the rock slope and to carry out a detailed parametric study as required in a specific field situation. There can be several special cases of Equation 6.14, including expressions in Equations 6.12 and 6.13, and many of them have been presented in the literature (Hoek and Bray, 1981; Ling and Cheng, 1997; Wyllie and Mah, 2004; Shukla and Hossain, 2011a, 2011b).

Seismic coefficients $k_{\rm h}$ and $k_{\rm v}$ are expressed as fractions of the gravitational constant. In conventional pseudostatic methods of analysis, the choice of horizontal seismic coefficient, $k_{\rm h}$, for design is related to the specified horizontal peak ground acceleration for the site, $a_{\rm h}$. The relationship between $a_{\rm h}$ and a representative value of $k_{\rm h}$ is, nevertheless, complex, and there does not appear to be a general consensus in the literature on how to relate these parameters. Values of $k_{\rm h}$ from 0.05 to 0.15 are typical for design, and these values correspond to one-third to one half of the peak acceleration of the design earthquake (Bathurst et al., 2012). In practice, the choice of $k_{\rm h}$ should be based on local experience or prescribed by local building codes or other regulations. The experience suggests that $k_{\rm h}$ may be as high as 0.5, and $k_{\rm v}$ is generally taken as half of $k_{\rm h}$.

 $\theta > \phi$; that is, the inclination of the joint/bedding plane to the horizontal should be greater than the angle of internal friction of the joint/bedding material, which has been stated in Section 6.2.

EXAMPLE 6.4

For the rock slope shown in Figure 6.12, consider the following: $i = 50^{\circ}$, $\theta = 35^{\circ}$, $\phi = 25^{\circ}$, $q^* = 0.5$, $T^* = 0.1$, $z^* = 0.1$, $z^* = 0.05$, $\gamma^* = 2.5$, $\alpha = 45^{\circ}$ and $c^* = 0.1$. Plot the variation of the factor of safety (FS) with vertical seismic coefficient (k_v) for horizontal

seismic coefficient, $k_h = 0.05$, 0.1, 0.15, 0.2, 0.25 and 0.3. Assume that the maximum value of $k_v = k_h/2$. What do you notice in this plot?

Solution

Using Equation 6.14, the variation of factor of safety (FS) with vertical seismic coefficient (k_v) for the given values of horizontal seismic coefficient (k_h) is shown in Figure 6.13.

The following two key observations are noted:

- 1. With an increase in k_v in the downward direction, FS decreases almost linearly, but it increases as k_v increases in the upward direction.
- 2. FS is greater than unity for any value of k_h less than 0.25, and it is higher for smaller values of k_h , which is an expected observation.

Following the graphical approach adopted in Example 6.2, Equation 6.14 can be used to develop design charts for specific field parameters. Shukla and Hossain (2010) have presented examples of some design charts for assessing the stability of anchored rock slopes against plane failure. Figure 6.14 shows a typical design chart.

6.4.3 WEDGE FAILURE

Figure 6.15 shows forces acting on a rock wedge $A_1A_2A_3$ in its two views: (a) view looking at the wedge face and (b) cross-sectional view. R_A and R_B are the normal

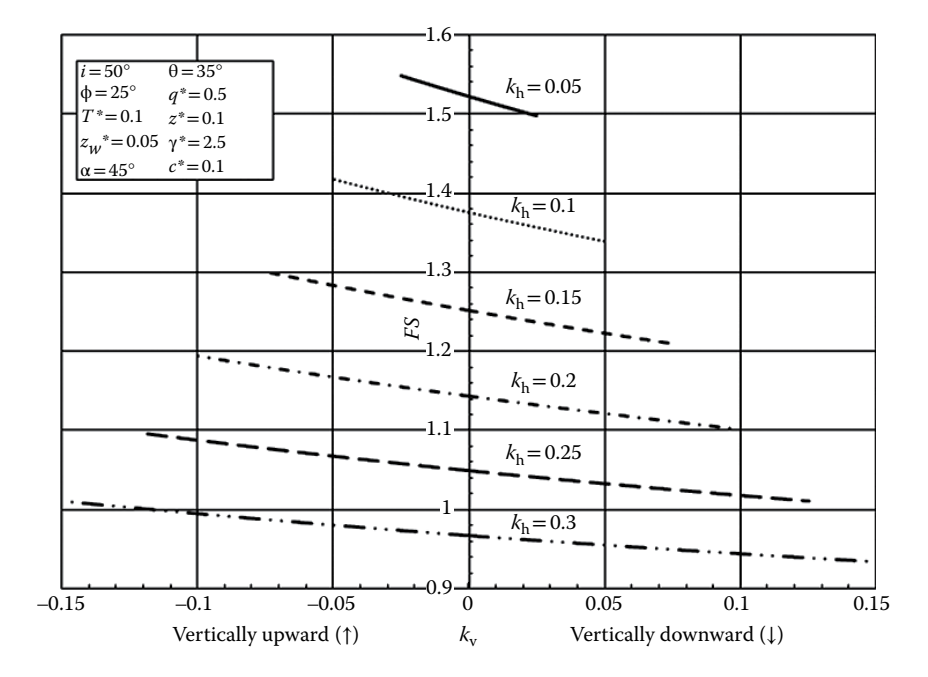


FIGURE 6.13 Variation of factor of safety (FS) with vertical seismic coefficient k_v .

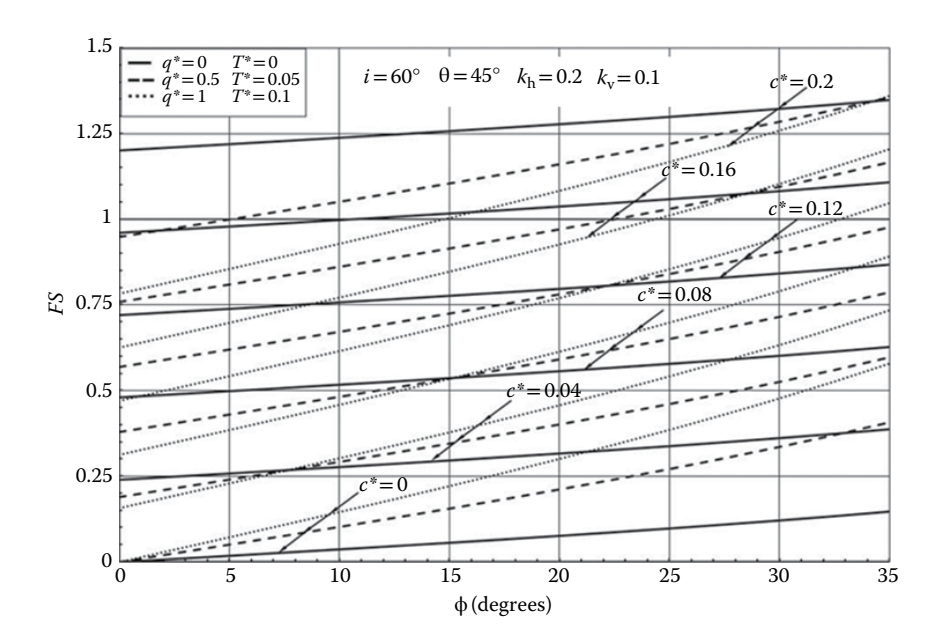


FIGURE 6.14 A typical design chart for estimating the stability of anchored rock slopes against plane failure. (Adapted from Shukla, S.K. and Hossain, M.M., Design charts for rock slope stability against plane failure under seismic loading condition. *Proceedings of the ISRM International Symposium 2010 and 6th Asian Rock Mechanics Symposium*, 23–27 October 2010, New Delhi, India, Paper No. 64, 2010.)

reactions provided to the sliding wedge by planes A and B, respectively. A condition of wedge sliding is defined by $i > \beta > \phi_{av}$, where i is the slope face inclination to the horizontal as considered in plane failure, β is the inclination to the horizontal of the line (i.e. plunge) of intersection of discontinuity planes A and B, and ϕ_{av} is the average angle of internal friction for the two discontinuity/slide planes A and B. If the angle of internal friction is the same for both planes and is ϕ , ϕ_{av} will be equal to ϕ . The cohesive forces at the discontinuity planes are assumed to be negligible.

The total force available to resist the sliding of the rock wedge along the line of intersection is

$$F_{\rm r} = R_{\rm A} \tan \phi + R_{\rm B} \tan \phi = (R_{\rm A} + R_{\rm B}) \tan \phi \tag{6.16}$$

The total force tending to induce sliding along the line of intersection is

$$F_{\rm i} = W \sin \beta \tag{6.17}$$

Substituting F_r and F_i from Equations 6.16 and 6.17, respectively, into Equation 6.1, the factor of safety is obtained as

$$FS = \frac{(R_{A} + R_{B})\tan\phi}{W\sin\beta}$$
 (6.18)

Resolving forces $R_{\rm A}$ and $R_{\rm B}$ into components normal and parallel to the direction along the line of intersection, we get

$$R_{\rm A}\sin\theta_{\rm A} = R_{\rm B}\sin\theta_{\rm B} \tag{6.19}$$

and

$$R_{\rm A}\cos\theta_{\rm A} + R_{\rm B}\cos\theta_{\rm B} = W\cos\beta \tag{6.20}$$

Solving Equations 6.19 and 6.20 for R_A and R_B , we obtain

$$R_{\rm A} = \frac{W \cos \beta \sin \theta_{\rm B}}{\sin (\theta_{\rm A} + \theta_{\rm B})} \tag{6.21}$$

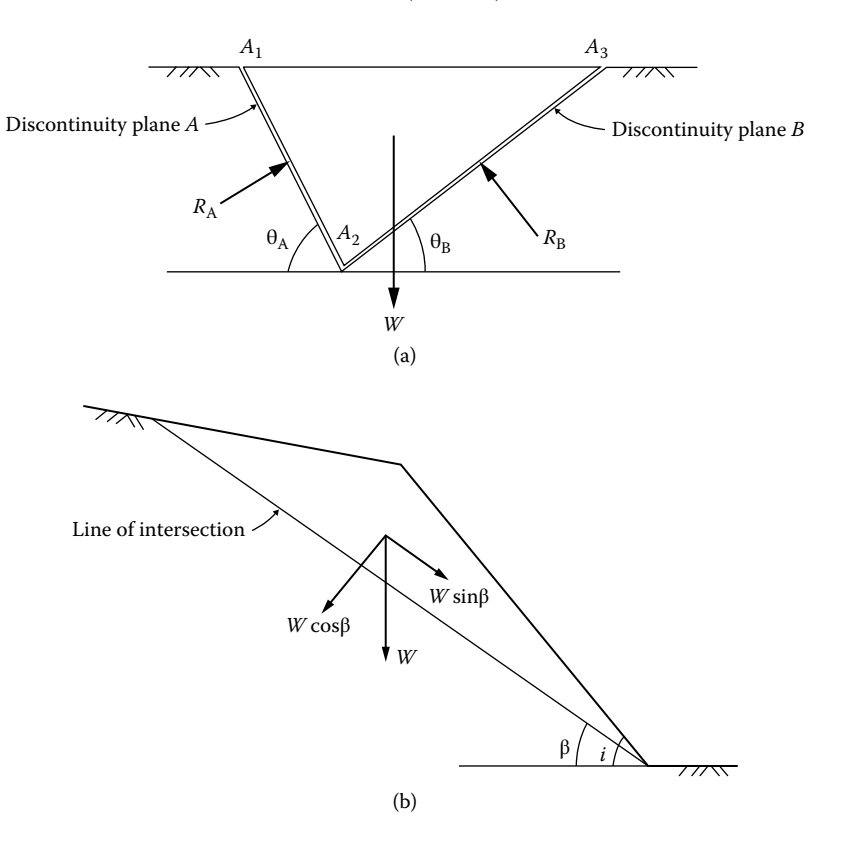


FIGURE 6.15 Forces acting on the rock wedge: (a) view of wedge looking at its face, showing definition of angles θ_A and θ_B and reactions R_A and R_B of discontinuity planes A and B, respectively; (b) cross section of the wedge showing resolution of the weight W.

and

$$R_{\rm B} = \frac{W \cos \beta \sin \theta_{\rm A}}{\sin(\theta_{\rm A} + \theta_{\rm B})} \tag{6.22}$$

Using Equations 6.21 and 6.22, Equation 6.18 can be expressed as

$$FS = \frac{\left(\sin\theta_{A} + \sin\theta_{B}\right)\tan\phi}{\tan\beta\sin\left(\theta_{A} + \theta_{B}\right)}$$
(6.23)

Or

$$FS = K \left(\frac{\tan \phi}{\tan \beta} \right) \tag{6.24}$$

where

$$K = \frac{\sin \theta_{A} + \sin \theta_{B}}{\sin(\theta_{A} + \theta_{B})}$$
 (6.25)

K is a wedge factor that depends on the inclinations of the discontinuity planes and is typically greater than 1. If the factor of safety FS against the wedge failure is denoted by FS_w, Equation 6.24 can be written as

$$FS_{W} = K(FS_{P}) \tag{6.26}$$

where FS_P (= $\tan \phi / \tan \beta$) is the factor of safety of the rock slope against plane failure, in which the slide plane – with an angle of internal friction ϕ – dips at the same angle β as the line of intersection of the planes A and B.

The wedge failure analysis presented here does not account for variations in friction angles and cohesions between the two sliding planes, nor does it consider groundwater seepage, surcharge or seismic loads. Incorporating these factors into the analysis significantly increases its complexity. For more detailed consideration of these aspects, refer to the works of Hoek and Bray (1981) and Wyllie and Mah (2004).

EXAMPLE 6.5

For the rock slope shown in Figure 6.15, consider the following: $i = 62^{\circ}$, $\beta = 53^{\circ}$, $\phi = 30^{\circ}$, $\theta_A = 45^{\circ}$ and $\theta_B = 48^{\circ}$. Calculate the factor of safety. Is the slope stable?

Solution

From Equation (6.25),
$$K = \frac{\sin 45^\circ + \sin 48^\circ}{\sin (45^\circ + 48^\circ)} = 1.45$$

From Equation (6.24),
$$FS = 1.45 \left(\frac{\tan 30^{\circ}}{\tan 53^{\circ}} \right) = 0.63$$

Since FS < 1, the slope is unstable.

6.4.4 CIRCULAR FAILURE

In the case of a closely jointed, fractured or highly weathered rock slope, the slide surface can naturally follow the path of least resistance through the slope. In such materials, it is observed that the slide surface generally takes the form of a cylindrical surface that has a circular cross-section; therefore, the failure is called circular failure (Figure 6.2c), which is the most common type of slope failure in soils. Various methods of analysis for circular failure in soils have been described in detail in textbooks dealing with soil mechanics; the readers may refer to Taylor (1948), Terzaghi (1943), Lambe and Whitman (1979), Terzaghi et al. (1996) and Das and Sivakugan (2017).

6.4.5 TOPPLING FAILURE

Toppling failures occur in a wide range of rock masses in both natural and engineered slopes. They involve the rotation of columns or blocks of rocks about their bases. The simplest toppling mechanisms involve a single block, resulting in single-block toppling or flexural toppling, as illustrated in Figure 6.16. The former mode of toppling occurs when the rock block is already detached from the rock mass of the slope, and the latter occurs when the rock block remains attached to the rock mass of the slope. The most common toppling failures involve several blocks, and they can be classified as block toppling, flexural toppling and block–flexural toppling (Figure 6.17) (Hoek and Bray, 1981; Goodman and Kieffer, 2000; Wyllie and Mah, 2004). Block toppling takes place in a hard rock mass when individual blocks or columns are composed of two normal joint sets, with the main set dipping steeply into the slope face. The upper blocks tend to topple and push forward on the short columns in the slope toe. Flexural toppling occurs when continuous columns of rock dipping steeply towards the slope break in flexure and tilt forward. Block–flexural toppling is a complex mechanism characterised by pseudocontinuous flexure along blocks that are divided by a number of cross-joints.

Note that block toppling is a form of *direct toppling*. In block toppling, individual rock blocks or columns, typically formed by discontinuities such as joints or fractures, rotate forward and topple under their own weight or due to slope instability. Direct toppling refers to this straightforward rotational movement of blocks, with little to no bending or deformation, distinguishing it from flexural toppling.

For a single-rock block resting on a discontinuity plane, as shown in Figure 6.18, if the width b and height h of the rock block are such that its weight acts outside its base, then there is a potential for the block to topple. For this condition to occur, the resisting moment about the outer lower edge of the block should be less than the driving moment about the same edge; that is,

$$(W\cos\theta)\left(\frac{b}{2}\right) < (W\sin\theta)\left(\frac{h}{2}\right)$$

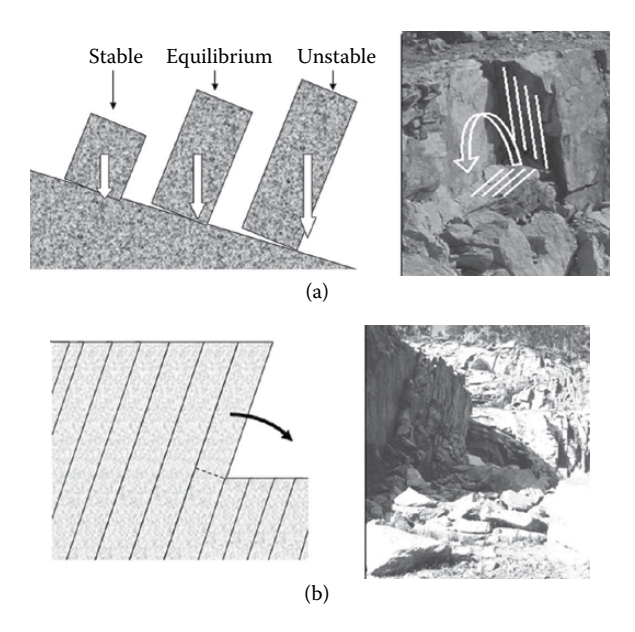


FIGURE 6.16 Simple toppling failures involving a single block: (a) single-block toppling; (b) single-block flexural toppling. (After Alejano, L.R., et al., *Eng. Geol.*, 114, 93–104, 2010.)

or

$$\frac{b}{h} < \tan \theta \tag{6.27}$$

For the sliding of the block,

$$W \sin \theta > \mu W \cos \theta$$

or

$$\tan\theta > \mu \tag{6.28}$$

where μ is the coefficient of friction between the sliding block and the joint/bedding plane. Since μ = tan ϕ , inequality 6.28 becomes

$$\theta > \phi$$
 (6.29)

Inequalities 6.27 and 6.29 define the following four conditions for toppling and/ or sliding of the block:

• Toppling only: $\frac{b}{h} < \tan \theta$ and $\theta < \phi$

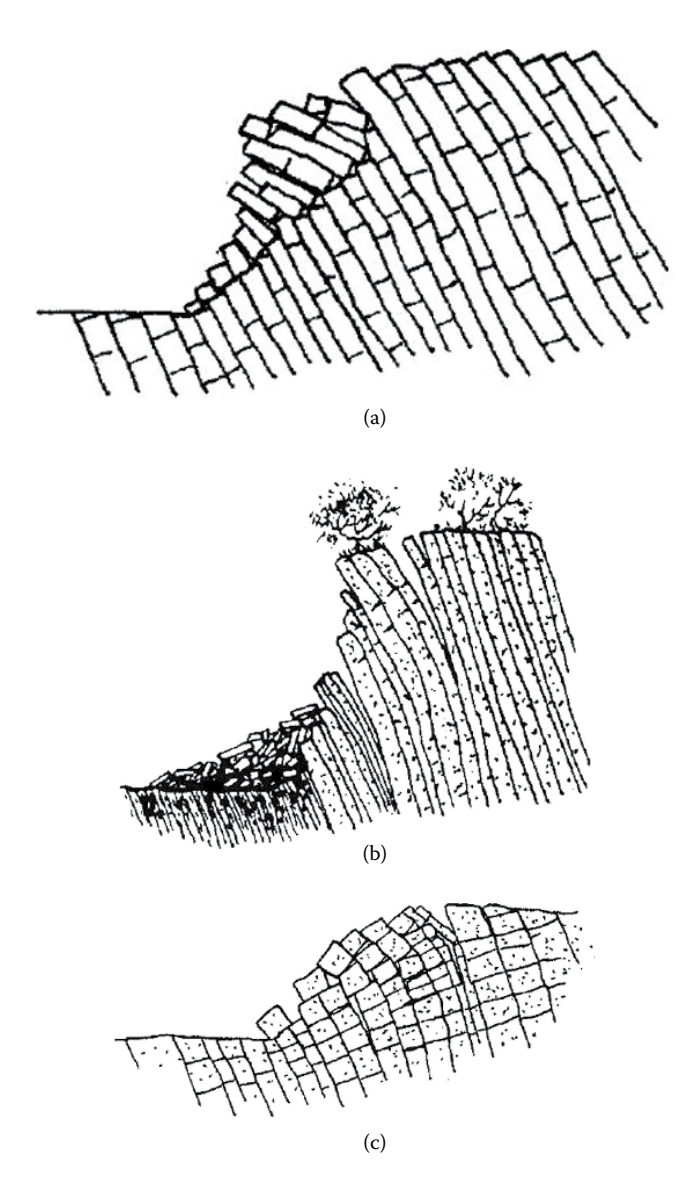


FIGURE 6.17 Common toppling failures involving several rock blocks: (a) block toppling; (b) flexural toppling; (c) block–flexural toppling. (From Goodman, R.E. and Kieffer, D.S., *J. Geotech. Geoenviron. Eng.*, 126, 675–684, 2000.)

- Toppling with sliding: $\frac{b}{h} < \tan \theta$ and $\theta > \phi$
- Sliding only: $\frac{b}{h} > \tan \theta$ and $\theta > \phi$
- No toppling and sliding, that is stable: $\frac{b}{h} > \tan \theta$ and $\theta < \phi$

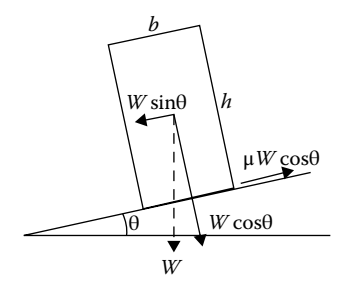


FIGURE 6.18 A rock block resting on a discontinuity plane.

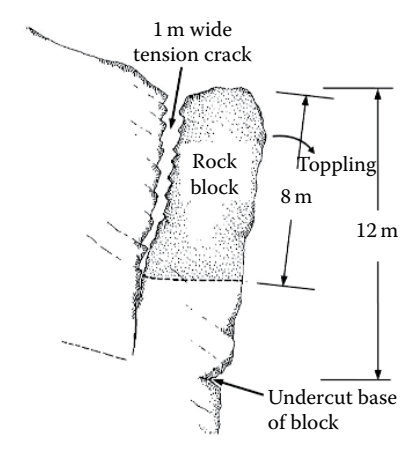


FIGURE 6.19 Single toppling block. (Adapted from Wyllie, D.C., *Rock Mech.*, 13, 89–98, 1980.)

The above four conditions have also been described by Hoek and Bray (1981) and Wyllie and Mah (2004), with analysis for other types of rock toppling failure. Wyllie (1980) has presented a field situation for a single-block toppling failure (Figure 6.19).

6.4.6 FALL

Rock fall involves the detachment of individual rock blocks or fragments from a slope, typically occurring through free fall, bouncing or rolling down the slope. This process is highly dynamic and sudden, making it difficult to apply traditional stability analysis methods such as those based on equilibrium, which are used for sliding failures. In plane, wedge and circular failures, the factor of safety is used to assess the stability of a rock mass moving along a defined failure surface. These mechanisms are more predictable, allowing engineers to calculate the factor of safety as the ratio of resisting forces to driving forces.

For rock falls, however, probabilistic assessments, rockfall modelling and trajectory analysis tools are commonly employed to predict rockfall behaviour and assess the associated risks rather than relying on factor of safety calculations. Rock

engineering programmes often generate a stone or rock block of random shape, initial rock energy, velocity and bounce height. The distribution of rock paths and endpoints could indicate dangerous zone for protection (Figure 6.20).

6.5 SLOPE STABILISATION

Civil and mining engineering projects often involve the creation of excavated rock slopes, which must remain stable for at least the project's design life. It is possible,

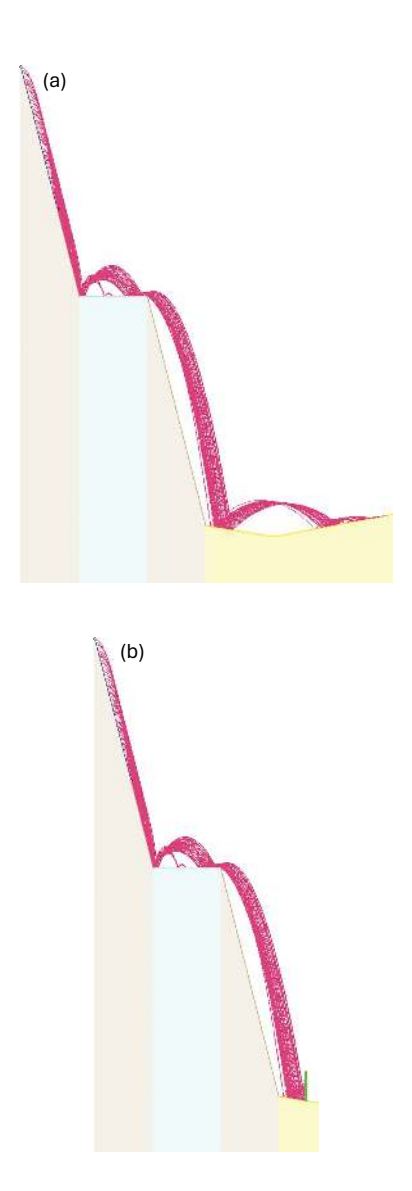


FIGURE 6.20 Distribution of rock fall paths: (a) without barrier; (b) with toe barrier; and (c) with slope barrier. (Continued)

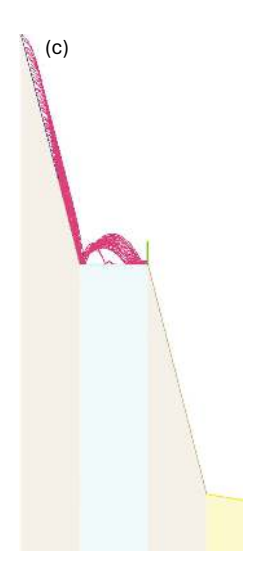


FIGURE 6.20 (Continued)

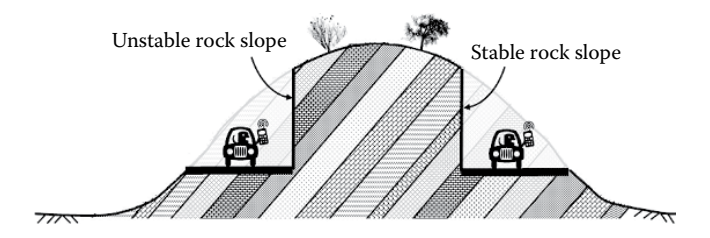


FIGURE 6.21 Rock slopes made through excavations for highways.

during site selection, to achieve a stable excavated rock slope without significant treatment or stabilisation, provided that the orientation of joints and bedding planes is carefully assessed before site selection. Figure 6.21 illustrates how site selection for a highway project can result in stable and unstable slopes. The excavated slope should only be created on the hillside where the rock strata dip away from the excavation.

In many field situations, site selection may not fully meet technical requirements or suitability criteria; in such cases, stabilisation or treatment techniques are employed to enhance slope stability. Several methods are available to increase the stability of slopes (Broms and Wong, 1991; Abramson et al., 2002; Shukla et al., 2012); these methods can be adopted singly or in combination. The choice depends primarily on the cost and the consequence of slope failure. The more commonly used slope stabilisation methods can be classified as follows (Broms and Wong, 1991):

- Geometric methods, in which the geometry of the slope is changed
- Hydrological methods, in which the groundwater table is lowered or the water content of the soil/rock is reduced

 Chemical and mechanical methods, in which the shear strength of the sliding soil/rock mass is increased or the external force causing the slope failure is reduced

Geometrical methods include slope flattening, removal of part of the soil/rock or load from the top of the slope, construction of pressure berms at the toe, terracing, replacement of slipped material by free-draining material and recompaction of slip debris. Hydrological methods include the installation of surface and subsurface drains, inverted filters and thermal methods (ground freezing and heating methods). Chemical and mechanical methods include grouting, construction of restraining structures (such as concrete gravity or cantilever walls), gabion structures, crib walls, embankment piles, lime and cement columns, ground anchors, rock bolting, soil nailing and root piles, earth reinforcement and plantation of grasses and shrubs.

Wyllie and Mah (2004) classified the methods of rock slope stabilisation into the following three groups:

- Reinforcement (rock bolts, dowels, tied-back walls, shotcrete, buttresses and so on)
- Rock removal (resloping, trimming and so on)
- Protection (ditches, mesh, catch fences, warning fences, rock sheds, tunnels and so on)

Rock reinforcement is a method of adding strength to the rock in order to prevent failure. The most useful forms of reinforcement are rock bolts and anchors, which can be used on both natural and engineered slopes to prevent blocks of rock from falling or sliding away from the main mass when isolated by discontinuity planes. They are installed in such a way that the axial load in the bolt or anchor increases the effective stress at depth in soil and rock, thus improving the strength, and a component of the anchor force may also act to reduce destabilising forces and moments. In the case of fractured rock slope, rock bolts and anchors are also used in combination with reinforced concrete walls, which cover the areas of fractured rock. In Figure 6.12, the anchor force T acts to restrain the sliding rock block $A_1A_2A_3A_4$. The parametric study conducted using Equation 6.14 shows that the factor of safety (FS) of the rock slope against plane failure increases non-linearly with an increase in T, and the rate of increase is higher for lower values of seismic coefficients. It is also found that the factor of safety increases non-linearly with an increase in its inclination (α) to the normal at the failure plane, and it becomes maximum for $\alpha \approx 70^{\circ}$, beyond which it decreases.

Steel rods, known as dowels, are sometimes installed and grouted into the jointed rock to act as reinforcement. Dowels are not stressed during the installation process unlike rock bolts and anchors.

Shotcrete is a pneumatically applied, fine-aggregate mortar that is usually placed in a 50–100 mm layer and is often reinforced for improved tensile and shear strength. It is generally applied along with drain holes as a surface protection layer to the excavated rock slope face before its significant deformation or alteration, in order to provide a high strength, vary rapidly. The shotcrete effectively controls the fall of loose, small rock blocks, but it provides little support against basic modes of slope failure discussed in the previous sections.

Grouting is a technique of injecting a fluid grout into the rock mass to replace all air or water present in its fissures and cracks. The grout consists of a mixture of cement and water. Sand, clay, rock flour, fly ash and other similar materials can be used as fillers in order to reduce the cost of the stabilisation work, especially where fissures and cracks are large in volume. Grouting is employed to reinforce mine slopes and roofs before excavation progresses and is also used ahead of tunnel construction through weak ground conditions. If a cavity is present in the slope face, a concrete buttress can be constructed in the cavity to prevent rock falls and support the overhang, if any.

Rock slope stabilisation is often carried out on a relatively ad hoc basis as the condition of the rock mass becomes exposed. Common stabilisation techniques used in practice include the following (Fookes and Sweeney, 1976; Bromhead, 1992; Wylie and Mah, 2004):

- Flattening of overburden slope
- · Trimming of unstable rock blocks
- · Scaling of small loose materials/blocks
- Construction of drains and drain holes
- Use of dowels
- Installation of rock anchors to prevent sliding along discontinuity plane
- Rock bolting to strengthen the jointed rock mass
- Construction of concrete or masonry walls with weep-holes
- Construction of rock trap ditches at the toe of the slopes
- Providing rock catch fences/walls along the slope to make the adjacent areas safe for public use
- · Hanging nets or chains to slow tumbling blocks
- Free-hanging mesh net to guide loose rock pieces to fall down near the slope toe only
- · Construction of berms/benches as a rock fall collector
- Mesh secured with bolts and shotcreted to stabilise and protect friable formations
- Construction of rock fall barriers (gabions and concrete blocks, reinforced soil barriers and so forth) at the toe of slopes
- · Construction of rock sheds and tunnels
- Providing warning signals in rock fall areas

Stabilisation measures such as rock bolts and anchors prevent the detachment of rock blocks from their original position; therefore, they are classified as active measures. Walls, ditches, catch fences, rock sheds, tunnels and so on are passive measures, as they do not directly interfere with the process of rock detachment but control the dynamic effects of moving or falling blocks.

The selection of a stabilisation technique or a combination of techniques requires consideration of geotechnical (geology, rock properties, groundwater and stability analysis), construction (type of equipment, construction access, construction cost and so on) and environmental (waste disposal, aesthetics and so on) aspects. The selection is also greatly controlled by the level of stabilisation and its design life, and finally the cost. For stabilisation to be effective over an extended period, the initial cost of the work may be higher.

6.6 SUMMARY

1. Rock slopes can be either natural or engineered (excavated). The primary modes of failure include plane, wedge, circular, toppling and fall.

- 2. Plane failures occur in rocks with well-defined discontinuities and jointing.
- 3. Wedge failures occur in blocky rocks with at least two continuous and non-parallel joint sets.
- 4. Circular failures are observed in the slopes of heavily jointed and weathered rock masses.
- 5. Toppling failures are generally noticed in hard rocks with regular, parallel joints dipping into the hillsides.
- 6. The objective of a slope stability analysis for a rock slope is to identify the most probable mode and mechanism of failure and to determine the corresponding minimum factor of safety.
- 7. The factor of safety for a rock slope is defined as the ratio of the total resisting force to the total driving force that induce sliding of the rock block. In practice, rock slopes with a factor of safety (FS) ranging from 1.3 to 1.5 are considered stable.
- 8. The analytical expressions for the factor of safety presented here can be used to investigate the effect of individual parameters on the stability of slopes against different modes of failure.
- Several stabilisation or treatment measures are available for increasing the stability of slopes, and their selection depends upon several considerations such as geotechnical conditions, construction, environmental impact, level of stabilisation and cost.
- 10. Some examples of stabilisation measures are slope flattening, trimming and scaling, reinforcement (rock bolting and anchoring), grouting, masonry walls and gabions, drains, hanging nets and chains, rock trap ditches, rock catch fences and rock sheds and tunnels.

REVIEW EXERCISES

Select the most appropriate answers to the following 10 multiple-choice questions.

- 6.1. Circular rock slope failure takes place in
 - a. hard or soft rocks with well-defined discontinuities
 - b. blocky rocks with at least two continuous and parallel joint sets
 - c. heavily jointed and weathered rock masses
 - d. hard rocks with regular, parallel joints dipping into the hillside
- 6.2. For plane rock slope failure,
 - a. $i > \phi$
 - b. $\theta > \phi$
 - c. $i > \theta$
 - d. all of the above

where i, θ and ϕ have their usual meanings.

- 6.3. The factor of safety considered for temporary slope designs is generally
 - a. 1
 - b. 1.3

- c. 1.5
- d 2
- 6.4. The factor of safety of a rock slope against plane failure does not depend on the
 - a. length of the slope
 - b. height of the slope
 - c. inclination of the slope
 - d. unit weight of the rock mass
- 6.5. Which of the following is generally considered in design practice?
 - a. $k_h = k_v$
 - b. $k_{\rm b} = 0.5k_{\rm v}$
 - c. $k_{\rm h} = 2k_{\rm v}$
 - d. $k_h < k_v$
- 6.6. The condition for a rock block to slide on a discontinuity plane is
 - a. $\theta > \phi$
 - b. $\theta < \phi$
 - c. $\theta = \phi$
 - d. $\theta \leq \phi$
- 6.7. In Figure 6.18, toppling failure only takes place when
 - a. $\frac{b}{h}\langle \tan\theta \text{ and }\theta \rangle \phi$
 - b. $\frac{b}{h} < \tan \theta$ and $\theta < \phi$
 - c. $\frac{b}{h} > \tan \theta$ and $\theta < \phi$
 - d. $\frac{b}{h} > \tan \theta$ and $\theta > \phi$
- 6.8. The excavated slope should be created on the hillside where rock strata
 - a. dip away from the excavation
 - b. dip towards the excavation
 - c. are vertical
 - d. are horizontal
- 6.9. Which of the following is not a geometrical method of rock slope stabilisation?
 - a. Slope flattening
 - b. Replacement of slipped material by free-draining material
 - c. Rock bolting
 - d. Construction of pressure berms at the toe
- 6.10. The selection of a stabilisation technique requires consideration of
 - a. geotechnical aspects
 - b. construction aspects
 - c. environmental aspects
 - d. all of the above

6.11. How does a natural rock slope differ from an engineered (excavated) rock slope?

- 6.12. Describe the effects of the following parameters on the stability of a rock slope against plane failure: strength parameters of joint material, depth of tension crack and inclination of the joint plane.
- 6.13. Derive an expression for the factor of safety of a rock slope against plane failure for a generalised field situation.
- 6.14. For the rock slope shown in Figure 6.11, consider that the joint material is cohesionless, and the values of the angle of internal friction and the inclination of the joint plane to the vertical are 30° and 60°, respectively. Calculate the factor of safety of the rock slope against plane failure.
- 6.15. Consider the rock slope shown in Figure 6.12 with the following details:

Height of the rock slope, H = 10 m

Unit weight of rock, $\gamma = 20 \text{ kN/m}^3$

Surcharge pressure, $q = 100 \text{ kN/m}^2$

Stabilising force, T = 100 kN/m

Depth of the tension crack, z = 2.5 m

Depth of water in the tension crack, $z_w = 2.5 \text{ m}$

Angle of inclination of stabilising force to the normal at the failure plane, $\alpha = 40^{\circ}$

Angle of shearing resistance of the joint material, $\phi = 25^{\circ}$

Cohesion of the joint plane material, $c = 32 \text{ kN/m}^2$

Angle of inclination of the slope face to the horizontal, $i = 50^{\circ}$

Angle of inclination of the joint plane/failure plane to the horizontal, $\theta = 35^{\circ}$

Horizontal seismic coefficient, $k_{\rm h} = 0.2$

Vertical seismic coefficient, $k_{x} = 0.1$

Calculate the factor of safety of the rock slope against plane failure. Assume that the height of tension crack is one-fourth of the height of the rock slope and the tension crack is completely filled with water.

- 6.16. Discuss about the optimum inclination of the anchor used for stabilising a sliding rock block separated by a sloping joint or bedding plane.
- 6.17. What is the difference between plane and wedge failures? Which one is the most common failure in field?
- 6.18. Derive an expression for the factor of safety of a rock slope against a simple wedge failure.
- 6.19. For the rock slope shown in Figure 6.15, consider the following: $i = 60^\circ$, $\beta = 40^\circ$, $\phi = 38^\circ$, $\theta_A = 40^\circ$ and $\theta_B = 45^\circ$. Calculate the factor of safety of the rock slope against wedge failure.
- 6.20. Is there any difference between slope failures in soils and rocks? Explain.
- 6.21. What are the different types of toppling failures? Explain with the help of neat sketches.
- 6.22. Discuss the conditions for toppling and sliding of a rock block resting in a joint plane.

- 6.23. What are the different rock slope stabilisation techniques and their classifications?
- 6.24. Discuss the suitability of rock bolting and anchoring for stabilising rock slopes.
- 6.25. What is the difference between a dowel and a rock bolt?
- 6.26. What is shotcrete? How does it differ from grouting?
- 6.27. Enumerate the factors that are considered for the selection of a stabilisation technique for a specific field application.

Answers:

6.1. c; 6.2. d; 6.3. b; 6.4. a; 6.5. c; 6.6. a; 6.7. b; 6.8. a; 6.9. c; 6.10. d

6.14. 1

6.15. 1.17

6.19. 126

REFERENCES

- Abramson, L.W., Lee, T.S., Sharma, S. and Boyce, G.M. (2002). *Slope Stability and Stabilization Methods*. John Wiley & Sons, New York.
- Alejano, L.R., Gomez-Marquez, I. and Martinez-Alegria, R. (2010). Analysis of a complex toppling-circular failure. *Engineering Geology*, Vol. 114, pp. 93–104.
- Bathurst, R.J., Hatami, K. and Alfaro, M.C. (2012). Geosynthetics-reinforced soil walls and slopes seismic aspects, in *Handbook of Geosynthetic Engineering*, 2nd edition, Shukla, S.K., editor, ICE Publishing, London, pp. 317–363.
- Bromhead, E.N. (1992). The Stability of Slopes. 2nd edition, Blackie Academic & Professional, Glasgow.
- Broms, B.B. and Wong, K.S. (1991). Landslides, in *Foundation Engineering Handbook*, Fang, H.Y., editor, Van Nostrand Reinhold. New York, pp. 410–446.
- Das, B.M. and Sivakugan, N. (2017). Fundamentals of Geotechnical Engineering. *Cengage*, pp. 774.
- Fookes, P.G. and Sweeney, M. (1976). Stabilization and control of local rockfalls and degrading rock slopes. *Quarterly Journal of Engineering Geology*, Vol. 9, pp. 37–56.
- Goodman, R.E. (1989). Introduction to Rock Mechanics. 2nd edition, John Wiley & Sons, New York.
- Goodman, R.E. and Kieffer, D.S. (2000). Behaviour of rock in slopes. *Journal of Geotechnical and Geoenvironmental Engineering*, Vol. 126, No. 8, pp. 675–684.
- Hoek, E. and Bray, J. (1981). Rock Slope Engineering. 3rd edition, Taylor & Francis, London. Hossain, M.M. and Shukla, S.K. (2010). Effect of vertical seismic coefficient on the stability of rock slopes against plane failure. Proceedings of the 6th Australasian Congress on Applied Mechanics, ACAM 6, 12–15 December 2010, Perth Convention Centre, Perth, Western Australia, Paper No. 1108.
- Lambe, T.W. and Whitman, R.V. (1979). Soil Mechanics, SI version. John Wiley & Sons, New York.
- Ling, H.I. and Cheng, A.H.D. (1997). Rock sliding induced by seismic force. *International Journal of Rock Mechanics and Mining Sciences*, Vol. 34, No. 6, pp. 1021–1029.
- Shukla, S.K. and Hossain, M.M. (2010). Design charts for rock slope stability against plane failure under seismic loading condition. *Proceedings of the ISRM International Symposium 2010 and 6th Asian Rock Mechanics Symposium*, 23–27 October 2010, New Delhi, India, Paper No. 64.

Shukla, S.K. and Hossain, M.M. (2011a). Analytical expression for factor of safety of an anchored rock slope against plane failure. *International Journal of Geotechnical Engineering*, Vol. 5, No. 2, pp. 181–187.

- Shukla, S.K. and Hossain, M.M. (2011b). Stability analysis of multi-directional anchored rock slope subjected to surcharge and seismic loads. *Soil Dynamics and Earthquake Engineering*, Vol. 31, Nos. 5–6, pp. 841–844.
- Shukla, S.K., Khandelwal, S., Verma, V.N. and Sivakugan, N. (2009). Effect of surcharge on the stability of anchored rock slope with water filled tension crack under seismic loading condition. *Geotechnical and Geological Engineering, an International Journal*, Vol. 27, No. 4, pp. 529–538.
- Shukla, S.K., Sivakugan, N. and Das, B.M. (2012). Slopes–stabilization, in *Handbook of Geosynthetic Engineering*, 2nd edition, Shukla, S.K., editor, ICE Publishing, London, pp. 223–243.
- Taylor, D.W. (1948). Fundamentals of Soil Mechanics. John Wiley & Sons, New York.
- Terzaghi, K. (1943). Theoretical Soil Mechanics. John Wiley & Sons, New York.
- Terzaghi, K., Peck, R.B. and Mesri, G. (1996). *Soil Mechanics in Engineering Practice*. John Wiley & Sons, New York.
- Wyllie, D.C. (1980). Toppling rock slope failures: Examples of analysis and stabilization. *Rock Mechanics*, Vol. 13, pp. 89–98.
- Wyllie, D.C. and Mah, C.W. (2004). Rock Slope Engineering. 4th edition, Spon Press, London.

7.1 INTRODUCTION

The word 'foundation' refers to both the load-bearing structural element of an engineering system (e.g. building, bridge, road, runway, dam, pipeline, tower or machine) located below the ground surface, and the earth mass that ultimately supports the loads from the engineering system.

Chapter 1 explains that rock is a hard, compact, naturally occurring earth material composed of one or more minerals, characterised by its permanence and durability in engineering applications. Most rocks generally require blasting for their excavation. Generally, a site consisting of rocks is usually recognised as the best foundation site for supporting structures because of the ability of rock mass to withstand much higher loads than the soil mass. In Chapters 1 and 4, we discussed that in situ rocks contain various types of discontinuities and planes of weakness (Figure 7.1), such as joints, fractures, bedding planes and faults. As a result, rocks at construction sites are often non-homogeneous and anisotropic in their properties. This complexity is why it has not been possible to develop a generalised approach for analysing foundations on rock. This chapter presents the description of shallow and deep foundations on rock to explain their fundamentals and some commonly used approaches to estimate the design value of their load-carrying capacity.

7.2 SHALLOW FOUNDATIONS

7.2.1 MEANING OF SHALLOW FOUNDATION

A foundation is classified as *shallow* if its depth (*D*) is typically less than or equal to its width (*B*). Therefore, for a shallow foundation,

$$\frac{D}{R} \le 1 \tag{7.1}$$

In practice, the ratio D/B of a foundation can be greater than unity and still be treated as a shallow foundation. The authors consider that a foundation can be described as shallow if its depth is less than or equal to about 3.5 m below the ground surface.

7.2.2 Types of Shallow Foundations

The most common types of shallow foundations on rock and soil are *spread footings* and *mats* (or *rafts*). A *spread footing* is simply an enlargement of a load-bearing wall or column that makes it possible to spread the load of the engineering system or structure over a large area of the rock and soil. The spread footing for supporting a long wall is called *strip footing*, which may have a length-to-width ratio more than 5.

DOI: 10.1201/9781032725161-7 **225**



FIGURE 7.1 Rock foundation for a barrel aqueduct at 44.900 km of the Bansagar Feeder Channel, Sidhi District, Madhya Pradesh, India: (a) foundation trench and (b) rock condition at the founding level. (After Sanjay Kumar Shukla, Allowable Load-Bearing Pressure for the Foundation of Barrel Aqueduct on Rock at km 44.900 of the Bansagar Feeder Channel, Dist. Sidhi, MP, India. A technical report dated 29 June 2007, Department of Civil Engineering, Institute of Technology, Banaras Hindu University, Varanasi, India, 2007.)

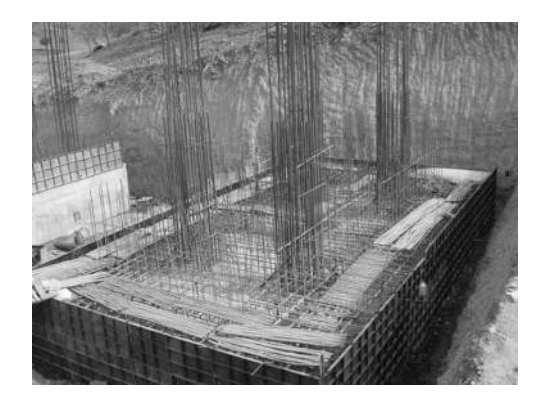


FIGURE 7.2 A raft foundation for an aqueduct under construction at 46.615 km of the Bansagar Feeder Channel, Sidhi District, Madhya Pradesh, India. (After Sanjay Kumar Shukla, Allowable Load-Bearing Pressure for the Foundation of Aqueduct on Rock/Soil at km 46.615 of the Bansagar Feeder Channel, Dist. Sidhi, MP, India. A technical report dated 7 June 2006, Department of Civil Engineering, Institute of Technology, Banaras Hindu University, Varanasi, India, 2006.)

A *mat* or *raft foundation* is a continuous slab constructed over the rock or soil bed to support an arrangement of columns and walls in a row or rows (Figure 7.2). Mat foundations are preferred for weak soils and heavily jointed and fractured rock masses that have low bearing capacities but that will have to support high column and/or wall loads. A mat that supports two columns is called *combined footing*. Mat foundations undergo significantly reduced differential settlements compared to those for spread footings.

7.2.3 DEPTH OF FOUNDATION

For shallow foundations resting on a rock, the depth of the rock, which is weathered or fissured, is generally excluded when determining the depth of foundation in the rock. The foundation level is established at sufficient depth so as to ensure that it is not undermined, keeping in view the continued erosion of the rock bed. In hard rocks, with an ultimate compressive strength of 10 MPa or above arrived at after considering the overall characteristics of the rock, such as fissures, joints and bedding planes, the minimum depth of foundation is taken as 0.6 m, whereas in all other types of rock, it is 1.5 m.

7.2.4 LOAD-BEARING CAPACITY TERMS

The load per unit area at the base level of foundation that causes shear failure to occur in the earth mass (soil or rock) is termed the *ultimate bearing capacity* (q_n) of the foundation. This capacity depends on the characteristics of the earth mass and is also governed by the geometric dimensions of the foundation and its depth below the ground surface. The safe bearing capacity (q_n) is the pressure at the base level of foundation that can be safely carried by the foundation without shear failure of the earth mass. The load per unit area at the base level of foundation that causes permissible or specified settlement of the engineering system is called the *safe bearing* pressure (q_s) . The lower of the safe bearing capacity and the safe bearing pressure is called the allowable bearing pressure (a_n). If the ultimate bearing capacity, safe bearing capacity, safe bearing pressure and allowable bearing pressure are estimated by deducting the effective overburden pressure at the base level of foundation, they are termed the net ultimate bearing capacity (q_{nn}) , net safe bearing capacity (q_{nn}) , net safe bearing pressure (q_{no}) and net allowable bearing pressure (q_{no}) , respectively. The value of the net allowable bearing pressure (q_{na}) is generally recommended for design of shallow foundations. Note that in practice, the term 'allowable bearing pressure' usually refers to 'net allowable bearing pressure'.

7.2.5 Estimation of Load-Bearing Capacity

The compressive strength of rocks varies widely, ranging from less than 10 MPa to over 300 MPa (see Figure 3.7 in Chapter 3). If a construction site consists of strong/hard rock, shallow foundations such as spread footings can support substantial loads; however, the presence of a single discontinuity plane in a particular direction (Figure 7.1) can cause sliding failure of the foundation. Discontinuities in rock also causes reduced bearing capacity of the foundation supported by the rock. Rock without discontinuities rarely occurs at or near the ground surface at the specific construction site. Therefore, it becomes essential to estimate the realistic values of the bearing capacity of foundations on rock, considering the presence of discontinuities.

Determining the bearing capacity of foundations on rock with inherent weaknesses is challenging due to significant variations in these weaknesses from site to site, and even within different locations of the same site. This variability is a result of the rock's non-homogeneous and anisotropic characteristics. Usually, the net allowable

bearing pressure to be used for design is restricted by the *local building code*; however, geology, rock type and quality (as RQD), as discussed in the previous chapters, are critical parameters that should be used together with the recommended code value. With the exception of a few porous limestone and volcanic rocks and some shales, the strength of bedrock in situ is greater than the compressive strength of the foundation concrete. Therefore, design values of net allowable bearing pressure are often limited by the strength of concrete. If concrete foundation is submerged under water, the bearing value of concrete should be reduced, and the allowable bearing pressure of a foundation on rock is further complicated by the possibility of rock softening. Common sandstones and limestones exhibit modulus of elasticity values that range from those similar to poor-quality concrete to those of high strength concrete. Very hard igneous and metamorphic rocks exhibit considerably greater modulus of elasticity values. Almost all rocks can withstand a compressive stress higher than concrete; the following are some of exceptions (Teng, 1962):

- 1. Limestones with cavities and fissures, which may be filled with clay or silt.
- Rocks with bedding planes, folds, faults or joints at an angle to the bottom of the footing.
- Soft rocks that reduce their strength after wetting; weathered rocks, which are very treacherous; and shale, which may become clay or silt in a matter of hours of soaking.

Some attempts have been made to present the theoretical solution for the bearing capacity of strip footings on jointed rock masses (Yu and Sloan, 1994; Prakoso and Kulhawy, 2004). The theoretical approach requires an idealisation of the strength of the intact rock, as well as the strength, spacing and orientation of the discontinuities. Because of a wide variation of these factors, it is rarely possible to present a generalised bearing capacity equation for foundations on rock in the way it is done for foundations on soil. In practice, empirical approaches of estimating the allowable bearing pressure are widely used, and some of them are discussed here.

Settlement of rock foundation is more often of concern than its bearing capacity. Therefore, for shallow foundations on rock, it is generally found that $q_{\rm np} < q_{\rm ns}$; therefore, $q_{\rm na} = q_{\rm np}$. If $q_{\rm np}$ is calculated based on the plate load test (Shukla and Sivakugan, 2011), the permissible settlement is taken as 12 mm even for larger loaded areas (BIS, 2005). In the case of rigid structures such as reinforced concrete silos, the permissible settlement may be increased judiciously, if required. If the spacing of discontinuities in rock foundation is wide (1–3 m) or very wide (>3 m), $q_{\rm np}$ for preliminary design of shallow foundations on rock can be determined from the classification of rock mass as given in Table 7.1.

The Indian Roads Congress (IRC) suggests that the allowable pressure values of rocks for average condition may be taken as follows (IRC, 2000): for hard rocks, $q_{\rm na} = 2-3$ MPa; for soft rocks, $q_{\rm na} = 1-2$ MPa; and for weathered rocks, conglomerates and laterites, $q_{\rm na} < 1$ MPa. These values should be modified after considering the various characteristics of rocks at the construction site.

If the spacing of discontinuities in a rock foundation is moderately close (0.3–3 m), $q_{\rm np}$ for design of shallow foundations on rock can be determined from the strength of the rock cores obtained during subsurface investigation.

TABLE 7.1

Net Safe Bearing Pressure Based on Classification

Type of rock	Net safe bearing pressure, q_{np} (MPa)
Massive crystalline bedrock including granite, diorite and gneiss	10
Foliated rocks such as schist and slate in sound condition	4
Bedded limestone in sound condition	4
Sedimentary rocks including hard shale and sandstone	2.5
Soft or heavily fractured bedrock (excluding shale) and soft limestone	1
Soft shale	0.4

Source: Adapted from BIS, Code of Practice for Design and Construction of Shallow Foundations on Rocks. IS: 12070–1987 (Reaffirmed 2005), Bureau of Indian Standards (BIS), New Delhi, India, 2005.

If the spacing of discontinuities in a rock foundation is moderately close (0.3–3 m), the net allowable bearing pressure ($q_{\rm np}$) for the design of shallow foundations on rock can be determined based on the strength of the rock cores obtained during subsurface investigation.

If $q_{\rm u(av)}$ is the average unconfined compressive strength of rock cores, the safe bearing pressure, $q_{\rm o}$, can be given as

$$q_{\rho} = q_{\mathrm{u(av)}} N_{\mathrm{d}} \tag{7.2}$$

where $N_{\rm d}$ is an empirical coefficient depending on the spacing of discontinuities and is expressed as

$$N_{\rm d} = \frac{3 + S/B}{10\sqrt{1 + 300(\delta/S)}} \tag{7.3}$$

where δ is the thickness (aperture) of discontinuities, S is the spacing of discontinuities and B is the width of footing. For spacing of discontinuities of 0.3–1, 1–3 and 3 m, the typical values of $N_{\rm d}$ are 0.1, 0.25 and 0.4, respectively. It may be noted that Equation 7.2 is valid under the following six conditions (BIS, 2005):

- 1. The rock surface is parallel to the base of the foundation.
- 2. The structural load is normal to the base of the foundation.
- 3. The spacing of discontinuities is greater than 0.3 m.
- 4. The aperture (opening) of discontinuities is less than 10 mm (15 mm if filled with soil and rock debris).

- 5. The foundation width is greater than 0.3 m.
- 6. The factor of safety is 3.

EXAMPLE 7.1

A strip footing of 1.2 m width rests on the bedrock exposed at the ground surface. The bedrock is horizontally bedded with spacing S = 0.8 m, aperture $\delta = 8$ mm and $q_{\text{n(av)}} = 80$ MPa. Estimate the safe bearing pressure.

Solution

Given: B = 1.2 m, S = 0.8 m, aperture $\delta = 8$ mm and $q_{u(av)} = 80$ MPa. From Equation 7.3,

$$N_{\rm d} = \frac{3 + (0.8)/(1.2)}{10\sqrt{1 + 300(0.008/0.8)}} = 0.18$$

From Equation 7.2,

$$q_{p} = (80)(0.18) = 14.4 \,\mathrm{MPa} \,\mathrm{or} \, 14400 \,\mathrm{kPa}$$

In many cases, the allowable bearing pressure is estimated as a fraction – typically between one-third and one-tenth – of the unconfined compressive strength obtained from intact rock sample, with the rock quality designation (RQD) used as a guide. For instance, a lower value, around one-tenth, is applied when RQD is small. When the RQD of the foundation rock tends to zero, one should treat it as soil mass and obtain the allowable bearing pressure using the bearing capacity theories for soils.

While recommending the allowable bearing pressure, it is important that the geological conditions and discontinuities present at the rock foundation site be analysed properly because they greatly control the net allowable bearing pressure compared to the strength of intact rock mass. For example, in Figure 7.3, the rock foundation

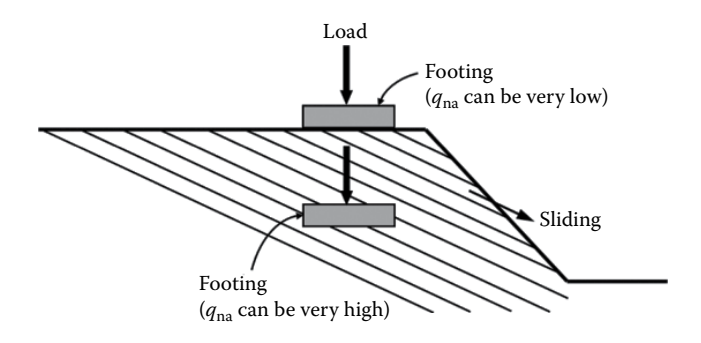


FIGURE 7.3 An example of the importance of consideration of geological condition and presence of discontinuities while recommending the net allowable bearing pressure for design of foundations on rock.

consists of rock beds dipping away from the slope, and therefore, a surface footing may be unstable due to the possible slides of the underlying top rock beds, while a footing at some depth may be stable. The readers can refer to the book by Wyllie (1999) for more geological details.

7.3 DEEP FOUNDATIONS

7.3.1 Meaning of Deep Foundation

The foundation is classified as deep if its depth (D) is greater than its width (B). Therefore, for a deep foundation,

$$\frac{D}{R} > 1 \tag{7.4}$$

Even if the condition in Equation 7.4 is not met, the authors suggest that a foundation can still be classified as deep if its depth extends more than approximately 3.5 m below the ground surface.

Deep foundations are commonly employed when the near-surface soil is highly compressible or too weak to support the load from the superstructure, enabling the load to be transferred to a stronger underlying soil layer or bedrock.

7.3.2 Types of Deep Foundations

The most common types of deep foundations on rock and soil are *piles* and *drilled piers*. *Piles* are structural members that are made of steel, concrete and/or timber. Placing a structure on pile foundations is much more expensive than having it on spread footings and is likely to be more expensive than a raft foundation. A *drilled pier* (also known as a *drilled shaft, drilled caisson* or simply *caisson*, or *bored pile*) is a cast-in-place pile, generally having a diameter of about 2.5 ft (\approx 750 mm) or more. It is constructed by drilling a cylindrical hole into the ground and subsequently filling it with concrete along with reinforcement (Figure 7.4) or no reinforcement.

If subsurface records establish the presence of rock or rock-like material at a site within a reasonable depth, piles are generally extended to the bedrock and socketed properly, if required (Figure 7.5a). In this case, based on the strength of bedrock or rock-like material, the *ultimate load-carrying capacity* ($Q_{\rm u}$) of the piles depends entirely on the load-bearing capacity of the bedrock or rock-like material, and the piles are called *point-bearing piles or end-bearing piles*, and therefore it is given as

$$Q_{\rm u} = Q_{\rm p} \tag{7.5a}$$

where Q_p is the *load-carrying capacity of the pile point/tip*, that is, the *point capacity* or *end-bearing capacity* of the pile. Rock-socketted piles are discussed separately in Section 7.4.

When bedrock or rock-like material is not available at a reasonable depth below the ground surface, piles can be designed to transmit the structural load through





FIGURE 7.4 A bored pile/drilled pier in fractured and weathered rock under construction at 52.106 km of the Bansagar Feeder Channel, Sidhi District, Madhya Pradesh, India: (a) before concrete filling and (b) after concrete filling. (After Sanjay Kumar Shukla, The pile termination at km 52.106 of the Bansagar Feeder Channel, Dist.—Sidhi, MP, India. A technical report dated 17 December 2008, Department of Civil Engineering, Institute of Technology, Banaras Hindu University, Varanasi, India, 2008.)

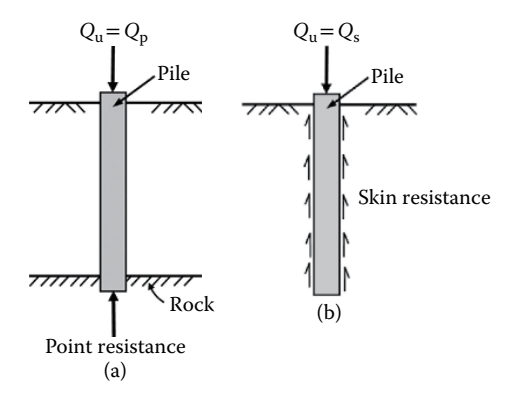


FIGURE 7.5 (a) Point-bearing pile and (b) friction pile.

friction and/or adhesion to the soil adjacent to the pile only or to both the adjacent soil and the underlying firm soil stratum, if available. The piles that transmit loads to the adjacent soil through friction and/or adhesion are called *friction piles* (Figure 7.5b) and therefore

$$Q_{\rm u} = Q_{\rm s} \tag{7.5b}$$

where Q_s is frictional resistance of the pile.

The piles in heavily jointed/fractured and weathered rocks, where bedrock does not exist at a reasonable depth, are generally designed considering them as both point-bearing and friction piles, the way they are designed in soils; thus, the *ultimate load-carrying capacity* of the pile is given as

$$Q_{\rm u} = Q_{\rm p} + Q_{\rm s} \tag{7.6}$$

The estimation of Q_p and Q_s for piles in soils, including heavily jointed/fractured and weathered rocks that behave similar to soils, is described in detail in most geotechnical books. This chapter discusses the estimation of load-carrying capacity of piles resting on bedrock only.

7.3.3 Estimation of Load-Carrying Capacity

A pile resting on bedrock or rock-like material is typically designed to transfer large structural loads, with its ultimate load-carrying capacity calculated based solely on its point or end-bearing capacity, $Q_{\rm p}$ (Equation 7.5a). The point capacity of a pile resting on bedrock or rock-like material is typically calculated in two steps: (1) determining the capacity based on the strength of the rock or rock-like material and (2) determining the capacity based on the yield strength of the pile material. The lower of these two values is then used as the design point capacity. Unless a pile is bearing on soft rock such as shale or other poor-quality rocks (RQD < 50), the capacity calculated from the strength of rock is higher than that calculated from the yield strength of the pile material. Therefore, in most cases, calculation of the load-carrying capacity of the pile resting on rock based on the yield strength of the pile material is sufficient (Kumar, 2011). The ultimate unit point resistance in rock is approximately (Goodman, 1980; Das, 2022)

$$q_{p} = q_{u} \left(N_{\phi} + 1 \right) \tag{7.7}$$

where $q_{\rm u}$ is the unconfined compressive strength of rock,

$$N_{\phi} = \tan^2 \left(45^{\circ} + \phi / 2 \right) \tag{7.8}$$

and ϕ is the drained angle of internal friction.

The unconfined compressive strength of rock is generally determined in the laboratory by conducting unconfined compression strength tests on small-diameter cylindrical intact rock specimens prepared from rock samples collected during subsurface investigation. It is observed that the unconfined compressive strength of rock decreases as the diameter of laboratory rock specimen increases, which is referred to as the *scale effect*. For rock specimens larger than about 1 m in diameter, the value of $q_{\rm u}$ remains approximately constant. There appears to be a fourfold to fivefold reduction in the magnitude of $q_{\rm u}$ in this process. The scale effect is primarily influenced by randomly distributed fractures, both large and small, as well as by progressive ruptures along the slip lines. Therefore, it is generally recommended that

TABLE 7.2

Typical Values of Laboratory Unconfined Compressive Strength and Drained Friction Angle of Some Rocks

Rock type	Unconfined compressive strength, q _u (MPa)	Drained angle of internal friction φ (Degrees)
Sandstone	70–140	27–45
Limestone	105–210	30–40
Shale	35–70	10–20
Granite	140–210	40–50
Marble	60–70	25–30

$$q_{\rm u(design)} = \frac{q_{\rm u(lab)}}{5} \tag{7.9}$$

Table 7.2 lists $q_{\rm u(lab)}$ and ϕ values for some rocks. Substituting $q_{\rm u}$ in Equation 7.7 with $q_{\rm u(design)}$ from Equation 7.9,

$$q_{\rm u} = \left[\frac{q_{\rm u(lab)}}{5}\right] \left(N_{\phi} + 1\right) \tag{7.10}$$

The point capacity or end-bearing capacity of the pile is

$$Q_{p} = q_{p}A_{p} \tag{7.11}$$

where $A_{\rm p}$ is the area of the pile point. Substituting $q_{\rm p}$ from Equation 7.10 into Equation 7.11,

$$Q_{\rm p} = \left[\frac{q_{\rm u(lab)}}{5} \right] \left(N_{\phi} + 1 \right) A_{\rm p} \tag{7.12}$$

From Equations 7.5a and 7.12,

$$Q_{\rm u} = \left[\frac{q_{\rm u(lab)}}{5} \right] \left(N_{\phi} + 1 \right) A_{\rm p} \tag{7.13}$$

The design load-carrying capacity or allowable load-carrying capacity of a pile is defined as

$$Q_{\rm a} = \frac{Q_{\rm u}}{\rm FS} \tag{7.14}$$

where FS is a factor of safety, depending on the uncertainties in the estimation of $Q_{\rm u}$. It is common to use large safety factors in estimating the load-carrying capacity of

rock foundation. The FS should be somewhat dependent on RQD, defined in Chapters 1 and 3. For example, an RQD of 80% would not require as high an FS as for ROD = 40%. It is common to use FS from 2.5 to 10.

From Equations 7.13 and 7.14,

$$Q_{\rm a} = \left[\frac{q_{\rm u(lab)}}{5} \right] \left[\frac{\left(N_{\phi} + 1 \right) A_{\rm p}}{\rm FS} \right] \tag{7.15}$$

Based on the yield strength (f_y) of the pile material, the ultimate load-carrying capacity of the pile is given as

$$Q_{\rm u} = f_{\rm v} A_{\rm p} \tag{7.16}$$

From Equations 7.14 and 7.16,

$$Q_{\rm a} = \frac{f_{\rm y}A_{\rm p}}{\rm FS} \tag{7.17}$$

The values of $Q_{\rm a}$ calculated from Equations 7.15 and 7.17 are compared, and the lower value is taken as the allowable point capacity of the pile for the design purposes.

EXAMPLE 7.2

A pile of diameter of 60 cm and length of 10 m passes through the highly jointed and weathered rock mass and rests on a shale bed. For shale, laboratory unconfined compressive strength = 38 MPa and drained friction angle = 26° . Estimate the allowable point capacity of the pile. Assume that the pile material has sufficient strength and use a factor of safety of 5.

Solution

Given that diameter D=60 cm = 0.6 m, length L=10 m, $q_{u(lab)}=38$ MPa and $\phi=26^\circ$, the area of the pile tip is

$$A_{\rm p} = \left(\frac{\pi}{4}\right)D^2 = \left(\frac{3.14}{4}\right)(0.6)^2 = 0.2826\,\mathrm{m}^2$$

From Equation 7.8,

$$N_{\phi} = \tan^2(45^{\circ} + 13^{\circ}) = 2.56$$

From Equation 7.15,

$$Q_{a} = \left[\frac{38}{5}\right] \left[\frac{(2.56+1)(0.2826)}{5}\right] = 1.529 \,\text{MN or } 1529 \,\text{kN}$$

7.4 ROCK-SOCKETTED PILES

Rock-socketted piles or shafts are the preferred option when there is possibility of transferring the loads from the superstructure to the competent bearing stratum located at a certain depth beneath the ground level. They also limit the settlements. They transfer the load to the sockets through the side shear resistance and end-bearing resistance.

7.4.1 Ultimate Load-Carrying Capacities $Q_{\text{side,uit'}}$ $Q_{\text{base,uit'}}$ and Q_{uit}

The ultimate load-carrying capacity of the rock socket can be determined as

$$Q_{ult} = Q_{side\ ult} + Q_{base\ ult} \tag{7.18}$$

where $Q_{\rm side,ult}$ and $Q_{\rm base,ult}$ are the ultimate load-carrying capacities of the side and the base, respectively, of the rock socket. They can be determined as

$$Q_{side,ult} = \pi B D_s f_s \tag{7.19}$$

$$Q_{base,ult} = \pi \frac{B^2}{4} q_b \tag{7.20}$$

where B = shaft diameter, D_s = socket length, f_s = ultimate unit side friction and q_b = ultimate end-bearing capacity (see Figure 7.6). Once f_s and q_b are known, the ultimate load-carrying capacity $Q_{\rm ult}$ of the rock-socketted pile can be determined from Equations (7.18), (7.19) and (7.20).

O'Neill and Reese (1999) noted that it only takes 6-10 mm movement for the entire side friction to be mobilised. This movement is in the order of 0.5-1.0% of the pile diameter (Haberfield and Collingwood, 2006). The mobilised friction along the socket walls remains constant with further movement. It requires much larger movements, in the order of few centimetres, for the entire base resistance to mobilise. This behaviour is similar to what has been seen with pile foundations in soils as well. It can be seen from Figure 7.7 that at working loads, even at relatively small pile head settlements, the load transferred to the base can be significant, in the order of 10% to 40% of the total load (Akgüner and Kirkit, 2012; Crapps and Schmertmann, 2002; Zhang and Xu, 2009). Therefore, it is necessary to compute the two components in determining the Q_{nl} . Nevertheless, some designers conservatively neglect the end bearing and assume that the entire load is carried by the side friction, which is fully mobilised. The most common reason given for neglecting the end-bearing resistance is the concern for underlying cavities, reluctance to inspect the bottom and the difficulty in estimating the end-bearing resistance. The larger the D/B ratio, lower the fraction of the load transferred to the base. The greater the rock stiffness, smaller the fraction of the load transferred to the base. The fraction of the load transferred to the base is influenced by D_s/B and E_r/E_c , where E_r and E_c are Young's moduli of the rock and concrete, respectively. Based on the theoretical studies carried out by Osterberg and Gill (1973) and their data, Ladanyi (1977) proposed Figure 7.8 as the

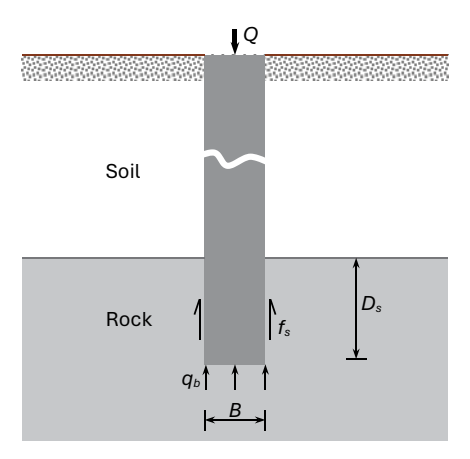


FIGURE 7.6 Schematic diagram of drilled shaft.

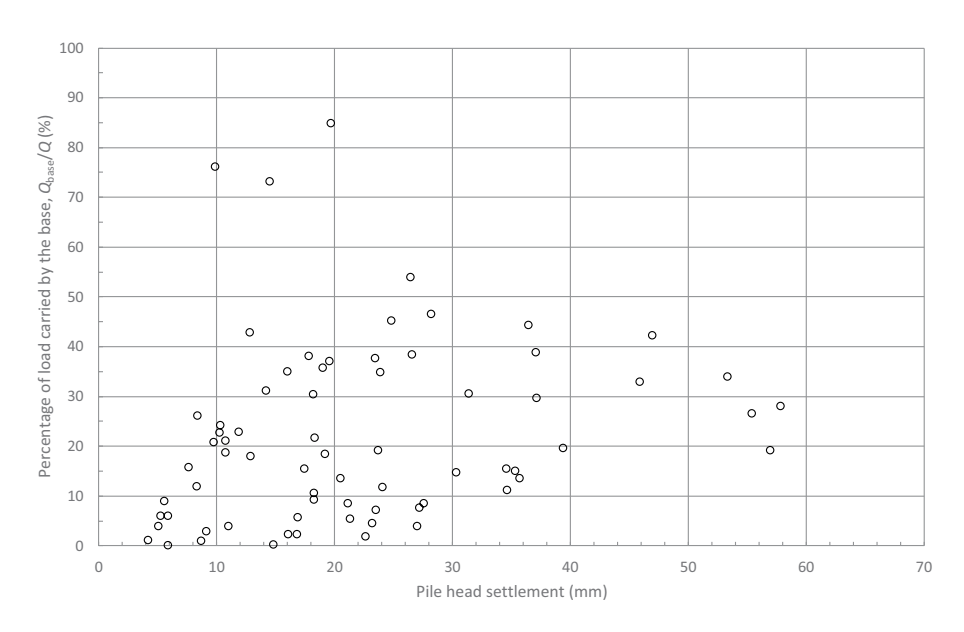


FIGURE 7.7 Percentage of the load carried by the base versus the pile head settlement. (Adapted from Zhang, 2010.)

basis for estimating the proportion of the pile load carried by the pile base, for D_s/B from 0.5 to 2.

Extensive field load test data on rock-socketted piles also suggest that up to 25% of the load applied at the top on the pile head can be carried by the base even at relatively small settlements, and the fraction carried by the base increases with time due to creep (Zhang, 2010).

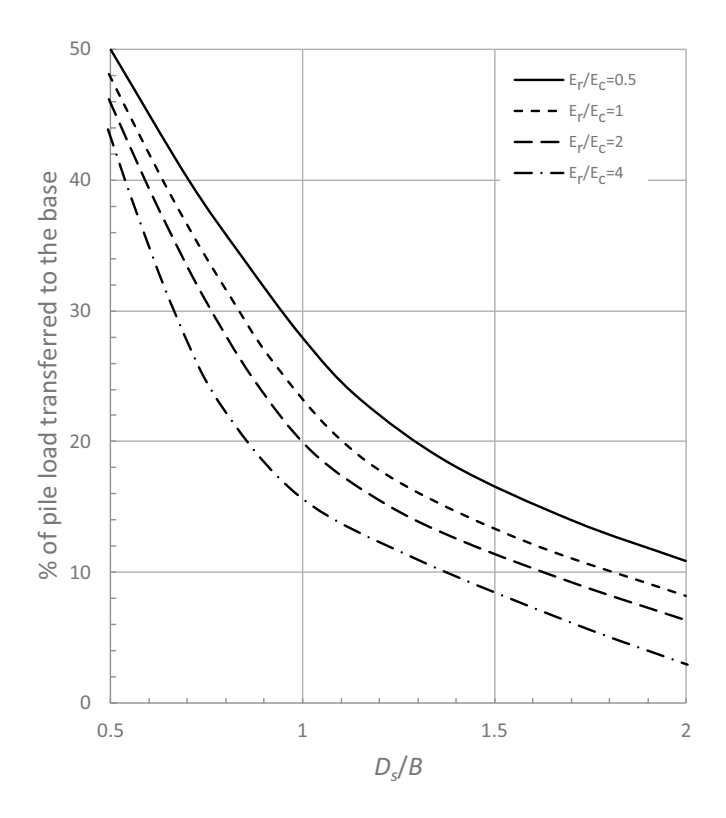


FIGURE 7.8 Percentage of pile load transferred to the base. (After Ladanyi, 1977.)

7.4.2 Ultimate Side Shear Resistance f_s

In its simplest form, the ultimate side friction f_s is expressed generally as

$$\frac{f_s}{p_a} = a \left(\frac{\sigma_c}{p_a}\right)^b \tag{7.21}$$

where a and b are constants, σ_c = unconfined compressive strength (UCS) of the *intact rock*, and p_a = atmospheric pressure (101.3 kN/m²). A range of values has been proposed for a and b based on load test data (see Table 7.3). While the study by Rowe and Armitage (1987) appears to be well received, the suggestion by Horvath and Kenney (1979) is seen as a good lower bound for 90% of the data (Carter and Kulhawy, 1988). CGS (1992) suggests b = 0.5 and a = 1.42, and endorses the Carter and Kulhawy (1988) value of a = 0.63 as the lower bound.

Carter and Kulhawy (1988) also suggested that in the absence of load test data, in situ tests or local experience, f_s should be computed conservtively as

$$f_s = 0.15\sigma_c \tag{7.22}$$

TABLE 7.3

Equations for the Ultimate Skin Friction f_s

Authors	Equation	Comments
Rosenberg and Journeaux (1976)	$\frac{f_s}{p_a} = 1.09 \left(\frac{\sigma_c}{p_a}\right)^{0.52}$	Based on only six data points with $\sigma_c/p_a = 5$ to 340.
Horvath and Kenney (1979)	$\frac{f_s}{p_a} = 0.65 \sqrt{\frac{\sigma_c}{p_a}}$	Diameter > 400 mm, with $\sigma_c/p_a = 1$ to 400. Lower bound.
Rowe and Armitage (1987)	$\frac{f_s}{p_a} = 1.42 \sqrt{\frac{\sigma_c}{p_a}}$	More than 80 piles from 20 sites, with $\sigma_e/p_a = 4$ to 400.
Meigh and Wolski (1979)	$\frac{f_s}{p_a} = 0.55 \left(\frac{\sigma_c}{p_a}\right)^{0.6}$ $f_s = 0.25\sigma_c$	Lower bound for weak rocks of σ_c/p_a = 7 to 125 For σ_c/p_a = 4 to 7
Williams et al. (1980)	$f_s = 0.230_c$ $\frac{f_s}{p_a} = 1.84 \left(\frac{\sigma_c}{p_a}\right)^{0.37}$	36 load tests from Australia with $\sigma/p_a = 5$ to 800.
Carter and Kulhawy (1988)	$\frac{f_s}{p_a} = 0.63 \sqrt{\frac{\sigma_c}{p_a}}$	From Rowe and Armitage data. Lower bound to 90% data. For $\sigma_c/p_a < 20$, $f_s = 0.15 \ \sigma_c$.
Fleming et al. (1992)	$\frac{f_s}{p_a} = 1.3 \sqrt{\frac{\sigma_c}{p_a}}$	Rough shaft and full keying between the concrete and host rock. f_s to be less than 5% of concrete strength f_c .
Zhang and Einstein (1998)	$\frac{f_s}{p_a} = 1.26 \sqrt{\frac{\sigma_c}{p_a}}$	All available data till then.
O'Neill and Reese (1999)	$\frac{f_s}{p_a} = 0.65 \sqrt{\frac{\sigma_c}{p_a}}$	Smooth socket
Prakoso (2002)	$\frac{f_s}{p_a} = \sqrt{\frac{\sigma_c}{p_a}}$	More systematic analysis of a larger database.
Brown et al. (2010)	$\frac{f_s}{p_a} = 0.65c_E \sqrt{\frac{\sigma_c}{p_a}}$	c_E is a coefficient to account for the degree of fracturing that can be determined from RQD. Default is 1.0.

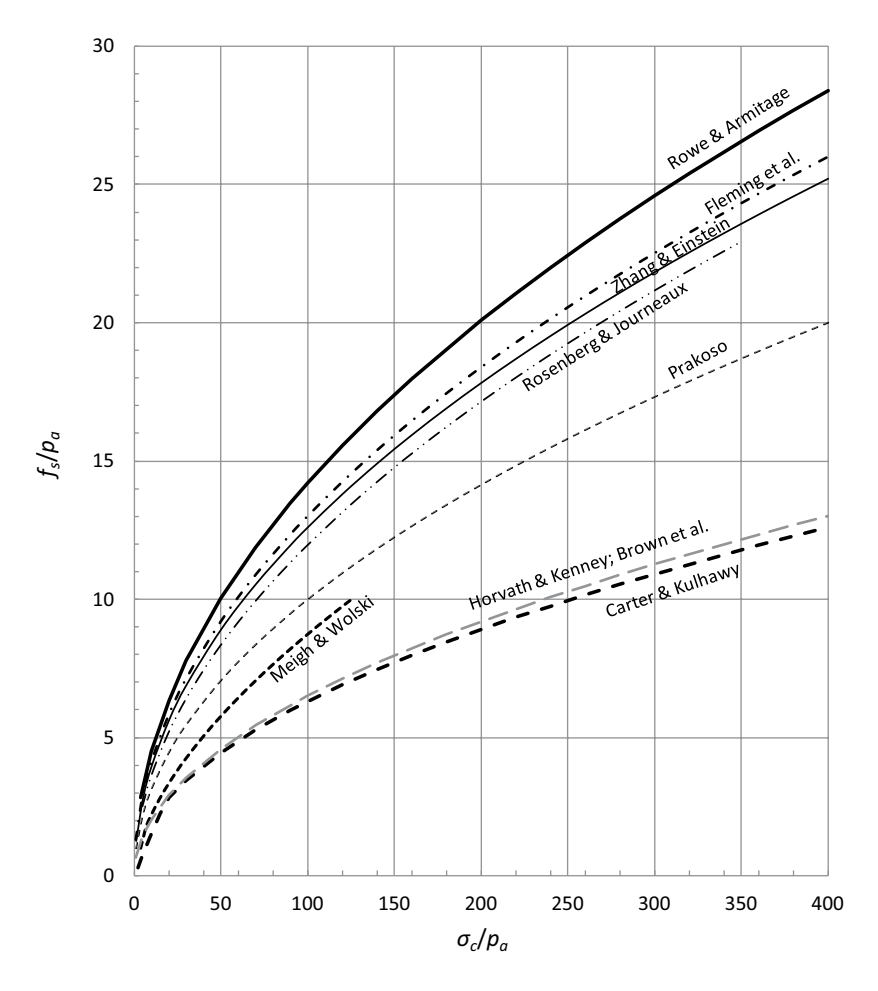


FIGURE 7.9 Normalised side friction values.

Equation (7.22) is generally preferred for situations where σ_c/p_a is less than 20. Further, f_s should not exceed 5% of the compressive strength of concrete f_c , to avoid bond failure at the interface, unless there is enough data to justify higher values. The different recommendations listed in Table 7.3 are compared graphically in Figure 7.9. Once f_s is determined, the ultimate load-carrying capacity of the side can be obtained from Equation (7.19).

Figure 7.10 shows the teeth of a drilling bucket that digs the soil or rock out of the formation. There are separate buckets to clean out the bases of the holes, which have cutting blades rather than teeth for better removal of the cuttings. Typically, they produce a rough socket.

7.4.3 Ultimate End-Bearing Capacity q_b

In its simplest form, the ultimate end-bearing capacity q_b is related to the uniaxial compressive strength of the intact rock σ_c . With the significant role played by the

Foundations on Rock 241



FIGURE 7.10 Drilling bucket used for bored pier.

discontinuities on q_b , it is even better to relate q_b to the uniaxial strength of the rock mass σ_{cm} .

q_b in terms of σ_c

The end bearing of socketed shafts is less understood than the side shear resistance. In its simplest form, the ultimate end-bearing capacity of the rock socket can be written as

$$q_b = N_{cr} \, \sigma_c \tag{7.23}$$

where N_{cr} is the bearing capacity factor for rock. Here, it is implied that the ultimate end-bearing capacity q_b is proportional to the unconfined compressive strength of the intact rock σ_c . Values for N_{cr} in the range of 2.5 to 8.0 have been suggested in the early years (e.g. Teng, 1962; Coates, 1967; Rowe and Armitage, 1987). Considering the work of Prakoso and Kulhawy (2004), Rowe and Armitage (1987) and Zhang and Einstein (1998), Brown et al. (2010) suggested N_{cr} be conservatively taken as 2.5, which is more or less the lower bound of the values suggested previously. These values appear to be reasonable when the rock is massive with no discontinuities.

Some researchers have suggested that the ultimate end-bearing capacity $q_{\rm b}$ and $\sigma_{\rm c}$ are related non-linearly by

$$q_b(MPa) = c\sigma_c^d \tag{7.24}$$

where σ_c is the UCS in MPa. In competent rock, the structural capacity of the concrete will govern the design. If the unconfined compressive strength of the concrete f_c is less than that of the rock, f_c it should be used in place of σ_c . Some values for c and d reported in the literature are given in Table 7.4.

In the different empirical equations for estimating the ultimate end-bearing capacity q_b (see Equation (7.24) and Table 7.4), the respective authors have very different definitions of q_b . Very often, q_b is defined as the bearing capacity of the base corresponding to settlement (either head or tip) of a fraction of the pile diameter (e.g. 10% of d).

TABLE 7.4	
Values of c and d for Equation	(7.24)

Authors	c	d	Comments
Zhang and Einstein (1998)	4.83	0.51	39 pile load tests
Vipulanandan et al. (2007)	4.66	0.56	21 pile load tests
Zhang (2008)	4.93	0.5	50 pile load tests
Rowe and Armitage (1987)	2.7	1	
Coates (1967)	3	1	
ARGEMA (1992)	4.5	1	$q_{\scriptscriptstyle b} \leq 10 \; \mathrm{MPa}$

All the above simplified methods relate q_b to the UCS of the intact rock, $\sigma_{\rm c}$. It is obvious that the presence of discontinuities can have significant influence here and hence it is appropriate to bring the rock mass quality into the picture.

AASHTO (1996) suggested that the end-bearing capacity can be estimated by

$$q_b = N_{ms}\sigma_c \tag{7.25}$$

where N_{ms} is a factor which depends on the rock type and the rock mass quality. These values are given in Table 7.5. It can be seen that N_{ms} is influenced more by the rock mass quality than the rock category. For example, rock mass quality described as 'Good' has N_{ms} in a narrow range of 0.28 to 0.46. However, for rock category D, depending on the rock mass quality, N_{ms} can be in a wide range of 0.02 to 5.2.

Rock categories for Table 7.5.

- A: Carbonate rocks with well-developed crystal cleavage (Dolostone, Limestone, Carbonatite, Marble, Tactite-Skarn)
- B: Lithified argillaceous rock (Argillite, Claystone, Marlstone, Phyllite, Siltstone, Shale, Slate)
- C: Arenaceous rocks with strong crystals and poor cleavage (Conglomerate, Sandstone, Quartzite)
- D: Fine-grained igneous crystalline rock (Andesite, Diabase)
- E: Coarse-grained igneous and metamorphic rock (Amphibolite, Gabbro, Gneiss, Granite, Quartzdiorite)

q_b in terms of σ_{cm}

Rock-socketted shafts are supported by the rock mass, where the socket strength is influenced by the discontinuities. A simple but crude measure of the discontinuities is the RQD. Goodman (1980) noted that the ultimate end-bearing capacity is theoretically given by

$$q_b = \sigma_{cm} \left[1 + \tan^2 \left(45 + \frac{\phi}{2} \right) \right] \tag{7.26}$$

TABLE 7.5 $N_{\rm ms}$ Coefficients

Rock mass		RMR	NGI	RQD		N _{ms}							
Quality	General description	Rating	Rating	(%)	Α	В	C	D	E				
Excellent	Intact rocks with joints spaced at $> 3 \text{ m}$ (10 ft)	100	500	95-100	3.8	4.3	5.0	5.2	6.1				
Very good	Tightly interlocking undisturbed rock with rough, unweathered joints spaced 0.9–3 m (3–10 ft) apart	85	100	90–95	1.4	1.6	1.9	2.0	2.3				
Good	Fresh to slightly weathered rock, slightly disturbed, with joints spaced 0.9–3 m (3–10 ft) apart	65	10	75–90	0.28	0.32	0.38	0.40	0.46				
Fair	Rock with several sets of moderately weathered joints spaced 0.3–0.9 m (1–3 ft) apart	44	1	50–75	0.049	0.056	0.066	0.069	0.081				
Poor	Rock with numerous weathered joints spaced 25–500 mm (1–20 inches) apart with some gouge	23	0.1	25–50	0.015	0.016	0.019	0.020	0.024				
Very poor	Rock with numerous highly weathered joints spaced < 50 mm (2 inches) apart	3	0.01	< 25	Use q_b for	or equivalen	t soil mass						

Note: After Hoek, 1983; AASHTO, 1996.

where σ_{cm} = unconfined compressive strength of the *rock mass*, which can be significantly less than that of the intact rock σ_c . AASHTO (1996) relates the uniaxial compressive strengths of the rock mass (σ_{cm}) and the intact rock (σ_c) by

$$\sigma_{cm} = \alpha_E \sigma_c \tag{7.27}$$

where $a_{\scriptscriptstyle F}$ is the reduction factor given by

$$\alpha_{\rm F} = 0.0231(RQD\%) - 1.32 \ge 0.15$$
 (7.28)

Equation (7.28) suggests that the reduction factor $a_E = 0.15$ when RQD < 64%. Zhang (2010) noted that the reduction factor a_E is applicable to the modulus of deformation E and not to the strength σ_c . He showed that $\alpha_E^{0.7}$ should be used on strength, when relating σ_{cm} and σ_c in Equation (7.27). Further, he showed that

$$q_b = 6.39\sigma_{cm}^{0.45} \tag{7.29}$$

EXAMPLE 7.3 (data from Zhang, 2010)

In Nashville, Tennessee, a 1.22 m diameter drilled shaft is socketed for 4.88 m into weathered limestone. RQD of the rock is in the range of 46–65%, with an average of 55.5%. The unconfined compressive strength of the intact rock varies in the range 34.5–55.2 MPa, with an average of 44.8 MPa. The unconfined compressive strength of the concrete is 39.8 MPa. Determine the ultimate end-bearing capacity q_b .

Solution

From Equation (7.28),

$$\alpha_{\rm F} = 0.0231(55.5) - 1.32 = -0.04 \ge 0.15$$

Let us take a_E as 0.15. With the modified Equation (7.27)

$$\sigma_{cm} = \alpha_F^{0.7} \sigma_c = 0.15^{0.7} \times 44.8 = 11.9 \text{MN/m}^2$$

The end-bearing capacity is governed by the lower rock mass strength (11.9 MN/m²) rather than the concrete strength (39.8 MN/m²) in this case.

From Equation (7.29)

$$q_b = 6.39\sigma_{cm}^{0.45} = 6.39 \times 11.9^{0.45} = 19.5 \text{ MN/m}^2$$

Note: The shaft was instrumented and the load test data were extrapolated to estimate q_b as 20.3 MN/m².

The load test data from 43 rock-socketted piles given in Zhang (2010) are summarised in Table 7.6. The table gives the intact rock UCS, RQD, socket dimensions

TABLE 7.6 Load Test Data for 43 Piles

No. I	No. Rock description		RQD(%)	B (mm)	D_s (m)	$\alpha_{\rm E}$ (Eq. (7.28))	q _b (MPa)	Reference
1.	Gypsum	2.1	100	1064	4.2	0.99	6.51	Leung and Ko (1993)
2.	Gypsum	4.2	100	1064	4.2	0.99	10.9	Leung and Ko (1993)
3.	Gypsum	5.4	100	1064	4.2	0.99	15.7	Leung and Ko (1993)
4.	Gypsum	6.7	100	1064	4.2	0.99	16.1	Leung and Ko (1993)
5.	Gypsum	8.5	100	1064	4.2	0.99	23	Leung and Ko (1993)
6.	Gypsum	11.3	100	1064	4.2	0.99	27.7	Leung and Ko (1993)
7.	Sandstone, horizontally bedded, shaley	8.36	74	610	15.6	0.38	10.1	Glos and Briggs (1983)
8.	with some coal stringers	9.26	88	610	16.9	0.71	13.1	Glos and Briggs (1983)
9.	Sandstone, fresh, defect-free	27.5	100	NA	NA	0.99	50	Thorne (1980)
10.	Siltstone, medium hard, fragmented	9	55	705	7.3	0.15	13.1	Radhakrishnan and Leung (1989)
11.	Marl, intact	0.9	100	1200	18.5	0.99	5.3	Carrubba (1997)
12.	Diabase Breccia, highly featured	15	10	1200	19	0.15	8.9	Carrubba (1997)
13.	Limestone, intact	2.5	100	1200	13.5	0.99	8.9	Carrubba (1997)
14.	Coal bed, Limestone	1.21	100	1189	29.9	0.99	5.83	Miller (2003)
15.	Very hard sandy Claystone	1.96	90	1067	7.7	0.75	11.3	Abu-Hejleh et al. (2003)
16.	Very hard clayey Sandstone	10.5	90	1372	14.4	0.75	15.2	Abu-Hejleh et al. (2003)
17.	Blue Claystone	1.21	95	787	6	0.87	9.48	Abu-Hejleh and Attwooll (2005)
18.	Weathered Claystone	0.48	0	762	6.1	0.15	2.25	Abu-Hejleh and Attwooll (2005)
19.	Claystone	1.1	43	762	8.53	0.15	5.03	Abu-Hejleh and Attwooll (2005)
20.	Weathered fossiliferous Limestone	1.5	39	1585	25.9	0.15	6.28	Bullock (2003)
21.	Weathered fossiliferous Limestone	3.8	35	1940	27.3	0.15	6.22	Bullock (2003)

 TABLE 7.6 (Continued)

Load Test Data for 43 Piles (Adapted from Zhang, 2010)

No. I	Rock description	σ_{c} (MPa)	RQD(%)	B (mm)	D _s (m)	$\alpha_{\rm E}$ (Eq. (7.28))	q _b (MPa)	Reference
22.	Weathered fossiliferous Limestone	0.92	12	1880	27.2	0.15	3.57	Bullock (2003)
23.	Clay Shale	1.5	85	762	11.2	0.64	3.6	Nam (2004)
24.	Gray Limestone	10.9	96	762	7.2	0.89	10.5	Nam (2004)
25.	Weathered Shale	2.21	79	1803	19.2	0.50	10.8	Thompson (1994)
26.	Greyish jointed Basalt	14.14	51	1000	12.7	0.15	11.3	Basarkar and Dewaikar (2006)
27.	Greyish jointed Basalt	19.43	10	1000	14.2	0.15	13.2	Basarkar and Dewaikar (2006)
28.	Moderately weathered Basalt	11.77	8	1000	14.9	0.15	10.3	Basarkar and Dewaikar (2006)
29.	Weathered Basalt	12.46	0	1000	11.9	0.15	10.6	Basarkar and Dewaikar (2006)
30.	Weathered amygdaloidal Basalt	7.07	30	1000	13.8	0.15	8	Basarkar and Dewaikar (2006)
31.	Jointed yellowish Tuff	11.49	37	1200	13.2	0.15	10.2	Basarkar and Dewaikar (2006)
32.	Greyish Tuff	28.5	30	1200	11.3	0.15	16	Basarkar and Dewaikar (2006)
33.	Volcanic Breccia	6.4	20	1200	19.1	0.15	7.6	Basarkar and Dewaikar (2006)
34.	Moderately weathered amygdaloidal Basalt	39.4	37	1200	12.1	0.15	18.8	Basarkar and Dewaikar (2006)
35.	Greyish jointed Basalt	28.04	10	1200	9.3	0.15	15.9	Basarkar and Dewaikar (2006)
36.	Jointed Basalt	35.7	37	900	10.4	0.15	17.9	Basarkar and Dewaikar (2006)
37.	Jointed Basalt	21.83	27	900	11.1	0.15	14	Basarkar and Dewaikar (2006)
38.	Moderately weathered Breccia	5.36	72	1200	22.7	0.15	7	Basarkar and Dewaikar (2006)
39.	Jointed amygdaloidal Basalt	40.8	42	1100	14	0.15	19.1	Basarkar and Dewaikar (2006)
40.	Greyish Basalt	15.3	43	1050	14	0.15	11.7	Basarkar and Dewaikar (2006)
41.	Greyish Basalt	11.8	0	600	11.2	0.15	10.3	Basarkar and Dewaikar (2006)
42.	Greyish Basalt	14.24	39	600	10.4	0.15	11.3	Basarkar and Dewaikar (2006)
43.	Granodiorite	35	49	1320	23.1	0.15	16	GEO (2006)

Note: Adapted from Zhang, 2010.

Foundations on Rock 247

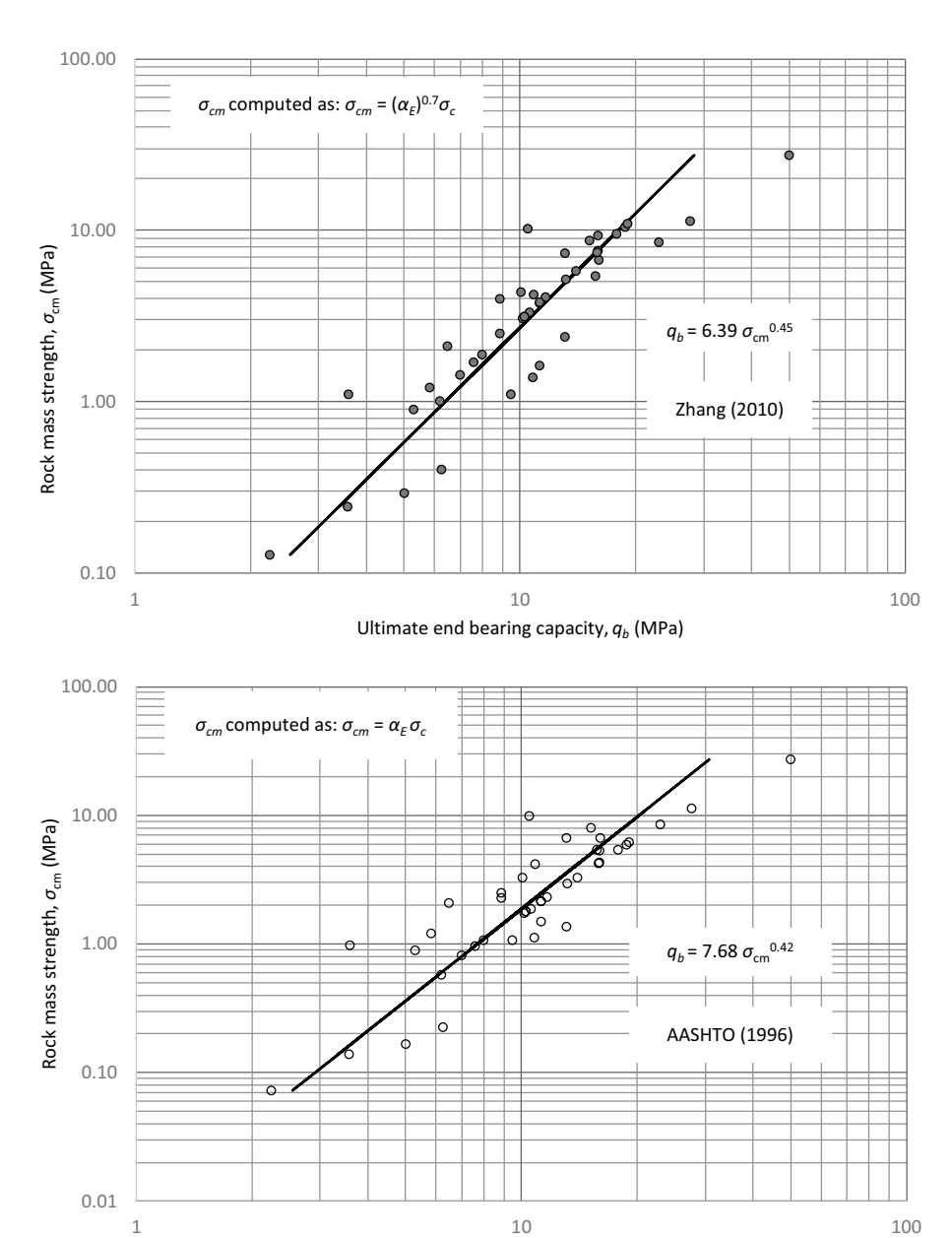


FIGURE 7.11 Comparison of AASHTO (1996) and Zhang (2010) suggestions for determining $q_{\rm b}$.

Ultimate end bearing capacity, q_b (MPa)

and the ultimate end-bearing capacity q_b . The method used for determining q_b from the load test data varied between the researchers. Figure 7.11 shows the comparison between the AASHTO (1996) and Zhang (2010) proposals for determining the ultimate end-bearing capacity q_b in the light of the load test data. They both give good predictions within the same order of accuracy.

When data are available and the discontinuities are mainly horizontal, a more refined approach would be to use the following equation for computing q_b (CGS, 1985).

$$q_b = 3\sigma_c \left(1 + 0.4 \frac{D_s}{B} \right) \left(\frac{3 + \frac{s_v}{B}}{10\sqrt{1 + 300 \frac{t_d}{s_v}}} \right)$$
(7.30)

where s_v = vertical spacing of the discontinuities, t_d = thickness (aperture) of the discontinuities, B = socket diameter and D_s = depth of the socket (embedment). The second term is the depth factor, which should be limited to 3.4. Equation (7.30) is valid for s_s/B in the range of 0.05–2.0, and $t_d/s_v \le 0.02$.

7.5 FOUNDATION CONSTRUCTION AND TREATMENT

The excavation of rocks for the foundation trench requires that they should be fragmented first by drilling and loading or by controlled blasting, without any damage to adjacent structures, if any. The excavation procedure is highly governed by the geological features of the site, as explained in Chapter 1, and by the experience of the person doing the excavation work.

Vertical joints, whether open or filled with soil, are commonly found even in unweathered rock formations. Such joints beneath the shallow foundations should be cleaned out to a depth of four to five times their width and filled with slush grout (cement-sand mixture in 1:1 ratio by volume with enough water). Grouting is also usually carried out where the shallow foundation bears on rock containing voids to strengthen the rock. Larger spaces, wider at the top, are likely to occur at intersecting joints, which are commonly filled with dental concrete (stiff mixture of lean concrete) placed and shaped by shovel. If horizontal joints are located beneath the shallow foundation, such joints may lead to differential and sudden settlements. If the estimated settlement exceeds the permissible limit, the rock above the joints may be removed if it is economically feasible; otherwise, deep foundations may be recommended. If the estimated settlement exceeds the permissible limit, the rock above the joints may be removed if it is economically feasible; otherwise, deep foundations may be recommended. If bedded limestones are present at the foundation site, there might be a possibility of solution cavities, which require a detailed investigation. Such cavities may be filled with cement grout. Solution cavities may render the foundation trench bed uneven; in that situation, the depth of foundation should be taken to a level such that at least 80% rock area is available to support the foundation. It is

Foundations on Rock 249

important to ensure that the base of the foundation does not overhang at any corner. If the filled up soil and loose pockets of talus deposit are present at the foundation site, they should be excavated, cleaned and backfilled with lean concrete of required strength. If a foundation is to be placed on sloping rock, particular attention should be given to the discussion on slope stability in Chapter 6.

For further geotechnical insights into foundations on rock, refer to *Foundation Engineering* by Peck et al. (1974).

7.6 SUMMARY

- A foundation is considered shallow if its depth is generally less than or equal to its width. The most common types of shallow foundations on rock and soil are *spread footings* and *mats* (or *rafts*).
- 2. In hard rocks, where the ultimate compressive strength is 10 MPa or higher, considering overall characteristics such as fissures, joints and bedding planes, the minimum foundation depth is set at 0.6 m. For all other types of rock, the minimum depth is 1.5 m.
- 3. The value of net allowable bearing pressure $(q_{\rm na})$ is generally recommended for design of shallow foundations. The allowable pressure values of rocks for average conditions may be taken as follows: for hard rocks, $q_{\rm na} = 2-3$ MPa; for soft rocks, $q_{\rm na} = 1-2$ MPa and for weathered rocks, conglomerates and laterites, $q_{\rm na} < 1$ MPa. These values should be modified after taking into account the various characteristics of rocks at the construction site.
- 4. In many cases, the allowable bearing pressure is set between one-third and one-tenth of the unconfined compressive strength obtained from intact rock samples, with the Rock Quality Designation (RQD) serving as a guide. For example, a lower value, such as one-tenth, is used when the RQD is low.
- 5. The foundation is considered deep if its depth is generally greater than its width. The most common types of deep foundations on rock and soil are *piles* and *drilled piers*.
- 6. In most cases, calculation of the load-carrying capacity of the pile resting on rock based on the yield strength of the pile material is sufficient.
- 7. It is common to use large safety factors (2.5–10) in estimating the bearing capacity of rock foundation.
- 8. The foundation excavation and treatment procedures are highly influenced by the site's geological features as well as by the expertise of the person doing the excavation work.

REVIEW EXERCISES

Select the most appropriate answers to the following 10 multiple-choice questions.

- 7.1. Which of the following ratios of width to depth of a foundation does not refer to a shallow foundation?
 - a. 0.5
 - b. 1.0

- c. 2.0
- d. Both (b) and (c)
- 7.2. A high-rise building site consists of a heavily jointed and fractured rock mass. The most suitable foundation for this site will be
 - a. strip footing
 - b. isolated square/rectangular footing
 - c. raft foundation
 - d. all of the above
- 7.3. Core drilling was carried out at a rock foundation site, and the RQD was estimated to be 25%. What will be the minimum depth of foundation at this site?
 - a. 0.6 m
 - b. 0.75 m
 - c. 1 m
 - d. 1.5 m
- 7.4. For the design of shallow foundation, which of the following value is generally recommended?
 - a. Safe bearing capacity
 - b. Net allowable bearing pressure
 - c. Allowable bearing pressure
 - d. Safe bearing pressure
- 7.5. The net safe bearing pressure of bedded limestone bedrock is generally
 - a. 0.4 MPa
 - b. 1 MPa
 - c. 2.5 MPa
 - d. 4 MPa
- 7.6. A drilled pier is also known as a
 - a. drilled shaft
 - b. drilled caisson
 - c. caisson
 - d. all of the above
- 7.7. For a point-bearing pile, the ratio of ultimate load-carrying capacity to the point capacity is
 - a. equal to 0.5
 - b. equal to 1
 - c. less than 1
 - d. greater than 1
- 7.8. The drained angle of friction (in degrees) for limestone ranges from
 - a. 10 to 20
 - b. 20 to 30
 - c. 30 to 40
 - d. 40 to 50
- 7.9. The factor of safety used in estimating the bearing capacity of a rock foundation ranges from
 - a. 1 to 2
 - b. 2 to 4

Foundations on Rock 251

- c. 2.5 to 10
- d. None of the above
- 7.10. Vertical joints in rock foundations are generally filled with slush grout that has a cement–sand mixture in the volume ratio of
 - a. 1:1
 - b. 1:1.5
 - c. 1.2
 - d. 1:3
- 7.11. What is meant by the term 'foundation'? Explain briefly.
- 7.12. Differentiate between shallow and deep foundations.
- 7.13. What type of shallow foundation would you recommend for a building on a heavily jointed and fractured rock site?
- 7.14. What should be the minimum depth of foundation on hard bedrock?
- 7.15. Define the following terms: ultimate bearing capacity, safe bearing capacity, safe bearing pressure and allowable bearing pressure.
- 7.16. Define the following terms: net ultimate bearing capacity, net safe bearing capacity, net safe bearing pressure and net allowable bearing pressure.
- 7.17. What are the parameters that govern the bearing capacity of foundations on rock?
- 7.18. A strip footing of 1.5 m width rests on bedrock exposed to the ground surface. The bedrock is horizontally bedded with spacing S = 1 m, aperture $\delta = 10$ mm and $q_{\text{n(av)}} = 60$ MPa. Estimate the safe bearing pressure.
- 7.19. How do geological site conditions affect the bearing capacity of rock foundation? Explain, giving some field examples.
- 7.20. How does a point-bearing pile differ from a friction pile? Explain with the help of neat sketches.
- 7.21. Explain the method of estimating the point-bearing capacity of a pile resting on rock.
- 7.22. A pile of diameter of 50 cm and length of 12 m passes through the highly jointed and weathered rock mass and rests on a sandstone bed. For sandstone, laboratory unconfined compressive strength = 90 MPa and drained friction angle = 38°. Estimate the allowable point capacity of the pile. Assume that the pile material has sufficient strength and use a factor of safety of 5.
- 7.23. Is it possible to excavate rock without blasting? Can you suggest some methods?
- 7.24. How are vertical joints in rock foundation treated before the construction of structural footings?
- 7.25. How will you deal with solution cavities located at a limestone foundation site?

Answers:

- 7.1. a; 7.2. c; 7.3. d; 7.4. b; 7.5. d; 7.6. d; 7.7. b; 7.8. c; 7.9. c; 7.10. a
- 7.18. 10.8 MPa
- 7.22. 3675 kN

REFERENCES

AASHTO (1996). *Standard Specifications for Highway Bridges*. 16th edition, American Association of State Highway Transportation Officials, Washington, DC.

- Abu-Hejleh, N. and Attwooll, W.J. (2005). *Colorado's Axial Load Tests on Drilled Shafts Socketed in Weak Rocks: Synthesis and Future Needs*. Colorado Department of Transportation, Research Branch, Denver, CO, Report CDOT-DTD-R-2005–4.
- Abu-Hejleh, N., O'Neill, M.W., Hanneman, D. and Attwooll, W.J. (2003). Improvement of the Geotechnical Axial Design Methodology for Colorado's Drill Shafts Socketed in Weak Rocks. Colorado Department of Transportation, Research Branch, Denver, CO, Report CDOT-DTD-R-2003–6.
- Akgüner, C. and Kirkit, M. (2012). Axial bearing capacity of socketed single cast-in-place piles. *Soils and Foundations*, Vol. 52, No. 1, pp. 59–68.
- ARGEMA (1992). Design Guides for Offshore Structures: Offshore Pile Design. Tirant, P.L., editor, Éditions Technip, Paris.
- Basarkar, S.S. and Dewaikar, D.M. (2006). Load transfer characteristics of rock socketed piles in Mumbai region. *Soils and Foundations*, Vol. 46, No. 2, pp. 247–257.
- BIS. (2005). Code of Practice for Design and Construction of Shallow Foundations on Rocks. IS: 12070–1987 (Reaffirmed 2005), Bureau of Indian Standards (BIS), New Delhi, India.
- Bowles, J.E. (1996). Foundation Analysis and Design. 5th edition, McGraw-Hill, New York.
- Brown, D.A., Turner, J.P. and Castelli, R.J. (2010). *Drilled Shafts: Construction Procedures* and LRFD Design Methods, Publication No. FHWA-NHI-10–016, Federal Highway Administration, USA.
- Bullock, P.J. (2003). A Study of the Setup Behaviour of Drilled Shafts. Report submitted to the Florida Department of Transportation, University of Florida, Gainesville, FL.
- Canadian Foundation Engineering Manual (1985). 2nd edition, *Canadian Foundation Engineering Manual*. Canadian Geotechnical Society (CGS), Canada.
- Carrubba, P. (1997). Skin friction of large-diameter piles socketed into rock. *Canadian Geotechnical Journal*, Vol. 34, No. 2, pp. 230–240.
- Carter, J.P. and Kulhawy, F.H. (1988). *Analysis and Design of Drilled Shaft Foundations Socketed into Rock*. Report EL-5918, Palo Alto: Electric Power Research Institute.
- CGS (1992). Canadian Foundation Engineering Manual. 3rd edition, Canadian Geotechnical Society (CGS), Canada.
- Coates, D.F. (1967). *Rock Mechanics Principles*. Monograph 874, Dept of Energy, Mines, and Resources, Mines Branch, Queen's Printer, Ottawa, Canada.
- Crapps, D.K. and Schmertmann, J.H. (2002). Compression top load reaching versus shaft bottom theory versus tests, in *Proceedings of the International Deep Foundation Congress*, Orlando, FL, 14–16 February 2002, Geotechnical Special Publication No. 116, O'Neill, M.W. and Townsend, F.C., editors, Geo-Institute, ASCE, Vol. 2m, pp. 1533–1549.
- Das, B.M. (2022). Principles of Geotechnical Engineering. 10th edition, Cengage Learning, Stamford.
- Fleming, W.G.K., Weltman, A.J., Randolph, M.F. and Elson, W.K. (1992). *Piling Engineering*. John Wiley & Sons, New York.
- GEO (2006). Foundation Design and Construction. Geotechnical Control Office, Hong Kong, GEO Publication, No. 1/2006.
- Glos, G.H. III and Briggs, O.H. Jr. (1983). Rock sockets in soft rocks. *Journal of Geotechnical Engineering, ASCE*, Vol. 109, No. 4, pp. 525–535.
- Goodman, R.E. (1980). Introduction to Rock Mechanics. John Wiley & Sons, New York.
- Haberfield, C.M. and Collingwood, B. (2006). Rock-socketed pile design and construction: A better way? *Proceedings of ICS Geotechnical Engineering*, Vol. 159, No. 3, pp. 207–217.
- Hoek, E. (1983). Strength of jointed rock masses, 23rd Rankine Lecture, *Geotechnique*, Vol. 33, No. 3, pp. 187–223.

Foundations on Rock 253

Horvath, R.G. and Kenney, T.C. (1979). Shaft resistance of rock-socketed drilled piers. Proceedings of Symposium on Deep Foundations, ASCE, pp. 182–214.

- IRC (2000). Standard Specifications and Code of Practice for Road Bridges. Indian Roads Congress, New Delhi, India, p. 54.
- Kumar, S. (2011). Design of pile foundations, in *Handbook of Geotechnical Engineering*, Das, B.M., editor, J. Ross Publishing, Inc., Fort Lauderdale, FL, pp. 5.1–5.73.
- Ladanyi, B. (1977). Discussion to "Friction and end bearing tests on bedrock for high capacity socket design". *Canadian Geotechnical Journal*, Vol. 14, No. 1, pp. 153–155.
- Leung, C.F. and Ko, H-Y. (1993). Centrifuge model study of piles socketed in soft rock. *Soils and Foundations*, Vol. 33, No. 3, pp. 80–91.
- Meigh, A.C. and Wolski, W. (1979). Design parameters for weak rock. *Proceedings of 7th European Conference on Soil Mechanics and Foundation Engineering*, British Geotechnical Society, Brighton, London, Vol. 5, pp. 59–79.
- Miller, A.D. (2003). *Prediction of Ultimate Side Shear for Drilled Shafts in Missouri Shafts*, M.Sc. thesis, University of Missouri, Columbia, MO.
- Nam, M.S. (2004). Improved Design for Drilled Shafts in Rocks, PhD thesis, University of Houston, Houston, TX.
- O'Neill, M.W. and Reese, L.C. (1999). Drilled Shafts: Construction Procedures and Design Methods. Department of Transportation, Federal Highway Administration, McLean, VA, Publication No. FHWA-IF-99–025.
- Osterberg, J.O. and Gill, S.A. (1973). Load transfer mechanism of piers socketed in hard soils and rock. *Proceedings of 9th Canadian Symposium on Rock Mechanics*, Montreal, Canada, pp. 235–262. The Canadian Advisory Committee on Rock Mechanics.
- Peck, R.B., Hanson, W.E. and Thornburn, T.H. (1974). *Foundation Engineering*. 2nd edition, John Wiley & Sons, New York.
- Prakoso, W.A. (2002). Reliability Based Design of Foundations on Rock for Transmission Lines and Similar Structures, PhD thesis, Cornell University, Ithaca, NY.
- Prakoso, W.A. and Kulhawy, F.H. (2004). Bearing capacity of strip footings on jointed rock masses. *Journal of Geotechnical and Geoenvironmental Engineering, ASCE*, Vol. 130, No. 12, pp. 1347–1349.
- Radhakrishnan, R. and Leung, C.F. (1989). Load transfer behaviour of rock socketed piles. *Journal of Geotechnical Engineering, ASCE*, Vol. 115, No. 6, pp. 755–768.
- Rosenberg, P. and Journeaux, N.I. (1976). Friction and end bearing for drilled piers in soft rock. *Canadian Geotechnical Journal*, Vol. 13, No. 3, pp. 324–333.
- Rowe, R.K. and Armitage, H.H. (1987). A design method for drilled piers in soft rock. *Canadian Geotechnical Journal*, Vol. 24, No. 1, pp. 126–142.
- Shukla, S.K. (2006). Allowable Load-Bearing Pressure for the Foundation of Aqueduct on Rock/Soil at km 46.615 of the Bansagar Feeder Channel, Dist. Sidhi, MP, India. A technical reported dated 7 June 2006, Department of Civil Engineering, Institute of Technology, Banaras Hindu University, Varanasi, India.
- Shukla, S.K. (2007). Allowable Load-Bearing Pressure for the Foundation of Barrel Aqueduct on Rock at km 44.900 of the Bansagar Feeder Channel, Dist. Sidhi, MP, India. A technical reported dated 29 June 2007, Department of Civil Engineering, Institute of Technology, Banaras Hindu University, Varanasi, India.
- Shukla, S.K. (2008). *The Pile Termination at km 52.106 of the Bansagar Feeder Channel, Dist.—Sidhi, MP, India.* A technical reported dated 17 December 2008, Department of Civil Engineering, Institute of Technology, Banaras Hindu University, Varanasi, India.
- Shukla, S.K. and Sivakugan, N. (2011). Site investigation and in situ tests, in *Geotechnical Engineering Handbook*, Das, B.M., editor, J. Ross Publishing, Inc., Fort Lauderdale, FL, pp. 10.1–10.78.
- Teng, W.C. (1962). Foundation Design. Prentice-Hall of India Pvt. Ltd., New Delhi.
- Thompson, R.W., III. (1994). Axial Capacity of Drilled Shafts Socketed into Soft Rock, M. Sc thesis, Auburn University, Auburn, AL.

Thorne, C.P. (1980). The capacity of piers drilled into rock. *Proceedings of International Conference on Structural Foundations on Rock*, Sydney, Australia, 7–9 May 1980, Taylor & Francis, London, Vol. 1, pp. 223–233.

- Vipulanandan, C., Hussain, A. and Usluogulari, O. (2007). Parametric study of open core-hole on the behaviour of drilled shafts socketed in soft rock, in *New Peaks in Geotechnics*, Contemporary Issues in Deep Foundations, Geo-Denver, pp. 1–10.
- Williams, A.F., Johnston, I.W. and Donald, I.B. (1980). Design of socketed piles in weak rock, in *Structural Foundations on Rock*, Pells, P.J.N., editor, A.A. Balkema, Rotterdam, pp. 327–347.
- Wyllie, D.C. (1999). Foundations on Rock. E&FN Spon, London.
- Yu, H.S. and Sloan, S.W. (1994). Bearing capacity of jointed rock. Proceeding of the 8th International Conference on Computer Methods and Advances in Geomechanics, A.A. Balkema, Rotterdam, The Netherlands, Vol. 3, pp. 2403–2408.
- Zhang, L. (2008). Predicting the end bearing capacity of rock socketed shafts. *Proceedings of the 33rd Annual and 11th International Conference on Piling and Deep Foundations*, New York, 15–17 October, pp. 307–316. BNP Media.
- Zhang, L. (2010). Prediction of end-bearing capacity of rock-socketed shafts considering rock quality designation (RQD). *Canadian Geotechnical Journal*, Vol. 47, pp. 1071–1084.
- Zhang, L. and Einstein, H.H. (1998). End bearing capacity of drilled shafts in rock. *Journal of Geotechnical and Geoenvironmental Engineering, ASCE*, Vol. 124, No. 7, pp. 574–584.
- Zhang, L. and Xu, J. (2009). Axial load transfer behaviour of rock socketed shafts, in Contemporary Topics in Deep Foundations, Selected Papers from the 2009 International Foundation Congress and Equipment Expo, Orlando, FL, 15–19 March 2009. Geotechnical Special Publication, 185, Iskander, M., Laefer, D.F. and Husein, M.H., editors, ASCE, Reston, VA, pp. 175–182.

8 Tunnelling within Rock Mass

8.1 INTRODUCTION

Tunnels are a vital type of infrastructure. In the last few decades, tunnels have become more popular due to safety requirements, economic efficiency and significant improvements in construction technologies. In general, there are three types of tunnels, which are associated respectively with typical cross sections: hydraulic, transportation and mining tunnels.

Hydraulic tunnels can be constructed to deliver fluids such as water or sewage. As pressurised fluid distributes stress equally in all directions, hydraulic tunnels often have a circular cross section (Figure 8.1a). This cross-sectional shape has the best durability and stability against high pressure and large impact. If maintenance requires heavy machinery, the cross section could be semicircular with a top arch, vertical walls and a flat floor (Figure 8.1b). In this case, drainage is often required to keep the floor dry during the maintenance.

Transportation tunnels often have circular, segmental, or horseshoe cross sections, with some variations. The circular cross section is popular for long subway tunnels, which frequently use boring machines to accelerate the construction. The conventional cross section of mining tunnels is semicircular. The arch roof distributes the load to sides, and the flat floor facilitates the ore transportation with trucks or trolleys. When the diameter of the arch exceeds the width of the tunnel, the roof is just a small segment of the circle, and the cross section is classified as a square cavern. If there are smooth transitions between the wall and the roof, the cross section is referred to as a shoulder cavern. Although the mining tunnels are heavily braced, there is no requirement for good-looking finish with shotcrete. If a protective mesh is not installed, stones and debris may fall off the roof. Safety warning and measures to protect miners are a must in mining tunnel design.

Meanwhile, segmental cross section is often used for multiple-lane highways when they go through mountains or hills. As this cross section is flat, pipe jacking may be required around the main course during the construction to avoid subsidence or collapse. The segmental of cross section of traffic tunnel often consists of four or five radii (Figure 8.1c). The ratio R_1/R_5 for two-lane tunnels is recommended to be near 2.5, while R_3/R_5 should be no less than 0.6. The radii R_2 should not be less than 1,500 mm due to stress flow and concentration.

A few recent urban projects proposed two-level tunnels with circular or horseshoe cross sections (Figure 8.1d). A traditional horseshoe cross section consists of a semicircle on the top and a trapezium underneath. A circular horseshoe profile has an invert dish at the bottom, while a curved horseshoe profile has different curvatures

DOI: 10.1201/9781032725161-8 **255**

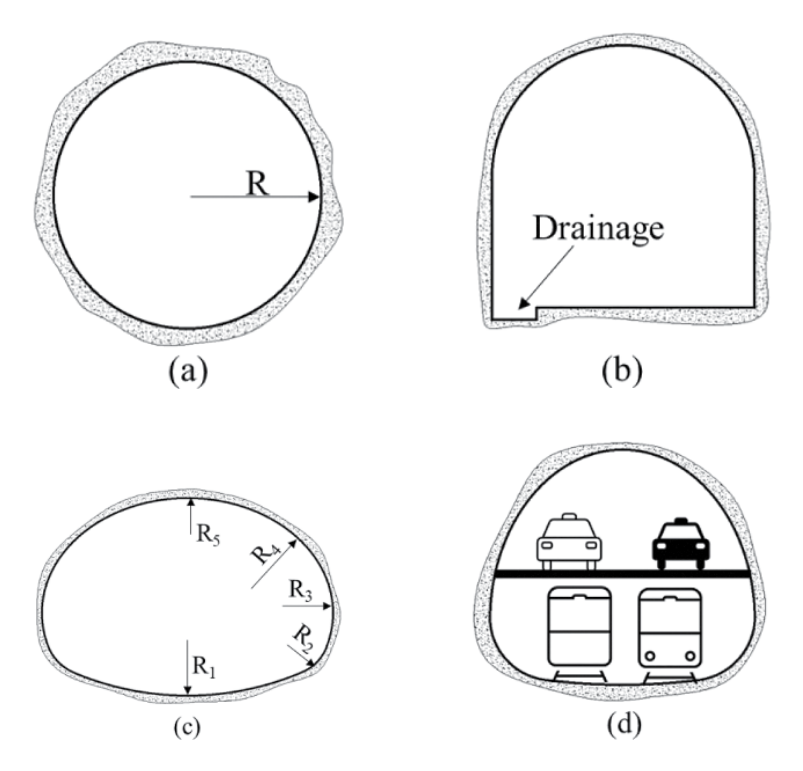


FIGURE 8.1 Typical cross sections of tunnels: (a) circular, (b) semicircular, (c) segmental and (d) horseshoe.

for roof, wall and floor. Apart from the financial benefits, these options reduce the number of tunnels and the impact on the foundations of existing skyscrapers as well as future ones.

The area of cross section of hydraulic tunnels is calculated from the required flow and pressure. Meanwhile, the cross section of transport tunnels is drafted from the required internal space for traffic (Figure 8.2). Although the structure of tunnels for different purposes can vary, Australian practice often employs guidelines from Austroads for general considerations and justifications (Austroads, 2018; Department of Transport and Main Roads, 2021). More detailed information could be found in guidelines from the Australian Tunnelling Society (Australian Tunnelling Society, 2020) or the US Federal Highway Administration (Federal Highway Adminstration, 2009). Currently there is no European standard or unified guideline for tunnel design at the European level. The design of tunnels in the EU is carried out based on national general guidelines and industrial knowledge. In 2022, a prospect for designing tunnels in the context of the Eurocodes was proposed (Athanasopoulou et al., 2022). In contrast, China has issued several technical guidelines for particular types of tunnels (China Oil & Gas Industry Standards, 2014; National Railway Administration of the People's Republic of China, 2016; Shanghai Engineering Construction Code, 2017). Russia has also provided a detailed guideline with some calculation

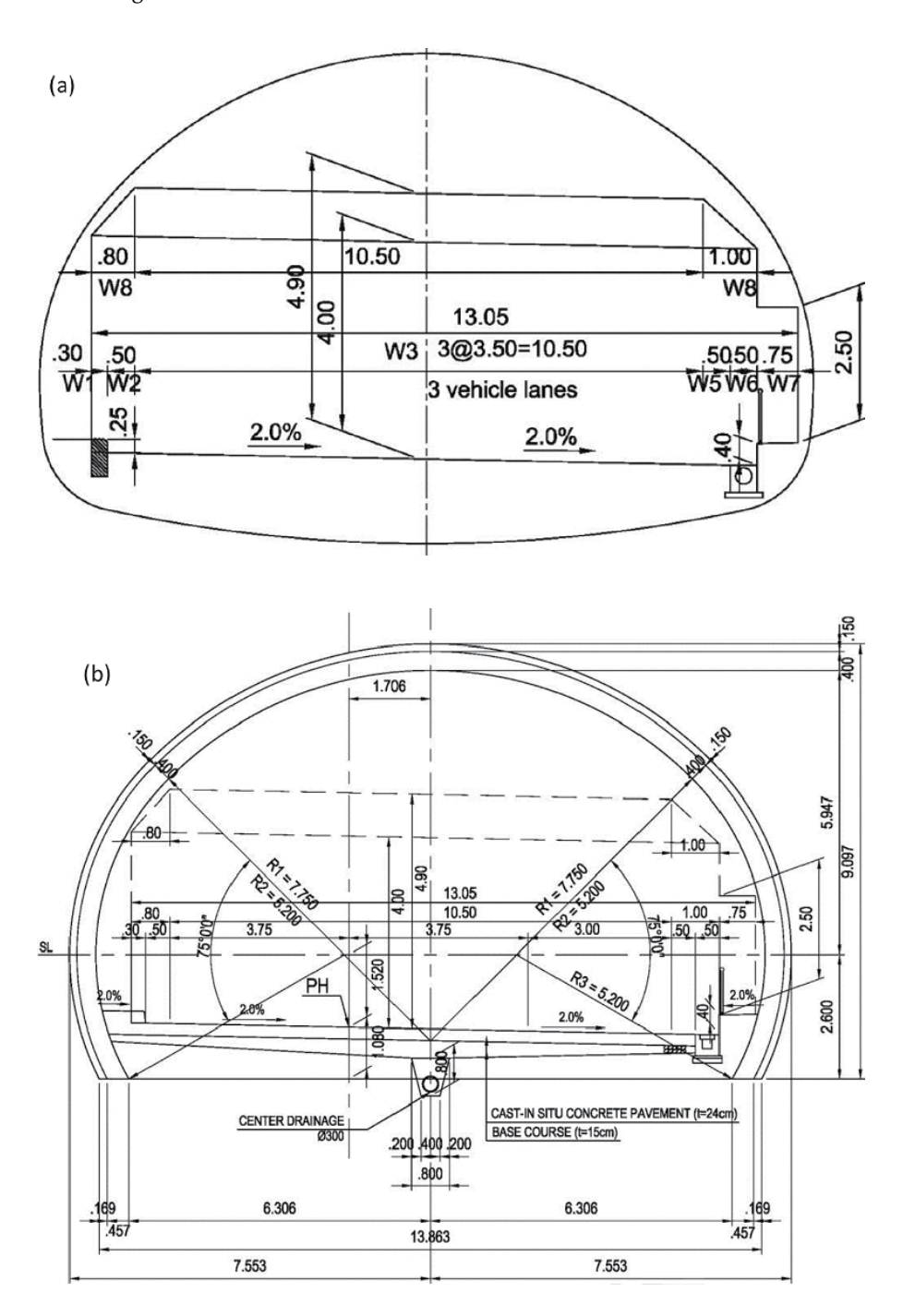


FIGURE 8.2 Sample dimensions of a cross-sectional area of three-lane traffic tunnel: (a) required internal dimensions and (b) proposed details. Unit is in metre.

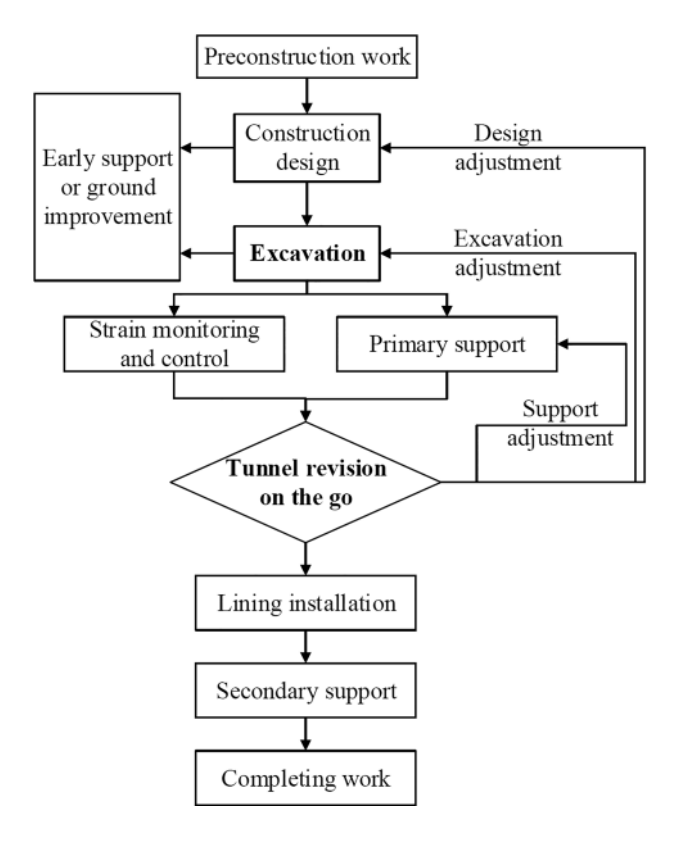


FIGURE 8.3 A typical flow chart of the New Austrian Tunnelling Method (NATM).

examples for seismic impact on tunnel (Federal Centre of Norms, 2018). The most popular method for tunnelling arguably could be New Austrian Tunnelling Method (NATM), which takes advantages of sophisticated monitoring to optimise the wall reinforcement techniques. Hence, this method is featured with flexible support and design adjustment during the construction (Figure 8.3).

This chapter presents essential engineering calculations for the design and technical principles for the construction of general tunnels in rock mass.

8.2 KEY ASPECTS OF DESIGN OF TUNNELS

In general, elements of a tunnel can be divided into two groups: structural and operational. Structural elements may consist of rock and lining supports. These elements ensure the stability of tunnels against internal and external loads, which act during and after construction. Early support can be installed before the drill, while late support can be installed during the operation of the tunnel. Operational elements can include drainage, ventilation and lighting. Besides, a monitoring system is a must for most of transport tunnels. Subway tunnels require a powerful electrical system with

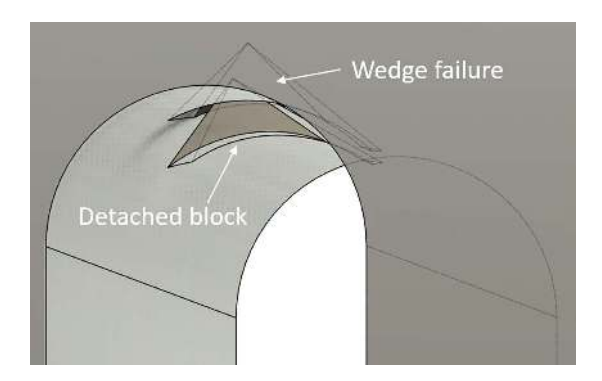


FIGURE 8.4 Schematic draft of wedge failure in rock tunnel.

technical hubs along the track. Pressurised tunnels at hydropower plants may have a heavy mechanical system to operate screens and gates, which are closed during turbine maintenance.

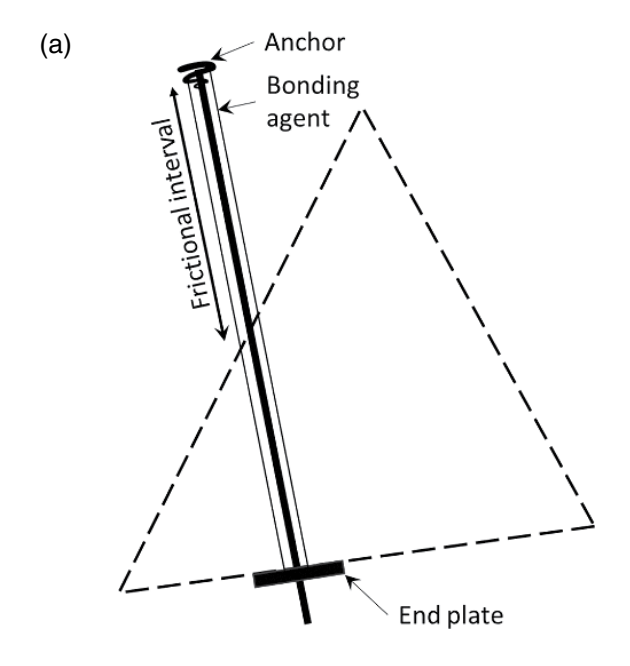
Tunnels have two frequent failure modes: wedge and crack. Either of these two failures could lead to the total collapse. Wedge failure occurs when a part of the roof or wall falls off due to the lack of support and binding force (Figure 8.4). Normal wedges are often formed by several significant discontinuities. When the falls occur in thin rock layers, it is called peeling. And when the falls consist of small rock blocks, it is called unravelling. Cracks occur due to high strain, which is caused by the stress acting on the tunnel. If the major stress acts along rock layers, it can cause buckling and rupture. When the stress acts perpendicularly to the rock layers, it can cause bending and flexural failures.

8.2.1 STABILISATION OF ROOF AND WALLS

Stabilisation of the roof and walls of a tunnel depends on the rock quality, which is usually reflected by rock mass rating (RMR) or rock quality designation (RQD) explained in Chapter 4. If RMR is high, the stabilisation focuses on the detachable rock block. When RMR is low, the rock is fragmented, and stabilisation aims to form an artificial arch to transfer rock stress to the base.

In general, wedges can be stabilised with rock bolts and cables. The length of rock bolts depends on the dimension of tunnels for the ease of installation. In 6 m mining drifts, point-anchored bolts are often less than 3 m, but they should be at least 1.5 m beyond the fractured zone. Cable bolts could exceed 20 m in length and may be used together with rock bolts. The factor of safety for wedge stabilisation is calculated in the sliding/falling direction:

$$FS = \frac{Total(passive)resisting force}{Total(active)driving force}$$
(8.1)



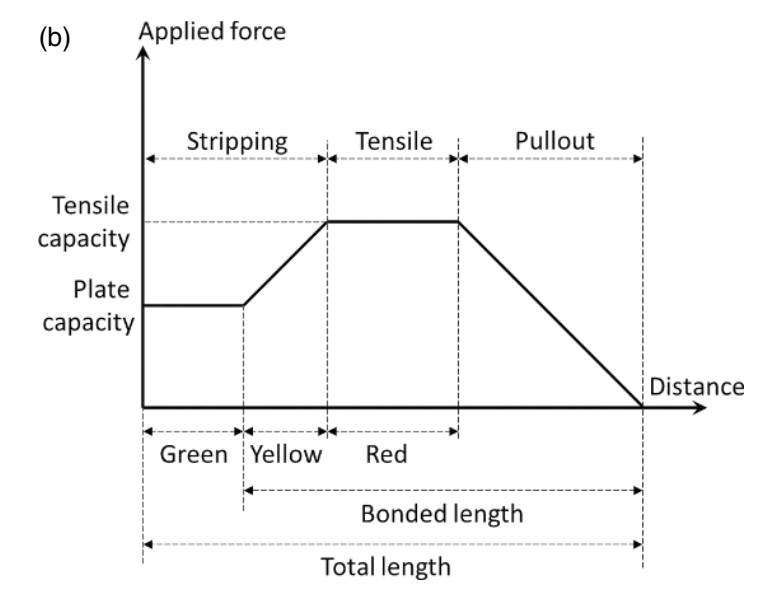


FIGURE 8.5 Work of a single rock bolt: (a) schematic diagram and (b) force-deformation graph.

The weight of the block can be estimated with a rock scan or calculated from joints. The passive force may include resultant bolt force, (internal) passive pressure force, shotcrete shear resistance force and frictional shear force along the failure surface. The capacity of a bolt is often provided by the manufacturer (Figure 8.5). It is required that at least 1% of installed bolt must be tested to verify the work in field of



FIGURE 8.6 Tension indicator for rock bolt.

rock bolts. Due to uncertainty in rock strength, the factor of safety should not be less than two in general rock bolting designs.

As bolts are usually installed at roughly 90° to the rock surface, they can have different orientations. Therefore, the equilibrium must be checked with force projections in the direction of potential failures. Cohesion between rock blocks should not be included in long-term as it can diminish over time. As the load distribution is not uniform, failure may occur first with a few bolts before a total collapse. Hence, rock bolts often have a colour indicator at the end to warn if they are over-tensioned (Figure 8.6). When the indicator warns, the bolt should be reinstalled as soon as possible, or another reinforcement must be in use.

The active driving force may include the wedge weight, shotcrete weight, (external) active pressure force and seismic force. Although the rock data is often given in the form of hemisphere coordination, the analytical solution requires this data to be converted into vector format to calculate the vertical forces using linear algebra. The resultant passive force \boldsymbol{P} is calculated as

$$P = S + I + B \tag{8.2}$$

where: S = shotcrete shear resistance force; I = resultant passive pressure force; and B = resultant bolt force. The resultant active force A is expressed as

$$A = W + M + U + X + E \tag{8.3}$$

where W = weight of the wedge; M = attached mesh and shotcrete weight; U = water force; X = active pressure force; and E = earthquake and dynamic impact force.

The passive forces in the sliding direction could be calculated with Mohr-Coulomb theory or the Hoek-Brown rock model. Rock engineers often use computer programs to calculate these components. The following is a simplified example that avoids the use of sophisticated vector algebra.

EXAMPLE 8.1

Three joints 42/005, 47/060 and 45/282 form a roof wedge on a traffic tunnel 0/20, as shown in Figure 8.7. The joints have no cohesion or tensile strength. The frictional angle of the rock is 38°. The volume of the wedge is estimated at 3.52 m³, and the average unit weight is 2.67 t/m³. A 12-ton rock bolt RSS-12 will be installed

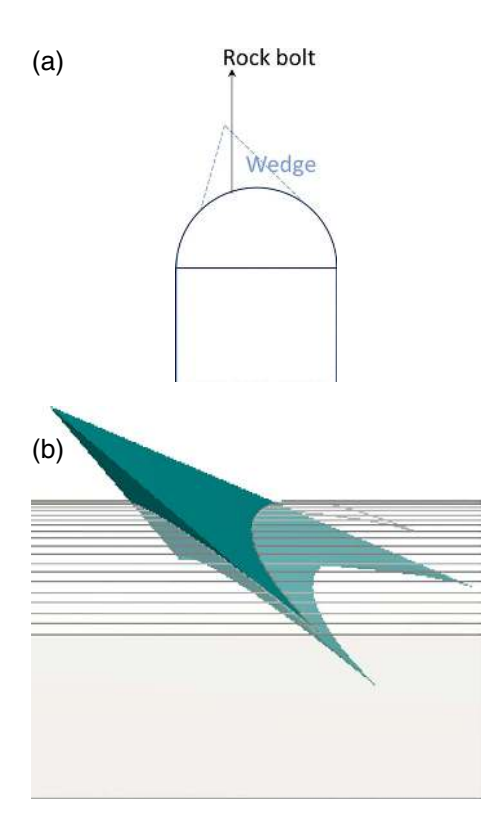


FIGURE 8.7 Rock wedge in Example 8.1: (a) schematic front view and (b) 3D side view.

vertically to prevent the possible failure. Determine the factor of safety for planar slide, assuming no groundwater or other external forces. The initial area of joint 1 face is 5.52 m^2 .

Solution

Set the coordinate system as x = East, y = Up, z = South. The normal vectors n of a joint plane is calculated as

$$\mathbf{n} = [\sin\alpha\sin\psi, \cos\alpha, -\sin\alpha\cos\psi]$$

Where α and ψ are direction and dip of the plane, respectively. Thereby,

$$\mathbf{n}_{1} = \left[sin\alpha_{1} sin\psi_{1}, cos\psi_{1}, -cos\alpha_{1} sin\psi_{1} \right] = \left[0.0583, \, 0.7403, \, -0.6666 \right]$$

$$\mathbf{n}_2 = \left[sin\alpha_2 sin\psi_2, cos\psi_2, -cos\alpha_2 sin\psi_2 \right] = [0.6334, 0.6820, -0.3660]$$

$$\mathbf{n}_3 = [\sin\alpha_3 \sin\psi_3, \cos\psi_3, -\cos\alpha_3 \sin\psi_3] = [-0.6917, 0.7071, -0.1470]$$

The rock block will not slide on Joint 2 and Joint 3 because the rock block is formed underneath these joints (Figure 8.7b). Assuming no groundwater pressure or external load, active force vector **A** could be calculated as

$$A = W = \gamma_{rock} V g = 2.67*3.52*[0, 1, 0] = [0, -9.3984, 0]$$

where W and V are the weight and volume of the wedge, respectively; γ_{rock} is the unit weight of the rock; and g is earth acceleration. Assuming no internal pressure (I) and no shotcrete (S) before stabilisation, I = S = 0. The bolt force is calculated as the sum of the resistance forces of all bolts.

$$P = B = \sum f(b \cdot s)$$

where f = bolt force vector, [0, 10, 0]; b = bolt direction, for a vertical bolt, b = [0, 1, 0]; s = sliding direction. As the wedge can slide only on joint 1:

$$s = \frac{(\mathbf{n}_1 \times \mathbf{A}) \times \mathbf{n}_1}{\|(\mathbf{n}_1 \times \mathbf{A}) \times \mathbf{n}_1\|} = [0.0648, 0.6691, 0.7403]$$

Because there is only one bolt required, the bolt force vector is

$$P = B = f(b \cdot s) = [0.10, 0] * ([0.1, 0] \cdot [0.0648, -0.6691, -0.7403]) = [0, 6.6913, 0]$$

The normal stress acting on the joint face is the ratio between force and sliding area:

$$\sigma = \frac{\left\| -\mathbf{A} \cdot \mathbf{n}_1 + \mathbf{P} \cdot \mathbf{n}_1 \right\|}{area}$$

$$- \left[0, -9.3984, 0 \right] \left[0.0583, 0.7403, -0.6666 \right] + \left[0, -6.6913, 0 \right]$$

$$= \frac{+0.0583, 0.7403, -0.66661}{5.52} = 0.3644 \text{ (t/m}^2)$$

Supported shear strength:

$$\tau = c + \sigma tan\varphi = 0 + 0.3644 * tan 38^{\circ} = 0.2847 \text{ (t/m}^2)$$

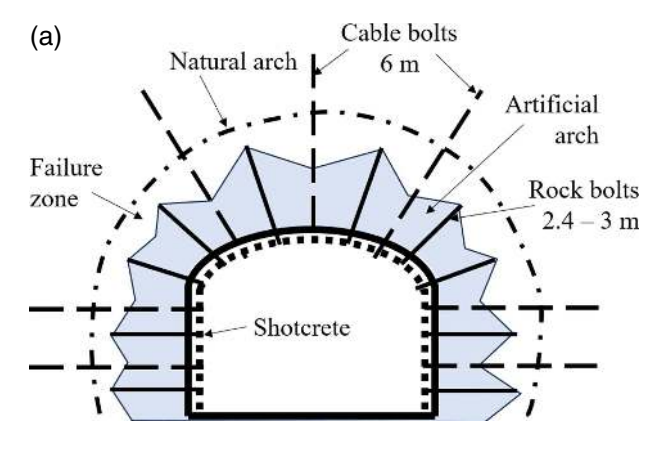
Factor of safety in the sliding direction:

$$F_s = \frac{\mathbf{P} \cdot \mathbf{s} + \tau * area}{\mathbf{A} \cdot \mathbf{s}} = \frac{\left[0, -6.6913, 0\right] \left[0.0648, -0.6691, -0.7403\right] + 0.2847 * 5.52}{\left[0, -9.3984, 0\right] \left[0.0648, -0.6691, -0.7403\right]} = \frac{6.0489}{6.2888}$$

When the rock is fragmented under high pressure, it could form a failure zone (Figure 8.8). Then, a strong reinforced concrete lining could be used in combination with other rock supports. The main idea of stabilisation is the formation of an artificial arch as a protective envelope which supports the loads acting on the tunnel. The untensioned length of rock bolt, L_b , in moderately jointed hard rock is recommended by the Norwegian Road Authority (Statens vegvesen, 2000):

$$L_{b} = 1.4 + 0.184B \tag{8.4}$$

where B =width of the tunnel.



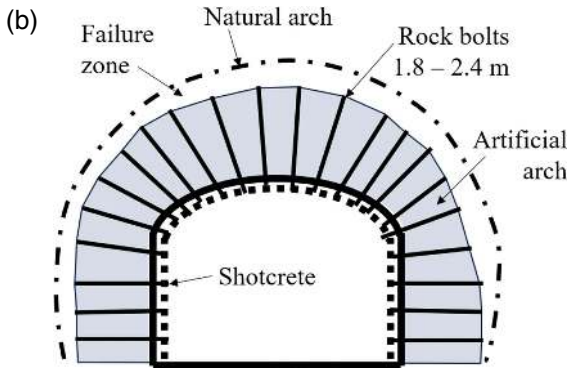


FIGURE 8.8 Examples of stabilisation for a shoulder cavern tunnel in fragmented rock: (a) combined rock bolting and (b) dense rock bolting.

Bolts should be installed in between joints, not directly at them. The position of rock bolts depends on joint sets in individual situations. Hence, engineering judgement is of vital importance for installation. If the rock is well fractured or moderately weathered, bolts should generate a dense triangular mesh. If the rock is fair or faintly weathered, bolts could form a few rows along the tunnel. A rule of thumb (Li, 2017) recommends bolt spacing, s, less than $L_b/2$ and:

$$s \begin{cases} \leq 3e & \text{to form artificial arch within the failure zone} \\ = 3e \rightarrow 4e & \text{to suspend the failure zone to the natural arch} \end{cases}$$
 (8.5)

where e = mean joint spacing.

The stability of the artificial arch should be computed using professional software due to the complicated geometry.

The thin layer of shotcrete is often not included in stability calculations. The application of shotcrete is based on rock behaviour and field stress. A general guidance adapted from (RocScience, 2023) is provided in Table 8.1.

TABLE 8.1

Application of Shotcrete

Rock	Rock behaviour	Requirements	Shotcrete
	Massive rock with no significant joints and defects		
Igneous and metamorphic	Surface defects, no significant joints.	Retention of broken pieces and control of rock mass dilation.	First layer: • Weldmesh & 50 mm shotcrete or • 50 mm of steel fibre reinforced shotcrete Second layer: 25 mm shotcrete for surface protection
	A few wide joints/ bedding planes, potential wedge failure.	Additional supports for rock bolts and cables.	50 mm of steel fibre reinforced shotcrete near the joints.
	Jointed.	Retention of broken pieces and control of rock mass dilation.	First layer: • 75 mm over weldmesh or • 75 mm of steel fibre reinforced shotcrete Second layer: 25 mm shotcrete for surface protection (thicker layer if stress concentration)
	Highly jointed and ravelling.	Prevention of progressive ravelling	50 mm of steel fibre reinforced shotcrete. Rock bolts or dowels may be required for large blocks.
	Heavily jointed.	Urgent control of rock mass failure and dilation	First layer: reinforced shotcrete with • Lattice girders or • light steel sets Inverted struts may be required. Second layer: thick steel fibre reinforced shotcrete. Extension of support down sidewalls may be required.
			(Continued)

(Continued)

Table 8.1 (Continued)

Application of Shotcrete

Rock	Rock behaviour	Requirements	Shotcrete
	Massive rock with minor surface defects	Sealing surface to prevent slaking	25 mm of shotcrete
	Surface defects, no significant joints.	Retention of broken pieces and control of squeezing.	75 mm of steel fibre reinforced shotcrete. Rock bolts and dowels may be needed.
	A few wide joints/ bedding planes, potential wedge failure.	Additional supports for rock bolts and cables.	50 mm of steel fibre reinforced shotcrete near the joints.
Sedimentary	Bedded and jointed, surface defects with squeezing.	Control of rock mass failure and squeezing.	First layer: 75 mm of steel fibre reinforced shotcrete. Rock bolts with face plates may be required. Second layer: 75 mm shotcrete.
	Highly jointed.	Control of bed separation and ravelling	Rock bolts or dowels are required. 75 mm of fibre reinforced shotcrete.
	Heavily jointed.	Control of rock mass failure and dilation	First layer: reinforced shotcrete with • Lattice girders or • light steel sets Inverted struts may be required. Second layer: thick steel fibre reinforced shotcrete. Gaps can be left to allow movement resulting from squeezing and swelling.

8.2.2 LINING SUPPORT SYSTEM

If the rock is very weak, a structural lining support system may be required. The internal support pressure must be larger than the critical value to avoid the plastic deformation developed around the circular tunnel:

$$p_{cr} = \left(p_0 - \frac{\sigma_{cm}}{2}\right) (1 - \sin\phi') \tag{8.6}$$

where p_0 = in-situ stress surrounding the tunnel; σ_{cm} = uniaxial compressive strength of rock mass; and ϕ' = effective frictional angle.

If there is only elastic deformation, the relative radial displacement at a distance x from the tunnel open end could be calculated approximately as (Panet and Sulem, 1995):

$$u^{*}(x) = \frac{u_{radial}(x)}{u_{max}} = 0.25 + 0.75 \left[1 - \left(\frac{3}{3 + 4\frac{x}{R}} \right)^{2} \right]$$
(8.7)

where: R = radius of the tunnel; and $u_{radial}(x) = \text{radial}$ displacement at the distance x from the end of the tunnel. The maximum radial displacement could be calculated approximately as:

$$u_{max} = \frac{R(p_0 - p_i)}{2G} = \frac{R(p_0 - p_i)(1 + v)}{E}$$

where: p_i = internal support pressure; G = shear modulus; E = Young's modulus; and v = Poisson's ratio.

EXAMPLE 8.2

A circular tunnel of 4.5 m diameter is proposed to be drilled at a mine near Pilbara. The in-situ pressure is estimated at 32 MPa. Young's modulus and UCS of the rock are 5GP and 30 MPa, respectively. The Poisson ratio is 0.2, and the frictional angle of the rock is 38°. The internal support pressure from the lining system is double the critical value. Calculate the displacement at 5 m from the tunnel open end.

Solution

Using Equation (8.5), the required pressure from the lining system is:

$$p_i = 2p_{cr} = 2\left(p_0 - \frac{\sigma_{cm}}{2}\right)(1 - \sin\phi') = 2\left(32 - \frac{30}{2}\right)(1 - \sin38^\circ) = 13.07 \text{ MPa.}$$

Using Equation (8.7), the maximum radial displacement is:

$$u_{max} = \frac{R(p_0 - p_i)(1 + v)}{E} = \frac{4.5(32 - 13.07)(1 + 0.2)}{5000} = 0.0204 \text{ m}$$

The relative radial displacement at 5 m from the open end of the tunnel is:

$$u^*(5) = 0.25 + 0.75 \left[1 - \left(\frac{3}{3 + 4\frac{x}{R}} \right)^2 \right] = 0.25 + 0.75 \left[1 - \left(\frac{3}{3 + 4\frac{5}{4.5}} \right)^2 \right] = 0.872$$

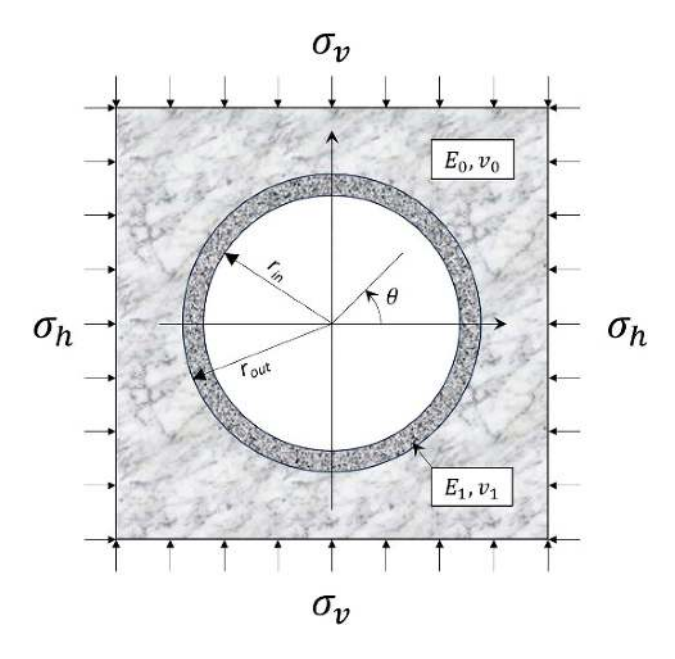


FIGURE 8.9 Symmetric circular tunnel model.

The absolute radial displacement at 5m from the open end of the tunnel is:

$$u_{2m}^{radial} = u_{2m}^* * u_{max}^{radial} = 0.0204 * 0.872 = 0.018$$
 (m).

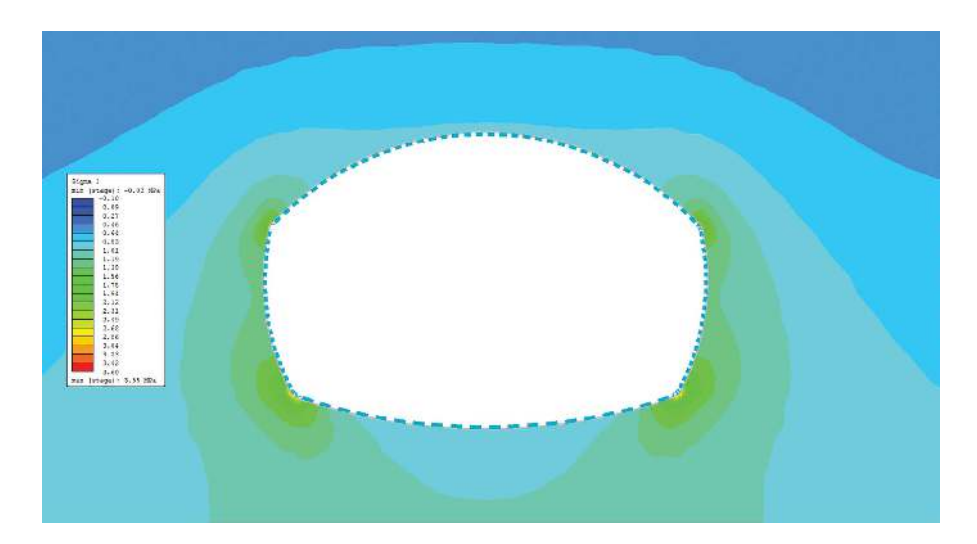


FIGURE 8.10 Stress distribution in rock surrounding a five-curve cross section of a tunnel with reinforced shotcrete.

If there is no plastic deformation (Figure 8.9), stress in the wall of a circular tunnel can be calculated using elastic theory, assuming (Анциферов, Деев et al., 2018):

$$\sigma_h = \frac{v_0}{1 - v_0} \sigma_v \tag{8.8}$$

Calculation for hydraulic tunnel should assume there is no water inside. An example of stress in the wall with v_0 of surrounding rock = 0.15 is given in Tables 8.2 and 8.3. Note that several tunnels may have only compressive stress. Hence, the tensile stress values in the table may be still negative.

In general, traffic tunnels have segmental cross sections. This form should be calculated using finite element programs due to its complexity (Figure 8.10).

8.2.3 Drainage and Ventilation System

Even when the tunnels are not designed for traffic, drainage and ventilation may still be considered for construction and maintenance. Tunnels are protected from water ingress with a circumferential waterproof layer (Figure 8.11). Right behind this layer is a system of longitudinal and cross-sectional diversion pipes, which lead water to a central drainage via one-way valves. Surface water inside the tunnel is collected via side ditches. Then, water may be led to the central drainage at some specific points.

Ventilation in tunnel provides oxygen for air comfort and reduces toxic content, including dust. The exposure to silica dust could pose a risk to lung health. Many countries set the work exposure limit to respirable crystalline silica for an eight-hour shift from 0.05 mg/m^3 to 0.1 mg/m^3 . As water spraying may add moisture content to the foundation, pressure air curtain is a popular choice to hinder the dispersion of dust. Besides, some tunnelling machines require compressed air, which can be supplied with a pumping system. The pumping station should have at least 75% extra reserved power, excluding the air leak via rubber pipes and accessories. If the tunnel is constructed at a significant elevation above the sea level, an elevation multiplier $K_{elevation}$ must be included in the pumping power (Table 8.4).

In terms of relative direction, ventilation in traffic tunnels could be classified as longitudinal, transverse and semi-transverse (Figure 8.12). To avoid the vacuum pressure, there should be only one main ventilation outlet near the exit of the tunnel. Two ventilation outlets may cause the lack of air in between them if there is no special air supply.

The minimum fresh air to be supplied per minute for people underground is roughly 5.7 m³ (200 cubic feet). The air supply for vehicles depends on type, load and speed of the vehicles. Electrical engines do not need air for combustion, but they may still need fresh air for heat removal. However, ventilation calculation for traffic tunnels is often based on wind speed for air comfort, as this number exceeds most of the need of fresh air. If the tunnel is extremely long, its ventilation will be sectioned to ensure the uniformity of oxygen concentration. Vertical inlets and outlets will be

Rock Mechanics

TABLE 8.2 Maximum Compressive Stress in the Wall of Circular Tunnels with $v_{\rm 0}$ = 0.15

	$\underline{\mathbf{r}_{\mathrm{out}}}$							E ₀ /E ₁							
Value	$\frac{\overline{\mathbf{r}_{in}}}{\mathbf{r}_{in}}$.04	0.08	0.12	0.16	0.2	0.4	0.6	0.8	1	1.2	1.4	1.6	1.8	2
σ	1.05	-1.22	-0.94	-0.77	-0.66	-0.57	-0.35	-0.25	-0.20	-0.16	-0.14	-0.12	-0.10	-0.09	-0.09
$\frac{\sigma_r}{}$	1.10	-1.36	-1.17	-1.02	-0.90	-0.81	-0.54	-0.41	-0.33	-0.27	0.24	-0.21	-0.18	-0.16	-0.15
$\sigma_{_{v}}$	1.20	0.26	-1.21	-1.12	-1.04	-0.97	-0.72	-0.57	-0.47	-0.41	-0.35	-0.31	-0.28	-0.26	-0.24
	1.30	-1.01	-1.07	-1.05	-1.00	-0.96	-0.76	-0.62	-0.53	_0.46	-0.41	-0.36	-0.33	-0.30	-0.28
σ^{ex}	1.05	-23.10	-18.90	-15.80	-13.60	-11.90	-7.35	-5.32	-4.17	-3.43	-2.91	-2.53	-2.24	-2.01	-1.82
$\frac{\sigma_{ heta}^{ex}}{}$	1.10	-10.10	-10.80	-10.10	-9.27	-8.52	-5.96	-4.56	-3.70	-3.11	-2.68	-2.35	-2.10	-1.90	-1.73
$\sigma_{_{_{\scriptscriptstyle \mathcal{V}}}}$	1.20	-0.31	-3.98	-4.88	-5.09	-5.07	-4.28	-3.56	-3.03	-2.63	-2.32	-2.08	-1.88	-1.72	-1.58
	1.30	2.76	-1.17	-2.51	-3.08	-3.34	-3.32	-2.94	-2.60	-2.31	-2.08	-1.88	-1.72	-1.59	-1.47
σ^{in}	1.05	-31.20	-23.20	-18.80	-15.90	-13.80	-8.32	-5.98	-4.67	-3.83	-3.25	-2.82	-2.49	-2.23	-0.04
$\sigma_{ heta}^{in}$	1.10	-24.50	-18.40	-15.30	-13.30	-11.80	-7.69	-5.75	-4.60	-3.84	-3.29	-2.88	-2.56	-2.31	-0.31
$\sigma_{_{v}}$	1.20	-22.40	-16.10	-13.30	-11.60	-10.40	-7.14	-5.53	-4.54	-3.85	-3.35	-2.97	-2.66	-2.42	-2.10
	1.30	-21.30	-15.40	-12.70	-11.10	-9.94	-6.91	-5.44	-4.51	-3.87	-3.39	-3.02	-2.73	-2.49	-6.10

Data edited from (Анциферов, Деев et al., 2018).

TABLE 8.3 Maximum Tensile Stress in the Wall of Circular Tunnels with $\nu_{\rm 0}=0.15$

	$\underline{\mathbf{r}_{\mathrm{out}}}$							Eo	Έ ₁						
Value	r_{in}	0.04	0.08	0.12	0.16	0.2	0.4	0.6	0.8	1	1.2	1.4	1.6	1.8	2
σ	1.05	-0.01	0.06	0.09	0.09	0.09	0.08	0.06	0.05	0.04	0.04	0.03	0.03	0.03	0.02
$\frac{\sigma_r}{}$	1.10	-0.14	-0.05	0.00	0.03	0.05	0.07	0.07	0.06	0.05	0.05	0.05	0.04	0.04	0.04
$\sigma_{_{v}}$	1.20	-0.45	-0.29	-0.21	-0.16	-0.12	-0.03	0.00	0.02	0.02	0.02	0.02	0.02	0.02	0.02
	1.30	-0.78	-0.55	-0.43	-0.36	-0.31	-0.16	-0.10	-0.07	-0.05	-0.04	-0.03	-0.02	-0.02	-0.02
σ^{ex}	1.05	-2.01	0.86	1.71	2.01	2.08	1.77	1.43	1.18	1.00	0.87	0.76	0.69	0.62	0.57
$\frac{\sigma_{ heta}^{ex}}{}$	1.10	-5.77	-1.96	-0.58	0.10	0.48	0.99	0.97	0.88	0.79	0.71	0.65	0.59	0.54	0.50
$\sigma_{_{v}}$	1.20	-9.19	4.32	-2.49	-1.54	-0.96	0.14	0.41	0.49	0.50	0.49	0.47	0.44	0.42	0.40
	1.30	-9.75	-5.15	-3.26	-2.23	-1.59	-0.28	0.10	0.25	0.32	0.34	0.35	0.34	0.34	0.33
σ^{in}	1.05	4.92	4.30	4.01	3.73	3.46	2.47	1.90	1.53	1.29	1.11	0.97	0.87	0.78	0.71
$rac{\sigma_{ heta}^{\scriptscriptstyle in}}{}$	1.10	7.09	4.43	3.65	3.27	3.01	2.25	1.81	1.51	1.30	1.14	1.01	0.91	0.83	0.76
$\sigma_{_{v}}$	1.20	11.20	6.32	4.64	3.81	3.31	2.25	1.81	1.53	1.33	1.18	1.06	0.97	0.89	0.82
	1.30	12.60	7.46	5.45	4.40	3.75	2.39	1.87	1.57	1.37	1.21	1.09	1.00	0.91	0.85

Data edited from (Анциферов, Деев et al. 2018).

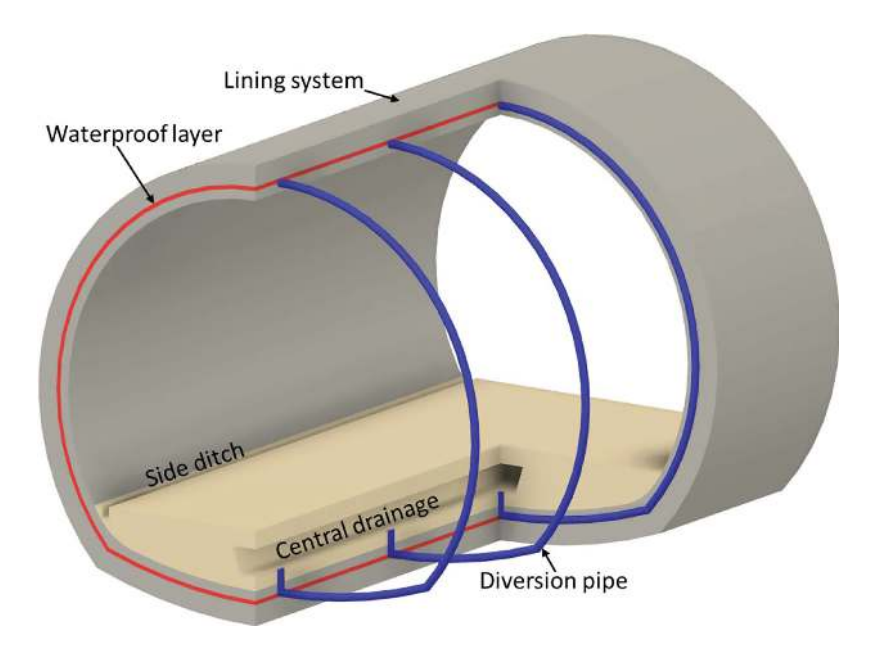


FIGURE 8.11 Drainage of a tunnel.

TABLE 8.4 Elevation Multiplier for Pumping Power

Elevation, m	0	300	600	900	1200	1500	1800	2100	2400	2700	3000	3600
$K_{\it elevation}$	1	1.03	1.07	1.10	1.14	1.17	1.20	1.23	1.26	1.29	1.32	1.37

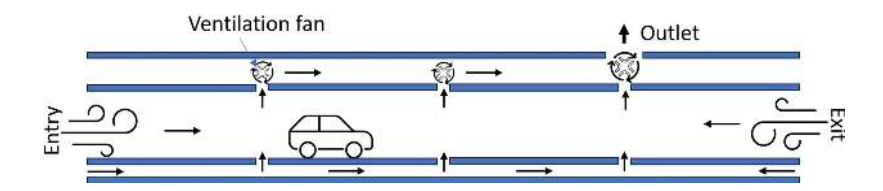


FIGURE 8.12 Semi-transverse ventilation system.

arranged alternatively. The International Tunnelling Association indicates that average wind speed in tunnel shall be from 0.3 m/s to 2 m/s during the operation. In the construction phase, dust will be upwind diffusion if the wind speed is less than 0.5 m/s (British Standards Institution, 2019).

EXAMPLE 8.3

A mining tunnel with a cross-sectional area of 29.5 m² near Tom Price uses an overlap ventilation system. There are no more than 120 workers in the tunnel at a time and machines require 540 m³ of fresh air per minute. Assuming a leaking rate of 20%, calculate the required wind speed and power of ventilation system.

Solution

As Tom Price town is at 747 m above sea level, $K_{\text{elevation}}$ is interpolated to be 1.085 (Table 8.4). Set the exceeding air volume at 75%. When the machine operated, the required fresh air volume per minute is:

$$V = (120*5.7+540)*1.085*(1+20\%)*(1+75\%)$$

= 2788.8 m³/minute = 46.48 m³/s.

As the tunnel employs the overlap ventilation system, the wind blows in two directions. Hence, the cross section for wind is halved, and the wind speed is calculated as:

$$v = \frac{46.48}{\frac{29.5}{2}} = 3.15 \text{ m/s}.$$

This wind speed is more than the recommended speed; workers may need PPE to keep their body heat. When the machine is not operated, the required fresh air volume per minute is:

$$V = (120*5.7)*1.085*(1+20\%)*(1+75\%)$$

= 1558.5 m³/minute = 25.97 m³/s.

The average wind speed is:

$$v = \frac{25.97}{\frac{29.5}{2}} = 1.76 \text{ m/s}.$$

This wind speed is in the air comfort zone.

8.3 CONSTRUCTION OF TUNNELS

From the standpoint of project management, a tunnel project can be typically divided into several stages with different focuses:

Planning and feasibility study: This is the most critical stage. Fieldwork
begins with general site investigations to obtain some primary understanding of geological conditions. An environmental impact assessment (EIA)
is required to evaluate potential environmental effects of the proposed
tunnel construction. Additionally, public consultations and stakeholder

engagement are necessary to gauge potential social impacts. Given all primary considerations assessed, an initial engineering design is developed, addressing technical feasibility, financial requirements and safety factors.

- Financing and approvals: This pass/fail test for the project is often done externally by non-engineering team. Bureaucratic procedures for approvals and permits are complex and time-consuming. An inadequate feasibility study without an understanding of regulations and legal requirements could cause a long delay in the project timeline.
- Detailed design and engineering: This stage focuses on detailed analyses to finalise the best construction method, which will be discussed later in this chapter. Ventilation, drainage and safety systems are detailed at this stage. Material and machines are selected to be employed in the tunnel. By this point, the certainty of the project is over 95%.
- Procurement and contractor selection: This stage may involve an invitation to tender or negotiation of other forms of contracts. Bidding companies must demonstrate financial capability and a proven track record in similar constructions. Specialised technical expertise is critical because tunnel construction requires distinct skills and precision compared to general construction, and any failure in construction could be costly to resolve.
- Construction: General tunnelling includes four components: excavation, support and lining, installation of system and services and testing and commissioning. These components may vary depending on the selected method.

Depending on the regulations of the country or territory, many authorities require additional approvals at each step.

8.3.1 Construction Methods

In general, the tunnel construction can be classified by the earth/rock removing methods. Cut-and-cover is an affordable method for shallow tunnels. This method excavates a trench and provides supports for the roof covering the tunnel. The earth or rock can be removed mechanically or with explosive materials. Conventional bottom-up constructions install temporary walls to support the later earth pressure (Figure 8.13). Thin sheet piles will be reused for the next projects, or they could stay as an additional safety measure. Meanwhile, top-down constructions install permanent walls in the first steps.

The tunnel boring machine (TBM) method is a highly automated method crushing though the earth or rock with a spinning cutter head. Some TBMs have pressurised compartments to accommodate the work under the groundwater level. Excavated earth and rock debris are transported via a chain inside the machine, and supports are installed as TBM advances. This method is often employed in long tunnel project, as it could significantly save the time. However, a TBM could only excavate fixed-size circular tunnels. As the shields of the tunnels are installed automatically on the go, there is very limited capability to amend the tunnel's cross section and profile.

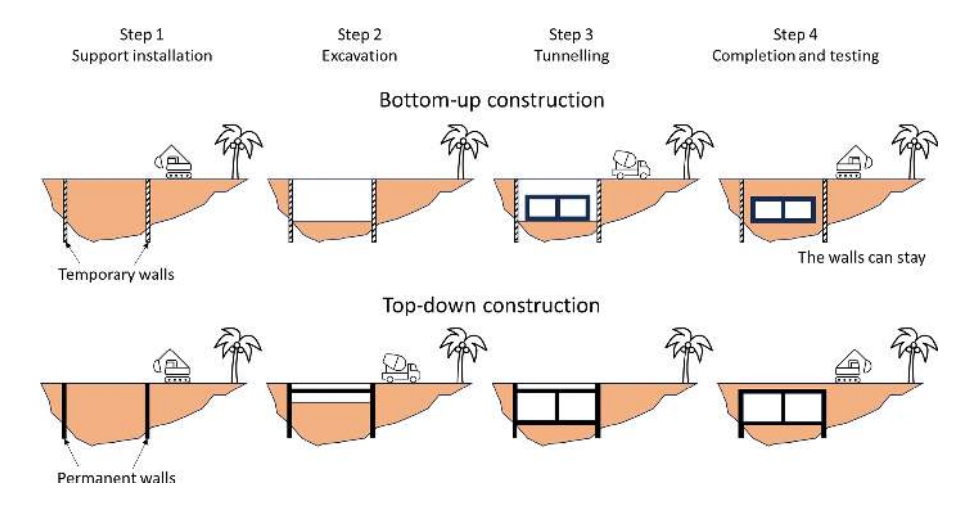


FIGURE 8.13 Cut and cover method for shallow tunnelling.

The new Austrian tunnelling method (NATM) is arguably the most popular method for mining and short traffic tunnels. This method may construct lattice girders and spray shotcrete to aid the stability. If the monitoring data indicated that the wall requires additional supports, rock bolts and cables can be installed at specific places or all over the perimeter to form an arch. Thereby, the tunnel is stabilised by the geotechnical stress of the surrounding rock mass. This method is featured with sophisticated monitoring and design on the go. Therefore, this method frequently uses the late supports, which are installed during or after the construction. NATM has many variances for specific purposes. Drill and blast (Figure 8.14) is

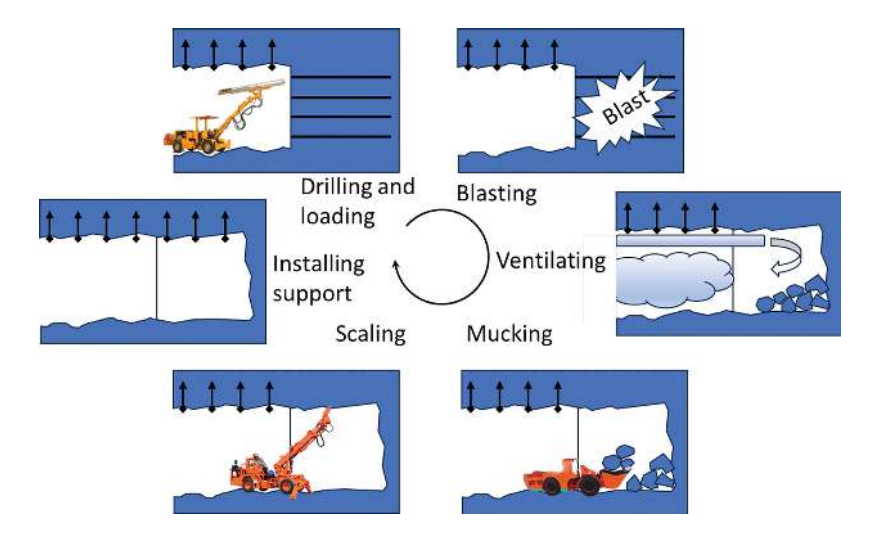


FIGURE 8.14 Drill and blast method.

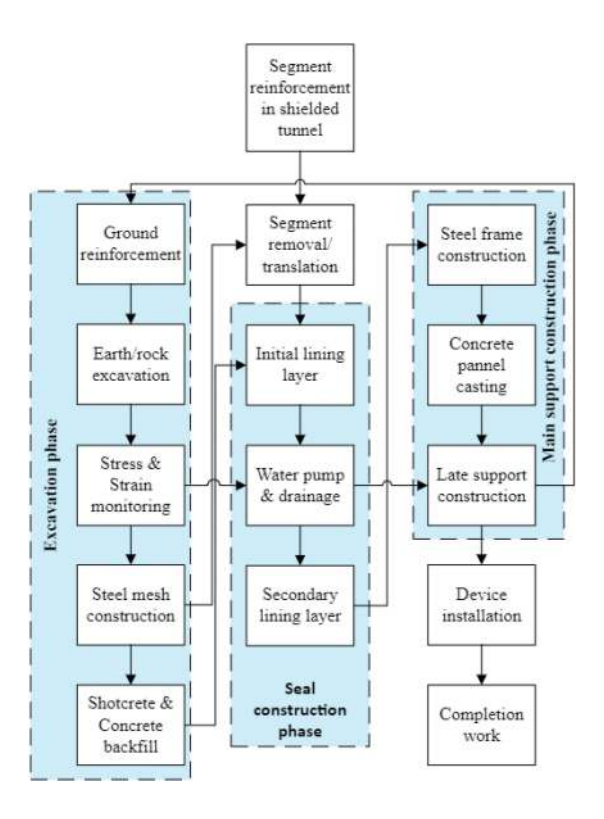


FIGURE 8.15 Sequential method.

often employed in mining while sequential method (Figure 8.15) can be adopted for traffic tunnels.

Multiple-lane traffic tunnels often have a very large radius of the top arch. Hence, the cross section may not be able to be excavated at once, as it may collapse during or right after the excavation. Therefore, the cross section of the tunnel is divided into several parts (Figure 8.16). One part is excavated first, and temporary supports are installed together with primary supports. Then another part will be excavated.

Jacking is a common choice if a new tunnel is constructed near other existing tunnels or under important structures because additional stress during the construction must be limited. If the size of the new tunnel is smaller than 10 feet, a pipe jacking system could be used (Figure 8.17). When the size is larger than 20 feet, box jacking system should be considered. To reduce the required power of hydraulic jacks, a micro tunnel boring machine can be employed to aid the forward moving to the reception shaft. Excavated debris will be transported to sedimentation tank via a conveyor pipe. A laser system could be used to ensure that the tunnel accurately turn on the predefined direction. Box jacking allows mini excavator to work within the box.

There are also several other tunnel construction methods, such as open building pit, clay-kicking, immersed and freezing. These methods do not focus on rock.

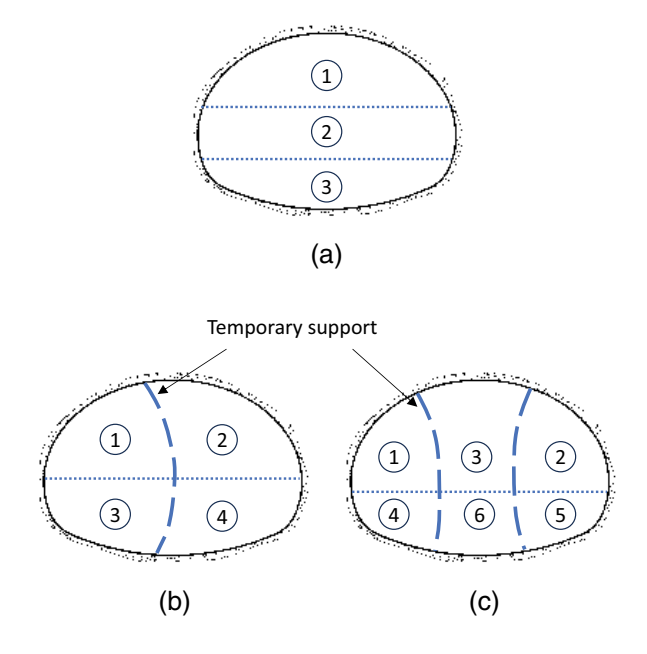


FIGURE 8.16 Excavation sequences for large tunnels: (a) head-bench; (b) central diaphragm and (c) side drift.

8.3.2 CARES AND CONSIDERATIONS

The biggest technical challenge in tunnelling is dealing with continually varying geological conditions. An unforeseen fractured zone of rock could abruptly elevate the rock pressure or increase groundwater inflow. Although thorough site investigations could assist in anticipating, the conditions could deteriorate due to the construction activities or simply with time. As rock stress is high, any movement in rock mass will crack tunnel shields. Hence, a comprehensive geotechnical investigation and sophisticated monitoring are a must in most tunnelling projects. The monitoring focuses on not only the rock at the excavation front but also installed structures and supports. A popular approach for geological investigation is seismic or acoustic survey. This non-destructive method initiates seismic waves from a seismic source. The waves travel through the ground and reflect at the interfaces between soil or rock layers, and they will be caught by several receivers at various places. The direction and amplitude of the waves indicate the geological properties underground.

When the new tunnel is placed near existing underground structures, a numerical study is often undertaken to evaluate the increase in stress on the existing structure, as this change was not proposed in the old design. The dynamic impact of traffic and hydraulic tunnel is complicated and depends on the shear wave velocity of the rock. In general, the distance to an existing tunnel should be three times the diameter of the larger tunnel. In the case of a weak foundation, this distance is recommended to be five times. When twin tunnels are constructed, the distance between

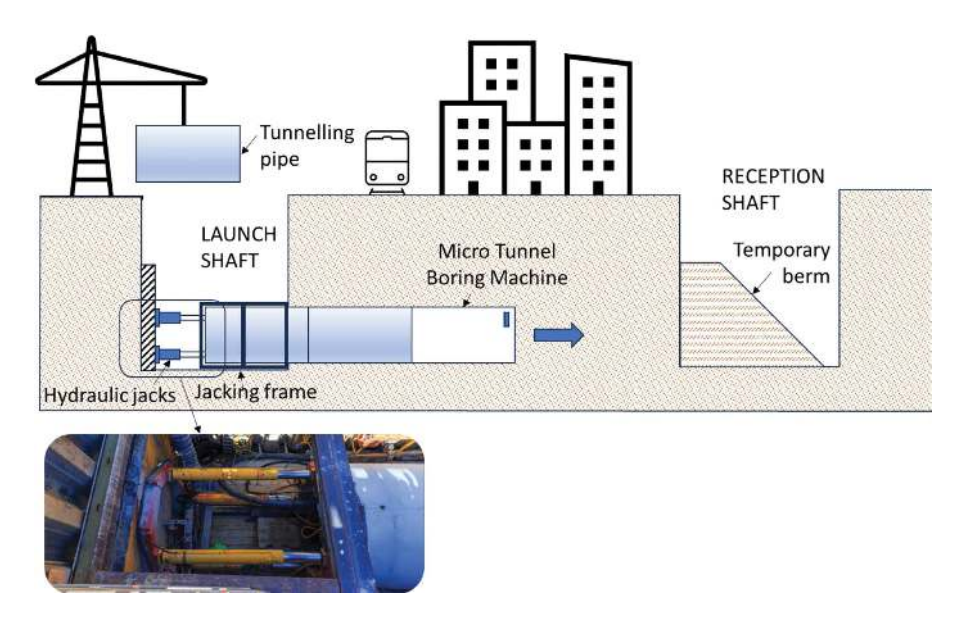


FIGURE 8.17 Pipe jacking.

the tunnels should be greater than 1.5 time the diameter if they are not constructed simultaneously.

Tunnel entries usually have unequal stress distribution and weak foundation. These places are prone to slide and erosion. If tunnels go into steep hill, the top of entries should have protection walls to stop rockfalls. Besides, the traffic entries are often smoothly elevated to prevent rainfall water ingress, or the tunnel trend outwards. Traffic tunnel should follow general guide of road planning (Department of Transport and Main Roads, 2021). In general, the grade of two-lane tunnels with two-way traffic is recommended to be less than 3%. If the slope must be higher, the design speed will decrease. For example, the slope of 8–9% sets the maximum speed in tunnels at 30 km/h. Emergency stops and service points must be designed to withstand dead loads.

A frequent substantial issue in tunnelling is groundwater inflow. Excessive groundwater can disrupt the construction with flooding, increase pressure on tunnel lining, damage machines and girders, and complicate the excavation process. Therefore, drainage systems must be well designed, and dewatering pumps must have backups readily available at any time during construction. In May 2024, water inflow has partially collapsed the hydraulic tunnel of Snowy 2.0 in New South Wales. This interruption is likely to put Snowy Hydro at risk of missing its deadline of being operational by late 2027.

Two significant lethal dangers in tunnelling are fire and explosion. Fire could be caused by equipment malfunction and electrical fault, while explosion could be caused by inappropriate use or storage of explosive materials. Therefore, fire detection and suppression must meet standards. Good evacuation plans and frequent drills could help to mitigate the consequences. Signboards and emergency phones are

required for traffic tunnels. Generators may be required as a backup for grid power. Limited access and egress, poor ventilation and potential entrapment could cause hazards in confined spaces. Tunnels longer than 500 m rely on an active ventilation system. Hence, a backup for the main ventilation fan is required.

As most tunnels are under groundwater levels, sealing lining system requires special care. Note that groundwater pressure can vary widely in rock when rain fully fills rock joints of tens metres. Segmental lining systems often seal with hollow rubber gaskets to prevent leaking due to aged materials.

8.4 NUMERICAL ANALYSIS AND SOFTWARE

Engineers are witnessing a crucial moment when tunnel design is getting rid of analytical calculations because these calculations could not anticipate complicated geological conditions and special, irregular tunnel shapes. The simplification requires a high safety factor, which add another dimension to the project budget. Besides, numerical computations are aided with detailed illustrations, which impress clients. This section will not depict the algorithm of numerical methods, which may need several thick books to explain in detail. It will skim through some main points of a few popular numerical methods for engineers to give consideration during the selection.

The finite element method (FEM) is an outstanding tool if the computation must deal with stress and non-linear physics. Therefore, FEM is often selected for the simulation of structural components of tunnels. FEM has some significant advantages with composite materials – such as concrete – and non-elastic deformation – such as lining layers' stretch. FEM is based on tessellation and can be applied with an irregular mesh. An appropriate meshing with the right type of elements could significantly reduce the computing workload. However, original FEM cannot simulate breakage, which requires remeshing.

The finite difference method (FDM) is fast for linear physics. FDM employs a square net, which may require adaptive meshing for irregular shapes. Hence, FDM is often used to simulate the state of the whole domain, such as heat transfer, water pressure or dust diffusion. However, this method is more research-oriented thanks to its simplicity.

The finite volume method (FVM) is the scientific foundation for most computational fluid dynamics simulation tools. FVM solves partial differential equations with linear algebra, like FEM and FDM. In FVM, the flux at the surface of a finite volume – a very small volume surrounding a node point in a mesh – is evaluated as a divergence term, using the divergence theorem. Theoretically, the flux entering a given volume via an interface equal to the flux leaving the adjacent volume. Thereby, FVM can be applied easily to unstructured meshes.

The discrete element method (DEM) is a relatively new tool to study the behaviour of rock mass. This explicit method treats each element as an individual object, which can move, slide, rotate and so on. Hence, DEM can be used to simulate breakage or behaviours of discontinuous media. However, DEM's computing workload can be significantly higher than of other methods. Based on the overlapping zone between elements, the interactions and deformation are computed.

TABLE 8.5
Numerical Methods and Objects of Simulation

Object	Finite element method	Finite difference method	Finite volume method	Discrete (distinct) element method
Tunnel structure	///	✓		
Rock mass	///	√ ✓		√ √
Jointed rock	✓			///
Ground water	///	/ / /	✓ ✓	
Support systems	///	✓		✓
Blast	✓	✓		///
Crush	✓	✓		✓
Stage of construction	///	✓		
Incidents			✓	✓
Drainage system	✓	✓✓	/ / /	
Ventilation	✓	√ √	///	

A few computer packages employ coupled FEM-DEM to study the behaviour of jointed rocks. The methods stated in Table 8.5 include their whole family with their coupled methods.

In tunnelling, software can be categorised into four main groups based on purpose:

- Geotechnical/Geological conditions: This type of software computes stress
 and strain in the ground, including the additional stress caused by construction stages on adjacent infrastructure. Geotechnical finite element software,
 such as Plaxis, RocScience (RS), FEM-Tunnel, Geo5 and GeoStudio, dominates this group.
- *Tunnel Support*: This group focuses on designing and computing specific types of tunnel supports. Due to the small scope of application within tunnel engineering, this group is the smallest group, with several specified software, such as Unwedge and OpenTunnel Designer.
- *Tunnel Structure*: This group simulates structural elements of tunnels. Examples of structural finite element software used in this area include ANSYS, Sap2000 and ProStructures.
- Monitoring and Data Collection: This group includes a variety of software,
 often tailored to specific projects. Nevertheless, many programmes integrate
 within a large environment and focus on digital twin/BIM capabilities. Some
 of them are web-based or app-based for real-time monitoring. Examples of
 platforms used in tunnel projects include iTwin, WeStatiX and TwinView.

Universities typically do not equip students with software skills because commercial programmes evolve annually. However, the use of numerical simulations has become essential in most tunnel designs.

8.5 SUMMARY

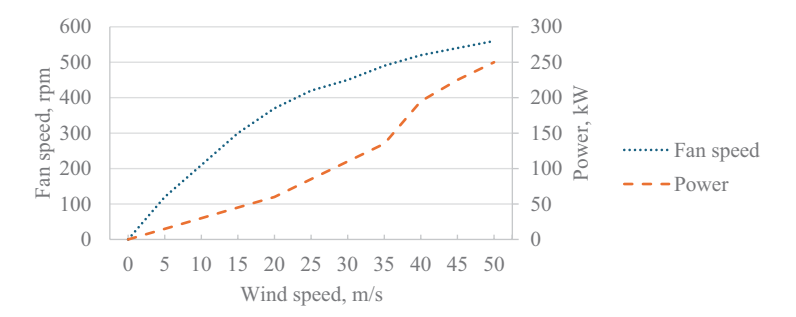
- Four popular methods for tunnel construction include: cut and cover (suitable
 for shallow tunnels), tunnel boring machine (TBM) for long-distance tunnelling, new Austrian tunnelling method (NATM) for general tunnelling, and
 jacking for short tunnels.
- 2. NATM is featured with adaptive design and sophisticated real-time monitoring to adjust support based on in-situ conditions.
- 3. Early support can be installed before the excavation, while late support can be installed during the tunnel operation phase.
- 4. Local rock reinforcement stabilises walls or roof by securing the wedge with surrounding rock. Global rock reinforcement stabilises the tunnel by forming an arch and transfer the stress to the rock base under the tunnel.
- 5. Tunnels in heavily jointed rock mass require two layers of shotcrete. The first layer can have lattice girders, while the second can be steel fibre reinforced.
- 6. A minimum interspace of three tunnel diameters is recommended between new and existing tunnel, and 1.5 tunnel diameters between twin tunnels excavated concurrently. If the tunnels are different in size, the largest diameter is used for calculation.
- For tunnel with large segmental cross-sectional area, the excavation proceeds in multiple phases. Temporary supports can be installed to stabilise the roof and walls.
- 8. Ventilation in the main tunnel space should control airflow from 0.5 m/s to 2 m/s for air comfort and prevention of dust upwind diffusion.
- 9. FEM dominates numerical packages in tunnel engineering. However, the modern large tunnel projects are powered with digital twin platforms.

REVIEW EXERCISES

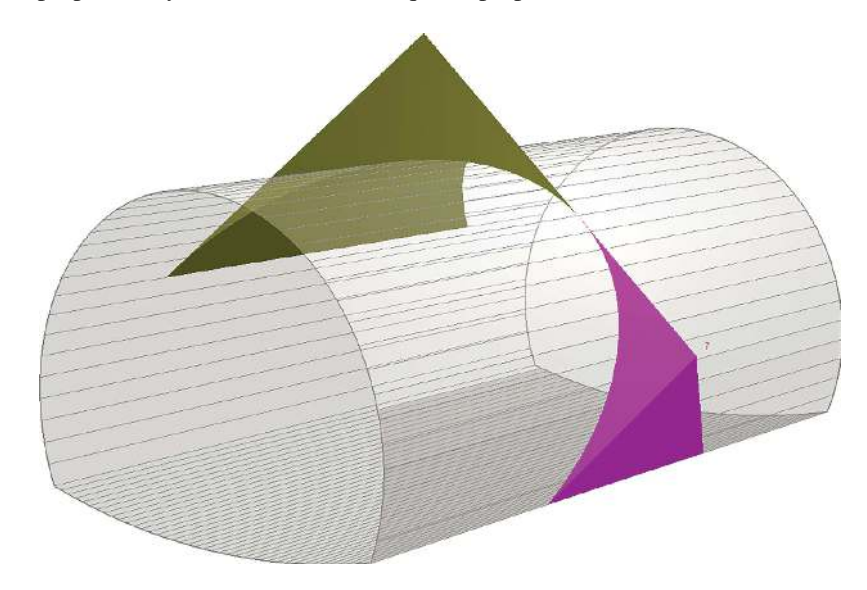
- 8.1. Discuss the advantages and disadvantages of each type of tunnel cross section described in Figure 8.1.
- 8.2. Compare bottom-up and top-down approaches in cut and cover method.
- 8.3. Discuss the features of NATM that make it a popular choice for mining tunnels.
- 8.4. Recent accidents on a four-lane highway perched on a slope requires a new tunnel to be constructed. Propose the required internal dimensions of the tunnel for traffic. Recommend a segmental cross section for the proposed tunnel. Given the allowable height of vehicles is 4.5 m. Lanes, including the service lane, have standard width of 3.5 m, and the minimum free space for inclining vehicles is 0.9 m.
- 8.5. Redo question 2 with two separate tunnels for two traffic directions. Which option will require more excavation?
- 8.6. A brochure of a rock bolt reads that plate capacity, tensile capacity and anchor capacity of the bolt are 0.6 MN, 1.2 MN and 0.5 MN, respectively. What is the maximum load that the bolt can carry safely?
- 8.7. A pumped hydro system requires a circular hydraulic tunnel of 4.5 m diameter to supply water to turbines. A part of the tunnel will be

underground with the highest vertical stress estimated to be 2.2 MPa. Given that the allowable stresses in concrete are 7.0 MPa in compression and 2 MPa in tension, calculate the required thickness of the concrete tunnel. Assume $\nu_0=0.15$. The measured elastic modulus of rock and concrete are 32 and 20 GPa, respectively.

8.8. An engineer is assigned to design ventilation for a long metro tunnel with a cross-sectional area of 25.5 m². In case of accidents, two trains with 648 passengers each could be detained in between the inlet and outlet shafts. The fan must increase its rotation speed to supply air for the detained passengers. Calculate the required fan speed at the outlet. Given the graph of tested in situ wind speed and fan speed as shown.



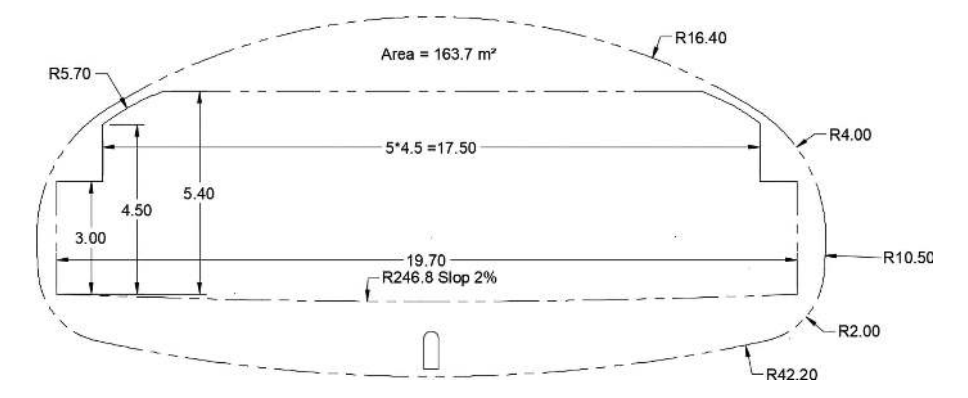
8.9. A tunnel of 10 m width has gone in the direction of 90/0 through a weak rock zone with three major joints of 60/30, 60/150 and 60/270, as shown in the following figure. The weights of the wedges on the roof and at the side wall are 67.4 and 15.9 tons, respectively. Using rock bolts HS26 with a maximum tensile capacity of 260 kN to stabilise the roof wedge, propose a layout and number of required perpendicular rock bolts.



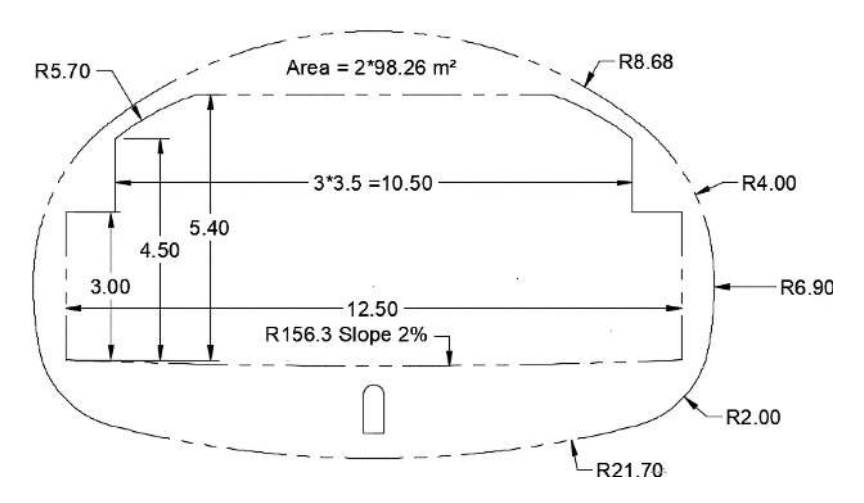
8.10. Calculate required number of bolts to stabilise the side wedge of the tunnel in question 9, if the internal friction angle of the rock is 35°, and the cohesion is 1 kPa. The area of the sliding surface is 11.78 m². The required safety factor is 1.5.

Answer

8.4. There are a few good variances. The following is one example with 0.5 m gap. Unit in metre.



8.5. The following is one example. Twin tunnels requires more excavation. However, the single-tunnel design may require more temporary supports and a thicker shield.



- 8.6. The max load is 0.5 MN. The capacities cannot be added together. The failure at anchor will occur first.
- 8.7. Calculate the stress ratios:

$$\frac{\sigma_{compressive}}{\sigma_{v}} = \frac{7}{2.2} = 3.18; \qquad \frac{\sigma_{tensile}}{\sigma_{v}} = \frac{2}{2.2} = 0.909$$

Using Table 8.2 for $E_0/E_1 = 32/20 = 1.6$. There is no significant requirement for compressive strength, but tensile strength requires $r_{\text{out}}/r_{\text{in}}$ to be equal or smaller than 1.1 so that $\frac{\sigma_{in}}{\sigma_{v}}$ will be equal or smaller 0.91. Select $r_{\text{out}}/r_{\text{in}} = 1.1$, then the required thickness should be 0.225 m because $r_{\text{in}} = 4.5/2 = 2.25$ m.

8.8. As the incident occurs in a long metro tunnel, the outlet take air from both sides. Set the exceeding air volume to be 75%. The required air volume rate is

$$V = 2 * (1+75\%) * (2*248*5.7) = 25855.2 \text{ m}^3/\text{min}.$$

Neglecting contraction, in-situ wind speed at free space could be

$$v = 25855.2/60/25.5 = 16.899 \text{ m/s}$$

Using the provided chart, the required fan speed to be 350 rpm.

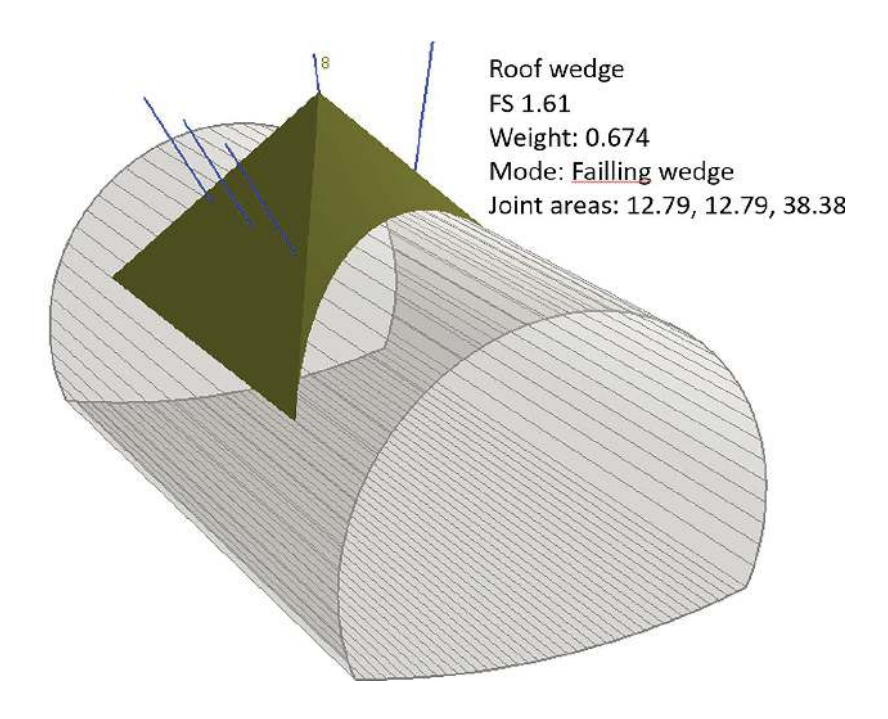
8.9. The weight of the roof wedge is

$$W = 67.4*9.81 = 661.194$$
.

As the curvature of the roof is not given, it may be the best to use three vertical rock bolts.

$$FS = \frac{resisting\ force}{driving\ force} = \frac{3*260}{661.19} = 1.8$$

Another numerical solution is provided as reference.



8.10. Weight force of the side wedge:

$$F = 15.9*9.81 = 156 \text{ kN}.$$

Normal vector of joint 60/270:

$$\mathbf{n}_{3} = \left[\sin\alpha_{3}\sin\psi_{3}, \cos\psi_{3}, -\cos\alpha_{3}\sin\psi_{3} \right] = [-0.866, 0.5, 0]$$

$$\mathbf{s} = \frac{(\mathbf{n}_{3} \times \mathbf{A}) \times \mathbf{n}_{3}}{(\mathbf{n}_{3} \times \mathbf{A}) \times \mathbf{n}_{3}} = [-0.4998, 0.8662, 0]$$

The bolt is perpendicular to the surface. Assume there is one horizontal bolt.

$$P = [260,0,0] * ([1,0,0] \cdot [-0.4998, 0.8662, 0]) = [-129.984 \ 0 \ 0]$$

$$\sigma = \frac{\|-A \cdot n_3 + P \cdot n_3\|}{area} = 16.1792 \text{ kPa}$$

$$\tau = c + \sigma tan\varphi = 1 + 16.1792 * tan35^\circ = 12.3288 \text{ kPa}$$

$$F_s = \frac{P \cdot s + \tau * area}{A \cdot s} = 1.556 \text{ Satisfy}.$$

REFERENCES

- Athanasopoulou, A., et al. (2022). Prospects for Designing Tunnels and Other Underground Structures in the Context of the Eurocodes. Joint Research Centre, Luxembourg.
- AustralianTunnelling Society (2020). *Tunnel Design Guideline*. https://australiantunnellingsociety.com.au/resources/ats-tunnel-design-guideline/
- Austroads (2018). *Guide to Road Tunnels*. https://austroads.gov.au/infrastructure/road-tunnels/guide-to-road-tunnels
- British Standards Institution (2019). BS 6164:2019 Health and Safety in Tunnelling in the Construction Industry Code of Practice. British Standards Institution.
- China Oil & Gas Industry Standards (2014). *Code for Design of Oil and Gas Transmission Pipeline Crossing by Shield Tunneling*. https://gbstandards.org/China_standard_english.asp?code=SY/T%207023-2014
- Department of Transport and Main Roads (2021). Road tunnels. *Road Planning and Design Manual*, Vol. 4. https://www.tmr.qld.gov.au/business-industry/technical-standards-publications/road-planning-and-design-manual-2nd-edition
- Federal Centre of Norms, S. and Assessment in Construction (2018). Calculation and Design Guideline: Transport Tunnels for Regions with Increased Seismicity. https://meganorm.ru/Data2/1/4293727/4293727747.pdf
- Federal Highway Administration (2009). *Technical Manual for Design and Construction of Road Tunnels Civil Elements*. https://www.fhwa.dot.gov/bridge/tunnel/pubs/nhi09010/tunnel_manual.pdf
- Li, C.C. (2017). Principles of rockbolting design. Journal of Rock Mechanics and Geotechnical Engineering, Vol. 9, No. 3, pp. 396–414.

National Railway Administration of the People's Republic of China (2016). *TB 10003 Code* for Design of Railway Tunnel. https://www.chinesestandard.net/PDF/English.aspx/TB10003-2016

- Panet, M. and Sulem, J. (1995). *Calcul des Tunnels par la Méthode Convergence-Confinement*. Presses de l'Ecole Nationale des Ponts et Chaussées.
- RocScience (2023). Shotcrete Support. https://static.rocscience.cloud/assets/resources/learning/hoek/Practical-Rock-Engineering-Chapter-15-Shotcrete-Support-Remediated.pdf
- ShanghaiEngineering Construction Code (2017). DG TJ 08–2033 Shanghai Construction Specification: Road Tunnel Design Standards. https://www.sanmin.com.tw/product/index/006613934
- Statens vegvesen (2000). Fjellbolting. Håndbok 215. Trykkpartner, Oslo.
- Анциферов, С.В., et al. (2018). РУКОВОДСТВО ПО РАСЧЕТУ И ПРОЕКТИРОВАНИЮ ТРАНСПОРТНЫХ ТОННЕЛЕЙ ДЛЯ РАЙОНОВ С ПОВЫШЕННОЙ СЕЙСМИЧНОСТЬЮ. Moscow.

Appendix

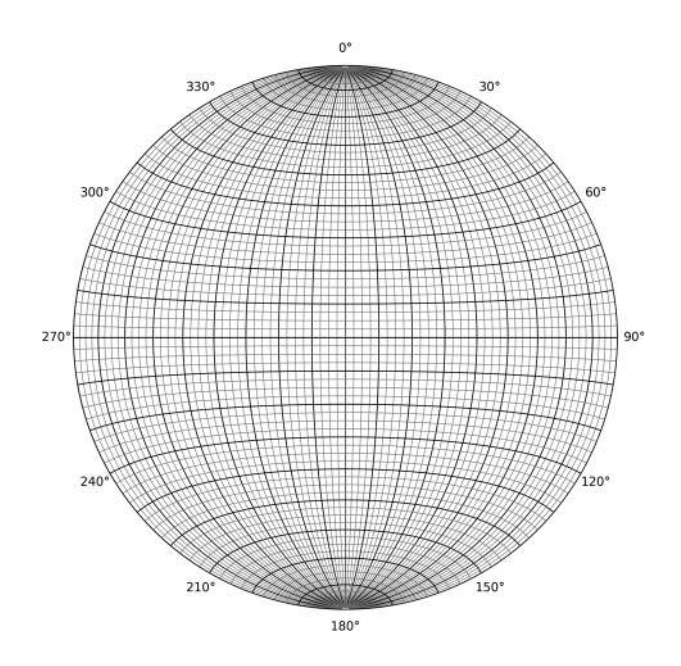


FIGURE A1 Schmidt equatorial stereonet (equal area projection)

Python code A1

```
To plot at any resolution and configuration using mplstereonet library in python
```

```
import matplotlib.pyplot as plt
import mplstereonet as mpl
import numpy as np
fig=plt.figure(figsize=(8,8),dpi=300)
                                           # add a new figure with defined size and solutions
ax=fig.add_subplot(1,1,1,projection='stereonet')
                                                               # add a stereonet to the figure
ax.minorticks_on()
                                                                           # add minor ticks
ax.grid(which='major',color='black',linewidth=0.8)
                                                           # set properties for the major grid
ax.grid(which='minor',color='gray',linewidth=0.5)
                                                           # set properties for the minor grid
                                                                          # get the axes limit
ymin, ymax = ax.get_ylim()
xmin, xmax = ax.get\_xlim()
y_ticks = np.arange(ymin, ymax, np.deg2rad(10))
                                                           # Set the minor grid of 10 degrees
x_ticks = np.arange(ymin, ymax, np.deg2rad(10))
ax.set_xticks(x_ticks)
                                                                              # Set the ticks
ax.set_yticks(y_ticks)
ax.set_azimuth_ticks(range(0, 360, 30))
                                                                # Set labels every 30 degrees
```

ax.set_longitude_grid_ends(89) ax.grid(True) plt.savefig('stereonet.png', dpi=300) plt.show() # Set the length of longitude grid # Show the grid # Save the plot # Show the plot (optional)

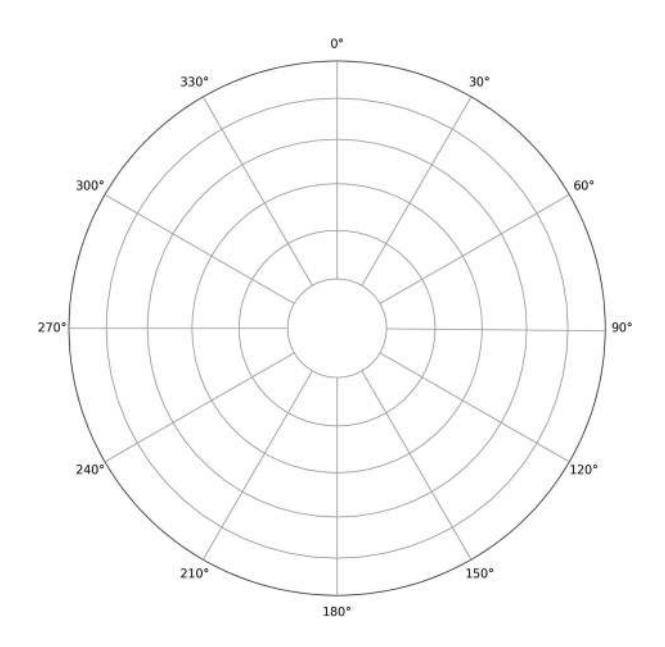


FIGURE A2 Polar overlay for hemisphere projection

Python code A2

The python library mplstereonet has limited option for polar overlay

import matplotlib.pyplot as plt import mplstereonet import numpy as np fig = plt.figure(figsize=(8,8),dpi=300) ax = fig.add_subplot(111, projection='stereonet') ax.grid(kind='polar') ax.set_azimuth_ticks(range(0, 360, 30)) plt.savefig('polar.png', dpi=300) plt.show()

Set type of the stereonet to polar # Set appropriate ticks

A	bored pile, <i>see</i> drilled piers
anaganamy mimamala 6	Bowen's reaction series, 19
accessory minerals, 6	Brazilian indirect tensile strength test, see
air-dried clay fraction, X-ray	indirect tensile strength test
diffractogram of, 6–7	broken rock, 148, 173
allowable bearing pressure, 90, 227–230	building materials, 10
allowable load-carrying capacity, see	building stones, 10
load-carrying capacity	bulk modulus K, 96
allowable pressure values, of rocks, 228, 249	•
alumina octahedron, 20	
American Society for Testing Materials (ASTM)	C
D3967, 102	caisson, see drilled piers
D6032, 90, 91, 110, 111	calcite, 6–10
angle of internal friction, 188-190	characteristics of, 9
angle of shearing resistance, see angle of internal	
friction	chemical methods, slope stabilisation, 218
anisotropic behaviours of rock, 156	chemical weathering of rocks, 16
anticline, 13, 14	circular failure, 212
aperture, 128	mode, 189–190
apparent dip, 12, 57	slope, 191–193
aquicludes, 30–31	clay minerals, 17–20
aquifers, 30–31, 51	coefficient of earth pressure, 156
aquifuges, 30–31	cohesive bonds, 169
aquitards, 30–31	combined footing, 226
•	compressional waves, 23
asthenosphere, 3, 22	confined aquifer, 30
ASTM, see American Society for Testing	conglomerate, 9, 11, 16
Materials	constant separation traversing, (CST), 45
augite, 6	coordinate system, 3, 60–62
axial plane, 13	core, 87–90
axis of fold, 13	core diameters, 89
axisymmetric loading, stress–strain relations, 162	core recovery ratio (CR), 89
	coring tools, 36
D.	correction factor (CF), 110
В	CR, see core recovery ratio
barrel aqueduct, rock foundation for, 226	crest of fold, 13
basalt, 8, 9, 11	critical distance, 40
basic friction angle, 127, 151, 169	crossover distance, 40
•	
bearing capacity factor, 241	crust, 1, 3
bedding plane, 14, 47, 48, 120	crustal rocks, 4
isometric view of, 69, 70	CST, see constant separation traversing
material, 189–190, 205	
bedrock, 228–231	D
determining depth, 45	
pile resting on, 232–233	deep-focus earthquakes, 22
Bhuj earthquake, 26	deep foundations on rock
biotite, 6	load-bearing capacity estimation, 233-236
black mica, see biotite	meaning of, 231
block-flexural toppling, 198, 199	types of, 231–232
block size, in rock mass, 129–130	deformation
block size index, 130	modulus of rock mass, 180-181
block toppling, 212–215	soils vs. rocks, 155–156
hody waves 23	degradation of rocks 17

degree of weathering, 17, 18 dental concrete, 248	elements of fault, 14 elements of folds, 13
diametrical strain, variation of, 95, 96	empirical correlations, intact rock, 112–113
diametric plane, 61	empirical correlations, rock mass, 147, 175, 181
dip, 57–60, 66	end-bearing capacity of pile, <i>see</i> point capacity
dip azimuth, see dip direction	of pile
dip direction, 12–13, 57–60, 72	end-bearing piles, <i>see</i> point-bearing piles
definition of, 51	engineering geology, 1
determining, 75	epicentric distance, 22–23
direct ray, 39	equal angle projection, 65, 66, 72, 81
discontinuities, 12–14, 50, 57, 119	equal area projection, 64–65, 81
factors affecting	equatorial plane, 61
block size, 129-131	equatorial stereonet, 72–76, 82
orientation, 124	excavation of rocks, 225, 248
roughness, 125-126	expanding probe, 45
seepage, 129	extrusive igneous rocks, 9
wall strength, 127–128	
measurements methods parameters, 132	F
rating increments for condition of, 135	
in rock foundation, 227–229	factor of safety (FS)
types of, 68	expression for, 202–206
disintegration of rocks, 9, 17	rock foundation, 225, 228
dispersed structure of soil, 19	for stability of rock slope, 202, 204, 205
double-tube core barrels, 87, 88	with vertical seismic coefficient, 208
dowels, 218	fall, 215
drainage & ventilation system, 269	fault estimation, 76
drilled caisson, <i>see</i> drilled piers drilled piers, 231	fault plane, 14
drilled shaft, see drilled piers	feeler gauge, for measuring aperture, 128
drilling	feldspars, 6, 8 filled fractures, within rock mass, 120, 121
rotary vs. percussion, 86	filling
wire line, 87	discontinuity parameters, 132
durability test, slake, 106–108	soil, 19
,,,	first-cycle slake durability index, 107
r.	flexural toppling, 191, 194, 196
E	flocculated structure of soil, 19
earth	focal depth, 22
coefficient of pressure, 156	folds, 12–13
crust of continental-sized plates, 22	foliation, 120
igneous rock, 8	formations of rock, types, 7–11
structure and composition of, 2–3	foundations on rock
earthquakes, 21, 22	construction and treatment, 248
human activities-based causes, 22	deep foundations, 231–235
intensity scale, 26–28	shallow foundations, see Shallow foundations
magnitude, 26	on rock
tectonic and non-tectonic causes, 22	fracture of rock, 14
types, 22	friction angle, 151
waves, 23–25	of rock specimen, 92
effective overburden pressure, 227	of rough discontinuity surface, 127
effective resistivity of rock, 42	friction piles, 232
elasticity, Young's modulus of, 25	FS, see factor of safety
elastic material, isotropic linear, 158	
electrical drilling, 45 electrical resistivity method, 41	G
electrode configuration used in, 44	geological compass, 59–60
resistivity parameters, 41	geological strength index (GSI), 133, 146
subsurface earth materials, 42	for jointed rocks, 148
5055011000 out in materials, 72	101 Jointou 10cks, 140

rock mass quality and, 150 Geomechanics Classification System, 133 geometrical methods, slope stabilisation, 217 geophysical investigation methods, 37 global rock mass strength, 177 gneisses, 11 good-quality rock mass, 149 granites, 8, 9, 11 gravity (Specific) of minerals, 5 great circle, see reference sphere groundwater, 27, 28, 45, 51, 132	intensity scale of earthquake, 27, 28 intermediate-focus earthquakes, 22 International Society for Rock Mechanics (ISRM), 90, 109, 110, 123 International Society of Soil Mechanics and Geotechnical Engineering (ISSMGE), 91 intrusive igneous rocks, 9 isoseismal line, 22 isotropic behaviour, 173 isotropic linear elastic material, 158 ISRM, see International Society for Rock
aquifer, 30–31	Mechanics
in joints, 136	ISSMGE, see International Society of Soil
grouting, 218-219	Mechanics and Geotechnical
GSI, see geological strength index	Engineering
Н	J
hard rocks, 227, 249	joint alteration number, 140–142
Hoek–Brown failure criterion, 111, 146–149, 170, 173 intact rock, 170–173 rock mass, 173–176	joint condition, rating increments for, 135–136 joint plane material, 202, 204–205 joint roughness coefficient (JRC), 126 joint roughness number, 140
Hoek–Brown parameters, 175–179	joints, 121
Hooke's law, 94, 158	groundwater in, 137
horizontal normal stress, 156, 165	Joint sets number, 129
horizontal planes, projections of	number of, 123
circles on, 66–67	for Q-system, 141
horizontal seismic coefficient, 207–208, 222	rating increments for spacing, 134
horizontal slip, 14	joint wall compressive strength (JCS), 127
hornblende, 6, 9	joint water reduction, 143
hydrogeology, 27–31	
hydrological methods, slope	K
stabilisation, 217	l1:-::- (7 20
hypocentric distance, 22	kaolinite, 6, 7, 20 kinematic analysis, 194–200
I.	Kinematic analysis, 174–200
	L
igneous rock, 8–11, 50	
illite, basic structure of, 20	labradorite, 6
Indian Roads Congress, 228	lambert projection, see equal area projection
indirect tensile strength test, 101–103, 105,	La Mécanique des Roches (Talobre), 1
112, 114 in situ stresses within rock mass, 156–157	large-scale surface undulations, 125–126
intact rock, 155, 170	latitudes, coordinate system with, 60–62 leaky aquifers, 31
Brazilian indirect tensile strength test in, 101	
engineering properties of, 86	limbs, 13 limestones, 9–11
rock coring, 87–88	bedded, 248
rock quality designation, 89–90	cores, 167, 171
test procedure standards, 91–92	modulus of elasticity values, 228
Hoek–Brown failure criterion, 170–173	limit equilibrium methods, for slope
isotropic behaviour of, 174	stability analysis, 202
and rock mass, 119–122	line of dip, 12, 50
state of stress in, 181	line of unconformity, 16
strength of, 116, 133, 230	lines
Young's modulus of, 180	angle between, 75–77, 84

of latitude, 61 orientations of, 57–60 lining support system, 266–267 lithosphere, 3 load-bearing capacity, 227–228 estimation of deep foundations, 233–235 shallow foundations, 227–229 load-carrying capacity of pile, 231–235 longitudes, coordinate system with, 60–62 Love waves, 23, 50 L-type hammers, 110	N net allowable bearing pressure, 218, 227, 230 net safe bearing capacity, 217, 228 pressure, 229 net slip, 14 net ultimate bearing capacity, 227 non-tectonic causes, earthquake, 22 normal fault, 14 N-type hammers, 110 numerical analysis, 279–280
M	O
magma, 6, 8, 9 chemical composition of, 9 magnitude of earthquake, 26 Malpasset concrete arch dam, 2 mantle, 3, 4 marbles, 10, 11, 50 mass, rock, <i>see</i> rock mass	organic soils, 19 orientation of discontinuities, 133 of plane, 12 rating adjustments for, 137
mat foundation, 46, 226 measuring tape, 125	peak shear strength, 168, 184
mechanical methods, slope stabilisation, 218 mechanical properties of rocks, 8 Mercalli maximum intensity scales, 27, 28 meridians, see longitudes meridional stereonet, see equatorial stereonet metamorphic minerals, 9 metamorphic rock, 8, 10, 11, 50 metamorphism, 9 minerals, 1, 4 clay, 5–7 grains, 8, 9, 11, 17 gravity (specific) of, 5 hardness of, 5, 50 metamorphism, 9 physical properties of, 4 quartz, 17, 176 rock-forming, 6–8, 41 mining rock mass rating (MRMR), 139 modulus ratio, see Young's modulus Mohr-Coulomb c' and φ' for rock mass, 176–179 Mohr-Coulomb failure criterion, 111, 155, 163, 166, 176, 184 adjustment for tensile normal stresses, 166 Hoek-Brown failure criterion and, 171 to rock mass, 169 from soil mechanics, 127	percussion drilling vs. rotary drilling, 81 permeability of rocks, 30, 33 petroleum geology, 31–34 piezometric surface, 31 piles, deep foundations, 231, 245 resting on bedrock, 233 pipe jacking, 255, 276, 278 plagioclases, 6 planar discontinuity, 192, 195 plane failure, 191–193 mode, 188–190 of rock slopes, 69, 194–198 plane of unconformity, 16–17 planes angle between, 75–76 intersection of, 62, 63, 74 orientations of, 57–60 plane strain loading, stress-strain relations, 160–162 plane stress loading, stress-strain relations, 162–163 plate tectonics, 22 plunge of fold, 13 point-bearing piles, 231 point capacity of pile, 231, 234, 235 point load strength anisotropy index, 105 point load strength index test, 103–105, 112, 114
Mohr-Coulomb failure envelope, 92 Mohs scale of hardness, 4–5 montmorillonite, 7, 20 MTS universal testing machine, UCS test on, 92, 93 muscovite, 6	point load test, 103, 104 advantage of, 105, 114 Poisson's ratio, 94, 95, 100 polar stereonet, 64, 67, 68, 72 pole of line, 64 pole of plane, 64
	-

poor-quality rocks, 149	heavy jointing, 15
porosity of rocks, 28-30	Hoek-Brown failure criterion, 173-175
primary openings in rock, 28	intact rock and, 119-123
primary rocks, see igneous rock	Mohr-Coulomb c' and ϕ' for, 176–179
	Mohr-Coulomb failure criterion to, 169
Q	persistence of, 125
	Q-system, see Q-system
Q-system, 133, 139	RMR, see rock mass rating
joint alteration number for, 141–142	seepage in, 129
joint set number for, 141	with several discontinuities, 87
rock mass classification, 145	strength of, 181–183
RQD values in, 139, 140	shear, 168–169
stress reduction factor for, 143–144	stress within, 156
quartz, 6, 8	triaxial tests, 176–179
weathering processes, 16–17	rock mass rating (RMR), 133, 151
quartzite, 9, 11, 31	rating increments
	for groundwater conditions, 137
R	for joint condition, 135–136
0.0 1.0 .0 1.0	for uniaxial compressive strength, 134
raft foundation, see mat foundation	value, 138
Rayleigh waves, 23	rock quality designation (RQD), 89–90, 130, 230, 249
reference sphere, 60–61	rating increments for, 134
reflection method, seismic, 40–41	values in Q-system, 140
refracted ray, 39–40	rock reinforcement, 218
refraction method, seismic, 40	rock slope
residual friction angle, 127 residual shear strength, 141, 168	failure modes of, 188–191
residual soils, 19	in plane failure, 193–203
resistivity of materials, 41, 42	stabilisation, 188, 216–220
reverse fault, 14	stability of, 201
rhyolite, 8, 9, 50	factor of safety, 202
Richter's earthquake magnitude, 26–28	Rock-socketted pile, 236
vs. Mercalli maximum intensity scales, 28	Rock wedge, forces acting on, 208, 210
Richter's earthquake magnitude vs., 28	rotary drilling, 36, 51
RMR, see rock mass rating	vs. percussion drilling, 86
rock beds, 47–51, 231	roughness
folded, 13	angle, estimation, 127–128
geological structures and orientation of,	of rock joint, 125–126
16–17	RQD, see rock quality designation
rock block resting on discontinuity plane, 215	
rock bolt, 138, 260, 261, 263	S
rock cores, 119	3
rock coring, 87–89	safe bearing capacity, 227
rock cycle, 10	safe bearing pressure, 227, 229
rock engineering, 1	sandstones, 9–11, 50–51
rock formations, types, 7–11	modulus of elasticity values, 228
rock-forming minerals, 6–8, 41	scale effect, 155, 233
rock foundation, 10–11, see also foundations on	Schmidt hammer test, 108–110, 127
rock granite	Schmidt projection, see equal area projection
rock joint, roughness of, 125-127	secant modulus, 94
rock mass, 57, 86	secondary minerals, 6
analysis of, 158	secondary openings in rock, 28
block size in, 129–139	secondary permeability, rocks, 129, 155
classes, 139	second-cycle slake durability index, 107, 108
classification, 89, 131–132	sedimentary rock, 8, 9, 11
deformation modulus of, 180–181	sedimentary soils, 17
GSL see geological strength index	seepage in rock mass, 129

seismic methods, 38–41	SRF, see stress reduction factor
seismic waves, 23	stability of rock mass, 119-120, 146
seismograph, 25-26, 51	state of stress in intact rock, 181
seismology, 22	steel rods, 218
shallow-focus earthquakes, 22, 50	stereographic projection, see equal angle projection
shallow foundations on rock, 225	stiffness, 180
depth of, 227	strain-displacement relationships, 163
load-bearing capacity, 227	strength
estimation, 227–228	of rock mass, 181-183
types of, 225	shear, see shear strength
shear modulus G, 96	in situ stresses and, 155-157
shear strength, 127–128	soils vs. rocks, 155
of rock mass, 165-170	tensile, see tensile strength
soils, 163	strength and durability of, 11
shear stress, 169	stress, within rock mass, 156
shear waves, 23	stress reduction factor (SRF), 140, 143-146
shock waves, 38, 40	stress-strain relations, 158-163
shotcrete, 218, 264–266	strike, 52, 58, 59
silica tetrahedron, 20	of plane, 12
single-tube core barrels, 88	strip footing, 160, 225
site investigation, 35–37	subsurface investigation, 36, 228-229
size-corrected point load strength index, 105	geophysical methods, 37
slake durability test, 106–108	subsurface water, 28
slickenside, 125	suggested methods for rock test, 91
sliding rock block, 190, 202-203	surface staining on rocks, 142
slope failure mechanisms, 191–192	surface waves, 23
slope stabilisation, 216–219	syncline, 13
slope stability analysis, 201–202	
plane failure in, 202–207	T
wedge failure in, 208–211	•
slush grout, 248	tangent modulus, 94
small-scale unevenness, 125, 126	tectonic earthquakes, 22
socket length, 236, 237	tensile normal stress, Mohr-Coulomb failure
soft rocks, 191, 228	criterion adjustment for, 166-167
software, 78, 80, 204	tensile strength, test
soil, 1, 17–19	indirect, 164–166
formation, weathering of, 17–22	of intact rock, 155
layer, 231	of rock mass, 175
mass, 170	test
mechanics, 1–2	Brazilian indirect, 165
particle, 21	indirect, 101–103, 114
vs. rocks strength and deformation, 155–156	uniaxial, 163
sedimentary, 19, 28, 32	tension crack, 205
shear strength, 163	water in, 206
strength, classification of, 122–123	Terzaghi's effective stress theory, 169
structure, 19–20	thermal conductivity of rock, 3–4
triaxial tests on, 111	toppling failure, 188–191, 199–200, 215
UCS test, 92–93	triaxial test, 111–114
soil-bedrock interfaces, 44	limestone cores, 167, 171
spacing of discontinuities, rock classification,	rock mass, 176-178
124, 125	trough, anticline, 13
sphere, intersection of, 62–64	true dip, 57, 59
spherical projections, 60, 64	tunnelling, 255
equal angle projection, 65	construction of, 273, 274
equal area projection, 65	designs of, 258
great circles, 66-67	drill and blast method, 275
spread footing, 225–227	excavation sequence, 277

tunnelling, discontinuity orientation effects in, vertical normal stress, 156, 165 135-139 vertical seismic coefficient, 207-209 tunnelling quality index, see Q-System volcanic causes, earthquake, 22 types of rock, 7-11 volumetric joint count, rock mass, 130 U W UCS, see uniaxial compressive strength ultimate bearing capacity, 227 wall strength of rock, 127-128 ultimate load-carrying capacity of piles, 231, 232 subsurface, 27-28 rock-socketted piles, 236 in tension crack, 205-206 unconfined aquifers, 30-31 water table well, 31 unconfined compressive strength, see uniaxial waves, earthquakes, 25-26 compressive strength weathering of rocks, 49 unconformity, plane of, 16 classification, 18 uncorrected point load strength index, 103 degradation, 17 unfilled fractures within rock mass, 120 in formation of soils and sediments, 19 uniaxial compressive strength (UCS), 86, 92 wedge failure, 82, 208 rating increments for, 134 mode, 188-194 ratio of, 105 wedge sliding, condition of, 209 of rock, 233, 234, 236 Wenner electrode configuration, 44 rock classification based on, 96, 98 white mica, see muscovite soils vs. rocks, 92-93 wire line drilling, 87 test, 92-97, 163, 166 Wulff projection, see equal values, 96, 100 angle projection uniaxial tensile strength test, 163-166 uniaxial tensile tests, 163, 164, 166 Young's modulus, 92-98, 100 V of elasticity, 25 Vajont dam, 1 of intact rock, 180

modulus ratio, 100, 101

vertical electrical sounding (VES), 45